Electron Spin Resonance Spectroscopy in Medicine

Ashutosh Kumar Shukla
Editor

Springer

Electron Spin Resonance Spectroscopy in Medicine

Ashutosh Kumar Shukla
Editor

Electron Spin Resonance Spectroscopy in Medicine

Springer

Editor
Ashutosh Kumar Shukla
Physics Department
Ewing Christian College
Allahabad
Uttar Pradesh
India

ISBN 978-981-13-2229-7 ISBN 978-981-13-2230-3 (eBook)
https://doi.org/10.1007/978-981-13-2230-3

Library of Congress Control Number: 2018958539

This Springer imprint is published by the registered company Springer Nature Singapore Pte Ltd.
The registered company address is: 152 Beach Road, #21-01/04 Gateway East, Singapore 189721, Singapore

To my parents

Preface

This collection intends to describe the applications of electron spin resonance (ESR) spectroscopy in the medical field. Mathematical details have been kept at a necessary minimum so as to make the collection more meaningful for readers from different disciplines.

Chapter 1 by Bernadeta Dobosz and Ryszard Krzyminiewski presents ESR study of human blood and its interaction with magnetite nanoparticles. Chapter 2 by Małgorzata Dutka, Janusz Pyka, and Przemysław M. Płonka presents ESR applications in understanding the physical intricacy of HbNO complexes. Germán Barriga-González and Claudio Olea-Azar have discussed the applications of ESR and spin trapping technique for the study of tropical parasitic diseases in Chap. 3. Detection and measurement of oxidative stress using ESR spectroscopy is discussed in Chap. 4 by Siavash Iravani. Seyda Colak has presented ESR spectroscopy investigations on radiosterilization feasibilities of sulfa-group drug raw materials in Chap. 5. Chapter 6 by Bruno Luiz Santana Vicentin and Eduardo Di Mauro presents ESR applications in identification of free radicals and monitoring of polymerization of resinous materials used in dentistry. Recent issues in X band ESR tooth enamel dosimetry have been addressed by Shin Toyoda in Chap. 7. Przemysław M. Płonka, Dominika Michalczyk-Wetula, and Martyna Krzykawska-Serda have presented dermatological applications of ESR in Chap. 8. Przemysław M. Płonka has coined and justified "paramagnetomics" for biologically and medically oriented ESR spectroscopy in Chap. 9.

I am especially thankful to the expert contributors for making this collection a unique addition to the existing knowledge base. I sincerely thank Dr. Naren Aggarwal, Executive Editor, Clinical Medicine, Springer (India) Private Limited, for giving me opportunity to present this book to the readers. I also thank Teena Bedi, Associate Editor (Clinical Medicine), Springer (India) Private Limited and Mr. Kumar Athiappan, Project Coordinator (Books), Springer Nature, for their support during the publication process.

I am grateful to Professor Ram Kripal, Department of Physics, University of Allahabad; Prof. Raja Ram Yadav, Vice-Chancellor, V.B.S. Purvanchal University, Jaunpur; Dr. A. D. M. David, Principal, Ewing Christian College, Allahabad; and my colleagues for their constant encouraging remarks and suggestions during the development of this volume.

I could complete this task with the blessings of my parents. My brother Dr. Arun K. Shukla, Department of Biological Sciences and Bioengineering, Indian Institute of Technology, Kanpur, has suggested the best in many ways and words are insufficient to thank him. I wish to thank my wife Dr. Neelam Shukla, my daughter Nidhi, and son Animesh for their patience during the progress of this work.

Allahabad, India
September 2018

Ashutosh Kumar Shukla

Contents

About the Editor

Ashutosh Kumar Shukla obtained his B.Sc., M.Sc., and D. Phil. degrees from the University of Allahabad. His doctoral research work involved using electron spin resonance spectroscopy and optical absorption spectroscopy to investigate transition ion-doped single crystals. He has teaching and research experience of more than 17 years and is currently an Associate Professor of Physics at Ewing Christian College, Allahabad, a University of Allahabad institution. He also served as an Associate Professor (Pure and Applied Physics) at Guru Ghasidas Vishwavidyalaya, Bilaspur, C.G. (a central university).

Dr. Shukla has successfully completed research projects in the area of electron spin resonance funded by the University Grants Commission, the apex body of higher education in India. He has visited different countries including U.S.A., U.K., Germany, Spain, and Russia to present his work at international events. He has published numerous research papers in peer-reviewed journals and has edited various volumes. He has delivered several invited lectures on characterization techniques at national and international conferences and workshops. He reviews manuscripts for a number of international journals.

He has received many scholarships and fellowships, including National Scholarship, Scholarship of Ministry of Higher Education, Government of U. P.; Research Fellowship of the Council of Science & Technology, Lucknow, U.P.; Research Fellowship of the Council of Scientific & Industrial Research, New Delhi; and the Indian National Science Academy-Bilateral Exchange Fellowship.

1 Electron Spin Resonance (ESR) Study of Human Blood and Its Interaction with Magnetite Nanoparticles

Bernadeta Dobosz and Ryszard Krzyminiewski

1.1 Introduction

Electron spin resonance (ESR) is a popular technic in various fields [1–3]. One of them is also medicine, where it can be used both for paramagnetic species and free radical study in so-called biologically active materials (e.g., blood, tissues) [4, 5].

The basic principles of ESR are very similar to the more popular nuclear magnetic resonance (NMR) technique. Both methods are based on the interaction of electromagnetic radiation with magnetic moments of electrons (ESR) and nuclei (NMR). When a sample with an unpaired electron will be placed in an external magnetic field, the electron spin will align parallel or antiparallel to the direction of the magnetic field. This situation corresponds to two energy states, and the energy difference between these is proportional to the applied magnetic field, what is described by the so-called resonance equation (Eq. 1.1):

$$h\nu = g\mu_B B \tag{1.1}$$

where h is Planck's constant, ν is the frequency of the electromagnetic radiation, g is a spectroscopic splitting factor characteristic for each paramagnetic center, B is applied magnetic field, and μ_B is the Bohr magneton.

In context of using ESR for paramagnetic species and free radicals present in blood study, two definitions are important: hyperfine and fine interaction.

The first one concerns the interaction between a spin of unpaired electron with a nucleus. It is particularly important in the case of free radical detection. It can be more precisely described on the example of the nitrogen nucleus which spin is $I_N = 1$. Nitrogen often occurs in special substances used for free radicals detections: spin labels, spin traps, and spin probes. In a case of one unpaired electron and one

B. Dobosz (✉) · R. Krzyminiewski
Medical Physics Division, Faculty of Physics, Adam Mickiewicz University, Poznan, Poland
e-mail: benia@amu.edu.pl; rku@amu.edu.pl

A. K. Shukla (ed.), *Electron Spin Resonance Spectroscopy in Medicine*,
https://doi.org/10.1007/978-981-13-2230-3_1

nitrogen nucleus, the ESR spectrum is a triplet of lines. However, the possibility of registering such a triplet depends on the environment and how far the radicals can interact. In the case of powder, when the radicals are in contact with each other, the multiplet averaging will occur, and only one line is observed. Using ESR not only a type of free radical can be determined but also the concentration of free radicals in a sample and their dynamics.

The second type of interaction, so-called fine interaction, concerns the situation when more than one unpaired electron is present in studied sample ($S > 1/2$). It is based on the interaction of unpaired electron spins with each other in the crystalline field. It refers to transition elements, including iron that is present in the blood [1, 6].

1.2 ESR Study of Human Blood

Full human blood is composed of fluid (plasma) and the morphological elements suspended in it: erythrocytes, thrombocytes, and leukocytes. Approximately 94% of the erythrocyte solid is hemoglobin, consisting of a prosthetic group (hem) and a protein part (globin). Hem is built of protoporphyrin and centrally located ferrous ion Fe^{2+}. In the lungs hemoglobin is saturated with oxygen. The binding of the oxygen molecule changes the electron system within the iron that moves in the porphyrin plane, which initiates the structural transformation of the molecule. Fe^{2+} ion in the hemoglobin has two possible spin states. In venous blood, deoxyhemoglobin is in a high-spin state ($S = 2$), while in arterial blood oxyhemoglobin is in a low-spin state ($S = 0$) [7]. The transition from the paramagnetic high-spin state to the diamagnetic low-spin state results in a decrease in the iron ion's radius so that it can slip into the porphyrin ring [8]. Both oxyhemoglobin and deoxidized hemoglobin, by various factors, can turn into methemoglobin, in which iron is at +3 oxidation state. The presence of methemoglobin is often disclosed in ESR study of blood by signal recording with $g_{\perp} = 6$ and $g_{\parallel} = 2$ from the high-spin form of Fe^{3+} [9–11]. An ESR study showed elevated methemoglobin level in people exposed to various types of radiation [7]. Excessive presence of this protein is not good because free radicals are produced in the blood mainly by reaction with hydrogen peroxide [9, 10]. When trivalent iron in the hem reacts with H_2O_2 or other peroxide, the hem is oxidized to the oxyferyl form ($Fe^{4+}{=}O$), and the H_2O_2 is reduced to H_2O by accepting two electrons. One of them comes from the transform of Fe^{3+} in Fe^{4+}, while the other is from the globin, where a porphyrin-based cationor $P^{+\cdot}$ is generated [9]. ESR spectroscopy revealed the formation of toxic methylene radicals from tryptophan residues ($g = 2.033$) and tyrosyl radicals ($g = 2.005$) in methemoglobin [9, 10]. It has been proven that ascorbate present in plasma can sweep off free radicals produced by H_2O_2. As a result of electron donating, ascorbate converts into an ascorbic radical $A^{-\cdot}$ which is much less reactive [9]. In addition, ascorbate as an antioxidant effectively prevents the formation of oxidative damage of coagulation factors in blood, including fibrinogen [12].

Human transferrin (Tf) is a protein, whose main role is an iron transport and delivers it to cells. It is also important in the processes of growth, proliferation,

differentiation, and apoptosis of cells [13, 14]. Transferrin only accepts Fe^{3+} ions, which occur here in a high-spin state ($S = 5/2$). Hence, during the full human blood investigation, a characteristic ESR signal is observed at $g = 4.2$ [4, 14, 15]. This signal is complex, which is related to the transition from the middle Kramers doublet [16]. On the other hand, the two peaks present at the low field correspond to the transitions between the levels of the lowest Kramers doublets [17]. Iron-deficient transferrin-apotransferrin does not give ESR signals [9]. Transferrin is a part of the defense system which defends the organism against the excess of free iron. Such iron, unbound to protein, leads in Fenton reaction to the formation of hydroxyl radicals, which are highly reactive and cause damages to lipids and DNA [18].

Human ceruloplasmin (hCP) is a glycoprotein found in the blood plasma. The ceruloplasmin contains about 95% of the total copper in the body. The hCP molecule contains six protein domains arranged in a triangular orientation and binds six copper atoms. Copper atoms are here divided into three types. Each copper atom of type I binds to cysteine and two histidine residues and to methionine residues. Type III copper atoms are associated with three histidines while type II with two. Copper atoms of type I are paramagnetic and give a more complex ESR spectrum than Cu type II. Conversely, a pair of antiferromagnetic-coupled type III copper ions is invisible in the ESR [19]. In ESR spectra of the purified human ceruloplasmin, one can distinguish the signal from Cu type II with $g_{\|} = 2.25$ and $A_{\|} = 18$ mT and two various signals from Cu type I centers with different values of the hyperfine splitting constant ($A_{\|} = 7.2$ mT and $A_{\|} = 9$ mT) but similar g values ($g_{\|} = 2.20$ and 2.21) [20]. Ceruloplasmin is synthesized in the liver, but cancer cells may it also produce. In malignant tumors both the level of copper in the plasma [21] and the concentration of ceruloplasmin increase [22, 23]. Significantly elevated serum ceruloplasmin level had patients with head and neck cancer comparing to healthy people, and this increase was proportional to the stage of the disease. A decrease in ceruloplasmin level was noticed after radiotherapy, but it was still higher than in the control group [24].

1.2.1 ESR Study: Chosen Examples

ESR has been used for years in medical research. There are many references in the literature on the use of this technique in blood study. In this part of this chapter, only a few chosen examples will be described.

One of them is a paper by Krzyminiewski et al. [4] in which human blood, taken from healthy people and patients with melanoma, was investigated using ESR to study the electron states of iron complexes and to find out if the ESR results can be related to a standard biochemical laboratory tests of different blood elements. Cells, both normal and neoplastic, take up iron by endocytosis with the help of transferrin receptors. The effectiveness of such process is different in these two cases. In melanoma there is a quick growth and numerous metastases. Melanotransferrin (MTf) present in the melanoma cells reveals a significant homology with transferrin and lactoferrin, and its expression does not depend on the iron concentration inside cells. With the mechanism of the iron concentration in the progress of the disease,

the released proinflammatory cytokines are probably related. They strengthen the production of ferritin, which is an iron-storing protein, and simultaneously induce a reduction in the expression of transferrin receptors. This leads to lower iron intake by the receptors and at the same time enhances the uptake of iron taking from the cells that change to phagocytes [25, 26]. The accumulation of iron in macrophages and the cells of the reticuloendothelial system lowers the availability of iron for the erythrocyte system, which can reduce the Hb concentration and lead to anemia. For this reason knowing the role and functions of the of iron ion complexes in cancer disease is very important.

Comparing the ESR spectra of healthy blood and blood from patients with melanoma, the basic difference is seen in the complexity of ESR spectrum, in which for healthy people there are more components which come from higher number of various types of Fe^{3+} complexes than in the case of people with melanoma. The second difference is that ESR signals from healthy samples are more intensive. In this study four different types of components of the EPR spectra were determined with g factor amounting to $g = 6.08–6.09$, $g = 4.14–4.22$, $g = 3.12$, and $g = 2.34–2.39$. Each line can be assigned to specific iron complexes present in the blood, and so on the signal at $g = 6.0$, it is due to the trivalent heme iron in methemoglobin (MetHb) [5, 27, 28] in which iron is at the third degree of oxidation instead of the second one. Trivalent iron cannot bind oxygen, the energy of the crystalline field at the Fe^{3+} ion is small, and iron is in the high-spin state ($S = 5/2$). A small percent of such Hb can be found in the blood of each person. The ESR line recorded at $g = 4.14–4.22$ is a typical signal for the nonheme iron Fe^{3+} ion in a system of low, rhombic symmetry in an octahedral or tetrahedral surrounding. Such systems give rise to low crystalline fields; hence iron is in the high-spin state ($S = 5/2$). This signal can occur as a single peak [5, 28–32] or it can be complex [33–36]. Most researchers have assigned this signal as originating from Fe^{3+} in transferrin [5, 28–32, 34–39]. The resonance lines at $g = 3.12$ and $g = 2.34–2.39$ are related to various heme protein complexes in which iron is on the third degree of oxidation, the so-called hematin or hemin. In contrast to the case of MetHb, iron in hemin is in the low-spin state. In this study the complexes of copper Cu^{2+} were observed only in healthy people. The exemplary ESR spectrum of whole human blood taken from patient with melanoma is shown in Fig. 1.1.

Similar investigation was done in a group of patients with a breast cancer [14, 40]. In this study the signals from high-spin Fe^{3+} ions in transferrin ($g = 4.2$) and Cu^{2+} ions in ceruloplasmin ($g = 2.05$) were obtained in the ESR spectra of frozen whole blood both in healthy people and patients suffering from cancer. ESR lines derived from high-spin Fe^{3+} ions in methemoglobin ($g = 5.8–6$) and various low-spin ferriheme complexes ($g = 2.21–2.91$) were detected in some patients and also in several healthy volunteers. Therefore, it cannot be clearly stated whether the presence of ESR line from specific trivalent iron complex is characteristic of particular disease entity and allows to differentiate patients from healthy people. However, significant changes in ESR signal amplitudes both from Cu^{2+} in ceruloplasmin and Fe^{3+} from transferrin were observed taking into account the influence of radiotherapy treatment.

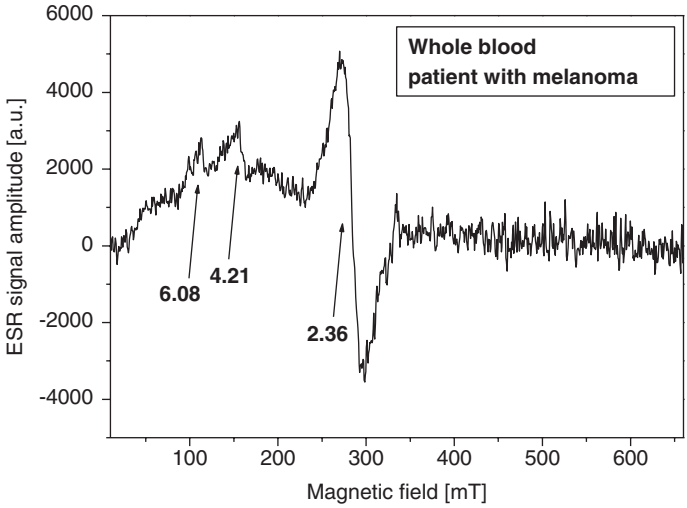

Fig. 1.1 Exemplary ESR spectrum of whole human blood taken from patient with melanoma, recorded at 77 K

The possibility of blood testing using ESR was described much earlier. Foster and Pocklington [41, 42] showed that ceruloplasmin and Fe transferrin levels can be measured by ESR in whole frozen blood. These works concerned studies in patients with cancer. In ESR spectra they observed lines with g factor typical for ceruloplasmin ($g = 2.049$) and transferrin ($g \sim 4.2$). Schwartz and Wiesner [43] also applied ESR for blood study in mixed cancer patients and observed an increase in ceruloplasmin signal size as compared with control samples and a decrease on response to radiotherapy.

Numerous other studies were dedicated to study ceruloplasmin and transferrin in various diseases like leukemia, Hodgkin's disease, and different types of cancer [16, 44, 45].

ESR is applicable for the studies of iron complexes not only in blood but also in remaining human tissues [5]. The researchers used lyophilized samples of various tissues: the human liver, brain, and blood to identify most typical iron forms in the human body. In liver sample they observed a signal from Fe^{2+} ions in hemoglobin ($g = 5.8$), a typical signal of high-spin Fe^{3+} ions which presence can be assigned to nonheme Fe^{3+} ions in transferrin ($g = 4.3$), a sharp signal at $g = 2.0$, which the authors ascribed to free radicals and the broad line at $g = 2.1$ attributed to the Fe^{3+} ions in grains of ferritin. Similar signals were observed in the brain tissue with the differences in shape and intensity. The signals of course changed depending on the temperature in which the sample was measured. The signals from hemoglobin and transferrin, because of their paramagnetic behavior, were hardly detectable at higher temperatures. It was concluded that brain tissue contains less blood than liver ones and the grains of ferritin in the brain are smaller than those present in the liver.

The scientists applied also ESR technique to estimate the age of human blood [28, 32]. In their investigation the authors found that ESR signals from

paramagnetic centers in human blood can be correlated with the time that has passed since bleeding. They used dried blood from healthy volunteers, and the measurements at 77 K were performed on the 1st day of sample preparation and 775th day after extraction. The ESR spectra obtained in the experiments consisted of typical lines observed in blood samples: ferric heme species at $g = 6.2$; ferric nonheme iron species at $g = 4.3$; two kinds of low-spin ferric heme species at $g_1 = 2.93$, $g_2 = 2.27$, and $g_3 = 1.54$ (A) and $g'_1 = 2.43$, $g'_2 = 2.27$, and $g'_3 = 1.90$ (B); and free radicals at $g = 2.005$. The low-spin species (A) and (B) were attributed to a bishistidinato-ferric heme complex and cysteine-heme-imidazole conformation, respectively [32, 46, 47]. The free radical signal was assigned to lipid peroxyl radicals formed by degradation of blood components [48]. The authors studied which parameter can be used for age determination. Important are that ESR measurement is a nondestructive technique and a 10 mg sample is enough to determine the age of a bloodstain. However, environmental factors (temperature and light) should be taken into account.

Other authors [49] applied ESR method in order to estimate the time of blood extravasation assuming that it can find application as a practical test in forensic medicine. Similarly to Fujita et al. [28], the authors stated that the conditions in which the samples are stored (temperature, humidity) have an impact on the results. Unfortunately in conclusions the authors stated that their results showed that the investigating ESR spectroscopic method is not valuable to be used in forensic medicine application and their experiments gave no confirmation of assumed concept.

1.3 ESR of Free Radicals

From a definition, a free radical is a molecule or molecular fragments with one or more unpaired electrons in its outermost orbit (atomic or molecular) which is capable of independent existence [50–52]. Free radicals can be created both from exogenous and endogenous substances. They are creating both in environment and in cells. There are many sources of free radicals generation [53–57]:

- Radiation (UV, X-ray, gamma rays, microwave)
- Inflammation initiates special elements (neutrophils and macrophages) to generate reactive oxygen species (ROS) and reactive nitrogen species (RNS)
- In various reactions, e.g., mitochondria-catalyzed electron transport
- Mitochondrial cytochrome oxidase, xanthine oxidases, neutrophils, lipid peroxidation
- Metabolism of arachidonic acid, platelets, macrophages, smooth muscle cells
- Interaction with chemicals, smoking, cars exhausts
- Burning of organic matter during cooking, volcanic activities
- Industrial wastewaters, excess of chemicals, drugs, asbestos, certain herbicides and pesticides, some metal ions, fungal toxins
- Metal-catalyzed reactions

1.3.1 ROS and RNS

Radicals coming from oxygen are the most important group of radical created in living systems [58, 59]. Molecular oxygen, because of its unique electronic configuration, is a free radical. By addition of one electron to such form, the superoxide anion radical ($O_2^{\cdot -}$) is created. Superoxide anion is forming either through metabolic processes or after oxygen "activation" by physical irradiation. It is capable of further interacting with other molecules, and "secondary" ROS can be generated. The formation of superoxide has a place mainly in the mitochondria of a cell [60]. The hydroxyl radical ($^{\cdot}OH$) is the neutral form of the hydroxide ion. It is characterized by a high reactivity, and it is very dangerous (half-life in vivo approx. 10^{-9} s) [61]. There are also additional reactive radicals from oxygen which can be formed in living systems like peroxyl radicals ($ROO^{\cdot}$), for example, $HOO^{\cdot}$, the protonated form of $O_2^{\cdot -}$ [58].

Free radical reactions derived from oxygen are involved in the pathogenesis of many human diseases [58, 62–69]:

- Neurodegenerative disorder: Alzheimer's disease, Parkinson's disease, multiple sclerosis, amyotrophic lateral sclerosis, memory loss, depression
- Cardiovascular disease: atherosclerosis, ischemic heart disease, cardiac hypertrophy, hypertension, shock and trauma
- Pulmonary disorders: inflammatory lung diseases (asthma, chronic obstructive pulmonary disease)
- Disease associated with premature infants: bronchopulmonary, dysplasia, periventricular leukomalacia, intraventricular hemorrhage, retinopathy of prematurity, and necrotizing enterocolitis
- Autoimmune disease: rheumatoid arthritis
- Renal disorders: glomerulonephritis and tubulointerstitial nephritis, chronic renal failure, proteinuria, uremia
- Gastrointestinal disease: peptic ulcer, inflammatory bowel disease, and colitis
- Tumors and cancers: lung cancer, leukemia, breast, ovary, rectum cancers, etc.
- Eye diseases: cataract and age related of retina, maculopathy
- Aging process
- Diabetes
- Skin lesions
- Immunodepression
- Liver disease, pancreatitis
- AIDS
- Infertility

The second "popular" group of free radicals are reactive nitrogen species (RNS). $NO^{\cdot}$ is a small molecule with one unpaired electron. In biological tissues is generated by specific nitric oxide synthases (NOSs). Nitric oxide is a reactive radical, an important biological signaling molecule in many physiological processes: blood pressure regulation, defense mechanisms, neurotransmission, smooth muscle relaxation, and

immune regulation [70]. Its half-life is only a few seconds in an aqueous environment and is greater in a lower oxygen concentration (half-life>15 s). Overproduction or RNS is called nitrosative stress [58, 71, 72].

The human body mainly consists of water. When water is exposed to radiation, the two-electron bondings between the oxygen and the hydrogen atoms can be interrupted, leaving one electron on the hydrogen and one on the oxygen, and thus two radicals are created. These radicals are commonly known as the hydrogen radical and the hydroxyl radical which are both very reactive [73]. The hydroxyl radical is the most reactive free radical which can attack almost every molecule in the body. In medicine important are two free radicals: the mentioned above hydroxyl radical and the superoxide radical. Free radicals are very dangerous because they are able to start a chain reaction that can destroy destructively the tissues. If hydroxyl radical attacks DNA, chain reactions run along the DNA molecule causing damage and mutations or even disruption of the DNA strands. During X or gamma radiation used to kill cancers, large numbers of hydroxyl free radicals are produced. But radiation and water are not the only ways to produce free radicals.

Inflammation is also associated with free radicals; however, in this case free radicals are probably the reason of the inflammation rather than the effect. The human body uses free radicals to kill bacteria within the phagocytes, the scavenging cells of the immune system. In the case when excessive numbers of the phagocytes are present in an inflamed area, the free radicals almost certainly increase tissue damage, making the situation worse. This situation is present, for example, in rheumatoid arthritis.

Oxygen free radicals are possible mediators of reperfusion-induced injury. Reperfusion corresponds to the restoration of oxygenated blood flow to ischemic tissue. During ischemia there is a reduction or even a complete blockade of blood flow to a tissue, with a rapid loss of oxygen supply to the cell [74].

The results of investigation suggest that hyperthermia promotes oxygen-centered free radical formation in cells [75–79]. Also in atherosclerosis, during atherosclerotic plaque formation, which can lead to stroke or myocardial infarction, oxygen free radicals may play a role [80]. Reperfusion of an injured region leads to increased formation of oxygen free radicals. It is a result of oxygen reintroduction to the injured region [81]. Toxic oxygen species can be produced either as a result of an increased xanthine oxidase pathways or neutrophil activity.

Free radicals in blood can be produced in the reaction of hydrogen peroxide with human methemoglobin [10]. Peroxyl radical, with $g = 2.033$, comes from tryptophan residues, while nonperoxyl, with $g = 2.005$, was identified as tyrosyl radical [10, 82]. Plasma ascorbate has the ability to scavenge globin free radicals. The reduction of these species by ascorbate causes the formation of less reactive ascorbyl radical. The increase in the concentration of ascorbyl radicals reflects the rate of the one-electron oxidation of ascorbate and shows oxidative challenges and also those caused by iron overload [83]. The ESR spectrum of ascorbyl radical is a doublet at room temperature and a narrow singlet ($\Delta B_{pp} = 0.9$ mT) at 10 K [82]. In blood at 77 K, the line has $g = 2.0057$ [11]. Human erythrocytes efficiently recycle ascorbate, because ascorbyl free radicals are reduced by the NADH- and

NADPH-dependent reductases [84]. Adrenaline radicals (singlet, ΔB_{pp} = 1.4 mT, g = 2.003) and adrenochrome radicals (singlet ΔB_{pp} = 0.9 mT, g = 2.004) were also detected in the blood [11, 14].

There are three mechanisms in which oxygen free radicals affect cells [73, 85]. First is a single reaction which they can initiate. This does not cause extensive cell damage. Second is in which the oxygen radicals may initiate a chain reaction and generate more radicals as a by-product. These radicals start the same reaction that can continue indefinitely. Such reaction can only stop when one free radical reacts with another one. However, the most destructive is the third mechanism. Initially, the oxygen radical generates more free radicals in the chain-type reaction. These radicals continually initiate reactions, and going further may start other types of reactions in which new kinds of radicals will arise. This mechanism named the branching mechanism can be continued until the structure and the function of the cell are destroyed.

Free radicals, besides their high reactivity, have very short half lifetime ($t_{1/2}$ 10^{-9}–10 s). For this reason there are two methods which allow the detection of free radicals: freezing the samples in liquid nitrogen (77 K) or adding special substance, called spin traps [75]. They are able to produce more stable secondary radicals, and thus they can be detected by ESR. Also the conditions of a measurement are important and temperature control. Figure 1.2 shows how it changes the ESR spectrum of free radicals after repassing through the liquid phase. This is particularly important when the concentration of free radicals in a sample has to be determined.

There are a lot of spin traps used in study of free radicals [86]. In biological systems most of them are nitroso and nitrone derivatives. For oxygen, carbon, or sulfur radicals, nitrone spin traps are usually applied, for example, the water-soluble DMPO (5,5-dimethyl-1-pyrroline-N-oxide) or the lipid-soluble α-phenyl-*N*-tert-butylnitrone (PBN). For NO, iron/sulfur cluster-containing spin traps have been developed, for instance, iron(II)-methyl glucamyldithiocarbamate

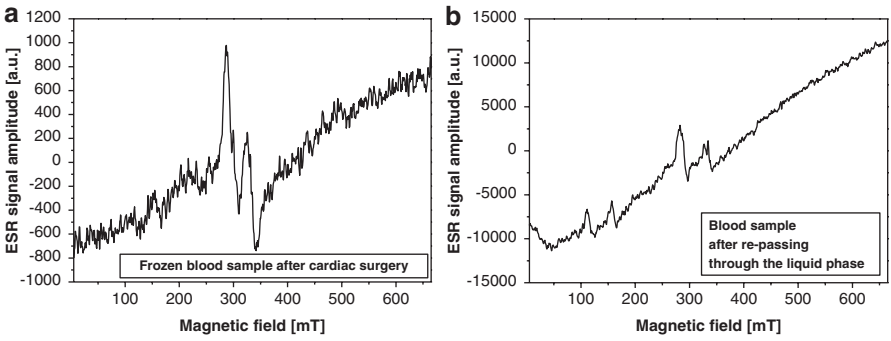

Fig. 1.2 ESR spectra of free radicals in human blood after cardiac surgery recorded at 170 K: (**a**) first measurement, (**b**) second measurement after repassing through the liquid phase, recorded at 170 K

(Fe-MGD_2). Depending on the properties (hydro- or liposolubility), they can diffuse through the cell membranes. The structure of ESR spectrum, number of lines, and their amplitudes can deliver information about the type of the radicals which were trapped [74].

The source of ESR signals in vitro can be vitamin C, present in vivo and known as a scavenger of free radicals. It also participates in the reduction of vitamin E, which is one of the important antioxidants. Thus, vitamin C level may indirectly indicate free radicals reactions in the body [87].

1.3.2 ESR of Free Radicals: Chosen Examples

Free radicals, using ESR spectroscopy, were studied in the blood taken from patients during open aortoiliac arterial reconstruction [88]. This kind of surgery can lead to development of ischemia-reperfusion injury and induces an inflammatory response and free radical production [89]. The authors compared the results of free radical study by ESR with a degree of inflammatory response monitored on the basis of standard parameters obtained from blood tests like Il-6, TNF-alfa, and CRP. To detect free radicals, the standard nitrosobenzene spin trap was added to blood samples. Free radical production during reperfusion of the first leg was observed 5 min after the aortic clamp removal. Twenty-four hours after the operation, free radicals decreased to the level observed before surgery. In the first minutes of reperfusion and reoxygenation of hypoxic tissue, high formation of oxygen radicals such as superoxide radicals ($O_2^{\cdot -}$), hydroxyl radicals ($^{\cdot}OH$), and hydrogen peroxide is observed [90]. The superoxide radicals in the reperfusion phase react with nitric oxide (NO) to generate peroxynitrite anions, which leads to the peroxidation of lipid and membrane proteins [91]. Increased formation of reactive oxygen radicals during reperfusion is associated with different mechanisms of mitochondrial function, DNA damage, activation of apoptosis, destruction of cellular membranes, capillary perfusion failure, interstitial edema, and multiorgan dysfunction syndrome [92–94]. Severity of ischemia and reperfusion cellular injury is dependent on overproduction of free radicals, duration of ischemia, degree of surgical trauma, endogenous antioxidant capacity, and antioxidant therapy. A significant increase in CRP, IL-6, and TNF-alfa was observed 24 h after the surgical treatment. It may cause not only tissue injury during surgery but also muscle ischemia during temporary aortic clamping and reperfusion. These markers decreased 6–8 days after the aortic reconstructive surgery in uncomplicated cases.

ESR spectroscopy was also used to monitor free radicals generation in peripheral blood inpatients subjected to angioplasty treatment [95, 96]. In this study the scientists also applied nitrosobenzene spin trap, and they determined the most appropriate experimental conditions (temperature of measurements and the concentration of spin trap-blood solution), the concentration of free radicals in patients subjected to angioplasty treatment, and compared the ESR results with myocardium damage markers (CPK, MB, and TnT). It is obvious that inflammation accompanies this type of surgery which, in turn, is associated with increased levels of free radicals. The increase

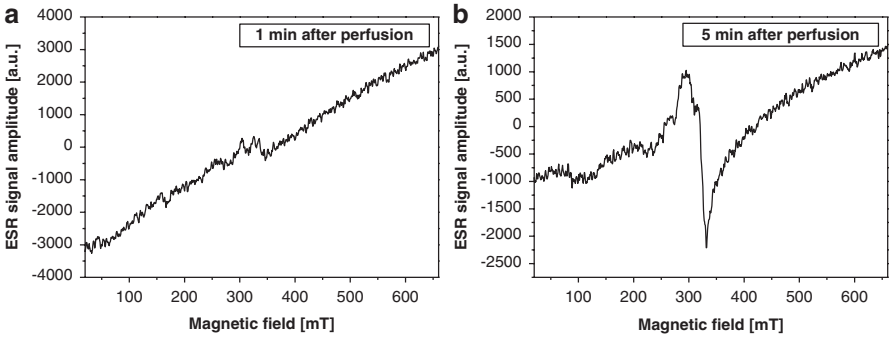

Fig. 1.3 Exemplary ESR spectra of free radicals in human blood generated after perfusion: (**a**) 1 min after perfusion, (**b**) 5 min after perfusion

in the concentration of free radical in the blood-spin trap conglomerate was observed 2 h after reperfusion. Twenty-four hours after reperfusion, the concentration of free radicals decreased, and maximum values for some medical markers were observed. This study shows that ESR is a sensitive method to detect heart damage and inflammation earlier than standard medical blood markers. In addition, it was found that such samples should be stored at liquid nitrogen temperature (77 K) to stabilize the concentration of free radicals over time. The exemplary results of free radicals generated in human blood after reperfusion is shown in Fig. 1.3.

Gonet et al. [87] applied ESR for study free radicals in ischemic heart disease in two groups: people with myocardial infarction and with angina pectoris. The role of free radicals in ischemia, atherosclerosis, and diabetes diseases was described in many papers [97–100]. Gonet et al. used lyophilized blood samples taking into account that this kind of sample preparation and exposure to air can affect the type of free radicals generated. Their results indicate a reduce level of vitamin C in blood in patients with ischemic heart disease that was in good agreement with the previous study [101–105]. Second, the shape and parameters of ESR signals from blood can be a useful method in studying free radicals in patients with ischemic heart disease.

Because free radicals are also associated with ionizing radiation, there are papers concerned to ESR study of irradiated blood or serum [7, 31]. Maghra by et al. [31] studied the effect of ionizing radiation of Cs-137 and Co-60 on powder bovine hemoglobin. In addition to the signals coming from iron (described earlier in this chapter), the authors also described the signal assigned to free radicals in hemoglobin created by the degradation of blood components [48]. In several papers two or more different kinds of radicals are considered as created on the protein [106, 107]. As the major contributor of this signal, the globin-based free radical (HB(Fe(IV) = O)) was suggested [10, 33]. It was observed that this signal significantly increased even for very low dose of irradiation (4.95 Gy), and the response to gamma radiation doses was linear. No new radicals were generated after irradiation. The researchers concluded that gamma irradiation of bovine hemoglobin causes conformational changes in Hb molecular structure, which may cause the changes in its function performance.

The ways of imposing oxidative stress are physical exercises [108, 109]. It is also a good model for studying the balance between oxidative challenge and antioxidant defense mechanisms in biological systems [110]. Physical exercises increase the generation of ROS [111, 112]. It is a response to increased use of oxygen that causes a disturbance in the prooxidant/antioxidant balance in favor of the former and leads to oxidative stress. On the other hand, antioxidant compounds can lead to a reduction in ROS production by alter redox status [113, 114]. Mrakic-Sposta et al. [108] successfully applies ESR to monitor ROS production in peripheral blood of athletes after controlled exercise. Although ESR can be used to measure many kinds of biological samples, blood is the most commonly used one. Based on the conducted research, the authors stated that by measuring of the capillary blood, a reliable information can be provided about free radicals appear in the skeletal muscle, heart, and liver.

1.4 Magnetite Nanoparticles as Potential Drug Carriers and Their Interaction with Human Blood

This part of the chapter will be dedicated to magnetite nanoparticles and their interaction with human blood. Both these materials are suitable to study using ESR. Various nanomaterials are of interest to researchers as future materials for applications in various fields of life including medicine [1]. The special place, because of their physical properties, occupies magnetite nanoparticles. Using a special configuration of magnetic field gradients, they could be directed to a place of disease that is particularly important in a case of cancer. Standard used chemotherapeutics destroy both cancer and healthy cells. Using magnetite nanoparticles as drug carriers, a drug attached to a magnetite core would be released at the site of the disease and only destroy diseased cells. Because such drugs are administered intravenously, it is important to study their interactions also with blood. This issue is very complex because the interaction between nanoparticles and the environment (e.g., blood) depends on their many properties such as a size, a shape, surface charge, coverage, etc. [115].

The previous experiments, in the case of iron oxide nanoparticles, shown that applying an external magnetic field near the target increases the circulation time of the nanoparticles in the bloodstream and increases their accumulation in the indicated organ [116, 117]. It is particularly important to determine how nanoparticles interact with the morphological elements of the blood. Studies show that they can be caught by monocytes or remain on the surface of cells [118]. They can also penetrate the nuclei of lymphocytes located in the capillaries [117]. There are also studies showing the use of ESR to investigate the interactions of nanoparticles with blood or plasma proteins. In one of them, such interactions with fibrinogen and albumin were studied [119], applying spin labels. It has been found that important is the distance between the magnetite nanoparticles and free radicals and the fibrinogen can adhere

to the surface of the magnetic nanoparticles. These results are important in relation to the coagulation system and the formation of possible clots. In addition to fibrinogen chains, other proteins can also adsorb to superparamagnetic iron oxide nanoparticles: immunoglobulins, antitrypsin, α1 transthyretin, or just transferrin [120, 121]. This adsorption depends not only on the characteristics of the nanoparticles but also on the properties of the proteins and the environment. Meaning it is also the type of interaction. It was thought that albumin, as the most abundant protein in plasma, would be the fastest in interacting with the nanoparticle surface. Meanwhile, experiments with iron oxide nanoparticles have shown that albumins attach to their surface only in small amounts. Dominated immunoglobulins and fibrinogen increased with increasing the incubation time [121]. The effect of magnetic nanoparticle coverage on the degree of their interaction with albumin was also studied [122]. For nanoparticles coated with dextran and polyvinyl alcohol, the studies have been performed to determine which proteins present in the serum adsorb to nanoparticles [123]. The presence or absence of coverage is of great importance in terms of the interaction of nanoparticles with proteins as well as their rapid elimination from the bloodstream.

Nanoparticles, because of their physical properties, offer great possibilities in terms of their functionalization. From ESR point of view, a group of materials which can give additional valuable information are spin labels, for example, 2,2,6,6-tetramethylpiperidine-N-oxyl (TEMPO) [124]. Attaching these types of materials to the surface of nanoparticles is also useful in studying the extent of their interaction with the environment (e.g., blood, serum) [125]. Interactions of spin label with proteins present in blood might also affect the ESR spectra, and the pH influences the conformation of proteins and molecular motions. Depending on the rate of rotation of the spin label changes the line shape of ESR spectrum. Besides attaching a spin label to nanoparticles to obtain the information about nanoparticles interaction with an environment, they can be also placed in the nanoparticle core and apply as ROS scavengers [126, 127]. Shimizu et al. [127] projected redox nanoparticles, prepared by self-assembly of amphiphilic block copolymers possessing 2,2,6,6-tetramethylpiperidine-N-oxyls as a side chain of hydrophobic segment. Using ESR method the authors investigated their behavior in blood. When 4-hydroxy-2,2,6,6-Tetramethylpiperidine-N-oxyl was added to rat whole blood, the ESR signal disappeared rapidly. In contrast, the signal from redox nanoparticles remained for a long time. It indicates that nitroxyl radicals were protected in the blood by combining with the core of nanoparticle. They have shown that redox nanoparticles are useful in therapy for various oxidative stress injuries including hemorrhage and stroke. Because this type of nanoparticles under appropriate conditions takes the form of micelles, ESR is also suitable for monitoring their opening that has a place, e.g., in a pH-adjusted environment.

The biggest hope is the application of functionalized magnetite nanoparticles as drug carriers in chemotherapy or treatment of inflammation [128, 129]. To

become so, the nanoparticles must be thoroughly investigated, both in terms of their physical properties (durability, quality) and their impact on the body. Since most standard chemotherapeutics are administered intravenously, the interactions between new potential nanodrugs with blood and proteins present in it should be investigated. Of course these interactions change when nanoparticles move through various regions of the body [130–133]. They cause changes in nanoparticle properties such as the aggregation state, surface charge, and chemistry, targeting capabilities. All these factors lead to changes in their function [134]. Moreover both cellular and acellular elements will interact with each other on the nanoparticle surface, changing protein conformation, function [131, 135, 136], binding affinity, and also blood physiology. These changes in properties of both blood and nanoparticle generate a complex system of biological interactions.

Nanoparticles added to blood attract many different proteins to their surface, and so-called "protein corona" is formed. Protein corona increases the nanoparticle size and changes the surface charge [137]. This structure can cause unexpected changes in cellular interactions, cellular uptake, biodistribution, and immunogenicity [138]. The protein corona influences nanoparticles to bind to a wide variety of cells [130]. Depending on the nanoparticle charge and size, they favor proteins in different manners: anionic-charged nanoparticles favor proteins with pH < 5.5 and cationic-charged nanoparticles with pH > 5.5 [135].

Because the most interesting is the use of nanoparticles as drug carriers, more papers are concerned to this issue [139]. However some researchers also try to investigate the interactions between nanoparticles and blood. Kubiak et al. [140] applied ESR for study PEG-coated magnetite nanoparticles in water and whole human blood. The determined ESR parameters were different for nanoparticles depending on the medium (water and blood), which may indicate the influence of the environment on the interactions between nanoparticles and thus the utility of ESR application in such study.

From the point of view of magnetite nanoparticle applications in medical therapy, their important features are the magnetic properties and hence the ability to control their movement using a special configuration of magnetic field gradients. Dobosz et al. [141, 142] applied ESR to study both the physical properties of chosen magnetite nanoparticles and their interactions with human blood in a presence of an inhomogeneous magnetic field. In this case ESR was also used to monitor the diffusion of magnetite nanoparticles forced by the inhomogeneous magnetic field (Fig. 1.4).

The solution of magnetite nanoparticle movement control is particularly important in context of nanodrugs focusing in affected area (e.g., tumor). This would allow to deliver the drug directly to a target, omitting healthy cells that are in standard chemotherapy also destroyed. The authors checked the influence of both nanoparticle coverage and the time during which the sample was kept in a magnetic field. Because these nanoparticles were functionalized with TEMPO, the results gave two sources of information, both from the magnetite core and TEMPO (Fig. 1.5).

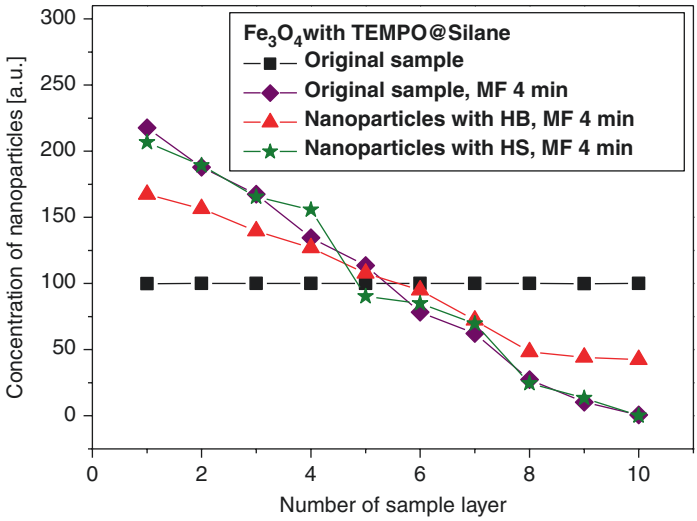

Fig. 1.4 The distribution of magnetite nanoparticles functionalized with TEMPO in particular layers of investigated sample after keeping it in the inhomogeneous magnetic field during 4 min (where MF, magnetic field; HB, human blood; HS, human serum)

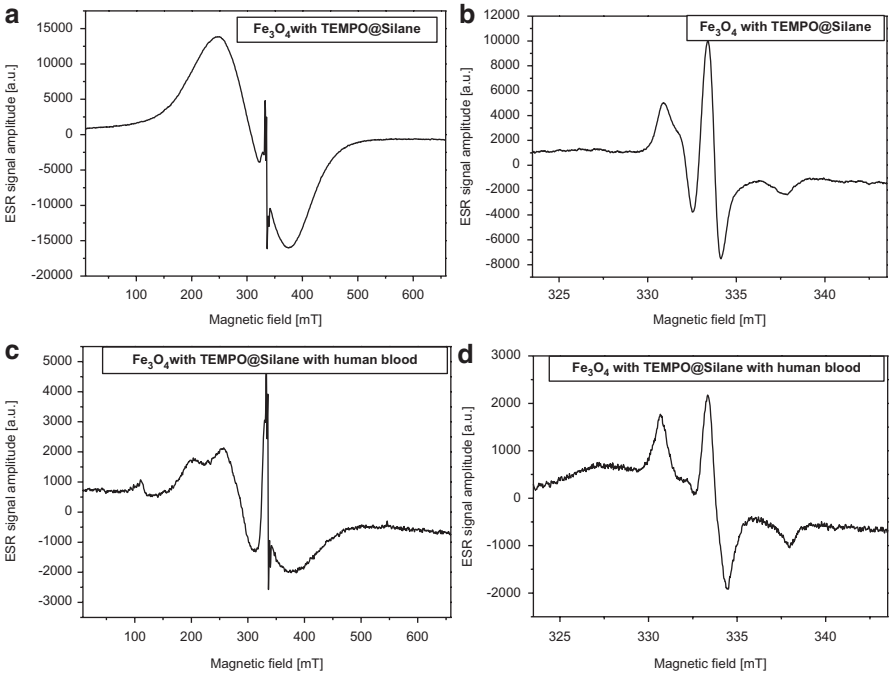

Fig. 1.5 Exemplary ESR spectra of magnetite nanoparticles functionalized with TEMPO coated with silane recorded at 230 K in a wide magnetic field range (**a** and **c**) and a narrow magnetic field range (**b** and **d**)

1.5 Summary

In this chapter electron spin resonance was shown as a method suitable for blood study, both paramagnetic species and free radicals, as well as magnetite nanoparticles as the example of a large group of nanomaterials. As scientists around the world work intensively on the use of nanomaterials in medicine, another advantage of the ESR technique is the ability to use it for the study of interactions between biologically active materials and potential nanodrugs (e.g., blood-functionalized magnetite nanoparticle interactions).

References

1. Kempe S, Metz H, Mäder K. Application of electron paramagnetic resonance (EPR) spectroscopy and imaging in drug delivery research – Chances and challenges. Eur J Pharm Biopharm. 2010;74:55–66.
2. Descrosiers M, Schauer DA. Electron paramagnetic resonance (EPR) biodosimetry. Nucl Instrum Methods Phys Res, Sect B. 2001;184:219–28.
3. Kumar Shukla A. EMR/ESR/EPR spectroscopy for characterization of nanomaterials. In: Springer series on Advanced Structured Materials, vol. 62. New York: Springer; 2017.
4. Krzyminiewski R, Kruczyński Z, Dobosz B, Zając A, Mackiewicz A, Leporowska E, Folwaczna S. EPR study of iron ion complexes in human blood. Appl Magn Reson. 2011;40:321–30.
5. Ślawska-Waniewska A, Mosiniewicz-Szablewska E, Nedelko N, Gałązka-Friedman J, Friedman A. Magnetic studies of iron-entities in human tissues. J Magn Magn Mater. 2004;272–276:2417–9.
6. Weil JA, Bolton JR. Electron Paramagnetic Resonance. Elementary theory and practical application. New Jersey: John Wiley & Sons; 2007.
7. Polakovs M, Mironova-Ulmane N, Pavlenko A, Aboltins A. Determination of methemoglobin in human blood after ionizing radiation by EPR. IOP Conf Ser: Mater Sci Eng. 2015;77:012028.
8. Hamirani YS, Franklin W, Grifka RG, Stainback RF. Methemoglobinemia in a Young Man. Tex Heart Inst J. 2008;35(1):76–7.
9. Dunne J, Caron A. Ascorbate removes key precursors to oxidative damage by cell-free haemoglobin in vitro and in vivo. Biochem J. 2006;399:513–24.
10. Svistunenko DA, Dunne J, Fryer M, Nicholls P, Reeder BJ, Wilson MT, Bigotti MG, Cutruzzolà F, Copper CE. Comperative study of tyrosine radicals in hemoglobin and myoglobins treated with hydrogen peroxide. Biophys J. 2002;83:2845–55.
11. Pulatova MK, Sharygin VL, Shlyakova TG, Sipyagina AE, Wasserman AM. Use of EPR spectroscopy to check the changes in organism radioresistance. Clinical Results Biophysics. 2009;54(2):223–31.
12. Parkkinen J, Vääränen O, Vahtera E. Plasma ascorbate protects coagulation factors against photooxidation. Thromb Haemost. 1996;75(2):292–7.
13. Gomme PT, McCann KB. Transferrin: structure, function and potential therapeutic actions. Drug Discov Today. 2005;10:267–73.
14. Kubiak T, Krzyminiewski R, Dobosz B. EPR study of paramagnetic centers in human blood. Curr Top Biophys. 2013;36:7–13.
15. Hirota Y, Haida M, Mohtarami F, Takeda K, Iwamoto T, Shioya S, Tsuji C, Hasumi K, Nakazawa H. Implication of ESR signals from ceruloplasmin (Cu^{2+}) and transferrin (Fe^{3+}) in pleural effusion of lung diseases. Pathophysiology. 2000;7:41–5.

16. Yang A, Gaffney BJ. Determination of relative spin concentration in some high-spin ferric proteins using E/D-distribution in electron paramagnetic resonance simulations. Biophys J. 1987;51:55–67.
17. Gaffney B, Maguire B, Weber RT, Maresch GG. Disorder at metal sites in proteins: a high frequency EMR study. Appl Magn Reson. 1999;16:207–21.
18. Liehr JG, Jones JS. Role of iron in estrogen-induced cancer. Curr Med Chem. 2001;8:839–49.
19. Healy J, Tipton K. Ceruloplasmin and what it might do. J Neural Transm. 2007;114:777–81.
20. KouohElombo F, Radosevich M, Poulle M, Descamps J, Chtourou S, Burnouf T, Catteau JP, Bernier JL, Cotelle N. Purification of human ceruloplasmin as a by- product of C1-inhibitor. Biol Pharm Bull. 2000;23:1406–9.
21. Zowczak M, Iskra M, Torliński L, Cofta S. Analysis of Serum Copper and Zinc Concentrations in Cancer Patients. Biol Trace Elem Res. 2001;82(1–3):1–8.
22. Senra Varela A, Bosco Lopez Saez JJ, Quintela Senra D. Serum ceruloplasmin as a diagnostic marker of cancer. Cancer Lett. 1997;121:139–45.
23. Özyilkan Ö, Baltali E, Özyilkan E, Tekuzman G, Kars A, Firat D. Ceruloplasmin level in women with breast disease. Acta Oncol. 1992;31:843–6.
24. Sachdeva OP, Girdhar V, Gulati SP, Lal H. Serum ceruloplasmin levels in head and neck cancers. Indian J Clin Biochem. 1993;8:51–3.
25. Feelders RA, Vreugdenhil G, Eggermont AM, Kuiper-Kramer PA, van Eijk HG, Swaak AJ. Regulation of iron metabolism in the acute-phase response: interferon γ and tumor necrosis factor α induce hypoferraemia, ferritin production and a decrease in circulating transferrin receptors in cancer patients. Eur J Clin Investig. 1998;28:520–7.
26. Weiss G. Iron and immunity: a double-edged sword. Eur J Clin Investig. 2002;32:70–8.
27. Nagai M, Mawatari K, Nagai Y, Horita S, Yoneyama Y, Hori H. Studies of the oxidation states of hemoglobin M Boston and hemoglobin M Saskatoon in blood by EPR spectroscopy. Biochem Biophys Res Commun. 1995;210(2):483–90.
28. Fujita Y, Tsuchiya K, Abe S, Takiguchi Y, Kubo S, Sakurai H. Estimation of the age of human bloodstains by electron paramagnetic resonance spectroscopy: Long-term controlled experiment on the effects of environmental factors. Forensic Sci Int. 2005;152(1):39–43.
29. Gamarra LF, Pontuschka WM, Amaro E Jr, Costa-Filho AJ, Brito GES, Vieira ED, Carneiro SM, Escriba DM, Falleiros AMF, Salvador VL. Kinetics of elimination and distribution in blood and liver of biocompatible ferrofluids based on Fe_3O_4 nanoparticles: An EPR and XRF study. Mater Sci Eng C. 2008;28:519–25.
30. Aasa R, Aisen P. An Electron Paramagnetic Resonance Study of the Iron and Copper Complexes of Transferrin. J Biol Chem. 1968;243(9):2399–404.
31. Maghraby AM, Ali MA. Spectroscopic study of gamma irradiated bovine hemoglobin. Radiat Phys Chem. 2007;76:1600–5.
32. Sakurai H, Tsuchiya K, Fujita Y, Okada K. Dating of human blood by electron spin resonance spectroscopy. Naturwissenschaften. 1989;76:24–5.
33. Svistunenko DA, Davies NA, Wilson MT, Stidwill RP, Singer M, Cooper CE. Free radical in blood: a measure of haemoglobin autoxidation in vivo? J ChemSoc Perkin Trans. 1997;2:2539–43.
34. Moreira LM, Poli AL, Lyon JP, et al. Ferric species of the giant extracellular hemoglobin of Glossoscolexpaulistus as function of pH: An EPR study on the irreversibility of the heme transitions. Comp BiochemPhys Part B. 2008;150:292–300.
35. Kolesar JM, Schelman WR, Geiger PG, Holen KD, Traynor AM, Alberti DB, Thomas JP, Chitambar CR, Wilding G, Antholine WE. Electron paramagnetic resonance study of peripheral blood mononuclear cells from patients with refractory solid tumors treated with Triapine. J Inorg Biochem. 2008;102(4):693–8.
36. Hubel CA, Kozlov AV, Kagan VE, Evans RW, Davidge ST, McLaughlin MK, Roberts JM. Decreased transferrin and increased transferrin saturation in sera of women with preeclampsia: implications for oxidative stress. Am J Obstet Gynecol. 1996;175:692–700.

37. Farnaud S, Amini M, Rapisarda C, Cammack R, Bui T, Drake A, Evans RW, SuryoRahmanto Y, Richardson DR. Biochemical and spectroscopic studies of human melanotransferrin (MTf): electron-paramagnetic resonance evidence for a difference between the iron-binding site of MTf and other transferrins. Int J Biochem Cell Biol. 2008;40:2739–45.
38. Bou-Abdallah F, Chasteen ND. Spin concentration measurements of high-spin ($g' = 4.3$) rhombic iron(III) ions in biological samples: theory and application. J Biol Inorg Chem. 2008;13:15–24.
39. Walker FA. Magnetic spectroscopic (EPR, ESEEM, Mössbauer, MCD and NMR) studies of low-spin ferriheme centers and their corresponding heme proteins. Coordin Chem Rev. 1999;185–186:471–534.
40. Winiecki T, Kazmierska J, Krzyminiewski R, Dobosz B, Kruczynski Z, Kubiak T. Utility of EPR for evaluation of free radicals and iron complexes in blood in patients before and after radiotherapy. Radiother Oncol. 2012;103(Suppl 1):S574.
41. Foster MA, Pocklington T, Miller JDB, Mallard JR. A study of electron spin resonance spectra of whole blood from normal and tumour bearing patients. Br J Cancer. 1973;28:340–8.
42. Pocklington T, Foster MA. Electron spin resonance of caeruloplasmin and iron transferrin in blood of patients with various malignant diseases. Br J Cancer. 1977;36:369–74.
43. Schwartz HM, Wiesner J. Radiation effects on plasma electron-spin resonance spectra of cancer patients. Radiology. 1972;104:209–10.
44. Horn RA, Friesen EJ, Stephens RL, Hedrick WR, Zimbrick JD. Electron spin resonance studies on properties of ceruloplasmin and transferrin in blood from normal human subjects and cancer patients. Cancer. 1979;43:2392–8.
45. Lohmann W, Schreiber J, Gerhardt H, Breithaupt H, Löffler H, Pralle H. Electron spin resonance (esr) investigations on blood of patients with leukemia. Blut. 1979;39:147–51.
46. Sakurai H, Yoshimura T. Models for coordination site of cytochrome P-450, characterization of hemin-thiolato complexes with S, O, and N donor ligands by electronic absorption and electron spin resonance spectra. J Inorg Biochem. 1985;24:75–96.
47. Tang SC, Koch S, Papaefthymiou GC, Foner S, Frankel RB, Ibers JA, Holm RH. Axial ligation modes in iron(III) Porphyrins. Models for the oxidized reaction states of cytochrome P-450 enzymes and the molecular structure of iron(III) protoporphyrin IX dimethyl ester p-nitrobenzenethiolate. J Am Chem Soc. 1976;98:2414–34.
48. Miki T, Ikeya M. Electron spin resonance of blood stains and its application to the estimation of time after bleeding. Forensic Sci Int. 1987;35:149–58.
49. Domek H, Sagan L, Piątek J, Gonet B. Electron spin resonance (ESR) as a method to estimate the time of blood extravasation in forensic medicine. Curr Top Biophys. 2010;33(Suppl A):39–42.
50. Sen S, Chakraborty R, Sridhar C, Reddy YSR, De B. Free radicals, antioxidants, diseases and phytomedicines: current status and future prospects. Int J Pharm Sci Rev Res. 2010;3(1):91–100.
51. Halliwell B, Gutteridge JMC. Free radicals in biology and medicine. 2nd ed. Oxford: Clarendon Press; 1999.
52. Mimić-Oka J, Simić DV, Simić TP. Free radicals in cardiovascular diseases. FU Med Biol. 1999;6(1):11–22.
53. Valko M, Rhodes CJ, Moncola J, Izakovic M, Mazur M. Free radicals, metals and antioxidants in oxidative stress-induced cancer. Chem Biol Interact. 2006;160:1–40.
54. Nagendrappa CG. An appreciation of free radical chemistry- 3, free radicals in diseases and health. Resonance. 2005;10:65–73.
55. Ali ATMM, Al-Swayeh OA, Al-Rashed RS, Al-Mofleh IA, Al-Dohayan AD, Al-Tuwaijri AS. Role of oxygen-derived free radicals on gastric mucosal injury induced by ischemia-reperfusion. Saudi J Gastroenterol. 1996;2:19–28.
56. Cadenas E. Biochemistry of oxygen toxicity. Annu Rev Biochem. 1989;58:79–110.
57. Bagchi K, Puri S. Free radicals and antioxidants in health and disease. East Mediterr Health J. 1998;4:350–60.
58. Valko M, Leibfritz D, Moncol J, Cronin MTD, Mazur M, Telser J. Free radicals and antioxidants in normal physiological functions and human disease. Int J Biochem Cell Biol. 2007;39:44–84.

59. Miller DM, Buettner GR, Aust SD. Transition metals as catalysts of "autoxidation" reactions. Free RadicBiol Med. 1990;8:95–108.
60. Cadenas E, Sies H. The lag phase. Free Radic Res. 1998;28:601–9.
61. Pastor N, Weinstein H, Jamison E, Brenowitz M. A detailed interpretation of OH radical footprints in a TBP DNA complex reveals the role of dynamics in the mechanism of sequence-specific binding. J Mol Biol. 2000;304:55–68.
62. Pham-Huy LA, He H, Pham-Huy C. Free radicals, antioxidants in disease and health. Int J Biomed Sci. 2008;4:89–96.
63. Agarwal A, Prabakaran SA. Mechanism, measurement and prevention of oxidative stress in male reproductive physiology. Indian J Exp Biol. 2005;43:963–74.
64. Pourmorad F, Hosseinimehr SJ, Shahabimajd N. Antioxidant activity, phenol and flavonoid contents of some selected Iranian medicinal plants. Afr J Biotechnol. 2006;5:1142–5.
65. O'donovan DJ, Fernandes CJ. Free radicals and diseases in premature infants. Antioxid Redox Signal. 2004;6:169–76.
66. Dufor D, Pichette A, Mshvildadze V, Bradette-Hebert M, Lavoie S, Longtin A, Laprise C, Legault J. Antioxidant, anti-inflammatory and anticancer activities of methanolic extracts from LedumgroenlandicumRetzius. J Ethnopharmacol. 2007;111:22–8.
67. Gupta SK, Joshi S, Velpandian T, Awor L, Prakash J. An update on pharmacological prospective for prevention and development of cataract. Indian J Pharm. 1997;23:3–10.
68. Kehrer JP, Smith CV. Free radicals in biology: sources, reactivities, and roles in the etiology of human diseases. In: Frei B, editor. Natural antioxidants in human health and disease. San Diego: Academic Press; 1994. p. 25–62.
69. Sen S, Chakraborty R, De B, Mazumder J. Plants and phytochemicals for peptic ulcer: an overview. Pharmacogn Rev. 2009;3:270–9.
70. Bergendi L, Benes L, Durackova Z, Ferencik M. Chemistry, physiology and pathology of free radicals. Life Sci. 1999;65:1865–74.
71. Klatt P, Lamas S. Regulation of protein function by S-glutathiolation in response to oxidative and nitrosative stress. Eur J Biochem. 2000;267:4928–44.
72. Ridnour LA, Thomas DD, Mancardi D, Espey MG, Miranda KM, Paolocci N, Feelisch M, Fukuto J, Wink DA. The chemistry of nitrosative stress induced by nitric oxide and reactive nitrogen oxide species. Putting perspective on stressful biological situations. Biol Chem. 2004;385:1–10.
73. Kerr ME, Bender CM. An introduction to oxygen free radicals. Heart Lung. 1996;25(3):200–9.
74. Vergely C, Maupoil V, Clermont G, Bril A, Rochette L. Identification and quantification of free radicals during myocardial ischemia and reperfusion using electron paramagnetic resonance spectroscopy. Arch Biochem Biophys. 2003;420:209–16.
75. Kopàni M, Celec P, Danišovič L, Michalka P, Biró C. Oxidative stress and electron spin resonance. Clin Chim Acta. 2006;364:61–6.
76. Gurbuz M, Yamanel L, Bulucu F, Inal V, Aydin A. Oxidative stress status in familial Mediterranean fever with or without proteinuria. Free RadicBiol Med. 2005;38(2):271–5.
77. Nomoto S, Shibata M, Iriki M, Riedel W. Role of afferent pathways of heat and cold in body temperature regulation. Int J Biometeorol. 2004;49(2):67–85.
78. Frohlich D, Wittmann S, Rothe G, Sessler DI, Vogel P, Taeger K. Mild hyperthermia downregulates receptor-dependent neutrophil function. Anesth Analg. 2004;99(1):284–92.
79. Cook JA, Gius D, Wink DA, Krishna MC, Russo A, Mitchell JB. Oxidative stress, redox, and the tumor microenvironment. Semin Radiat Oncol. 2004;14(3):259–66.
80. Haberland ME, Smith CV. Lipid peroxide-dependent modifications of lipoprotein in atherosclerosis. In: Moslen MT, Smith CV, editors. Free radical mechanisms of tissue injury. London: CRC Press; 1992.
81. Rubin E, Faraber JL. Cell injury. In: Rubin E, Farber JL, editors. Pathology. Philadelphia: JB Lippincott C0; 1994. p. 16–7.
82. Dunne J, Caron A, Menu P, Alayash AJ, Buehler PW, Wilson MT, Silaghi-Dumitrescu R, Faivre B, Cooper CE. Ascorbate removes key precursors to oxidative damage by cell-free haemoglobinin vitro and in vivo. Biochem J. 2006;399:513–24.

83. Vasquez-Vivar J, Santos AM, Junqueira VBC, Augusto O. Peroxynitrite-mediated formation of free radicals in human plasma: EPR detection of ascorbyl, albumin-thiyl and uric acid-derived free radicals. Biochem J. 1996;314:869–76.
84. May JM, Qu Z, Cobb CE. Human erythrocyte recycling of ascorbic acid. J Biol Chem. 2004;279(15):14975–82.
85. Koppenol WH. Chemistry of iron and copper in radical reactions. In: Rice-Evans CA, Burdon RH, editors. Free radical damage and its control. Amsterdam: Elsevier; 1994.
86. Bartosz G. Use of spectroscopic probes for detection of reactive oxygen species. Clin Chim Acta. 2006;368:53–76.
87. Gonet B, Szmatłoch E, Nowacka-Pietrzak M, Domański L. Electron spin resonance spectroscopy for examination of human ischemic heart disease. Eur J Intern Med. 1999;10:214–7.
88. Majewski W, Krzyminiewski R, Stanisić M, Iskra M, Krasiński Z, Nowak M, Dobosz B. Measurement of free radicals using electron paramagnetic resonance spectroscopy during open aorto-iliac arterial reconstruction. Med Sci Monit. 2014;20:2453–60.
89. Miller FJ, Sharp WJ, Fang X, Oberley LW, Oberley TD, Weintraub NL. Oxidative stress in human abdominal aortic aneurysms. A potential mediator of aneurismal remodeling. Arterioscler Thromb Vasc Biol. 2002;22:560–5.
90. Irie H, Kato T, Ikebe K, Tsuchida T, Oniki Y, Takagi K. Antioxidant effect of MCI-186, a New free- vadical scavenger, on ischemia-reperfusion injury In a rat hindhimb amputation model. J Surg Res. 2004;120:320–19.
91. Crimi E, Ignarro LJ, Napoli C. Microcirculation and oxidative stress. Free Radic Res. 2014;41:1364–75.
92. Murphy MP. How mitochondria produce reactive oxygen species. Biochem J. 2009;417:1–13.
93. Demirbag R, Yilmaz R, Gur M, Celik H, Guzel S, Selek S, Kocyigit A. DNA damage in metabolic sundrome and its association with antioxidative and oxidative measurements. Int J Clin Pract. 2006;60:1187–93.
94. Kotani Y, Ishino K, Osaki S, Honjo O, Suezawa T, Kanki K, Yutani C, Sano S. Efficacy of MCI-186, a free-radical scavenger and antioxidant, for resuscitation of nonbeating donor he arts. J Thorac Cardiovasc Surg. 2007;133:1626–32.
95. Krzyminiewski R, Kruczynski Z, Stepien A, Dobosz B. Free radicals in a conglomerate of peripheral blood with a spin trap investigated by the EPR method before and after angioplasty treatment. Pol J Med Phys Eng. 2008;14(1):1–12.
96. Krzyminiewski R, Kruczynski Z, Stepien A, Dobosz B. Spin traps in the detection of free radicals in the blood of patients with ischemia. Pol J Med Phys Eng. 2009;15(1):47–54.
97. Pincemail J. Free radicals and antioxidants in human diseases. In: Favier AE, et al., editors. Analysis of free radicals in biological systems. Basel: BirkhäuserVerlag; 1995. p. 83–98.
98. McCord J. Oxygen-derived free radicals in post ischemic tissue injury. N Engl J Med. 1985;312:159–63.
99. Thompson JA, Hess ML. The oxygen free radical system: a fundamental mechanism in the production of myocardial necrosis. Prog Cardiovasc Dis. 1986;28(6):449–62.
100. Pietri S, Culcasi M, Cozzone PJ. Real-time continuous-flow spin trapping of hydroxyl radical in the ischemic and post-ischemic myocardium. Eur J Biochem. 1989;186:163–73.
101. Gey KF, Stähelin HB, Eichholzer M. Poor plasma status of carotene and vitamin C is associated with higher mortality from ischemic heart disease and stroke. Clin Investig. 1993;71:3–6.
102. Mosca L, Rubenfire M, Mandel C, Cheryl R, Tarshis T, Tsai A, Pearson T. Antioxidant nutrient supplementation reduces the susceptibility of low density lipoprotein to oxidation in patients with coronary artery disease. J Am Coll Cardiol. 1997;30:392–9.
103. Brown CJ. Lack of vitamin C linked to heart attacks. Can Med Assoc J. 1997;156(10):1373.
104. Van de Vijver LPL, Kardinaal AFM, Grobbee DE, Princen HMG, Van Poppel G. Lipoprotein oxidation, antioxidants and cardiovascular risk: epidemiologic evidence. Prostaglandins Leukot Essent Fatty Acids. 1997;57(4–5):479–87.
105. Güler K, Palanduz S, Ademoglu E, Salmayenli N, et al. Total antioxidant status, lipid parameters, lipid peroxidation and glutathione levels in patients with acute myocardial infarction. Med Sci Res. 1998;26:105–6.

106. Kelman DJ, DeGraz JA, Mason RP. Reaction of myoglobin with hydrogen peroxide forms a peroxyl radical which oxidizes substrates. J Biol Chem. 1994;269:7458–63.
107. Gunther MR, Kelman DJ, Corbett JT, Mason RP. Self peroxidation of methmyoglobin results in formation of an oxygen reactive tryptophan-centered radical. J Biol Chem. 1995;270:16075–81.
108. Mrakic-Sposta S, Gussoni M, Montorsi M, Porcelli S, Vezzoli A. Assessment of a standardized ros production profile in humans by electron paramagnetic resonance. Oxidative Med Cell Longev. 2012;2012:973927. 10 pages
109. Davies KJA, Quintanilha AT, Brooks GA, Packer L. Free radicals and tissue damage produced by exercise. Biochem Biophys Res Commun. 1982;107(4):1198–205.
110. Ji LL. Antioxidants and oxidative stress in exercise. Proc Soc Exp Biol Med. 1999;222(3):283–92.
111. Bailey DM, Young IS, McEneny J, Lawrenson L, Kim J, Barden J, Richardson RS. Regulation of free radical outflow from an isolated muscle bed in exercising Humans. Am J Phys. 2004;287(4):H1689–99.
112. Bailey DA, Lawrenson L, McEneny J, Young IS, James PE, Jackson SK, Henry RR, Mathieu-Costello O, Mccord JM, Richardson RS. Electron paramagnetic spectroscopic evidence of exercise-induced free radical accumulation in human skeletal muscle. Free Radic Res. 2007;41(2):182–90.
113. Gomez-Cabrera MC, Domenech E, Viña J. Moderate exercise is an antioxidant: upregulation of antioxidant genes by training. Free Radic Biol Med. 2008;44(2):126–31.
114. Poljsak B. Strategies for reducing or preventing the generation of oxidative stress. Oxidative Med Cell Longev. 2011;2011:194586. 15 pages
115. Mahmoudi M, Shokrgozar MA, Sardari S, Moghadam MK, Vali H, Laurent S, Stroeve P. Irreversible changes in protein conformation due to interaction with superparamagnetic iron oxide nanoparticles. Nanoscale. 2011;3:1127–38.
116. Mykhaylyk O, Cherchenko A, Ilkin A, Dudchenko N, Ruditsa V, Novoseletz M, Zozulya Y. Glial brain tumor targeting of magnetite nanoparticles in rats. J Magn Magn Mater. 2001;225:241–7.
117. Mykhaylyk O, Dudchenko N, Dudchenko A. Doxorubicin magnetic conjugate targeting upon intravenous injection into mice: high gradient magnetic field inhibits the clearance of nanoparticles from the blood. J Magn Magn Mater. 2005;473:482–247.
118. Diaz B, Sánchez-Espinel C, Arruebo M, Faro J, de Miguel E, Magadán S, Yagűe C, Fernández-Pacheco R, Ibarra MR, Santamaria J, González-Fernández A. Assessing methods for blood cell cytotoxic responses to inorganic nanoparticles and nanoparticle aggregates. Small. 2008;4(11):2025–34.
119. Bychkova AV, Sorokina ON, Kovarskii AL, Leonova VB, Rozenfel'd MA. Interaction between blood plasma proteins and magnetite nanoparticles. Colloid J. 2010;72(5):696–702.
120. Saptarshi SR, Duschl A, Lopata AL. Interaction of nanoparticles with proteins: relation to bio-reactivity of the nanoparticle. J Nanobiotechnology. 2013;11:26.
121. Jansch M, Stumpf P, Graf C, Rűhl E, Műller RH. Adsorption kinetics of plasma proteins on ultra small superparamagnetic iron oxide (USPIO) nanoparticles. Int J Pharm. 2012;428:125–33.
122. Lartigue L, Wilhelm C, Servais J, Factor C, Dencausse A, Bacri JC, Luciani N, Gazeau F. Nanomagneting sensing of blood plasma protein interactions with iron oxide nanoparticles: impact on macrophage uptake. ACS Nano. 2012;6(3):2665–78.
123. Sakulkhu U, Mahmoudi M, Maurizi L, Salaklang J, Hofmann H. Protein corona composition of superparamagnetic iron oxide nanoparticles with various physico-chemical properties and coatings. Sci Rep. 2014;4:5020.
124. Dobosz B, Krzyminiewski R, Schroeder G, Kurczewska J. Electron paramagnetic resonance as an effective method for a characterization of functionalized iron oxide. J Phys Chem Solids. 2014;75:594–8.
125. Cavalu S, Damian G, Dânşoreanu M. EPR study of non-covalent spin labeled serum albumin and hemoglobin. Biophys Chem. 2002;99:181–8.

126. Nagasaki Y. Nitroxide radicals and nanoparticles: a partnership for nanomedicine radical delivery. Ther Deliv. 2012;3(2):165–79.
127. Shimizu M, Yoshitomi T, Nagasaki Y. The behavior of ROS-scavenging nanoparticles in blood. J ClinBiochem Nutr. 2014;54(3):166–73.
128. AroraWahajuddin S. Superparamagnetic iron oxide nanoparticles: magnetic nano platforms as drug carriers. Int J Nanomedicine. 2012;7:3445–71.
129. Issa B, Obaidat IM, Albiss BA, Haik Y. Magnetic nanoparticles: surface effects and properties related to biomedicine applications. Int J Mol Sci. 2013;14:21266–305.
130. Lazarovits J, Chen YY, Sykes EA, Chan WCW. Nanoparticle–blood interactions: the implications on solid tumour targeting. Chem Commun. 2015;51:2756–67.
131. Casals E, Pfaller T, Duschl A, Oostingh GJ, Puntes V. Time evolution of the nanoparticle protein corona. ACS Nano. 2010;4(7):3623–32.
132. Lundqvist M, Stigler J, Cedervall T, Berggård T, Flanagan MB, Lynch I, Elia G, Dawson K. The evolution of the protein corona around nanoparticles: a test study. ACS Nano. 2011;5(9):7503–9.
133. Dell'Orco D, Lundqvist M, Oslakovic C, Cedervall T, Linse S. Modeling the time evolution of the nanoparticle-protein corona in a body fluid. PLoS One. 2010;5(6):e10949.
134. Alkilany AM, Nagaria PK, Hexel CR, Shaw TJ, Murphy CJ, Wyatt MD. Cellular uptake and cytotoxicity of gold nanorods: molecular origin of cytotoxicity and surface effects. Small. 2009;5:701–8.
135. Prapainop K, Witter DP, Wentworth P. A Chemical approach for cell-specific targeting of nanomaterials: small-molecule-initiated misfolding of nanoparticle corona proteins. J Am Chem Soc. 2012;134:4100–3.
136. Kittler S, Greulich C, Gebauer JS, Diendorf J, Treuel L, Ruiz L, Gonzalez-Calbet JM, Vallet-Regi M, Zellner R, Köller M, Epple M. The influence of proteins on the dispersability and cell-biological activity of silver nanoparticles. J Mater Chem. 2010;20:512–8.
137. Choi HS, Liu W, Misra P, Tanaka E, Zimmer JP, Itty Ipe B, Bawendi MG, Frangioni JV. Renal Clearance of Nanoparticles. Nat Biotechnol. 2007;25(10):1165–70.
138. Tenzer S, Docter D, Kuharev J, Musyanovych A, Fetz V, Hecht R, Schlenk F, Fischer D, Kiouptsi K, Reinhardt C, Landfester K, Schild H, Maskos M, Knauer SK, Stauber RH. Rapid formation of plasma protein corona critically affects nanoparticle pathophysiology. Nat Nanotechnol. 2013;8(10):772–81.
139. Hałupka-Bryl M, Bednarowicz M, Dobosz B, Krzyminiewski R, Zalewski T, Wereszczyńska B, Nowaczyk G, Jarek M, Nagasaki Y. Doxorubicin loaded PEG-b-poly(4-vinylbenzylphosphonate) coated magnetic iron oxide nanoparticles for targeted drug delivery. J Magn Magn Mater. 2015;384:320–7.
140. Kubiak T, Krzyminiewski R, Dobosz B, Schroeder G, Kurczewska J, Hałupka-Bryl M. A study of magnetite nanoparticles in whole human blood by means of electron paramagnetic resonance. Acta Bio-Optica et Informatica Medica Inżynieria Biomedyczna. 2015;21(1):9–15.
141. Dobosz B, Krzyminiewski R, Schroeder G, Kurczewska J. Diffusion of functionalized magnetite nanoparticles forced by a magnetic field studied by EPR method. Curr Appl Phys. 2016;16:562–7.
142. Dobosz B, Krzyminiewski R, Kurczewska J, Schroeder G. The influence of surface modification, coating agents and pH value of aqueous solutions on physical properties of magnetite nanoparticles investigated by ESR method. J Magn Magn Mater. 2017;429:203–10.

2 EPR Studies on Understanding the Physical Intricacy of HbNO Complexes

Małgorzata Dutka, Janusz Pyka, and Przemysław M. Płonka

2.1 Introduction

Heme-based proteins play a key role in many basic life processes; they are involved in oxygen transport, catalysis, and electron transfer [1]. Versatile spectroscopic techniques (electron and nuclear magnetic resonance, Mössbauer and Raman spectroscopy, magnetic circular dichroism, vibrational spectroscopy, X-ray diffraction) and theoretical calculations (applying density function theory or quantum mechanics/molecular mechanics approach) are used in the research of these systems. Application of the electron paramagnetic resonance spectroscopy enormously contributed to understanding of structure–function relationship of proteins with heme cofactors, starting from the pioneering publication of Peisach and Blumberg [2].

The electron paramagnetic resonance signal directly probes the electronic structure of the active metal center and provides detailed information about the changes caused by the rearrangement of the nearest molecular structure of the heme pocket. The use of this technique for investigations on biological NO–heme complexes is exceptionally justified: the heme ligand NO is paramagnetic by itself; in turn the heme center constitutes the natural "spin trap" for NO. The paramagnetic nitrosyl hemoglobin exhibits a characteristic EPR spectrum with distinct features being a unique fingerprint of the molecular geometry and electronic structure around the unpaired electron.

The hemoglobin–NO complex (HbNO) has been extensively studied with application of electron paramagnetic resonance for more than 40 years [3–5]. The EPR spectra of HbNO derivatives directly proved the preferential NO bounding to α subunits within the hemoglobin tetramer [5]. The shape of nitrosyl hemoglobin EPR spectrum differentiated the conformation (R- or T-state) [6] of the whole tetramer

M. Dutka (✉) · J. Pyka · P. M. Płonka
Faculty of Biochemistry, Biophysics and Biotechnology, Jagiellonian University, Kraków, Poland
e-mail: malgorzata.dutka@uj.edu.pl

A. K. Shukla (ed.), *Electron Spin Resonance Spectroscopy in Medicine*,
https://doi.org/10.1007/978-981-13-2230-3_2

and demonstrated the direct observation of R/T transition taking place in the arterial-venous cycle [7, 8]. The EPR signal measurements remain the only direct and unambiguous technique to quantify HbNO in blood [9, 10], regardless of complex and demanding protocols for the whole blood samples assays [9, 11, 12]. Recently EPR studies on HbNO are a part of research of endogenous NO-derived paramagnetic species in biological systems [13]. The recent investigations of the electronic structures with EPR and other spectroscopic properties of heme–nitrosyls have been recently reviewed in [14, 15].

Investigations on nitrosyl hemoglobin complexes delivered a strong basis for understanding the role of NO in biology. The chronological stages of that research have been described in [16]. In the late sixties of the twentieth century, the experimental methodology for recording the nitrosylated hemoglobin EPR spectra had been settled; and the interest of the researchers focused on linking the EPR signatures of the HbNO sample to the structural conformations of the tetrameric hemoglobin [4–6]. Achieving this goal was a real challenge, due to molecular complexity of the protein composed of four polypeptide chains, with four reaction sites and extremal sensitivity of the EPR spectrum shape to minute structural modifications of hemoprotein. Identification of the component spectra within the recorded signal of HbNO complex [6] opened the road to the use of EPR for the quantitative measurement of HbNO in biological samples [8, 9, 12].

2.2 Nitrosyl Hemoglobin

The physiological function of hemoglobin is to transport oxygen in blood. This intracellular protein exhibits millimolar concentrations within mammals' erythrocytes. Under normal conditions, in human blood, approximately only 1 per 1000 hemoglobins binds nitric oxide [17]. The hemoglobin molecule is composed of four subunits: two α-chains, each with 141 amino acid residues, and two β-chains, each with 146 residues. Each chain carries one cofactor, heme group, which consists of a flat porphyrin ring molecule with an iron ion at the center (Fig. 2.1) with the ability to cycle between the ferrous (Fe^{2+}) and ferric (Fe^{3+}) redox states. The iron ion has the octahedral coordination: the nitrogen atoms of the porphyrin ring account for four ligands, and the remaining two ligand positions lie along an axis perpendicular to the porphyrin plane. The fifth coordination site is occupied by the nitrogen of proximal histidine F8. At the sixth position, different diatomic ligand can be bound. Binding of oxygen or carbon monoxide to a heme group takes place provided that initially the iron is in the Fe^{2+} (ferrous) form and the resulting complex is diamagnetic. In contrast to that, nitric oxide can be bounded to ferrous as well to ferric hem, with affinity exceeding considerably the affinities for CO and O_2 binding, and the resulting nitrosylated hem is paramagnetic [18]. There is also a difference of ligand-ferrous iron bonding geometry. Fe^{2+}–C–O bonds have linear arrangement, whereas Fe^{2+}–N–O or Fe^{2+}–O–O are bent at 130°–150° angle. The structural effects of binding the sixth ligand to a ferrous hem were precisely explained on the model tetraphenyl porphyrin complexes. The main changes are lengthening of the Fe–N(NO) bond and a decrease in the Fe–N–O angle

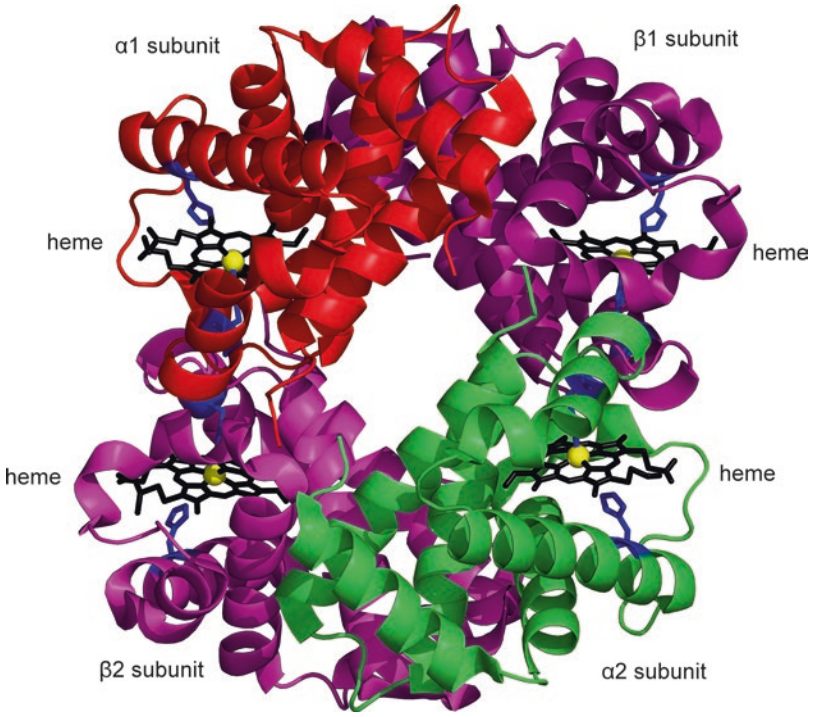

Fig. 2.1 Cartoon diagram of a three-dimensional structure of human hemoglobin in the deoxy form (PDB entry 2DN2). The heme planes and histidines (proximal and distal) are shown as a stick model. The heme irons are shown as a space-filling model. The figure was generated by the freeware PyMOL Molecular Graphics System, Version 1.6 Schrödinger, LLC

[19]. There exists to some extent the resemblance of oxyheme complexes to the analogous nitrosyl heme complexes. In the last case, the presence of at least two different geometries of the N(imidazole)–Fe–N(NO) bonds is postulated.

Three-dimensional crystal structure of human, physiologically formed adduct HbNO was reported for T- and R-state [20, 21]. Crystallographic studies confirmed earlier spectroscopically based conclusions that binding of NO to the heme groups of deoxyhemoglobin ruptures the Fe–proximal histidine bond of the alpha subunits (but not the beta units). The iron atom is displaced from the average porphyrin plane "upward," toward the NO ligand. In T-state HbNO, the iron heme from alpha unit is five-coordinate (proximal ligand, N from histidine is dissociated). In R-state both hemes remain six-coordinate but with a slightly different geometry: a greater length and more acute angle of Fe–N–O bond in beta chain are observed. The displacement of the proximal imidazole, induced by the R–T transition, is different for alpha and beta subunits (Fig. 2.2). It is clearly seen that the β-NO chain heme remains six-coordinate in R- and T-state.

The binding of NO to heme in hemoproteins has been investigated theoretically with Density Function Theory (DFT) methods. The effect of the protein environment

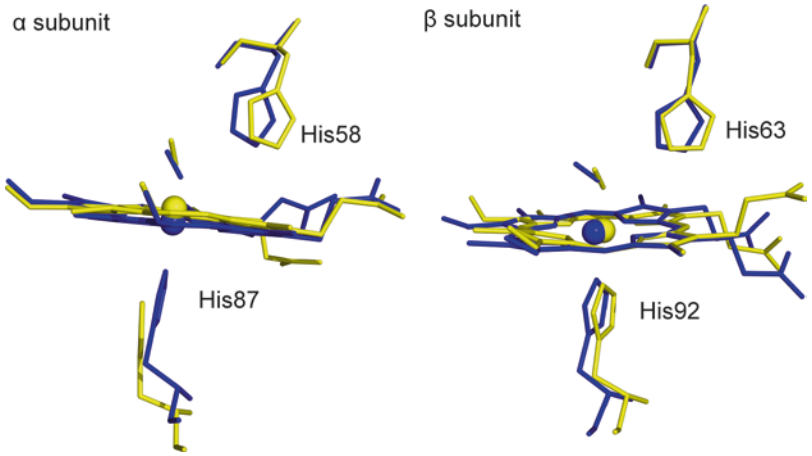

Fig. 2.2 Models of the heme active sites in alpha and beta subunits of human HbNO. The superimposed structures present configurations adopted T-state (yellow, PDB entry 1RPS) and R-state (blue, PDB entry 4N8T). The figure was generated by the freeware PyMOL Molecular Graphics System, Version 1.6 Schrödinger, LLC

was concerned as the possible key determinant whether the bond of His to Fe is broken or maintained upon binding of NO to iron [22]. Defining the factors controlling the coordination state of NO complexes in different hemoproteins remains still a real challenge. The extensive and complementary studies—including crystallography, EPR spectroscopy, and quantum chemical calculations—are reported for nitrosyl myoglobin complexes [23, 24]. The secondary and tertiary structures of myoglobin and the alpha subunits of hemoglobin are very similar; thus the results obtained from experiments on monomeric nitrosyl myoglobin pave the way for explaining the complexity of HbNO electron paramagnetic signals.

2.3 Electron Paramagnetic Resonance Phenomenon

2.3.1 Macroscopic Observation of Paramagnetic Resonance Signal

The EPR experiment offers the macroscopic method for establishing the microscopic parameters of the paramagnetic molecule. The complex of nitric oxide and heme is paramagnetic, with resulting electron spin $S = 1/2$, and can be subjected to measurements of electron paramagnetic resonance. The complete description of the EPR fundamentals in theoretical and practical aspects can be found in numerous textbooks. This technique becomes a more and more powerful tool of biophysical research on molecular biosystems. Consequently the number of handbooks and volumes reporting the development in this field is systematically increasing. Some of them are especially dedicated to the biomedical researchers [25–29].

The informative description of the basic EPR spectroscopic rules can be found in introductory parts of reviews published recently [10, 30, 31].

The most intuitive, classical explanation of the electron paramagnetic resonance describes the sample's magnetization reaction to the imposed static magnetic field $\mathbf{B_o}$ and microwave radiation $\mathbf{B_1}(t)$ with constant frequency ω and amplitude $B_1 << B_o$. The macroscopic magnetization of the sample is the sum of individual magnetic moments ("electronic spins") of the paramagnetic molecules. At the beginning we assume the paramagnetic centers are "diluted" within the sample and neglect interaction with other electron or nuclear magnetic moments. The number of spins in a typical sample reaches up to 10^{10}.The corresponding detectable concentration of active sites can be very low, compared to the other spectroscopic techniques. If the magnetization vector is inclined toward the direction of the static magnetic field, it undergoes a precession motion around it with a Larmor angular frequency $\omega_o = \gamma B_o$, where γ is the "gyromagnetic ratio." The value of γ directly connects the microscopic magnetic moment of the paramagnetic molecule $\boldsymbol{\mu}$ and its total electronic angular momentum $\mathbf{J}$ via relation:

$$\boldsymbol{\mu} = \gamma \mathbf{J} \tag{2.1}$$

Imposing the microwave field in the reciprocal plane (with respect to $\mathbf{B_o}$ direction) leads to the tilt of the precession axis of the magnetization motion. The tilt angle θ is determined by the equation:

$$tg(\theta) = \gamma B_1 / (\omega - \omega_0) \tag{2.2}$$

As the difference $(\omega - \omega_o)$ approaches zero, the tilt angle θ goes to $\pi/2$. The resonance takes place at the moment when the frequency of an alternating field ω (controlled by the experimenter) is matched to the Larmor frequency ω_o—an individual signature of the paramagnetic center. In practice the resonance condition is achieved by keeping microwave frequency ω constant and changing B_o—magnitude of the static magnetic field. EPR signal, proportional to a transverse component $M_\perp$ of the magnetization, is recorded for systematically swept magnitude B_o. The signal intensity changes abruptly at a field position characteristic for a given sample, where the static magnetic field B_o fulfills the resonance condition (the magnetization nutation frequency ω_o in this field becomes matched to the frequency of the imposed microwaves ω). For a basic sample, being an ensemble of diluted isotropic paramagnetic centers, non-interacting with each other, its related "continuous wave EPR spectrum" consists of one "resonance line" at uniquely defined position $B_{rez} = \omega/\gamma$, where γ characterizes the magnetic properties of the paramagnetic sample.

2.3.2 "Structural Fingerprints" of the Paramagnetic Center Read from EPR Signals

In the EPR experiment, the actual detected quantity is the macroscopic magnetization $\mathbf{M}$, which is a resultant vector of large ensemble of microscopic magnetic

moments ("spins" of unpaired electrons). The recorded EPR spectrum results from interaction of **M** with the external magnetic fields. Detailed analysis of that spectrum (the positions and shapes of "resonance lines") extracts basic parameters, encoding information about the structural properties of the paramagnetic center. In case of nitrosyl hemoglobin samples, the focus is on nitrosylated heme group and its interactions with ligands. Simplified, intuitive reasoning presented below illustrates the connection between macroscopic features/numbers (the resonance line position and shape) read from the recorded EPR spectrum and their meanings as representing microscopic properties of the molecular center. The amplitude of the EPR signal at the position B on the spectrum represents the answer of these magnetic moments, which possess the same γ value (calculated as a quotient of B, line position read from the spectrum, and ω, frequency of the applied electromagnetic field in the experiment). The value of γ [rad/T·s] directly refers to the intrinsic, dimensionless individual magnetic property of the paramagnetic center, Landè g-factor:

$$|\gamma| = \frac{\mu_B}{\hbar} g \tag{2.3}$$

In the above equation, μ_B is the Bohr magneton (elementary atomic unit of the magnetic moment), and $\hbar$ is the reduced Planck constant. For molecular systems the value of g-factor for bound unpaired electron deviates from the value g_e = 2.00231930436182(52), characterizing the free electron (the most accurately known physical constant). The Landè g-factor links to the individual magnetic properties of the molecule hosting an unpaired electron and depends on the electron density distribution, resulting from the given molecular structure and microenvironment conditions. Thus the value of g is very unique as is coding quantitatively the properties of the investigated paramagnetic complex on the molecular and quantum mechanical level. Recently, it has become possible to obtain the Landè g-factor straightforwardly from density functional theory for some molecular paramagnetic complexes, but for many, it still has to be established experimentally. When the EPR signal is used for this purpose, it must be taken into account that the measured interaction depends on the absolute orientation of the molecule with respect to the external magnetic field: the molecular system with anisotropic electron density distribution produces an "EPR" answer, dependent on its orientation with respect to the static magnetic field direction. Owing to that the EPR spectroscopy is an excellent tool to detect and study molecular systems exhibiting 3D anisotropy. For each position of the spectrum (given magnetic field B coordinate), the scalar value, called "effective g-factor" g_{eff}, can be calculated from formula:

$$g_{\text{eff}} = \frac{\hbar \cdot \omega}{B \cdot \mu_B} \tag{2.4}$$

where ω denotes frequency of the applied electromagnetic field in the experiment, set constant, and B is the magnitude of the static magnetic field, systematically

"swept" during detection of EPR signal. Intensity of the spectrum at a given value of B represents the total signal from selected spins: those with identical g_{eff}.

Numerous paramagnetic complexes manifest spatial anisotropy of their magnetic moment; especially nitrosyl hemoglobin is one of them. This entails that individual spins in the sample fulfill the resonance condition at different magnetic field positions, depending on their orientation. In consequence, for anisotropic molecular systems, the g_{eff} reflects the magnitude of the magnetic moment at a given orientation. Experimentally such anisotropy can be recognized when the crystalized sample is measured and the position of the resonance line on the recorded EPR spectrum varies with the changed orientation of the crystal within the static magnetic field. Such experiment reveals obviously the inherent magnetic anisotropy of the paramagnetic site. The set of the "single crystal" EPR spectra for systematically changing orientations of the crystal axes with respect to the direction of the static magnetic field, encoded as (Θ,φ), yields the data for $g_{\text{eff}} = g_{\text{eff}}(\Theta,\varphi)$. For anisotropic molecular systems, the value of g_{eff}, recovered from position of the single resonance line, usually departs from g_e—free electron value—and depends on angles (Θ,φ). In that case the complete description of magnetic properties for a given complex cannot be represented by the scalar quantity. The tensor is adequate to represent a set of these orientation-dependent factors: $g_i(\Theta,\varphi)$. Thus the **g**-tensor (more exactly 3 × 3 matrix) becomes a generalization of the scalar gyromagnetic g-factor. In Eq. 2.1, instead of scalar coefficient g, the multiplier relating the total angular momentum **J** to magnetic moment $\boldsymbol{\mu}$ becomes now **g**-tensor quantity. The necessity of introducing tensor quantity for concise description of the paramagnetism appears in these molecular centers where the electron possesses both spin and orbital angular momentum. The concise and complete definition of magnetic properties of the studied paramagnetic center is expressed by the three principal **g**-tensor values g_{xx}, g_{yy}, and g_{zz} ("eigenvalues") and set of angle orientations of the principal **g** axes within the molecular frame. In case of nitrosyl heme, the inner, molecular reference system is based on a heme system geometry. The principal axis systems for **g**-tensor are not collinear with heme-based molecular frame (e.g., the angle between the principal Z axis of the **g**-tensor and the heme normal is about 10°). The widely used classification of the paramagnetic complexes is based on the "**g**-tensor symmetry." If all eigenvalues are equal, the system is isotropic; when all values g_{xx}, g_{yy}, and g_{zz} are different, the "rhombic" symmetry is present; and when only two parameters are equal, this is the case of "axial symmetry." Knowledge of the principal **g**-tensor values of the investigated paramagnetic molecular system is the basic step for the proper interpretation of the measured EPR spectrum. After introducing the **g**-tensor—the real paramagnetic center "fingerprint"—the link between "g_{eff}" factor and the paramagnetic molecule orientation (Θ,φ) with respect to the B_o direction can be written as:

$$g(\theta,\varphi) = g_{\text{eff}} = \sqrt{\sin^2\theta\cos^2\varphi g_{xx}^2 + \sin^2\theta\sin^2\varphi g_{yy}^2 + \cos^2\theta g_{zz}^2} \tag{2.5}$$

This formula for g_{eff} separates the contribution of molecule orientation during EPR measurements and its individual magnetic signature, expressed by **g**-tensor components.

The routinely prepared and measured experimental samples of HbNO complexes are not "crystals" but frozen solutions of proteins. Such samples are classified within the magnetic resonance spectroscopy, as "disordered systems"—they are an ensemble of paramagnetic molecules adopting distinct, random orientations (θ,ϕ) versus the fixed magnetic field $\mathbf{B_o}$. The "lines" observed in their EPR spectra are very broad due to cumulation of the individual resonance signals from different orientations, with distinct "g_{eff}" value. Usually the distribution of magnetic moment orientations (θ,ϕ) is uniform in case of frozen solution samples. The measured EPR spectrum of such a "powder sample" is a superposition of individual signals, and the obtained final shape encompasses broadened, poorly resolved, and overlapping lines. Even then the resulting "powder profile" transfers the information about the intrinsic anisotropy of microscopic paramagnetic unit: the positions relating to the three principal values of **g**-tensor are easily discernable. The estimate values of eigenvalues g_{xx}, g_{yy}, and g_{zz} can be revealed directly from EPR powder spectrum (for the centers dominated by **g** anisotropy). In Fig. 2.3, the typical "powder pattern" of an EPR spectrum paramagnetic center with rhombic symmetry is displayed. In simulation the following values were assumed: $g_{xx} = 2.06$, $g_{yy} = 2.00$, and $g_{zz} = 1.96$. The coordinates of distinguishing points, the first maximum, the middle line cross point, and the last minimum, correspond to the molecular orientation in which a given principal **g** axis (x, y or z) is parallel to the magnetic field direction. When the molecule is found in one of these characteristic orientations, the effective value (g_{eff}) is equal to, consecutively, g_{xx}, g_{yy}, or g_{zz}. In general, the interpretation of experimental powder EPR spectra may be very demanding, due to the presence of other paramagnetic active sites, magnetic interactions, and distribution of magnetic parameter values. Samples of proteins are collection of molecules with distribution of conformations, and the paramagnet in each molecule may have slightly different **g**-tensor values. The exact determination of **g**-tensor values from experimental data is possible using simulation of "powder spectra" and least-squares fitting methods (*see*, e.g., ref. [27]).

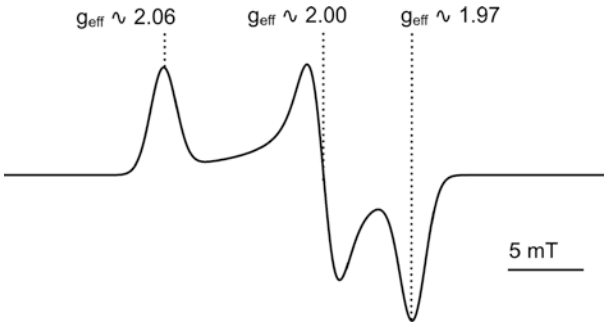

Fig. 2.3 Simulated EPR line shape for a randomly oriented $S = 1/2$ spin system with rhombic symmetry (in the absence of any hyperfine interaction). The simulation of powder profile was performed assuming $g_{xx} = 2.06$, $g_{yy} = 2.00$, $g_{zz} = 1.96$, and microwave frequency 9.5 GHz. The field positions related to the orientations, $\theta = 90°$ ($g_{\text{eff}} = g_{zz}$), $\theta = \varphi = 90°$ ($g_{\text{eff}} = g_{yy}$), and $\theta = 90°$; $\varphi = 0°$ ($g_{\text{eff}} = g_{\text{xx}}$), are indicated

The strict, theoretical interpretation of **g**-tensor is presented by the quantum mechanics approach. In brief, information about the wave function of the molecule in its electronic ground state is required to calculate **g**-tensor ab initio for a given molecular structure. This still remains a difficult task especially for heme–NO complexes, where sometimes large discrepancies between calculated and experimental **g**-tensor values appear [15]. Although theoretical predictions of **g**-tensors for model heme–NO compounds are obtained more routinely [32], the incorporation of the protein environment into calculations is a real challenge. Recently interesting results [24] have been published for nitrosyl myoglobin, a genuine prototype for the study of heme proteins. The insight into collection of **g**-tensor data established for the different ferrous heme–NO proteins reveals their general similarity: three principal *g*-values are around 2.07, 2.00, and 1.98, indicating the case of "rhombic" symmetry of these centers. Confrontation of the experimentally established *g*-values and those predicted from quantum mechanics confirmed the hypothesis that the orientations of the principal **g**-tensor axes are closely related to the orientation of the NO bond in ferrous NO–heme complexes [23].

2.3.3 Hyperfine Splitting of the Resonance Line

The magnetic moment of an unpaired electron senses not only the external applied field but also the presence of local nuclear magnetic moments in its vicinity. For the case of NO–heme unit, magnetic moments of the closest nuclei ^{1}H and ^{14}N exert a significant effect on the actual magnetic field experienced by the unpaired electron. The additional magnetic field provided by these nuclear "magnetic dipoles" can either add or subtract from the external magnetic field $\mathbf{B_o}$ and causes the splitting of the observed EPR spectrum line. Although the magnitude of this local field (up to few mT) exerted by the nuclear spins is small compared to the $\mathbf{B_o}$ (hundreds of mT), the interaction between the electron magnetic moment (determined by its spin **S**) and a nearby nuclear magnetic moment (originating from its spin **I**) introduces the visible changes in the EPR spectrum of the paramagnetic center. There are 2I + 1 different orientations of the nuclear spins in the external magnetic field $\mathbf{B_o}$, adopted statistically. Because the local field of the nucleus either adds or subtracts from the applied $\mathbf{B_o}$ field, therefore a certain fraction of the unpaired electrons experiences a larger, another lower magnetic field, and a bunch of 2I + 1 resonance lines appear in the spectrum instead of one (as in the absence of the interaction). The hyperfine interaction between the electronic and nuclear magnetic moments depends on the distance *r* between them and electron density distribution at the nucleus. The "hyperfine constant" *A* is introduced to express the strength of the coupling: its magnitude indicates the extent of delocalization of the unpaired electron over the nucleus. If the unpaired electron is delocalized over several ligands, it can interact with nuclear spins of all these atoms, and the resulting *A* value depends on the bond strength in the molecule. If the local field is strong, the separation between the hyperfine lines increases. The important hyperfine effect in case of NO–ligated hemes is the interaction of the unpaired electron and the nitrogen nucleus ^{14}N with

spin I = 1. In five-coordinate hemes (5C), the three-line splitting of the resonance line is expected due to the local field produced by nitrogen nucleus from NO. In six-coordinate hemes (6C), there are two nitrogen ligands: from NO and from proximal histidine. The pattern of hyperfine splitting becomes more complex, and the resulting local field from both N nuclei has $(2I + 1)\cdot(2I + 1) = 9$ possible magnitudes. Thus nine-line splitting pattern is expected for six-coordinate NO–hemes. It is worth to notice that use of ^{15}N-labeled NO changes the hyperfine pattern observed in the spectrum of NO–ligated hemes: the nuclear spin of ^{15}N is equal to 1/2. The hyperfine structure for 5C hemes consists of two lines only, and for 6C the number of lines is $(2\cdot 1/2 + 1)(2\cdot 1 + 1) = 6$.

In the molecular system, the coupling between the unpaired electron and a given paramagnetic nucleus is anisotropic; the magnitude of the splitting can differ significantly in each direction within the molecule. Generally the effect of the local nuclear field exerted on the unpaired electron must be represented by the tensor quantity **A**, which can be diagonalized by a suitable choice of principal axes. The principal values $[A_{xx}, A_{yy}, A_{zz}]$ of the tensor completely characterize the anisotropy of the interaction. They also constitute an individual molecular signature and complement the information about the paramagnetic center obtained from EPR signal. **A** tensor data for the iron–porphyrin–NO model compound, Fe(T*o*-F_2PP-BzIM)(NO) [14], can be an illustrative example of the hyperfine interaction strength in NO–hemes. The experimental spectrum for that compound was reconstructed by simulation with best parameters for **g**-tensor: $g_{xx} = 2.077$, $g_{yy} = 2.009$, and $g_{zz} = 1.978$. Hyperfine interaction with nitrogen from NO was determined by the following eigenvalues of $\mathbf{A^{NO}}$ (in gauss): 13.2, 22.1, and 13.9; the effect of interaction with nitrogen from imidazole was resolved on the spectrum only in "g_y" region; only one component of the $\mathbf{A^{IM}}$ tensor could be established: $A_{yy}^{IM} = 6.8$ G. These numbers directly indicate that the interaction with nitrogen nucleus from imidazole is much weaker than with that from NO. The quoted data represent typical magnitudes of hyperfine effects observed also in biological NO–heme complexes.

The hyperfine structure of the EPR resonance line is not always resolvable in the acquired spectrum, especially when the coupling constant is rather small, as compared with line broadening. In such case the experimental evaluation of these coupling parameters is possible using pulse EPR methods, e.g., electron spin echo envelope modulation (ESEEM) spectroscopy [33]. The knowledge of true **A**-tensor values is crucial for understanding of the relationship between molecular structure and electronic configurations of the paramagnetic heme complexes.

Put together, the **g**- and **A**-tensors reveal important information about local geometric and electronic structure of the metalloprotein's paramagnetic center. These parameters can be experimentally determined using "continuous wave" and pulse methods of electron paramagnetic spectroscopy [34]. The effect of hyperfine coupling between the unpaired electron and nuclear magnetic moments is essential in the utilization of EPR spectroscopy for structural studies. Especially unravelling the ligation scheme around paramagnetic transition metal ions is possible.

2.4 The EPR Spectra of the Nitrosyl Hemoglobin

From the very beginning, recording "continuous wave EPR spectrum" of HbNO complex has been the basic spectroscopic technique employed in Hb and HbNO studies. Detailed analysis of EPR spectral features corroborated the information obtained from other methods as well as provided new facts [3, 6, 35] concerning the bonding of diatomic ligands to heme. The complexity of nitrosyl hemoglobin EPR CW (continuous wave) spectrum arises from the fact that this macromolecule is composed of four subunits: two α- and two β-chains, each of them possibly contributing to the overall signal shape. In real samples, not all four units are necessarily nitrosylated. Additionally the variation of the HbNO EPR spectra with temperature as well as the effect of pH can be observed. Historically the first step toward unambiguous interpretation of that complex signals was proving that the EPR spectrum of the $Hb_4(NO)_4$ tetramer is a linear combination of the isolated subunit spectra [3]. Though the specific HbNO spectral features cannot be discussed without consideration of the protein environment of heme–NO complex, it was very advantageous to study monomeric species: model complexes and monomeric enzyme, myoglobin. The progress in thorough, quantitative understanding of the EPR spectra of ferrous heme-nitrosyls was achieved by combining the data retrieved from experiments and quantum mechanical calculations [15, 24].

2.4.1 EPR Signatures of HbNO-α and HbNO-β Subunits

As the decades passed, the consistent interpretation of the manifold of experimental EPR spectra recorded for nitrosyl proteins emerged. The routine is to measure the EPR spectrum of the frozen solution of the HbNO at liquid nitrogen temperatures. In such sample all possible orientations of the paramagnetic center occur, and the recorded signal belongs to the "powder-pattern" type. The EPR spectrum of the tetrameric hemoglobin appears to be composite, first because of contributions from the two types of subunits (α and β). The molecular surroundings of hem units slightly differ in α- and β-chains; thus the different sets of **g**- and **A**-tensor values are expected. Additionally, the hem in alpha subunit can occur as five- or six-coordinate unit, which may increase the number of spectral components required for reconstruction of tetrameric HbNO spectrum. Furthermore, the stereochemical variability of the Fe–NO bond in the sixfold coordinated systems may lead to the presence of "structural HbNO micropopulations," characterized by individual magnetic tensors.

2.4.1.1 Six-Coordinate Nitrosyl Hemes

The first attempts to determine principal **g**-tensor values for heme–NO utilized EPR spectra of isolated α_{NO}- and β_{NO}-chains recorded at low temperature [3, 36]. The approximate *g*-values for separate subunits were dissimilar and both demonstrated

Table 2.1 The principal values of **g**- and $\mathbf{A}_{NO}$-tensors for six-coordinate heme-NO in α and β subunits of human nitrosyl hemoglobin at 87 K, ref. [37]

	g-Tensor principal values			$\mathbf{A}_{NO}$-Tensor principal values [MHz]		
α-Chain	2.0604(52)	1.9653(9)	1.9995(56)	29.6(1.4)	32.9(1.0)	63.6(0.7)
β-Chain	2.0817(15)	1.9782(5)	1.9999(16)	26.9(0.9)	44.2(0.5)	62.3(0.2)

temperature dependence. The latter effect was explained as a result of altered orientation of the NO molecule with respect to heme at both room and low temperatures. The EPR spectra of isolated subunits, recorded at room temperature, gave broad, overlapping lines, and their hyperfine splitting was practically unresolvable. The spectral features, remarkably hallmarking the subunits, appear only at low temperatures, when they are not masked by the averaging dynamics of the molecules. Even since early experiments [3], the similarity of the EPR spectral shapes for β_{NO}-unit—but not α_{NO}—and NO-myoglobin has been noticed. The more precise and reliable disentangling of **g**-tensors was possible to gain from measurements on "single crystal" tetrameric HbNO sample. The study on the crystallized form of nitrosyl hemoglobin with preserved tetrameric structure and quaternary interactions [37] supplied the basic electronic parameters: the principal values and axis directions of the **g**-tensors adequate for an alpha and a beta subunit. The obtained EPR spectra indicated the presence of unpaired electron hyperfine interaction with NO and proximal histidine N, which corresponds to the fully liganded state of hemoglobin, with all hemes being six-coordinate. The established tensors [37] are summarized in Table 2.1.

The EPR data allowed establishing the principal axis directions for **A**- and **g**-tensors, and then the geometry difference between α and β subunit was clearly discerned. The principal axes of **A**- and **g**-tensors were not collinear. There was also no exact coincidence between the hem geometry and the directions of **g** principal axes: the angle between heme normal and the axes at which **g** component adopts nearly-free-electron values was about 10° in the alpha and about 8° in beta subunit. After experimental establishing of **g**-tensor, the model of geometry, orientation, and orbital spin distribution at NO ligand site was proposed; especially the Fe–N–O bond angles were calculated for α- and β-units as 135° [18] and 105° [5]. Putting all together, the obtained EPR spectroscopic data demonstrated subtle differences in the binding of NO to the heme between α and β subunits. It turned out that **g**-tensor was sensitive not only to the local properties of the heme unit but also the quaternary structure of the protein. The values for β_{NO} units from tetrameric hemoglobin could be compared with **g**-tensor of NO–myoglobin, determined also from the "single-crystal" study [38] at 77 K: $g_{xx} = 2.076$, $g_{yy} = 1.979$, and $g_{zz} = 2.002$. The Fe–N–O bond angle in the monomeric MbNO was estimated as 109°. Those nitrosyl myoglobin parameters were temperature dependent, in a similar way observed in nitrosyl hemoglobin samples.

The experimental determination of *g*-values and hyperfine coupling constants for crystal samples of nitrosyl hemoproteins must be recognized as a valuable contribution to the field, made by EPR spectroscopy. These parameters provided direct insight into the real electron spin density distribution in the heme–NO complexes.

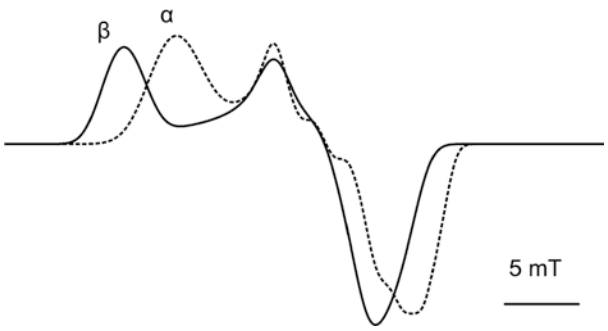

Fig. 2.4 Spectral simulation showing the separate contributions of α-NO and β-NO subunits. The EPR "powder spectra" at 9.5 GHz were simulated. The **g** and **A** tensors corresponds to the values established for six-coordinate alpha and beta subunits (ref. [37])

The results showed that practically no electron density is located on the four pyrrole nitrogens. Comparative studies [39] with use of ^{14}NO and ^{15}NO showed that the unpaired electron is delocalized mainly on iron and nitrogen N_ε (from proximal histidine) orbitals. On the other hand, the recognized structural flexibility of the NO ligand coordinated to ferrous heme has made the exact determination of Fe–NO electronic structure and formal oxidation states difficult both for proteins and model complexes. Recently it has been remarked that the geometry of Fe–NO observed in crystal structures of protein not necessarily represents the conformation executed during binding NO to hem in solution [40].

The consequence of different magnetic tensors **A** and **g** for alpha and beta subunits (both with six-coordinate heme) is the unequivalence of their EPR powder spectra. The simulated traces, corresponding to the parameters presented in Table 2.1, are displayed in Fig. 2.4. The large effect of resonance line broadening, similar to the experimental conditions, makes the details of hyperfine interaction unresolved. The general impression is that α- and β-chain spectra are fairly similar in the sixfold coordinated conformation. The real, HbNO samples would give the spectra which contain these basic components (besides others) in different proportions.

2.4.1.2 The Effect of Temperature on HbNO Spectra

Comparison of theoretical, simulated profiles and experimental spectra requires all constituents to be identified and their separate shapes properly set. Only then can the decomposition procedure explain the reliable proportion of these basic components. In case of nitrosyl hemoglobin, as well as six-coordinate heme complexes, the additional difficulty arises: their experimental EPR spectra exhibit a temperature-induced variation. That effect was observed in experiments on nitrosyl myoglobin and HbNO (for isolated chains and tetramers): in the recorded EPR spectra, two components were recognized, distinguished as an R (rhombic—three different **g**-tensor components) or A (axial—two different **g**-tensor components) species, characterized by the different **g**-tensor values. As temperature increased, the conversion of R-form into A-form was noticed [41].

The general explanation of that phenomenon could refer to the protein-specific effect: their backbone structure is temperature dependent. That intriguing observation was known also for small molecules: heme-model compounds [15]. Its elucidation could focus on the common feature: the temperature-dependent stereochemical variability of the Fe–NO bond in the six-coordinate hemes. Recently the explanation of the origin of these two forms "R" and "A" was suggested [23, 24]. That explanation consistently combined the spectroscopic data and theoretical, quantum mechanical calculations. The authors aimed to explain the geometric differences between the R- and A-forms and reproduced the experimental values of **g**-tensors from theoretical model for monomeric protein: nitrosyl myoglobin. They showed that at higher temperature (>77 K), rotation of the NO molecule with respect to the heme plane is probable and may be responsible for adopting the A-form. A similar hypothesis, concerning two differing geometries for six-coordinate heme–NO complex, was proposed for interpretation of the model complex experimental EPR data, collected over the 4–300 K range [42]. The "axial form" was related to the structure, where N(imidazole)–Fe–NO axis was parallel to the heme normal, whereas the "rhombic form" is related to the geometry assuming the tilt angle between N(imidazole)–Fe–NO axis and the heme normal. The authors postulated the presence of the axial and rhombic form for both α and β subunits (giving four different spectrum shapes). The further investigation of spectral components corresponding to distinct structural subtypes of HbNO involved measurements of EPR signal at higher microwave frequency (95 GHZ, W-band), offering better resolution [43]. The important finding was that the critical temperature, characterizing the structural change from R- to A-form, is much lower for β subunit than for α. In most HbNO measurements with the use of EPR, the temperature is set ~77 K; in this range, the β subunit is converted to the axial form, whereas α remains rhombic. The similar conclusion was earlier supported [42] by results obtained with ENDOR (electron-nuclear double resonance).

2.4.1.3 EPR Spectral Response to the R–T Transition of HbNO

Upon NO binding to the heme cofactor, a six-coordinate intermediate conformation forms until the heme-trans ligand is dissociated, leaving a five-coordinate complex. Crystallographic study of T-state human HbNO [21] presented explicitly a cleavage of the proximal Fe–His bond in the α subunit (whereas that bond was retained in the β subunit). A number of characteristic changes are observed in the EPR spectra of five-coordinate (5C) ferrous heme–nitrosyls. The average **g**-tensor values of Fe–NO unit (in model systems and proteins) are around 2.10, 2.06, and 2.01 [14]. These values can be compared with markedly smaller typical parameters for six-coordinate NO–hemes, 2.08, 2.00, and 1.98, which illustrated the profound effect of binding N-donor ligand trans to NO. The most striking evidence of Fe–N (imidazole) bond cleavage is the appearance of three-line hyperfine pattern. At the spectral line corresponding to $g \sim 2.01$, a very characteristic, three-line splitting is present. That very well-resolved hyperfine structure results from an unpaired electron interaction with nitrogen (NO) nuclear spin $I = 1$ in five-liganded NO–heme unit. In case of six-coordinate hemes, that interaction is also present but is further splitted by

interaction with the N (imidazole) of the proximal N-donor ligand, generating the final, nine-line hyperfine pattern with lower intensity.

The solid, theoretical explanation of the nitrogen hyperfine interactions during the change of heme coordination form 6C to 5C was given by Mun [44]. He directly proved that extensions of the Fe–N (imidazole) bond produce a significant decrease of the related hyperfine interaction constant; thus weakening or cleavage of that bond is unequivocally manifested by only three-line (not nine) splitting on the EPR spectrum.

When it comes to HbNO tetramers, formation of a pentacoordinate iron–NO–heme complex, manifested by the presence of "triplet" on the EPR spectrum in the high-field region, has been correlated to the T–R transition. The pentacoordinate heme–NO unit is formed only in α subunit. There is a preferential affinity of α subunits for nitric oxide, and, in turn, an equilibrium between hexa- and pentacoordinate α-NO hemes occurs in the low-affinity conformation of hemoglobin. If hemoglobin is in the quaternary T-state, the strain on heme-proximal histidine bond is present, and binding of NO to α-chain can finally lead to cleavage of the Fe-axial nitrogen bond resulting in the five-coordinate state of heme. This process is reversible and accompanied by the switch from T to R quaternary state of the tetramer. Owing to the fact that the molecular coordination of heme (5C or 6C) can be related to the physiological states of hemoglobin, T (low-affinity tense) or R (high-affinity relaxed) form, the transition from R to T structures can be monitored via changes from a nine- to a three-line hyperfine pattern in the EPR spectrum. The complicated, allosteric mechanism of hemoglobin structural transition is responsible for the fact that under physiological conditions, the α-NO fraction is a mixture of five- and six-fold coordination [42]. Experimentally, the formation of an intense "triplet" structure on the EPR spectrum of the tetrameric nitrosyl hemoglobin can be enhanced by the presence of inositol hexaphosphate [6]. The effect of hyperfine interaction on the CW EPR spectrum of HbNO is frequently obscured by the large resonance line widths, but this is not in the case of pentacoordinated α-NO. The prominent three-line splitting is resolved even on "powder" EPR spectra of frozen solution samples. The simulated EPR spectra for six- and pentacoordinated α-NO (in a presence of inositol hexaphosphate, IHP), with parameters proposed in [6], are presented in Fig. 2.5. The evident spectral differences indicate that the breakage of the bond between Fe and proximal histidine results in changes in **g**-tensor components and hyperfine interaction pattern. Generating the pentacoordinate α-NO heme (5C) in the HbNO sample is very efficient in the presence of IHP, but the presence of this chemical allosteric modulator can introduce some additional structural disturbances of the tetramer and, consecutively, recorded EPR spectra. The characteristic "triplet" on the EPR spectrum, accompanying formation of 5C NO–heme, appears also when pH in the sample containing tetrameric or monomeric HbNO is lowered from 7.3 to 3.0. The effect of pH on the X-band EPR parameters of HbNO was studied by Ascenzi et al. [45]. The presented spectroscopic data illustrated the "quaternary effect": the equilibrium constants, characterizing the pH-dependent spectroscopic transition R/T, were different between the tetramer and the isolated monomeric α- and β-chains.

The physiological role of NO as an enhancer of oxygen release is realized via NO-induced trans-axial cleavage of the heme Fe-proximal His bond in tetramer

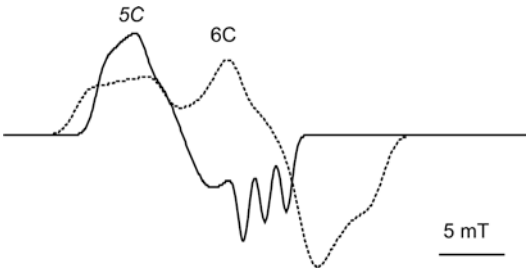

Fig. 2.5 The simulated EPR "powder" spectra corresponding to 5C-α-NO and 6C-α-NO (in the presence of inositol hexaphosphate, IHP). Values for *g* and *A* parameters are taken from ref. [6]

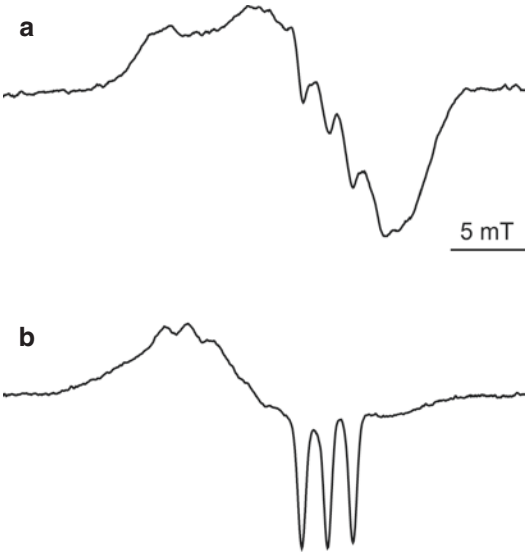

Fig. 2.6 Experimental continuous wave EPR (9.5 GHz) spectra detected ex vivo at 77 K in solid samples of human lung adenocarcinoma tumors growing in nude mouse model. A and B represent two different tumors. The difference between the spectra results from various levels of NO generation, thus various saturation of hemoglobin with NO. (**a**) The HbNO triplet signal overlaps with the signal of the six-coordinate HbNO, suggesting a considerable saturation of hemoglobin with NO. (**b**) The five-coordinate HbNO "triplet signal" has a predominant contribution to the whole spectrum

hemoglobin. The presence of the five-coordinate spectral component with distinct three-line pattern was demonstrated in venous blood samples [7, 46]. Moreover, due to a different ratio between five- and six-coordinate α-NO in venous and arterial blood, the structural transition of α-NO during arterial and venous circulation could be proved [8]. The presence of HbNO with characteristic signal was reported also in tumor tissue [47]. The examples of EPR tumor sample spectra are shown in Fig. 2.6. The signals exhibit different levels of 5C-α-NO versus 6C-α-NO in photodynamically stressed tumors.

2.5 Quantification of HbNO Signal

The EPR spectroscopy is an indispensable tool for research on endogenous NO-derived paramagnetic species in biological systems. However the researcher meets some challenges of EPR application to quantification of HbNO in biological samples. Interpretation of the experimental spectra of HbNO samples must take into account their composite character. There are many spectrally distinct subtypes of HbNO with temperature-dependent contributions. As a routine, in medical and biological applications, the "in vivo" samples are immediately frozen in liquid nitrogen, and then EPR measurements are taken at 77 K (and lower temperature). The general approach is to use three basis spectra for decomposition of the recorded spectrum, representing five-coordinate α-chain, six-coordinate α-chain, and six-coordinate β-chain. That procedure allows the quantification of HbNO fractions present in the sample. The standard EPR shapes of the basic components have to be measured separately for synthesized HbNO variants. A regression-based spectrum analysis technique was developed [12], which successfully allowed to quantify the HbNO levels in blood during NO inhalation. In the measurements on physiological material, the background signal is frequently problematic. One solution is to use "the spectral subtraction method," as proposed in [9]. The absolute concentrations of HbNO in venous and arterial blood from rats were determined using that method.

Because the five-coordinate α-NO spectrum exhibits the well-resolved nitrogen hyperfine splitting from NO, it is relatively easy to determine the height of one of the "triplet" inverted peaks and use it for monitoring the increase of 5C-α-NO subunit in the whole pool of HbNO. It must be noted that this height cannot be taken directly to quantify the absolute concentration neither "T-state" nor the whole pool of nitrosyl hemoglobin present in the sample. The magnitude of "triplet" peak neglects the contribution of 6C-α-NO to the spectrum. On the other hand, in biological tissue and blood samples, there are present other non-HbNO overlapping signals on the recorded EPR spectrum, but 5C-α-nitrosyl hemoglobin is the only form that gives a three-line hyperfine structure around $g \sim 2$. This fact motivates to use that distinct feature for approximate estimation of HbNO content. The procedure of calibration of "triplet" signal intensity versus NO concentration was proposed in [48]. The exemplary illustration of the pronounced increment of the hyperfine line heights on the EPR spectrum is presented in Fig. 2.7. The collected EPR spectra reflect increasing 5C-α-NO formation after exposure to growing concentrations of NO. The similar approach was used in [49] to reveal physiologic regulation of 5C-α-NO level in human pathophysiologic states.

In order to obtain the reliable concentrations of the active center in the biological sample, the sample processing procedures must be strictly followed, especially in case of HbNO. It is also essential to set conditions for EPR spectra acquisition properly. Due to the difference in the relaxation rates between the distinct structural subtypes of HbNO [50], the conditions under which the EPR spectra are taken are of great importance.

The recorded EPR spectrum of HbNO sample is composed of at least three contributing components. The process of spectral decomposition still uses experimentally

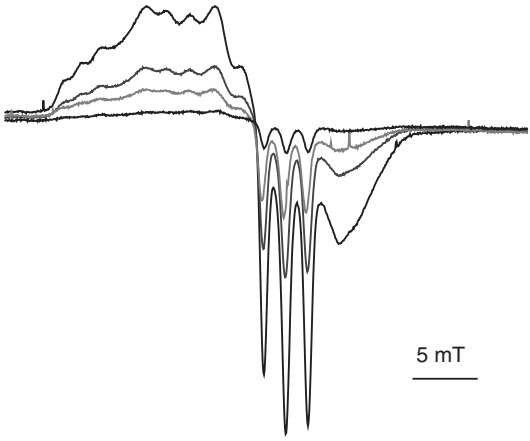

Fig. 2.7 . The increase of the "triplet signal" on the EPR spectrum of chemically pure nitrosyl hemoglobin, exposed to the increasing NO concentration, in the absence of allosteric agents, and anaerobic conditions. Continuous wave EPR spectrum (9.5 GHz) recorded at 77 K

prepared basis spectra [6, 12]. Their shapes cannot be reproduced in simulation with satisfactory fit quality, required for reliable quantification. In fact, due to conformational heterogeneity of 6C-NO hemes, the actual number of spectrally distinct HbNO subtypes must be greater than three. In simulations each of the conformation must be defined by the adequate set of magnetic tensors **A** and **g**. The number of required parameters increases enormously due to the presence of two types, α- and β-chains, and possible 5C or 6C heme coordination. Another difficulty arises from inhomogeneous broadenings occurring in the experimental spectrum. In simulation these irregular broadenings must be modelled mathematically, which is nontrivial. Even in case of much simpler model compounds, the obtained simulated EPR spectra diverge from experimental ones (*see*, e.g., ref. [14]). The successful attempts to fit CW EPR "powder" spectrum of HbNO have not been reported yet. Even in case of much simpler, monomeric myoglobin, it still becomes a challenge. Recently the successful reconstruction of EPR spectrum for heme protein was obtained for 5C heme−NO complexes of soluble guanylate cyclase [51]. In that case two components were identified, corresponding to two conformations of the investigated complex.

Conclusions

The analysis of experimental HbNO EPR spectrum must take into account the complex molecular composition of the protein determining its specific structure and electronic surrounding of the NO-ligated heme. Signals recorded at room temperatures exhibit a single and broad absorption with unresolved hyperfine splittings. The informative signal, hallmarking the conformations present in the sample, comes from the measurements at liquid nitrogen temperatures. The experimental EPR settings must be carefully chosen, especially when it comes to the microwave power. The recorded spectrum of the biological HbNO sample exhibits a variety of features, which can be utilized to recognize and monitor changes which take place in the investigated system. The application of EPR technique in medical and biological research gives the unique possibility to detect HbNO derivatives in complex biological tissues, without purification.

A more detailed insight into molecular structural details of nitrosylated hemoglobin must be supported by the advanced quantum mechanical calculations. Such approach seems indispensable in search of biological consequences of changeable and intricate interactions between hemoglobin and its paramagnetic ligand—nitric oxide.

References

1. Angelo M, Hausladen A, Singel DJ, Stamler JS. Interactions of NO with hemoglobin: from microbes to man. Methods Enzymol. 2008;436:131–68.
2. Peisach J, Blumberg WE, Wittenberg BA, Wittenberg JB. The electronic structure of protoheme proteins III. Configuration of the heme and its ligands. J Biol Chem. 1968;243:1871–80.
3. Henry Y, Banerjee R. Electron paramagnetic studies of nitric oxide haemoglobin derivatives: Isolated subunits and nitric oxide hybrids. J Mol Biol. 1973;73:469–82.
4. Szabo A, Perutz MF. Equilibrium between six- and five-coordinated hemes in nitrosyl hemoglobin: interpretation of electron spin resonance spectra. Biochemistry. 1976;15:4427–8.
5. Taketa F, Antholine WE, Chen JY. Chain nonequivalence in binding of nitric oxide to hemoglobin. J Biol Chem. 1978;253:5448–51.
6. Hille R, Olson JS, Palmer G. Spectral transitions of nitrosyl hemes during ligand binding to hemoglobin. J Biol Chem. 1979;254:12110–20.
7. Kosaka H, Sawai Y, Sakaguchi H, Kumura E, Harada N, Watanabe M, Shiga T. ESR spectral transition by arteriovenous cycle in nitric oxide hemoglobin of cytokine-treated rats. Am J Phys. 1994;266:C1400–5.
8. Jaszewski AR, Fann YC, Chen Y-R, Sato K, Corbett J, Mason RP. EPR spectroscopy studies on the structural transition of nitrosyl hemoglobin in the arterial-venous cycle of DEANO-treated rats as it relates to the proposed nitrosyl hemoglobin/nitrosothiol hemoglobin exchange. Free Radic Biol Med. 2003;35:444–51.
9. Jiang J, Corbett J, Hogg N, Mason RP. An electron paramagnetic resonance investigation of the oxygen dependence of the arterial-venous gradient of nitrosyl hemoglobin in blood circulation. Free Radic Biol Med. 2007;43:1208–15.
10. Hogg N. Detection of nitric oxide by electron paramagnetic resonance spectroscopy. Free Radic Biol Med. 2010;49:122–9.
11. Hawkins CL, Davies MJ. Detection and characterization of radicals in biological materials using EPR methodology. Biochim Biophys Acta. 1840;2014:708–21.
12. Piknova B, Gladwin MT, Schechter AN, Hogg N. Electron paramagnetic resonance analysis of nitrosyl hemoglobin in humans during NO inhalation. J Biol Chem. 2005;280:40583–8.
13. Dikalov S, Fink B. ESR techniques for the detection of nitric oxide in vivo and in tissues. Methods Enzymol. 2005;396:597–610.
14. Goodrich LE, Paulat F, Praneeth VK, Lehnert N. Electronic structure of heme-nitrosyls and its significance for nitric oxide reactivity, sensing, transport, and toxicity in biological systems. Inorg Chem. 2010;49:6293–316.
15. Lehnert N, Scheidt WR, Wolf MW. Structure and bonding in heme-nitrosyl complexes and implications for biology. Struct Bond. 2014;154:155–224.
16. Henry YA, Guissani A. EPR detection of nitrosylated compounds: introduction with some historical background. In: Lukiewicz S, Zweier JL, editors. Nitric Oxide in Transplant Rejection and Anti-Tumor Defense. New York: Springer Science + Business Media; 1998. p. 3–35.
17. McMahon TJ, Bonaventura J. The Main Players: Hemoglobin and Myoglobin; Nitric Oxide and Oxygen. In: Mozzarelli A, Bettati S, editors. Chemistry and biochemistry of oxygen therapeutics: from transfusion to artificial blood. New Jersey: John Wiley & Sons, Ltd; 2011. p. 47–62.

18. Cooper CE. Nitric oxide and iron proteins. Biochim Biophys Acta. 1999;1411:290–309.
19. Wyllie GR, Schulz CE, Scheidt WR. Five- to six-coordination in (nitrosyl)iron(II) porphyrinates: effects of binding the sixth ligand. Inorg Chem. 2003;42:5722–34.
20. Yi J, Soares AS, Richter-Addo GB. Crystallographic characterization of the nitric oxide derivative of R-state human hemoglobin. Nitric Oxide. 2014;39:46–50.
21. Chan NL, Kavanaugh JS, Rogers PH, Arnone A. Crystallographic analysis of the interaction of nitric oxide with quaternary-T human hemoglobin. Biochemistry. 2004;431:118–32.
22. Liao MS, Huang MJ, Watts JD. Binding of O_2 and NO to heme in heme-nitric oxide/oxygen-binding (H-NOX) proteins. A theoretical study. J Phys Chem B. 2013;117:10103–14.
23. Radoul M, Sundararajan M, Potapov A, Riplinger C, Neese F, Goldfarb D. Revisiting the nitrosyl complex of myoglobin by high-field pulse EPR spectroscopy and quantum mechanical calculations. Phys Chem Chem Phys. 2010;12:7276–89.
24. Sundararajan M, Neese F. Detailed QM/MM study of the electron paramagnetic resonance parameters of nitrosyl myoglobin. J Chem Theory Comput. 2012;8:563–74.
25. Eaton SS, Eaton GR, Berliner LJ, editors. Biomedical EPR–part A: free radicals, metals, medicine, and physiology. BiolMagnReson, vol. 23. New York: Kluwer Academic/Plenum Press; 2005.
26. Eaton SS, Eaton GR, Berliner LJ, editors. Biomedical EPR–part B: methodology, instrumentation, and dynamics. BiolMagnReson, vol. 24. New York: Kluwer Academic/Plenum Press; 2005.
27. Hagen WR, Biomolecular EPR Spectroscopy. Florida: CRC Press, Taylor & Francis Group; 2009.
28. Corvaja C. Introduction to Electron Paramagnetic Resonance. In: Brustolon M, Giamello E, editors. Electron paramagnetic resonance: a practitioner's toolkit 2009. New Jersey: John Wiley & Sons; 2009. p. 1–36.
29. Petasis DT, Hendrich MP. Quantitative interpretation of multifrequency multimode epr spectra of metal containing proteins, enzymes, and biomimetic complexes. Methods Enzymol. 2015;563:171–208.
30. Rizzi AC, Neuman NI, González PJ, Brondino CD. EPR as a tool for study of isolated and coupled paramagnetic centers in coordination compounds and macromolecules of biological interest. Eur J Inorg Chem. 2016;2016:192–207.
31. Van Doorslaer S, Desmet F. The power of using continuous-wave and pulsed electron paramagnetic resonance methods for the structure analysis of ferric forms and nitric oxide-ligated ferrous forms of globins. Methods Enzymol. 2008;437:287–310.
32. Patchkovskii S, Ziegler T. Structural origin of two paramagnetic species in six-coordinated nitrosoiron(ii) porphyrins revealed by density functional theory analysis of the g tensors. Inorg Chem. 2000;39:5354–64.
33. Deligiannakis Y, Louloudi M, Hadjiliadis N. Electron spin echo envelope modulation (ESEEM) spectroscopy as a tool to investigate the coordination environment of metal centers. Coord Chem Rev. 2000;204:1–112.
34. Van Doorslaer S, Vinck E. The strength of EPR and ENDOR techniques in revealing structure-function relationships in metalloproteins. Phys Chem Chem Phys. 2007;9:4620–38.
35. Dickinson LC, Symons MCR. Electron spin resonance of haemoglobin and myoglobin. Chem Soc Rev. 1983;12:387–414.
36. Shiga T, Hwang RJ, Tyuma I. Electron paramagnetic resonance studies of nitric oxide hemoglobin derivatives. I. Human hemoglobin subunits. Biochemistry. 1969;7:378–83.
37. Utterback SG, Doetschman DC, Szumowski J, Rizos AK. EPR study of the structure and spin distribution at the binding site in human nitrosyl hemoglobin single crystals. J Chem Phys. 1983;78:5874–80.
38. Hori H, Ikeda-Saito M, Yonetani T. Single crystal EPR of myoglobin nitroxide. Freezing-induced reversible changes in the molecular orientation of the ligand. J Biol Chem. 1981;256:7849–55.
39. Chien JCW, Dickinson LC. Nonequivalence of subunits in ^{15}N Nitrosyl hemoglobin Kansas. A single crystal electron paramagnetic resonance investigation. J Biol Chem. 1977;252:1331–5.

40. Copeland DM, Soares AS, West AH, Richter-Addo GBJ. Crystal structures of the nitrite and nitric oxide complexes of horse heart myoglobin. Inorg Bio Chem. 2006;100:1413–25.
41. Schmidt PP, Kappl R, Hüttermann J. On the mode of hexacoordinated NO-binding to myo- and hemoglobin: variable-temperature EPR studies at multiple microwave frequencies. App Magn Reson. 2001;21:423–40.
42. Hüttermann J, Burgard C, Kappl R. Proton ENDOR from randomly oriented NO-ligated haemoglobin: approaching the structural basis for the R–T transition. J Chem Soc Faraday Trans. 1994;90:3077–87.
43. Luchsinger BP, Walter ED, Lee LJ, Stamler JS, Singel DJ. EPR studies of the chemical dynamics of NO and hemoglobin interactions. In: Hanson G, Berliner L, editors. High resolution EPR. Berlin, Heidelberg: Springer Science+Business Media; 2009. p. 419–38.
44. Mun SK, Chang JC, Das TP. Origin of observed changes in ^{14}N hyperfine Interaction accompanying R → T transition in nitrosyl hemoglobin. Proc Natl Acad Sci U S A. 1979;76:4842–6.
45. Ascenzi A, Bocedi A, Fasano M, Gioia M, Marini S, Coletta M. Proton-linked subunit heterogeneity in ferrous nitrosylated human adult hemoglobin: an EPR study. J Inorg Biochem. 2005;99:1255–9.
46. Kosaka H. Nitric oxide and hemoglobin interactions in the vasculature. Biochim Biophys Acta. 1999;1411:370–7.
47. Jakubowska M, Michalczyk-Wetula D, Pyka J, Susz A, Urbanska K, Płonka BK, Kuleta P, Łącki P, Krzykawska-Serda M, Fiedor L, Płonka PM. Nitrosyl hemoglobin in photodynamically stressed human tumors growing in nude mice. Nitric Oxide. 2013;35:79–88.
48. Plonka PM, Chlopicki S, Plonka BK, Jawien J, Gryglewski RJ. Endotoxaemia in rats: detection of nitrosyl-haemoglobin in blood and lung by EPR. Curr Top Biophys. 1999;23:47–53.
49. Lobysheva II, Biller P, Gallez B, Beauloye C, Balligand JL. Nitrosylated hemoglobin levels in human venous erythrocytes correlate with vascular endothelial function measured by digital reactive hyperemia. PLoS One. 2013;8:e76457. https://doi.org/10.1371/journal.pone.0076457.
50. Wajnberg E, Linhares MP, EI-Jaick J, Bemski G. Nitrosyl hemoglobin: EPR components at low temperatures. Eur Biophys J. 1992;21:57–61.
51. Gunn A, Derbyshire ER, Marletta MA, Britt RD. Conformationally distinct five-coordinate heme−no complexes of soluble guanylate cyclase elucidated by multi frequency electron paramagnetic resonance (EPR). Biochemistry. 2012;51:8384–90.

3 Use of Electron Spin Resonance and Spin Trapping Technique in the Studies of Tropical Parasitic Diseases

Germán Barriga-González and Claudio Olea-Azar

3.1 Chagas Disease: An Example of Tropical Parasitic Disease

Parasitic diseases represented a major health and economic problem mainly for developing nations. Bearing in mind the development that has taken humanity during the twentieth and twenty-first centuries, parasitic diseases are associated mainly with ignorance and low educational and economic level. About 8 million people worldwide, mostly in Latin America, are infected. About 25 million people are at risk to be infected (WHO 2016) (Table 3.1) [1].

Chagas disease or American trypanosomiasis is a zoonosis caused by the flagellate protozoan *Trypanosoma cruzi*, described for the first time in 1909 by Carlos Chagas, in Minas Gerais, Brazil. It is a debilitating chronic disease that affects the health, welfare, and productivity of a great number of human beings and represents a public health problem in Latin America. The infection occurs mainly by the contact of the skin or mucous membranes of human beings or of other mammals, with feces or urine of insects of the hemipteran subfamily Triatominae, *Trypanosoma cruzi*.

T. cruzi is a unicellular parasite that alternates its life between two multicellular hosts, one invertebrate, and one vertebrate, presenting a digenetic life cycle. Depending on the general shape of the cells (spherical, pear-shaped, or elongated),

G. Barriga-González
Departamento de Química, Facultad de Ciencias Básicas, Universidad Metropolitana de Ciencias de la Educación, Santiago, Chile

C. Olea-Azar (✉)
Departamento de Química Inorgánica y Analítica, Facultad de Ciencias Químicas y Farmacéuticas, Universidad de Chile, Santiago, Chile
e-mail: colea@uchile.cl

A. K. Shukla (ed.), *Electron Spin Resonance Spectroscopy in Medicine*,
https://doi.org/10.1007/978-981-13-2230-3_3

Table 3.1 Countries affected by parasitic disease *T. cruzi*

Endemic countries	Non-endemic countries (but present)
Chile	United States
Argentina	Canada
Uruguay	Portugal
Paraguay	Spain
Bolivia	France
Peru	Belgium
Brazil	United Kingdom
Ecuador	Netherlands
Colombia	Denmark
Venezuela	Norway
Guyana[a]	Sweden
Suriname[a]	Germany
French Guiana[a]	Austria
Panama	Italy
Costa Rica	Greece
Nicaragua	Switzerland
Honduras	Japan
El Salvador	Australia
Belize	
Guatemala	
Mexico	

[a]No data available

the relative position between the core and the extranuclear kinetoplast DNA (located in the mitochondria; this DNA represents a major proportion of the total DNA of the cell because, depending on the species, it may contain from 10% to 20% of the total DNA in the cell), the position in which the flagellum emerges from the parasite (central or lateral), defines the following evolutionary forms for the trypanosomatids (Fig. 3.1):

- Trypomastigote, the kinetoplast is located after the kernel, usually in the posterior portion of the parasite. The flagellum exits the back end and bends forward along the body of the parasite, forming an undulating membrane throughout the parasite and emerge in a manner that is free in its front end.
- Epimastigote, the kinetoplast is in the middle part of the body just in front of the core. The flagellum emerges from the middle part of the parasite and forms an undulating membrane smaller than the observed in the trypomastigotes.
- Promastigote, the kinetoplast has on the front and a flagellum free (may be present or absent) without an undulating membrane.
- Amastigote is more ball and has no free flagellum. The kinetoplast is a dark body near the nucleus.

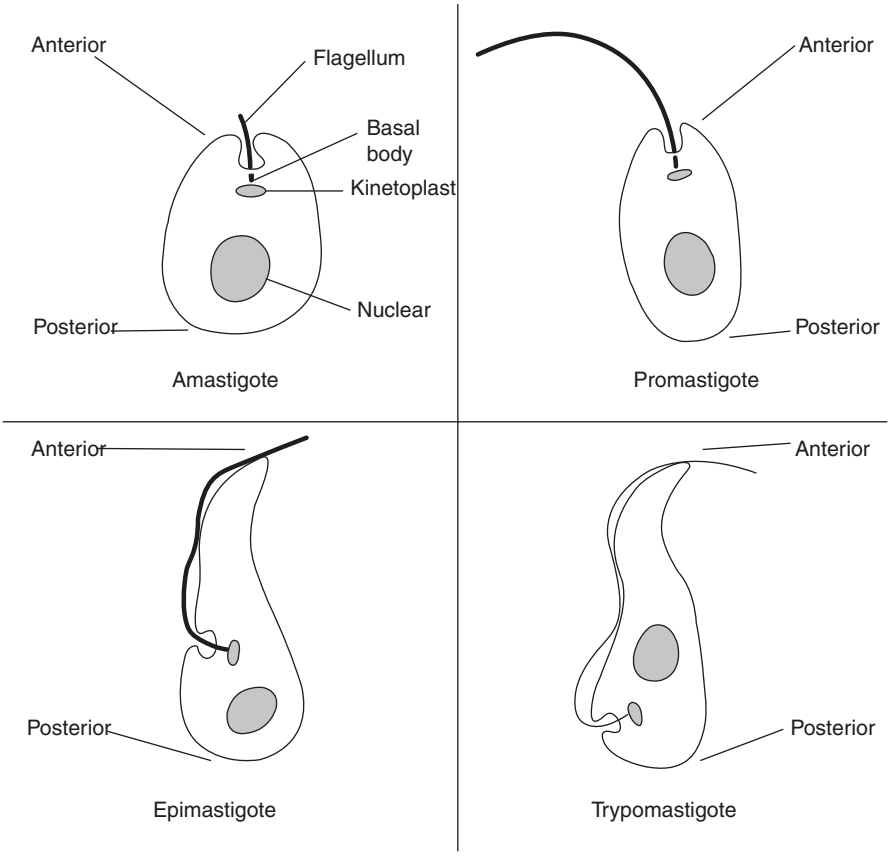

Fig. 3.1 Evolutionary forms of trypanosomatids. Image from https://commons.wikimedia.org/wiki/File:Trypanosomatid_Cellular_Forms.png

3.2 Transmission of *T. cruzi*

The main route of transmission of *T. cruzi* among their hosts is the vectorial transmission (through the vector) in which two cycles can be distinguished: wild and domestic. The wild cycle or primitive cycle of *T. cruzi* is essential, where the zoonotic protozoan circulates between vectors and wild reservoirs throughout most of the American continent from millions of years ago. The primitive ecosystems of *T. cruzi* are very diverse, through the North American deserts, Andean highlands, Amazonian forests, and Atlantic. Wild trypanosomiasis prefers closed or semi-open environments, varying in the proportions of hosts to vectors, depending on several factors such as climate, altitude, humidity, characteristic of flora and fauna, and availability of food. In this context, it is found in all America, keeping the parasite in mammals of medium and small size and the insect vectors. Among others, it prevails in those ecosystems where the vectors can form its colonies such as palm trees,

coconuts, trunks, stony ground, etc. This is a state of balance developed through a long adaptation that translates into the low or no pathogenic action of the protozoan on their natural hosts. The domestic transmission cycle of Chagas disease corresponds to a situation that is much more recent in the historical context, defined by anthroponotic factors (cycle, man-insect-man) and making the man one of the last natural reservoirs of *T. cruzi*. The expansion of Chagas disease is the product of an erratic occupation and of a deprogrammed occupation of Latin America based on three main elements:

- Deep actions on the natural environment as burning and cutting down on the large tracts of forests, promoting the opening of natural spaces, and bringing to artificial ecosystems the reservoirs and vectors of the parasite
- Providing the existence of ranches and households of poor quality as an excellent shelter of the vectors
- Inducing the migration of peasants, conveyors of the infection, toward large cities and the existence of vectors with a high capacity to settle, a typical case of *Triatoma infestans*

In the domestic transmission cycle, man stands out as the main reservoir of infection, which leads the parasite to urban areas and to new regions and non-endemic countries. In addition to the vector path (which represents 80%–90% of transmission), there are various forms of secondary transmission, being the main transmission by blood transfusion, which corresponds to 5%–20% of the cases, and the congenital path that corresponds to the range between the 0.5% and 8% of the cases. The other routes of transmission are exceptional (accidental, organ transplantation, other vectors, lactogenic, etc.) and do not represent a significant importance in terms of public health. Transmission by blood transfusion is mainly due to the economic difficulties present in Latin America, which has stimulated the migration to urban areas in the past six decades. Currently, in most of the countries, cities have 60% of the population. The migration from rural to urban areas, while reducing the number of people exposed to the vector infected, increases the probability of transmission by blood transfusion. Insofar as they do not discard donor blood contaminated, there is the likelihood of transmitting the disease by this path, being the most exposed individual poly-transfused, such as hemophiliacs and dialyzed. Fortunately, only one party (12%–18%) of those receiving a transfusion with infected blood contracts the disease. On the other hand, the infection by blood transfusion has become a serious problem in the developed countries (where there is no vector transmission) due to the tens of millions of Latin Americans who migrate to these countries, being North America the main destination of Latin American immigrants.

T. cruzi has different host-parasite relations, depending directly on the type of host you are in. If your host is the insect, the *T. cruzi* will behave and develop in a way, while if your host is a mammal, their relationship changes like its cycle. These relations are divided in two: insect-parasite and mammal-parasite. The insect-parasite relationship is one in which the biological cycle of *T. cruzi* starts when the insect

ingests the blood of infected animals. To reach the stomach, trypomastigote shapes are transformed to spheromastigotes and epimastigotes; sometimes the spheromastigote shapes are added, giving the impression of multinucleate masses. Soon the parasites migrate toward the intestine, where they are multiplied as epimastigote forms (25 h after the infection). An essential stage of the interaction of *T. cruzi* with the invertebrate host is the adhesion of the epimastigote forms to the surface of the epithelium of the midgut and later to the cuticular layer of the epithelium of the rectal gland and the rectal pouch, which can be observed 8 days after infection. The accession of the epimastigotes occurs by hydrophobic interactions with a layer of wax that covers the cuticle [2–4]. In opposition, the mammal-parasite relationship directly affects the man, and in it, the evolutionary cycle of *T. cruzi* in the vertebrate host begins when the epimastigote and trypomastigote forms are removed in the feces and urine of the insect vector and are inoculated into the skin or mucous membranes of the vertebrate. The forms of trypomastigotes can penetrate any type of cell that you find at the site of inoculation, less in eosinophils and neutrophils. For its part, the epimastigote forms are phagocytosed by cells with phagocytic capacity that are in the area and are rapidly digested. After entering the host cell, the trypomastigotes can be found in the interior of a vacuole, called parasitophorous vacuole. After some time, it transforms to amastigote form, which is now free in the cytoplasm of the host cell. The process of binary cell division starts 35 h after the infection, which continues for several days depending on the strain of *T. cruzi* and the host cell. The generation time is approximately 14 h; after 5 days, approximately, when the host cell contains around 500 amastigotes, an almost synchronized process of transformation to the trypomastigote form starts, passing through an intermediate state. When the trypomastigote shapes have a longer flagellum, an intense movement begins that seems to be responsible for the breakdown of the host cell, with the subsequent release of hundreds of trypomastigotes to intercellular space. The available data suggest that all these forms are able to invade new cells at the same site where they were released or exit to the bloodstream and distributed throughout the body (Fig. 3.2) [5].

3.3 Chagas Disease: Clinical Manifestations

Chagas disease presents a series of clinical manifestations. The disease occurs initially with a high parasitemia (acute phase), which is limited by the immune response of the host. In the acute stage, infected individuals pass through a period without clinical symptoms called indeterminate phase or asymptomatic. The patients in the chronic phase present subpatent levels of parasitemia, which largely hinders the parasitological diagnosis. Approximately 70% of asymptomatic patients remain so throughout their lives. However, 30% of the patients after remaining asymptomatic for years develop slowly but progressively a cardiomyopathy. In addition to the cardiac alterations, one can observe a syndrome of dilation of viscera, being the most frequent the dilation of the colon and/or esophagus, caused by the development of megaesophagus or megacolon. The clinical

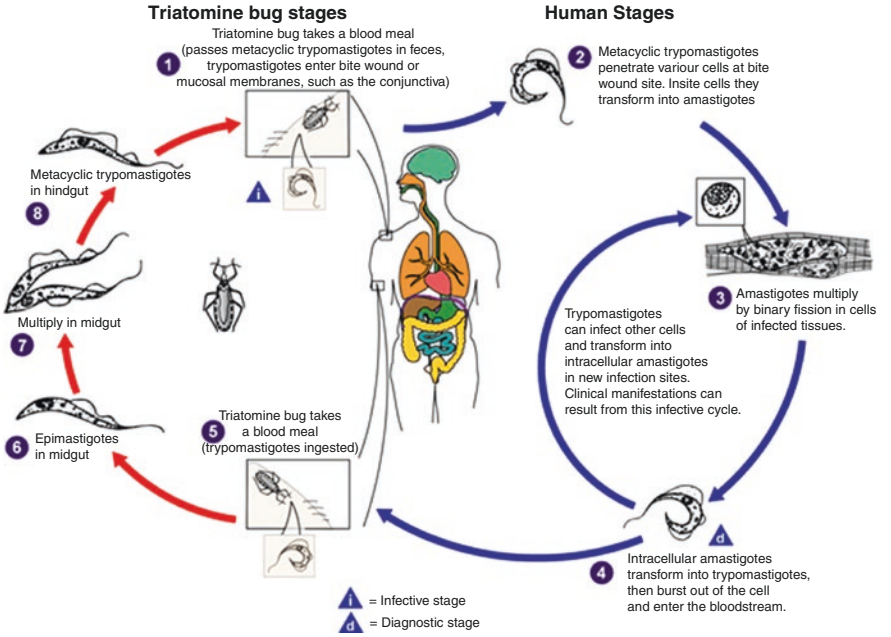

Fig. 3.2 The cycle of *Trypanosoma cruzi* and its relationship with the host. Image modified from https://www.cdc.gov/dpdx/trypanosomiasisAmerican/index.html

manifestations of the disease vary depending on the stage of the infection. The acute phase may occur with or without symptoms. The symptoms can be varied. For example, the Romana's sign that manifests as unilateral or bilateral bi-palpebral edema of a purple tone, painless and durable, accompanied by facial edema, conjunctivitis, keratitis, and dacryocystitis. This sign is accompanied by preauricular lymphadenopathy uni- or bilateral [6–8]. Lymph more committed are usually preauricular, parotid, sternocleidomastoid, and submaxillary [9, 10], in addition to the systemic manifestations common to other diseases [1]. At this stage, the clinical manifestations are more frequently observed in children, where the disease can be fatal. Cases of mortality can be observed in the adults but with greater frequency can go unnoticed or presented in a moderate way. In this phase, the trypomastigote forms can be detected in the blood due to the high levels of parasitemia, which are subsequently controlled by the immune response. This response does not eradicate completely to the parasite, maintaining a subpatent parasitemia throughout the life of the host. Once the acute stage begins, the infected individuals pass through a period without clinical symptoms called indeterminate phase or asymptomatic. Approximately 70% of infected patients remains so throughout its life, coexisting with the parasite, without developing significant damage in their tissues. In the absence of evidence of significant damage in cardiac and/or digestive tissue, the seroreactivity to *T. cruzi* is the only thing that differentiates clinically to an asymptomatic patient from a normal individual. Of these patients, approximately 30% of

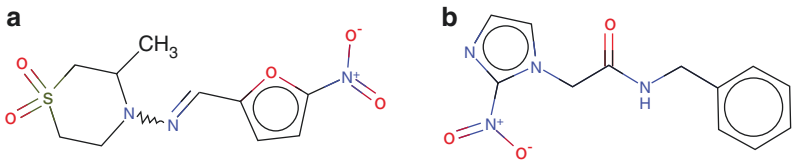

Fig. 3.3 Structures of the current drugs available for the treatment of *T. cruzi*. (**a**) Nifurtimox; (**b**) benznidazole

them, after remaining asymptomatic for a time, develop the symptomatic phase or chagasic cardiomyopathy. This phase is characterized by a slow evolution, usually between 10 and 20 years, between the end of the acute phase and the establishment of the heart damage. Those patients who are going to develop the cardiomyopathy usually die of a heart failure, by severe arrhythmia or conduction disorders advanced. The different tests that are performed to detect this disease are:

- Physical examination (This procedure let to recognize symptoms associated and confirm the existence of heart failure in the chronic phase.)
- Peripheral blood smear (It shows the presence of trypanosome mobiles in the acute phase.)
- Cultivation of blood (It shows the presence of *T. cruzi* in the acute phase.)
- ELISA assay (It could detect past infection with *T. cruzi* in the chronic phase.)

The treatment that is done involves the use of two drugs. For the acute phase, it is recommended to use the benznidazole (Fig. 3.3b) that has proven to be effective; treatment may also include the use of nifurtimox (Fig. 3.3a). There is not much use in treating the chronic phase with antibiotics; should be addressed, in contrast, the symptoms of heart and intestinal disease.

In the present, there is a wide diffusion of pharmaceutical products and/or cosmetic that exalt the benefits of using antioxidant with many different purposes, such as prevention or improvement to diseases, improvement in the quality of life, anti-aging treatments, etc. Terms such as oxidative stress, free radicals, antioxidants, reactive oxygen species, vitamins, etc. are used (with a greater or lesser degree of accuracy) in the advertising of these products trying to explain.

3.4 Free Radicals

Free radicals are atoms or molecules in general of high reactivity that can damage important biomolecules because of their short half-life. They can produce damage to proteins and nucleic acids and cause inactivation of enzymes. Free radicals have unpaired electrons either by gain or loss of these or by breaking of covalent bonds. Due to these unpaired electrons, free radicals show paramagnetic properties. Depending on the atom in which the unpaired electrons are located, these can be classified as free radical centered on oxygen, nitrogen, carbon, etc.

Oxidative stress is a state of the cell in which the intracellular oxide-reduction homeostasis is altered, i.e., the balance between prooxidant and antioxidants. This imbalance occurs because of an excessive production of reactive oxygen species (ROS) and/or deficiency in the antioxidative mechanisms, leading to cell damage. In analogy to the term oxidative stress, Hausladen and Stambler have called nitrosative stress to excessive or deregulated formation of nitric oxide radical ($NO^{\cdot}$) and reactive species of nitrogen (RNS) arising from the same [11]. The main ROS are the superoxide anion radical ($O_2^{\cdot -}$), hydrogen peroxide (H_2O_2), and hydroxyl radical ($^{\cdot}OH$). One of the main sources of ROS is the respiratory chain, where the following transfers of electrons can occur:

$$O_2 \xrightarrow{e^-} O_2^{\cdot -} \xrightarrow[2H^+]{e^-} H_2O_2 \xrightarrow[H^+]{e^-} {}^{\cdot}OH_{(+H_2O)} \xrightarrow[H^+]{e^-} H_2O \tag{3.1}$$

Approximately 3% of the electrons from NADH is diverted toward the formation of ROS by the incomplete reduction of oxygen. These species are able to oxidize biological macromolecules such as proteins, lipids, and nucleic acids [12–14]. On the other hand, these can react with divalent metals (free or attached to proteins) and produce a Fenton reaction:

$$Fe^{2+} + H_2O_2 \rightarrow Fe^{3+} + {}^{\cdot}OH + OH^- \tag{3.2}$$

In a similar way, these can also react with the prosthetic group of metalloproteins containing iron through the reaction of Haber-Weiss:

	$2O_2^{\cdot -} + 2H^+ \rightarrow H_2O_2 + O_2$
	$M^{(n)} + O_2^{\cdot -} \rightarrow M^{(n-1)} + O_2$
Fenton	$M^{(n-1)} + H_2O_2 \rightarrow {}^{\cdot}OH + OH^- + M^{(n)}$
Haber-Weiss	$\overline{O_2^{\cdot -} + H_2O_2 \rightarrow O_2 + {}^{\cdot}OH + OH^-}$ (3)

The hydroxyl radical can react with different macromolecules (proteins, lipids, and nucleic acids, mainly), through the donation of an electron, through producing other reactive species, and through unknown mechanisms and intermediaries. In these cases, it is said to have intervened the hydroxyl radical, understanding as such a free radical from univalent oxidation initiated by a Fenton-type reaction [15]. In this type of reactions, the hydroxylation and the removal of hydrogen are the most common modifications that suffer the organic substrate involved, generating other organic free radicals such as the alcohoxile ($RO^{\cdot}$), peroxyl ($ROO^{\cdot}$), and sulfur-containing radicals. There are two other ROS, with special features: the singlet oxygen ($^1O_2$) and hypochlorite (in protonated and deprotonated form).

The main RNS are nitric oxide ($NO^{\cdot}$) and peroxynitrite ($ONOO^-$) considered as one of the most potent biological oxidants [16]. RNS can damage and kill cells by various mechanisms: inactivation of the various complexes of the respiratory chain [17], damage to proteins and lipids [12, 14, 18, 19], inhibition of protein or DNA synthesis [20, 21], and GSH or ATP depletion [22, 23]. While all living organisms support a number of endogenous and exogenous factors of oxidative stress, at the

same time, they have many systems of enzymatic and nonenzymatic antioxidant defenses. There are enzymes that act specifically on certain reactive species [15]. Thus, the superoxide dismutase disproportionates (reaction through which two molecules that are equal are transformed into two other different molecules) $O_2^{\cdot -}$ to O_2 and H_2O_2, the catalase transforms the H_2O_2 in O_2 and water, and the GSH peroxidase catalyzes the reduction of peroxyl radicals (ROOH) to alcohols (ROH), taking advantage of the reduction potential of the GSH [24].

The research focused on the study of free radical, in the last 30 years, has provided important evidence about the production of free radical species at a physiological level and because of the actions of drugs in biological systems, including parasitic diseases. Although different mechanisms of action of drugs with anti-parasitic action are known, most of the compounds studied, which showed the best results as anti-parasitic drugs, are those that act through mechanisms of generation of free radicals. The principal families studied as free radical-producing drugs are mainly quinones, quinonimines, aminoquinolines, and nitro-heterocyclic compounds [25].

3.5 Electron Spin Resonance Spectroscopy

The development of the magnetic spectroscopic techniques has allowed us to develop extensively the electron spin resonance (ESR) spectroscopy. The direct detection of free radicals by ESR is only possible if the free radicals are produced in relatively high concentrations in the cavity of the ESR spectrometer by in situ irradiation or by mixed by flows systems. Unfortunately, free radicals of greater biological interest present very short half-life ranging from milliseconds to nanoseconds, making it impossible to its correct characterization, and it is therefore very difficult to study.

ESR is like nuclear magnetic resonance (NMR), being the main difference between both techniques that ESR is based on the splitting of the electronic spin states due to the action of an external magnetic field, while the nuclear magnetic resonance studies the splitting of the nuclear spin states. In both techniques, the sample is affected by a strong static external magnetic field, and in the case of ESR, the radiation used to correspond to a microwave-frequency radiation (GHz). The energy is absorbed by the sample if the frequency of the radiation corresponds to the energy difference between two electronic states in it, and the transition will occur if it complies with the appropriate selection rules. The division will occur when the electron has a total angular momentum other than zero. In the case of the free electron, the angular momentum of spin can have two possible values of inverse values which will generate two different states. In the absence of the external magnetic field, the two states of spin degenerate. By applying an external magnetic field, the degeneration "breaks," resulting in two different energy states; this separation corresponds to the electronic Zeeman effect. A maximum absorption will occur when the magnetic field "tunes" the two spin states so that their energy difference matches the energy of the radiation [25].

Once the measurement has been made, parameters are obtained that will allow the identification of the radical species. The parameters obtained correspond to the *g* values and the hyperfine interactions which provide information about the electron distribution within the molecule. Free radicals are generally found as intermediates during a reaction, and their identification will give information about the reaction mechanism. Measurement of the variation of their concentration with time will give kinetic data information [25].

3.6 Spin Trapping Technique

Spin trapping technique has emerged as an interesting tool to understand kinetics and mechanisms of certain reactions [26–29], such as sonolysis [30], lipid peroxidation [31, 32], Fenton-type reactions [23, 24], and enzymatic-type reactions in vivo/in vitro [33–38]. The emergence of spin traps is based on the addition of free radicals to compounds such as nitroso compounds (Fig. 3.4b) and nitrones (Fig. 3.4a) [39–47]. The product of this reaction, a nitroxide-based persistent radical (widely known as spin adduct) presents a half-life considerably higher than free radical without trap (Fig. 3.4).

Nitrones are currently the most widely used compound for free radical trap because they allow the characterization of free radicals of great biological interest such as the superoxide anion radical ($O_2^{\cdot -}$), hydroxyl radical ($^{\cdot}OH$), and several other secondary radicals formed mainly in the reaction between the hydroxyl radical and various cellular targets. There are two structural groups of nitrones in which the attention to the development of spin traps has focused, mainly the aromatic compounds conjugated alkane-*N*-oxides that include the α-phenyl-*N*-tert-butylnitrone (PBN) (Fig. 3.5b) and the Δ^1-pyrroline-*N*-oxides compounds such as 5,5-dimethyl-1-pyrroline-*N*-oxide (DMPO) (Fig. 3.5a) [48, 49].

The family of nitroso compounds has ceased to be used as spin traps due in the first instance that these compounds are subject to a series of chemical reactions, producing mainly nitroxides, which in general do not have any relationship with the

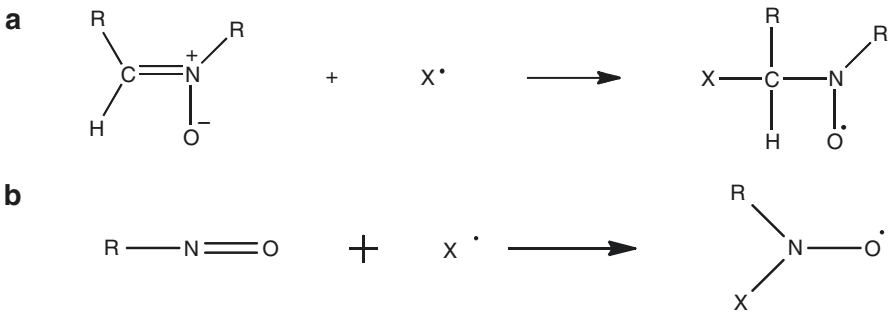

Fig. 3.4 Spin trapping reaction showing the formation of spin adducts using nitrones as spin traps (**a**) and nitroso compound (**b**)

radical in the study [50]. A clear example of this fact corresponds to trap the superoxide anion radical using 3,5-dibromo-4-nitrosobenzenesulfonic acid (DBNBS) (Fig. 3.6) [51].

It has been found that with the use of dimethyl sulfoxide (DMSO) as a solvent in the reaction mixture, the obtained spectrum actually shows the hyperfine pattern of sulfur trioxide anion radical from DMSO and not the superoxide anion radical ($O_2^{\cdot -}$) [52]. Secondly, the low stability of the spin adducts by trapping radicals centered on oxygen restricts the use of these compounds as free radical spin traps for specific radical or at low temperatures [53]. The main advantages and disadvantages of the nitroso compounds are summarized below [54]:

Advantages:

- The multiplicity of the hyperfine splitting pattern immediately delivers the number of hydrogens that are attached to the carbon in the trapped alkyl radical.
- Trapping of aryl radicals can be easily distinguished by the additional hyperfine splitting pattern from protons due to the delocalization of electrons over aromatic carbon atoms.
- Radicals, in which the electron is located on atoms with nuclear spin, show a characteristic hyperfine splitting pattern.
- The magnitude of the hyperfine splitting of nitrogen (A_N) varies considerably depending on the atoms that are attached.
- The values of *g* of the spin adducts vary with the type of atom that is attached to the nitroxide function.

Disadvantages:

- Strong tendency to dimerize.
- Some spin adducts are unstable.

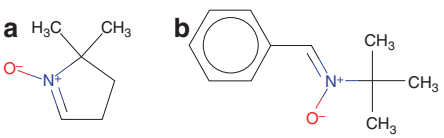

Fig. 3.5 Structures of commonly used spin traps. (**a**) 2,2-Dimethyl-3,4-dihydro-2*H*-pyrrole-1-oxide (DMPO), (**b**) *N*-(2-methyl-2-propanyl)-*N*-[(*Z*)-phenylmethylene]amine oxide (PBN)

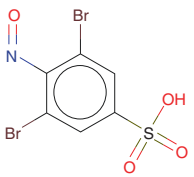

Fig. 3.6 Structure of nitroso compound 3,5-dibromo-4-nitrosobenzenesulfonic acid (DBNBS)

- Photolysis in presence of oxygen or thermal decomposition leads to the formation of nitroxide radicals.

The following is a summary of the main advantages and disadvantages of nitrones as free radicals spin traps [54]:

Advantages:

- Nitrones are stable compounds and as solids are not too sensitive to light, oxygen, or water vapor.
- In inert solvents, photolysis produces an insignificant concentration of nitroxide radicals.
- Spin adducts are very stable. This is due to a carbon atom that separates the nitroxide moiety that has trapped the radical.

Disadvantages:

- Information about the nature and structure of the trapped radicals is difficult to interpret from the obtained spectra of the spin adducts formed. Generally, the spectrum always consists of a triplet of doublets due to the coupling between the nitrogen and β-hydrogen atoms present in the structure of spin adduct.
- Photolysis of these types of compounds, in some solvents, quickly produces radical from the solvent.
- Low selectivity as spin traps in some cases and low solubility in aqueous media.

Detection and characterization of the formed spin adducts are performed by electron spin resonance (ESR) spectroscopy. Unpaired electron interacts with local magnetic fields from neighboring atoms with nuclear magnetic moments. Therefore, the different nuclear magnetic fields will be added or subtracted from the external magnetic field imposed as a fixed amount, depending on the quantization of its orientation. This phenomenon causes the division of the absorption line. The magnitude of the division of the absorption line depends on the size of the nuclear magnetic moment and the fraction of the electronic distribution of the atom. The variation of the magnitude of the split or division of the absorption line from the nucleus whose magnetic moment affects the unpaired electron results in an ESR spectrum composed of multiple lines. These lines are important because they allow the characterization of the paramagnetic molecule. From a hyperfine pattern, it is possible to calculate the hyperfine coupling constants whose values allow the discrimination of the formed spin adduct [55, 56]. This feature is one of the main advantages of using spin traps. Even small differences between free radicals can frequently cause significant changes in the spectra and in the hyperfine coupling constants. An example of this feature is observed in the hyperfine patterns of the DMPO spin trap when it is used to trap superoxide anion radical ($O_2^{\cdot -}$) and the hydroxyl radical ($^{\cdot}OH$), allowing to distinguish, by simple visual inspection of the spectrum, the trapped radical (Fig. 3.7) [57]. This aspect has a great relevance in the study of biological

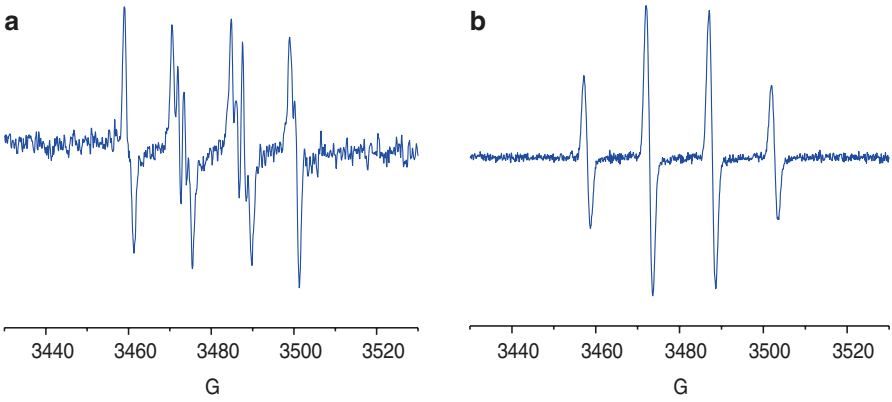

Fig. 3.7 (**a**) Superoxide radical anion spectrum ($O_2^{\cdot -}$). (**b**) Hydroxyl radical spectrum ($^{\cdot}OH$). DMPO was used in both cases

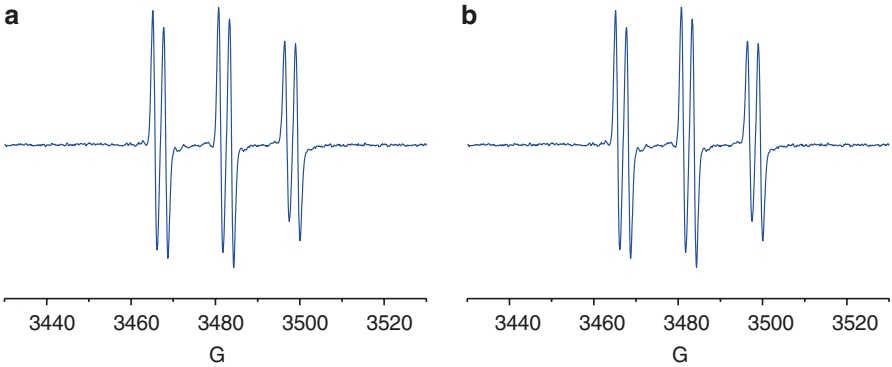

Fig. 3.8 (**a**) Superoxide radical anion spectrum ($O_2^{\cdot -}$). (**b**) Hydroxyl radical spectrum ($^{\cdot}OH$). PBN was used in both cases

processes where radical species are involved. However, these differences in the hyperfine patterns and in the hyperfine coupling constants are not noticeable with other nitrones. Example of this is the great difficulty of distinguishing between radicals centered on oxygen when PBN is used. The hyperfine patterns and coupling constants for superoxide anion radical and hydroxyl radical are very similar for PBN, and it cannot be distinguished which radical has been trapped (Fig. 3.8).

3.7 Anti-parasitic Agents

As mentioned above, several anti-parasitic agents have shown to exert their actions via free radical metabolism. In this sense, nitro and *N*-oxide compounds have been used against trypanosomatids, anaerobic protozoa, and

helminths. Antimalarial compounds such as primaquine, chloroquine, qinghaosu, and quinines have shown to be active in vitro and in vivo against different parasites [58].

Currently, the only available drugs used for the treatment of Chagas disease are nifurtimox (Nfx) and benznidazole (Fig. 3.3). It is believed that nitro-heterocyclic compounds have important biological effects, especially in *T. cruzi*, since they would be involved in a redox cycling of these compounds and oxygen radical production. In both processes, the nitro anion radicals formed to play a vital role [59–62]. When Nfx is added to intact *Trypanosoma cruzi* cells, a characteristic ESR signal appears corresponding to the nitro radical formed. It should be noted that the causative agent of Chagas disease (American trypanosomiasis) is *Trypanosoma cruzi* cells [63]. A series of experiments indicate that the major mode of action against *T. cruzi* corresponds to an intracellular reduction of Nfx followed by redox cycling [64]. Numerous side effects occur when using these drugs. Some of these side effects are fever, muscle weakness, abdominal or stomach pain, vomiting, etc. preventing in some cases to continue with these drugs as treatments [65]. The mechanisms of these side effects are not fully understood, but it is believed that peroxynitrite formation from Nfx resulting from the interaction of nitric oxide radical and superoxide anion radical generated during biotransformation of the Nfx could play a role in the toxicity of Nfx [66].

Our research group reported a series of nitro compounds with the ability to generate nitro anion radicals, which was verified by ESR spectroscopy [67, 68]. Also, our group has studied new analogs of Nfx (Fig. 3.9) [69]. The following ESR spectra were obtained for these compounds (Fig. 3.10). These results indicated that at least one of these compounds (compound 2) possesses similar or better activity than that presented by Nfx and produced an oxygen redox cycling in *T. cruzi* epimastigotes. In a *T. cruzi* incubation solution, the presence of the compound (2) showed an increase in the oxygen uptake. This indicated that the anti-chagasic activity of this compound was carried out by an oxidative stress mechanism.

Other studies focused on the bioreductive activation of megazol (Fig. 3.11) through the use of the following conditions: ferredoxin-NADP$^+$ reductase (FNR), rat liver microsome, and cell fractions of T. *cruzi* [70]. The detection was made using ESR and the characterization through the use of computational simulations. The presence of this radical was only detected under anaerobic conditions in the presence of NADPH and FNR. No evidence was found in the formation of the

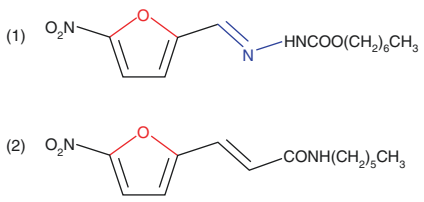

Fig. 3.9 Nitro compounds analog to Nfx studied by our group as potential trypanomicide drugs

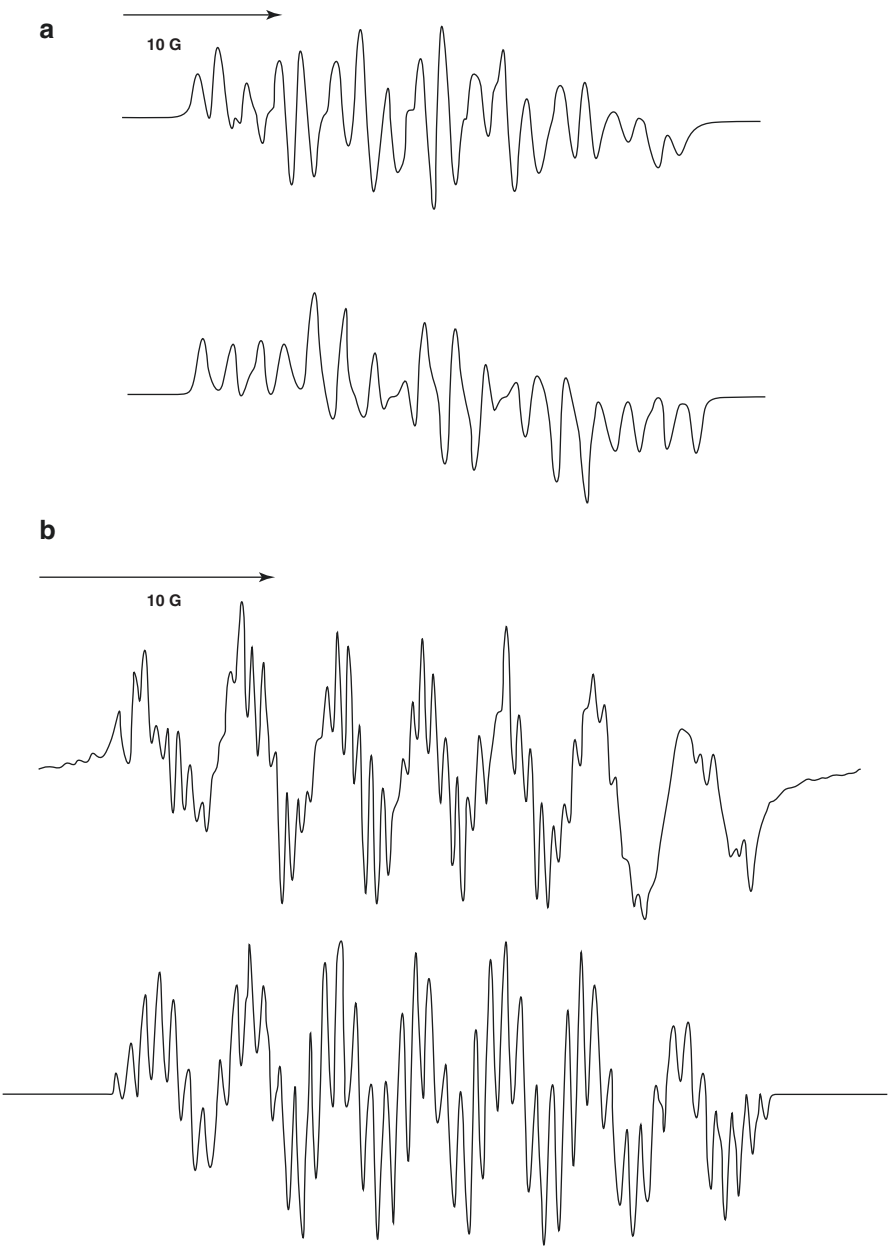

Fig. 3.10 (**a**) Experimental spectrum of the radical anion of (1) (Fig. 3.9) in DMSO and simulation of the same spectrum. (**b**) Experimental spectrum of the radical anion of (2) in DMSO and simulation of the same spectrum (Fig. 3.9)

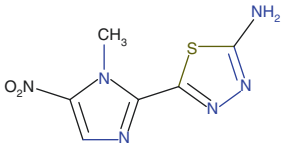

Fig. 3.11 Structure of megazol

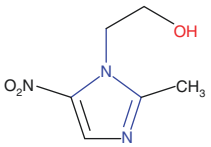

Fig. 3.12 Structure of metronidazole

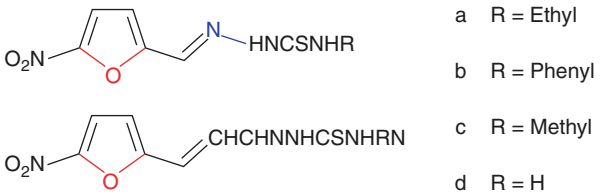

Fig. 3.13 Structure of 5-nitrofuryl thiosemicarbazone derivatives as potential drugs

megazol radical, the presence of rat liver microsome, and *T. cruzi* cell fractions. This would indicate that his bioreductive metabolism has no relation to a redox process.

Other studies on megazol showed that it is highly active against several strains of *T. cruzi* [71]. The interactions shown by Nfx, metronidazole (Fig. 3.12), and megazol with different redox enzymes were compared. The results showed that these compounds could be reduced by L-lactate cytochrome c reductase, adrenodoxin reductase, and NADPH-cytochrome P-450 reductase. These reductions were related to the reduction potentials of these pseudo-substrates. However, the enzyme responsible for the reduction of megazol is unknown. On the other hand, the effect of megazol in the presence of the enzymes lipoamide dehydrogenase of *T. cruzi* and trypanothione reductases was analyzed. It was found that megazol cannot inhibit physiological reactions, but it turned out to be a weak substrate of both flavoenzymes. The monoelectronic reduction of megazol, Nfx, and metronidazole, by NADPH-cytochrome P-450 reductase, rat liver, and trypanosome, was monitored through ESR experiments. It was confirmed that megazol interferes with the oxygen metabolism of the parasite such as Nfx and metronidazole, but its extra activity compared to Nfx may be related to other properties not determined [71]. In addition, it should be noted that these results are interesting since the serious side effects and their carcinogenicity of the nitro compounds must be considered.

In other research, 5-nitrofuryl thiosemicarbazone derivatives (Fig. 3.13) were used as potential drugs [72]. In vitro activity and the mechanism of action of these compounds against *T. cruzi* showed that they are capable of free radical production when were incubated in the presence of mammalian liver microsomes. All studied compounds showed an ESR spectrum in microsomal incubations after a brief induction period of 1–2 min. The theoretical rationalization for this biological behavior

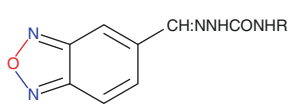

a R = Buthyl
b R = Hexyl
c R = 3-(dimethylamino)propyl
d R = 3-(diethylamino)propyl

Fig. 3.14 Structure of 1,2,5-oxadiazole *N*-oxide family studied as an antitrypanosomal drug

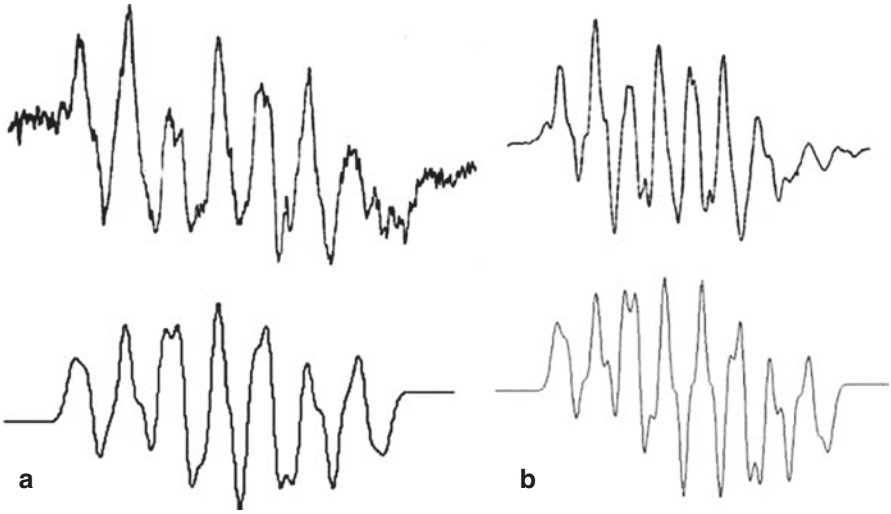

Fig. 3.15 (**a**) Experimental spectrum of *N*-oxide derivate generated by the microsomal system (Fig. 3.14a) and the corresponding computer simulation (bottom). (**b**) Experimental spectrum of *N*-oxide derivate generated by the microsomal system (Fig. 3.14c) and the corresponding computer simulation of the same spectrum (bottom)

showed similar values of atomic charge on NO_2 nitrogen, confirming the results obtained in the ESR experiments. Thus, studied compounds have similar electrochemical behavior, so they could act biologically in an initial redox pathway.

The *N*-oxide moiety from diverse compounds studied has shown to be responsible for the biological activity of a wide variety of families of drugs (with antitumor or antibacterial activities) through the production of free radical species such as the nitro pharmacophore of antitrypanosomal drugs [73, 74].

Other studies have reported the behavior of 1,2,5-oxadiazole *N*-oxide family (Fig. 3.14) against epimastigote form of *T. cruzi* to determine their antitrypanosomal activities in vitro [75].

ESR assays showed the easy reduction of the *N*-oxide fragment. In addition, these compounds possess within their skeleton the conjugation of an *N*-oxide fragment and another semicarbazide fragment such as trypanothione, the substrate of the trypanothione reductase enzyme. This substrate is used in the protection system of trypanosomatids, against oxidative stress. The research group of Dr. Olea described the formation of the free radical that is generated through the microsomal reduction of these *N*-oxide compounds, using ESR spectroscopy (Fig. 3.15) [69].

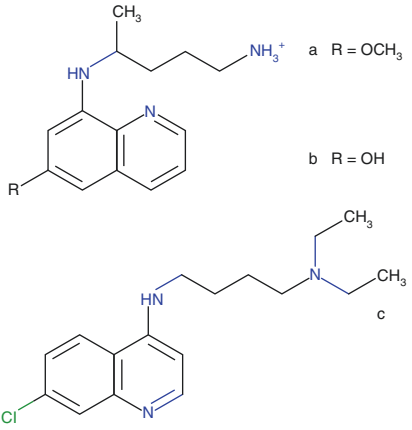

Fig. 3.16 Structure of different 8-aminoquinoline compounds. (**a**) Primaquine; (**b**) 6-hydroxyprimaquine; (**c**) chloroquine

The same hyperfine patterns were obtained either by a biochemical generation or by electrochemical reduction. In addition, the ESR spectra allowed to determine that the reduction mechanism of these compounds includes the protonation of the *N*-oxide fragment, also confirmed by cyclic voltammetry.

As seen, oxidative stress would possibly play a key role in several fatal endpoints caused by other diseases, and it represents the most promising explanation for antiprotozoal therapy. The detoxification of ROS could be a challenge for erythrocytes infected with plasmodia. In this regard, it's attention-grabbing to notice that a variety of medicine presently in clinical use exert their activities, a minimum of parts, by increasing oxidative stress within the parasitized blood cell [76]. That's the case of antimalarial compound primaquine belonging to the pharmacological family of 8-aminoquinolines (Fig. 3.16a), because it is the sole tissue schizonticide presently out there for free radical treatment of this protozoal infection. Its utility is compromised by its toxicant effects on erythrocytes and so was one among the primary agents recognized to produce oxidative stress [77, 78].

A controversy that still had to be settled corresponded to whether the pharmacological effects of antimalarial were due to the original compound or to some of its metabolites. The presence of the radical derived from primaquine was detected through ESR spectroscopy caused by protein oxidation catalyzed by horseradish peroxidase-H_2O_2 or methaemoglobin-H_2O_2. A series of oxidations that occur to the original product alter its composition through various rearrangements and addition reactions. Despite these oxidations, the ESR parameters obtained were compared with data reported in the literature. It was found that the parameters correspond to a benzidine-type rearrangement. The occurrence of this benzidine-type radical is mainly due to the presence of nucleophilic groups that cause condensation reactions which accounts for the polymeric nature of the reaction products. A similar ESR pattern was obtained by studying the protein oxidation of 6-hydroxyprimagine (Fig. 3.16b) at pH 9.0. Computational simulations of the ESR spectra indicated that the radicals contain two primaquine fragments. In vitro oxidation of this compound leads to the formation of a stable radical intermediate in the presence of oxygen.

This opens a new a new route to explore an alternative to analyze the effects of primaquine.

Several mechanisms of action have been determined for the drugs used in antimalarial chemotherapy. Chloroquine compound (Fig. 3.16c) acts by inhibiting the malarial heme detoxification (ferri-/ferroprotoporphyrin IX, FP), and its activity increases when GSH levels are reduced. It was determined that the redox cycle of the primaquine metabolites (Fig. 3.16a) exerts a tremendous oxidative stress; the same thing happens when artemisinin was used (Fig. 3.17) (usually called qinghaosu), which reacts with heme fragment forming cytotoxic radicals [79, 80].

In other studies was found another mechanism of action for primaquine and has been characterized by ESR [81]. Erythrocytes from mice with or without the malarial parasite *Plasmodium berghei* reduce the water-soluble spin probes, such as 2,2,6,6-tetramethylpiperidine-*N*-oxyl (TEMPO) (Fig. 3.18a), 2,2,6,6-tetramethylpiperidine-4-hydroxy-*N*-oxyl (TEMPOL) (Fig. 3.18b), and 2,2,6,6-tetramethylpiperidine-4-keto-*N*-oxyl (TEMPONE) (Fig. 3.18c) at similar rates in the presence or absence of oxygen.

ESR spectrum for the lipid-soluble spin probe 5-doxylstearate (Fig. 3.19) showed a stable incorporation into erythrocytes from mice without the infection. In the assessment, parasitized red cells lessen this nitroxide probe, at a fee which increases

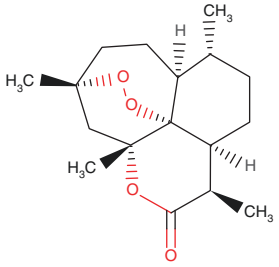

Fig. 3.17 Structure of artemisinin

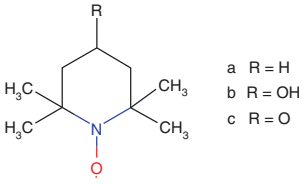

Fig. 3.18 The general structure for the spin probes TEMPO, TEMPOL, and TEMPONE

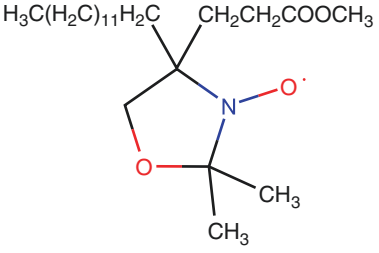

Fig. 3.19 Spin probe 5-doxylstearate

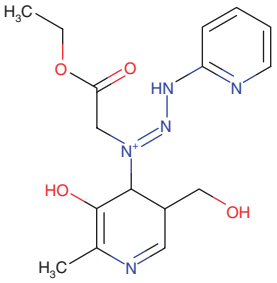

Fig. 3.20 Structure for iron chelator code-named L2-9

with the extent of parasitemia and inhibitors of electron transport chain such as KCN and NaN_3 growth the reduction.

This would assume then that nitroxide reduction occurs through the electron transport chain in the parasite. Primaquine causes reduction for as well as in water-soluble and lipid-soluble spin probes, demonstrating that this behavior is independent of their potential to liberate H_2O_2 from oxyhemoglobin. The increase of NADPH increases the speed of the reduction of the nitroxide radicals. Chloroquine has no such behavior.

Six hours prior to ESR measurements, parasitized mice treated with chloroquine display less nitroxide decreasing capability than untreated mice. It is possible to conclude that these antimalarial drugs have diametrically different behaviors.

Malaria parasites are more susceptible to oxidative stress than their host erythrocytes in general terms. There is an exception founded in the parasite *Plasmodium falciparum* (FCR-3). This parasite proved to be resistant to chloroquine. In vitro studies showed that it is susceptible when using an iron chelator (1-[*N*-ethoxycarbonylmethylpyridoxylidenium]-2-[2′-pyridyl]hydrazine bromide (code-named L2-9)) (Fig. 3.20) as a treatment. This allowed determining that the presence of iron is necessary and not the presence of oxygen. Spectrophotometric studies confirmed that an electron transfer process would generate radical species, which were detected by ESR using spin traps. L2-9-Fe(II) could generate radicals in the presence or absence of cells. In addition, it was found that L2-9-Fe(III) produced radicals only in the presence of actively metabolizing cells [76].

Another interesting group of molecules, quinones, are pigments located in different plants and fungi, and some have been shown to be antitumor drugs [82]. They are substrates for flavoenzymes and might go through mono- or bi-electron reduction, an important behavior in determining the cytotoxic and antitumor impact of quinones [83–85].

Quinones shown through one-electron reduction generate semiquinone radicals, which may reduce molecular oxygen to superoxide anion radical in a redox-cycle process under aerobic environments. Some research investigated the possible role of cytochrome P-450 in the one-electron reduction of quinoid compounds as well as in the formation of reduced oxygen species. ESR spin trapping technique has been used to detect the free radicals formed [86].

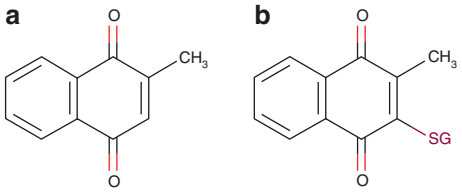

Fig. 3.21 (**a**) Structure of compound menadione; (**b**) structure for compound thiodione

Fig. 3.22 Structure of MNP spin trap

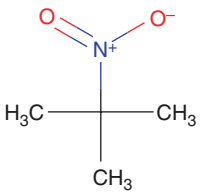

Transient radical intermediaries of the semiquinone type were identified by ESR spectroscopy and by the nonenzymatic reaction of menadione (Fig. 3.21a) and 1,4-naphthoquinone [87]. It was found that the first compound causes the loss of cellular thiols since it could react with ROS and by arylation of GSH and other sulfhydryl groups. This causes the formation of thiodione (Fig. 3.21b) [88]. The compounds were subjected, in the presence of GSH, to form the corresponding semiquinones. It was determined that at low concentrations of GSH only a reduction of the corresponding semiquinones (1,4-naphthoquinone) was detected [89].

Artemisinin (Fig. 3.17) (and derivatives) does not share structural structures common to other known antimalarial drugs. This structural difference would imply that its mechanism of action was different. Certain studies carried out showed or revealed part of the mechanism of this compound. The results showed that the endoperoxide bridge plays an important role in the antimalarial properties of artemisinin [90, 91]. The presence of a peroxide fragment implies that it is a source of ROS which would generate oxygen-centered radicals such as hydroxyl and superoxide. This fact would indicate that free radicals would be related to the mechanism of action of artemisinin. This was corroborated during the decade of the 1980s [92]. Experimental evidence suggests that the most likely mechanism of action would involve the heme-mediated breakdown of the endoperoxide bridge which will produce free radicals centered on carbon. The use of the 2-methyl-2-nitrosopropane trap (MNP) (Fig. 3.22) provided evidence on the participation of free radicals in the in vitro cleavage of artemisinin-like compounds [93, 94].

The behavior of the bacterium *Mycobacterium leprae* (responsible for leprosy) and the parasite *Leishmania donovani* (responsible for visceral leishmaniasis (VL)) was studied. It was determined that both pathogens persist in the human host staying in mononuclear phagocytes. This comparison showed that the control of parasites comes from the activation of macrophages with an expression of inducible nitric oxide synthase (*i*NOS), synthesis of nitric oxide, and extensive nitration of parasites. The

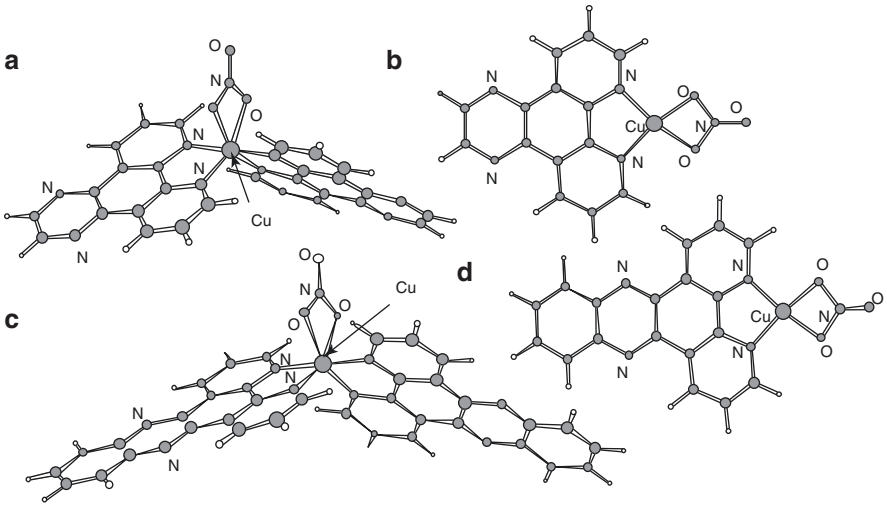

Fig. 3.23 Structure for the paramagnetic complex with the capacity of intercalated DNA

nitration agent was identified as a peroxynitrite derivative. In vitro studies confirmed that peroxynitrite is cytotoxic to parasites, while nitric oxide is cytostatic. This would imply that the peroxynitrite would react with the carbon dioxide forming the carbonate radical anion on the one hand and the formation of nitrogen dioxide. The joint action of both compounds leads finally to the nitration of the parasite [95, 96].

Several research groups have studied the mechanism of action that involves free radicals. Other research groups have focused on the design and synthesis of new antiprotozoal agents. The synthesis and characterization of new compounds through the coordination of antiprotozoal organic drugs have shown to have an important biological activity [97]. These compounds interact with DNA and establish that one of the possible mechanisms is the generation of free radicals [98].

Another example of synthesized compounds corresponds to the paramagnetic organometallic complexes $[Cu(dppz)(NO_3)]NO_3$ (Fig. 3.23d), $[Cu(dppz)_2(NO_3)]NO_3$ (Fig. 3.23c), $[Cu(dpq)(NO_3)]NO_3$ (Fig. 3.23b), and $[Cu(dpq)_2(NO_3)]NO_3$ (Fig. 3.23a). It was determined that these organometal complexes possess antiparasitic activity through the DNA interchange mechanism [99].

The biological activity of these copper complexes was determined using ESR spectroscopy and was evaluated in promastigotes of *Leishmania braziliensis*. These compounds showed activity as leishmanicidal, especially the compound $[Cu(dppz)_2(NO_3)]NO_3$ (Fig. 3.23c). In this case, the use of ESR was limited to studying geometric changes of symmetry in the copper plane.

References

1. WHO. What is chagas disease? WHO. Available at: http://www.who.int/chagas/disease/en/. Accessed 24 May 2017.
2. Schaub GA. Direct transmission of Trypanosoma cruzi between vectors of Chagas' disease. Acta Trop. 1988;45:11–9.

3. Schaub GA, Böker CA. Colonization of the rectum of Triatoma infestans by Trypanosoma cruzi studied by scanning electron microscopy: influence of blood uptake by the bug. Parasitol Res. 1987;73:417–20.
4. Schaub GA, Lösch P. Trypanosoma cruzi: origin of metacyclic trypomastigotes in the urine of the vector Triatoma infestans. Exp Parasitol. 1988;65:174–86.
5. Rodríguez EM, Briceño L, Chiurillo MA, Mosca W, Campos Y. Tripanosomiasis americana: aspectos teóricos. Curso Latinoamericano sobre Enfermedades Infecciosas, Instituto de Biomedicina UCV. 25 Octubre - 12 Noviembre 2004.
6. Kelly JM, Taylor MC, Rudenko G, Blundell PA. Transfection of the African and American trypanosomes. Methods Mol Biol Clifton NJ. 1995;47:349–59.
7. Goldsmith RS. Infectious disease: protozoal. In: Schroeder SA, editor. Current medical diagnosis and treatment. New York: Appleton & Lange; 1991. p. 536–50.
8. Prata A. American trypanosomiases (Chagas disease). In: Goldsmith R, Heyneman D, editors. Tropical medicine & medical parasitology. New York: Lange Medical Publications; 1990. p. 274–5.
9. Hoffand R, Boyer MH. Immunology of Chagas' disease. In: Tizard I, editor. Immunology and pathogenesis of trypanosomiasis. Florida: CRC Press; 1985. p. 145–83.
10. Solana ME, Katzin AM, Umezawa ES, Miatello CS. High specificity of Trypanosoma cruzi epimastigote ribonucleoprotein as antigen in serodiagnosis of Chagas' disease. J Clin Microbiol. 1995;33:1456–60.
11. Hausladen A, Stamler JS. Nitrosative stress. In: Oxidants and antioxidants. Texas: Gulf Professional Publishing; 1999.
12. Berlett BS, Stadtman ER. Protein oxidation in aging, disease, and oxidative stress. J Biol Chem. 1997;272:20313–6.
13. Henle ES, Linn S. Formation, prevention, and repair of DNA damage by iron/hydrogen peroxide. J Biol Chem. 1997;272:19095–8.
14. Steinberg D. Low density lipoprotein oxidation and its pathobiological significance. J Biol Chem. 1997;272:20963–6.
15. Fridovich I. Superoxide anion radical (O2-.), superoxide dismutases, and related matters. J Biol Chem. 1997;272:18515–7.
16. Schöpfer F, et al. Oxidation of ubiquinol by peroxynitrite: implications for protection of mitochondria against nitrosative damage. Biochem J. 2000;349:35–42.
17. Brown GC. Nitric oxide and mitochondrial respiration. Biochim Biophys Acta. 1999;1411:351–69.
18. Prescott SM. A thematic series on oxidation of lipids as a source of messengers. J Biol Chem. 1999;274:22901.
19. Tien M, Berlett BS, Levine RL, Chock PB, Stadtman ER. Peroxynitrite-mediated modification of proteins at physiological carbon dioxide concentration: pH dependence of carbonyl formation, tyrosine nitration, and methionine oxidation. Proc Natl Acad Sci U S A. 1999;96:7809–14.
20. Bundy RE, Marczin N, Chester AH, Yacoub M. A redox-based mechanism for nitric oxide-induced inhibition of DNA synthesis in human vascular smooth muscle cells. Br J Pharmacol. 2000;129:1513–21.
21. Kim YM, et al. Inhibition of protein synthesis by nitric oxide correlates with cytostatic activity: nitric oxide induces phosphorylation of initiation factor eIF-2 alpha. Mol Med. 1998;4:179–90.
22. Lu SC. Regulation of glutathione synthesis. Curr Top Cell Regul. 2000;36:95–116.
23. Pieper AA, Verma A, Zhang J, Snyder SH. Poly (ADP-ribose) polymerase, nitric oxide and cell death. Trends Pharmacol Sci. 1999;20:171–81.
24. de Molina R, del María C. El estrés oxidativo y el destino celular. QuímicaViva. 2003;2:17–28.
25. Olea-Azar C, Rigol C, Mendizabal F, Briones R. Applications of electron spin resonance and spin trapping in tropical parasitic diseases. Mini Rev Med Chem. 2006;6:211–20.
26. Rojas Wahl RU, Zeng L, Madison SA, DePinto RL, Shay BJ. Mechanistic studies on the decomposition of water soluble azo-radical-initiators. J Chem Soc Perkin Trans 2. 1998;9:2009–18.
27. Jenkins CA, Murphy DM, Rowlands CC, Egerton TA. EPR study of spin-trapped free radical intermediates formed in the heterogeneously-assisted photodecomposition of acetaldehyde. J Chem Soc Perkin Trans 2. 1997:2479–86.

28. Santos CX, Anjos EI, Augusto O. Uric acid oxidation by peroxynitrite: multiple reactions, free radical formation, and amplification of lipid oxidation. Arch Biochem Biophys. 1999;372:285–94.
29. Hawkins CL, Davies MJ. Degradation of hyaluronic acid, poly- and mono-saccharides, and model compounds by hypochlorite: evidence for radical intermediates and fragmentation. Free Radic Biol Med. 1998;24:1396–410.
30. Misík V, Riesz P. Recent applications of EPR and spin trapping to sonochemical studies of organic liquids and aqueous solutions. Ultrason Sonochem. 1996;3:S173–86.
31. Stolze K, Udilova N, Nohl H. Spin trapping of lipid radicals with DEPMPO-derived spin traps: detection of superoxide, alkyl and alkoxyl radicals in aqueous and lipid phase. Free Radic Biol Med. 2000;29:1005–14.
32. Dikalov SI, Mason RP. Spin trapping of polyunsaturated fatty acid-derived peroxyl radicals: reassignment to alkoxyl radical adducts. Free Radic Biol Med. 2001;30:187–97.
33. Ma Z, Zhao B, Yuan Z. Application of electrochemical and spin trapping techniques in the investigation of hydroxyl radicals. Anal Chim Acta. 1999;389:213–8.
34. Gianni L, Zweier JL, Levy A, Myers CE. Characterization of the cycle of iron-mediated electron transfer from Adriamycin to molecular oxygen. J Biol Chem. 1985;260:6820–6.
35. Sankarapandi S, Zweier JL. Evidence against the generation of free hydroxyl radicals from the interaction of copper, zinc-superoxide dismutase and hydrogen peroxide. J Biol Chem. 1999;274:34576–83.
36. Zweier JL, Flaherty JT, Weisfeldt ML. Direct measurement of free radical generation following reperfusion of ischemic myocardium. Proc Natl Acad Sci U S A. 1987;84:1404–7.
37. Zweier JL, Kuppusamy P, Lutty GA. Measurement of endothelial cell free radical generation: evidence for a central mechanism of free radical injury in postischemic tissues. Proc Natl Acad Sci U S A. 1988;85:4046–50.
38. Zweier JL, et al. Measurement and characterization of postischemic free radical generation in the isolated perfused heart. J Biol Chem. 1989;264:18890–5.
39. Mackor A, Wajer TAJW, de Boer TJ. C-nitroso compounds. Part VI. Acyl-alkyl-nitroxides from acyl radicals and nitroso compounds as studied by ESR. Tetrahedron. 1968;24:1623–31.
40. Mackor A, Wajer TAJW, de Boer TJ, van Voorst JDW. C-nitroso compounds. Part I. The formation of nitroxides by photolysis of nitroso compounds as studied by electron spin resonance. Tetrahedron Lett. 1966;7:2115–23.
41. Mackor A, Wajer TAJW, de Boer TJ, van Voorst JDW. C-nitroso compounds. Part III. Alkoxy-alkyl-nitroxides as intermediates in the reaction of alkoxy-radicals with nitroso compounds. Tetrahedron Lett. 1967;8:385–90.
42. Iwamura M, Inamoto N. Novel radical 1,3-addition to nitrones. Bull Chem Soc Jpn. 1967;40:702.
43. Iwamura M, Inamoto N. Novel formation of nitroxide radicals by radical addition to nitrones. Bull Chem Soc Jpn. 1967;40:703.
44. Iwamura M, Inamoto N. Reactions of nitrones with free radicals. II. Formation of nitroxides. Bull Chem Soc Jpn. 1970;43:860–3.
45. Chalfont GR, Perkins MJ, Horsfield A. Probe for homolytic reactions in solution. II. Polymerization of styrene. J Am Chem Soc. 1968;90:7141–2.
46. Janzen EG, Blackburn BJ. Detection and identification of short-lived free radicals by an electron spin resonance trapping technique. J Am Chem Soc. 1968;90:5909–10.
47. Lagercrantz C, Forshult S. Trapping of Free Radicals formed by g-Irradiation of Organic Compounds. Nature. 1968;218:1247–8.
48. Emmons W, The D. Preparation and properties of oxaziranes. J Am Chem Soc. 1957;79:5739–54.
49. Bonnett R, Brown RFC, Clark VM, Sutherland IO, Todd A. Experiments towards the synthesis of corrins. Part II. The preparation and reactions of D1-pyrroline 1-oxides. J Chem Soc Resumed. 1959:2094–102.
50. de Boer TJ. Spin-trapping in early and some recent nitroso chemistry. Can J Chem. 1982;60:1602–9.

51. Ozawa T, Hanaki A. Spin-trapping of superoxide ion by a water-soluble, nitroso-aromatic spin-trap. Biochem Biophys Res Commun. 1986;136:657–64.
52. Stolze K, Mason RP. Spin trapping artifacts in DMSO. Biochem Biophys Res Commun. 1987;143:941–6.
53. Wargon JA, Williams E. Electron spin resonance studies of radical trapping in the radiolysis of organic liquids. I. Evidence for the primary formation of the methoxy radical in methanol. J Am Chem Soc. 1972;94:7917–8.
54. Janzen EG. Spin trapping. Acc Chem Res. 1971;4:31–40.
55. Buettner GR. Spin trapping: ESR parameters of spin adducts 1474 1528V. Free Radic Biol Med. 1987;3:259–303.
56. Li ASW, Chignell CF. The NoH value in EPR spin trapping: a new parameter for the identification of 5,5-dimethyl-1-pyrroline-N-oxide spin adducts. J Biochem Biophys Methods. 1991;22:83–7.
57. Finkelstein ELI, Rosen GM, Rauckman EJ, Paxton J. Spin Trapping of Superoxide. Mol Pharmacol. 1979;16:676–85.
58. Docampo R. Sensitivity of parasites to free radical damage by antiparasitic drugs. Chem Biol Interact. 1990;73:1–27.
59. Cerecetto H, et al. Formal potentials of new analogues of nifurtimox: relationship to activity. Farmacoterapia. 1992;47:1207–13.
60. Cerecetto H, et al. Synthesis and anti-trypanosomal activity of novel 5-nitro-2-furaldehyde and 5-nitrothiophene-2-carboxaldehyde semicarbazone derivatives. Il Farmaco. 1998;53:89–94.
61. Maio RD, et al. Synthesis and antichagasic properties of new 1,2,6-thiadiazin-3,5-dione 1,1-dioxides and related compounds. Arzneimittelforschung. 1999;49:759–63.
62. Cerecetto H, et al. Synthesis and antitrypanosomal evaluation of E-isomers of 5-nitro-2-furaldehyde and 5-nitrothiophene-2-carboxaldehyde semicarbazone derivatives. Structure–activity relationships. Eur J Med Chem. 2000;35:343–50.
63. Docampo R, Moreno SN. Free radical metabolites in the mode of action of chemotherapeutic agents and phagocytic cells on Trypanosoma cruzi. Rev Infect Dis. 1984;6:223–38.
64. Hazra B, Sur P, Roy DK, Sur B, Banerjee A. Biological activity of diospyrin towards Ehrlich ascites carcinoma in Swiss A mice. Planta Med. 1984;50:295–7.
65. Estani SS, Segura EL. Treatment of Trypanosoma cruzi infection in the undetermined phase. Experience and current guidelines of treatment in Argentina. Mem Inst Oswaldo Cruz. 1999;94:363–5.
66. Díaz EG, Montalto de Mecca M, Castro JA. Reactions of nifurtimox with critical sulfhydryl-containing biomolecules: their potential toxicological relevance. J Appl Toxicol. 2004;24:189–95.
67. Olea-Azar C, et al. Cyclic voltammetry and electron paramagnetic resonance studies of some analogues of nifurtimox. Spectrosc Lett. 1998;31:99–109.
68. Olea-Azar C, Atria AM, di Maio R, Seoane G, Cerecetto H. Electron spin resonance and cyclic voltammetry studies of nitrofurane and nitrothiophene analogues of nifurtimox. Spectrosc Lett. 1998;31:849–57.
69. Olea-Azar C, et al. ESR spin trapping studies of free radicals generated from nitrofuran derivative analogues of nifurtimox by electrochemical and Trypanosoma cruzi reduction. Free Radic Res. 2003;37:993–1001.
70. Tsuhako MH, Alves MJM, Colli W, Brener Z, Augusto O. Restricted bioreductive metabolism of a nitroimidazole-thiadiazole derivative with curative action in experimental Trypanosoma cruzi infections. Biochem Pharmacol. 1989;38:4491–6.
71. Viodé C, et al. Enzymatic reduction studies of nitroheterocycles. Biochem Pharmacol. 1999;57:549–57.
72. Aguirre G, et al. In vitro activity and mechanism of action against the protozoan parasite Trypanosoma cruzi of 5-nitrofuryl containing thiosemicarbazones. Bioorg Med Chem. 2004;12:4885–93.
73. Cahill A, White INH. Reductive activation of N-oxides to cause DNA strand breakage in cell lines in vitro. Biochem Soc Trans. 1991;19:127S.

74. Brown JM. redox activation of benzotriazine n-oxides: mechanisms and potential as anticancer drugs. In: Adams PGE, Breccia PA, Fielden DEM, Wardman PP, editors. Selective activation of drugs by redox processes. New York: Springer; 1990. p. 137–48. https://doi.org/10.1007/978-1-4615-3768-7_12.
75. Cerecetto H, et al. 1,2,5-oxadiazole n-oxide derivatives and related compounds as potential antitrypanosomal drugs: structure−activity relationships. J Med Chem. 1999; 42:1941–50.
76. Iheanacho EN, Sarel S, Samuni A, Avramovici-Grisaru S, Spira DT. Growth inhibition of Plasmodium falciparum involving carbon centered iron-chelate radical (L., X-)-Fe(III) based on pyridoxal-betaine. A novel type of antimalarials active against chloroquine-resistant parasites. Free Radic Res Commun. 1991;15:1–10.
77. Cohen G, Hochstein P. Generation of hydrogen peroxide in erythrocytes by hemolytic agents. Biochemistry. 1964;3:895–900.
78. Holtzman JL. Role of reactive oxygen and metabolite binding in drug toxicity. Life Sci. 1982;30:1–9.
79. Vásquez-Vivar J, Augusto O. Oxidative activity of primaquine metabolites on rat erythrocytes IN vitro and in vivo. Biochem Pharmacol. 1994;47:309–16.
80. Becker K, et al. Oxidative stress in malaria parasite-infected erythrocytes: host–parasite interactions. Int J Parasitol. 2004;34:163–89.
81. Deslauriers R, Butler K, Smith ICP. Oxidant stress in malaria as probed by stable nitroxide radicals in erythrocytes infected with Plasmodium berghei. The effects of primaquine and chloroquine. Biochim Biophys Acta. 1987;931:267–75.
82. Driscoll JS, Hazard GF, Wood HB, Goldin A. Structure-antitumor activity relationships among quinone derivatives. Cancer Chemother Rep 2. 1974;4:1–362.
83. Lind C, Hochstein P, Ernster L. DT-diaphorase as a quinone reductase: A cellular control device against semiquinone and superoxide radical formation. Arch Biochem Biophys. 1982;216:178–85.
84. Thor H, et al. The metabolism of menadione (2-methyl-1,4-naphthoquinone) by isolated hepatocytes. A study of the implications of oxidative stress in intact cells. J Biol Chem. 1982;257:12419–25.
85. Thor H, Smith MT, Hartzell P, Orrenius S. Toxic and nontoxic pathways during metabolism of menadione (2-methyl-1,4- naphthoquinone) in isolated hepatocytes. In: Hietanen E, Laitinen M, Hanninen O, editors. Cytochrome P-450, biochemistry, biophysics and environmental implications. New York: Elsevier; 1982. p. 729–32.
86. van de Straat R, de Vries J, Vermeulen NPE. Role of hepatic microsomal and purified cytochrome P-450 in one-electron reduction of two quinone imines and concomitant reduction of molecular oxygen. Biochem Pharmacol. 1987;36:613–9.
87. Takahashi N, Schreiber J, Fischer V, Mason RP. Formation of glutathione-conjugated semiquinones by the reaction of quinones with glutathione: An ESR study. Arch Biochem Biophys. 1987;252:41–8.
88. Wefers H, Sies H. Hepatic low-level chemiluminescence during redox cycling of menadione and the menadione-glutathione conjugate: Relation to glutathione and NAD(P)H:quinone reductase (DT-diaphorase) activity. Arch Biochem Biophys. 1983;224:568–78.
89. Gant TW, Doherty M, Odowole D, Sales KD, Cohen GM. Semiquinone anion radicals formed by the reaction of quinones with glutathione or amino acids. FEBS Lett. 1986;201:296–300.
90. Chemical studies on qinghaosu (artemisinine). China Cooperative Research Group on qinghaosu and its derivatives as antimalarials. J Tradit Chin Med. 1982;2:3–8.
91. Brossi A, et al. Arteether, a new antimalarial drug: synthesis and antimalarial properties. J Med Chem. 1988;31:645–50.
92. Halliwell B, Gutteridge JM. Free radicals in biology and medicine. Oxford: Oxford University Press; 2015.
93. Wu W-M, et al. Unified mechanistic framework for the Fe(II)-induced cleavage of Qinghaosu and derivatives/analogues. The first spin-trapping evidence for the previously postulated secondary C-4 Radical. J Am Chem Soc. 1998;120:3316–25.

94. Wu W-M, Chen Y-L, Zhai Z, Xiao S-H, Wu Y-L. Study on the mechanism of action of artemether against schistosomes: the identification of cysteine adducts of both carbon-centred free radicals derived from artemether. Bioorg Med Chem Lett. 2003;13:1645–7.
95. Chan J, et al. Microbial glycolipids: possible virulence factors that scavenge oxygen radicals. Proc Natl Acad Sci U S A. 1989;86:2453–7.
96. Linares E, et al. Role of peroxynitrite in macrophage microbicidal mechanisms in vivo revealed by protein nitration and hydroxylation. Free Radic Biol Med. 2001;30:1234–42.
97. Navarro M, et al. Toward a novel metal-based chemotherapy against tropical diseases. Part 5. Synthesis and characterization of new Ru(II) and Ru(III) clotrimazole and ketoconazole complexes and evaluation of their activity against Trypanosoma cruzi. Polyhedron. 2000;19:2319–25.
98. Cerecetto H, et al. 1, 2, 4-Triazine n-oxide derivatives: studies as potential hypoxic cytotoxins. Part III. Arch Pharm (Weinheim). 2004;337:271–80.
99. Navarro M, et al. Design of copper DNA intercalators with leishmanicidal activity. J Biol Inorg Chem. 2003;8:401–8.

Measurement of Oxidative Stress Using ESR Spectroscopy

4

Siavash Iravani and Ghazaleh Jamalipour Soofi

4.1 Introduction

In general, reactive oxygen species as free radicals (e.g., superoxide, hydrogen peroxide, hydroxyl radical, and singlet oxygen) contribute to the event of quite few very important ailments by inflicting oxidative stress and might damage cellular targets [1, 2]. Reactive oxygen species will initiate cellular tissue injury by approach of modifying lipids, proteins, and deoxyribonucleic acid, which might considerably subsume cell health and viability or induce a spread of cell responses via an era of secondary reactive species, mainly to cell dying by necrosis or apoptosis. However, entire signal for this association is frequently deficient, thanks to the fact of known shortcomings with strategies accessible to examine oxidative stress status in vivo in humans [3]. Oxidative stress is related to the pathogenesis of diabetes, cancer, obesity, aging, neurodegenerative disorders, inflammation, hypertension, cardiovascular disease, apoptosis, heart failure, and cardiovascular ailments [4]. Oxidative stress triggered by reactive oxygen species takes place when the formation of reactive oxygen species exceeds the potential of the cell to detoxify these doubtlessly injurious oxidants using endogenous antioxidant protection systems. But, wherever associate degree excessive amount of reactive oxygen species is generated or protection mechanisms are impaired, oxidative stress resulting in events together with lipid peroxidation [5, 6]. This matter is extremely illustration in countless pathological conditions within the central nervous system (e.g., stroke) [7]. Oxidative stress occurs when the formation of reactive oxygen species exceeds the capability of the cell to detoxify these most likely injurious oxidants using endogenous antioxidant defense systems. Conditions connected with oxidative stress include

S. Iravani (✉)
Faculty of Pharmacy and Pharmaceutical Sciences, Isfahan University of Medical Sciences, Isfahan, Iran

G. J. Soofi
Radiology Department, Isfahan University of Medical Sciences, Isfahan, Iran

A. K. Shukla (ed.), *Electron Spin Resonance Spectroscopy in Medicine*,
https://doi.org/10.1007/978-981-13-2230-3_4

ischemia/reperfusion, hypercholesterolemia, diabetes, cardiovascular disease, and hypertension [8–10]. The adhesion of circulating blood cells (leukocytes and platelets) to vascular endothelium is an important factor in the pro-inflammatory and prothrombogenic phenotype assumed by the vasculature in these and totally different ailment states that are associated with oxidative stress. There are a lot of evidences that hyperlink the blood cell-endothelial cell interactions in these prerequisites to the additional appropriate production of reactive oxygen species [11].

Electron spin resonance (ESR) is one in all the foremost dependable and powerful strategies for the detection of reactive oxygen species (in the structure of free radicals) in biological tissues and cells. As an example, ESR-based technique in order to decide the outcomes of reactions caused with the aid of reactive oxygen species in bio-organic systems in vitro and in vivo with an emphasis on a rodent disease model has been developed [12–14]. Relating to in vitro ESR applications, spin trapping method is well acknowledged as ESR spin adduct to discover reactive oxygen species, quantifying spin concentration in experimental systems. Furthermore, for in vivo ESR applications, nitroxyl radicals are very appropriate as exogenous spin probes to measure free radical distribution, oxygen concentration, and redox metabolism in biological systems [15–18]. It was demonstrated that the blood-brain barrier (BBB)-permeable molecule 3-methoxycarbonyl-2,2,5,5-tetramethyl-pyrrolidine-1-oxyl (MC-PROXYL) is an appropriate spin probe for the study of free radical reactions induced by reactive oxygen species in the brains of small animal models using in vivo ESR detection technique. Quantitative ESR analysis using MC-PROXYL is useful for understanding redox status under conditions of oxidative stress in the rodent brain [12–14]. Findings from researches and literatures showed that oxidative stress played an indispensable function in the vascular injury which took place in cardiovascular disease, hypertension, and stroke [19–21]. In this chapter, some necessary issues about the detection and measurement of oxidative stress using ESR spectroscopy have been mentioned.

4.2 ESR Spectroscopy and Oxidative Stress

By using ESR, free radicals can be seen quickly and specifically, since it detects the presence of unpaired electrons. However, ESR detects only fairly unreactive radicals, thanks to the fact that reactive ones do not accumulate to sufficiently high ranges to be measured. Therefore, spin traps or spin probes (agents that intercept reactive radicals) can be used in order to react with reactive radicals to form stable ones which can be detected via ESR spectroscopy. Relating to in vitro ESR applications, spin trapping technique could be a recognized approach for detection and quantification of reactive oxygen species concentrations in experimental systems. Moreover, vital developments in $_{L}$-band and in vivo ESR methods have provided helpful data on oxidative stress in biological structures [7, 20–26].

Recently, massive enhancements within the subject of ESR imaging have currently created it doable to examine the distribution and metabolism of free radicals, and also the degree of tissue oxygenation, in vivo. ESR is beneficial for investigation of the redox status of living organisms, noninvasively. This method is especially

helpful for distinctive in vivo spatial distribution of free radicals in animals. It was demonstrated that the in vivo ESR/nitroxyl spin probe strategies may well be an efficient tool to become aware of free radicals selectively and to monitor free radical reactions in vivo [27–29]. An in vivo ESR imaging system was developed with high-quality ESR-computed tomography images or reconstructed three-dimensional images by using MC-PROXYL in a rodent model [13]. Consequently, it was suggested that ESR-computed tomography imaging could be a useful tool for monitoring and detecting the areas of oxidative stress in the brains of rodent animal models [13]. It needs to be mentioned that such a medical indicator of acute stroke gives little information in relation to the prevention of stroke. In the near future, further improvements in the instrumentation used for ESR imaging and in the improvement of optimized nontoxic spin probes will make ESR one of the most novel diagnostic tools for acute stroke or clinical predictors for prevention of stroke. Moreover, it was indicated that ESR assessment can characterize the degree of oxidative stress in the spontaneously hypertensive rat model of hypertension and the stroke-prone spontaneously hypertensive rat model of stroke through ESR imaging system [14].

Ashton et al. [30] reported the utilization of ESR spectroscopy in conjunction with the spin trapping technique, to determine directly and immediately the formation of radical species in the venous blood of healthful human volunteer's pre- and post-exhaustive aerobic exercise. Consequently, increased lipid peroxidation and total antioxidant ability post-exercise were demonstrated. Moreover, free radical species were measured by the usage of ESR spectroscopy in the coronary sinus blood of sufferers undergoing elective cardioplegia and coronary angioplasty [31, 32].

Reactive oxygen species might be involved in the gastric ulcer formation induced by indomethacin [33]. The noninvasive measurement of reactive oxygen species to indomethacin-treated rats was done in order to assess the sites of reactive oxygen species generation. By giving orally a membrane-permeable or impermeable probe, the spectra were collected as a function of time by in vivo 300-MHz ESR spectroscopy analysis. The ESR signal-decay rates of membrane-permeable probes, hydroxy-2,2,6,6-tetramethylpiperidine-N-oxyl (TEMPO) and 3-methoxycarbonyl-2,2,5,5-tetramethyl-pyrrolidine-1-oxyl, in the gastric mucosal region were considerably increased 1 h after indomethacin treatment, and they both caused the protection of ulcer formation; however, membrane-impermeable probes, carboxy- and trimethylammonium-TEMPO, which did not exhibit the improved signal decay, had no result on ulcer formation. Findings suggested that the enhanced signal-decay rates in the gastric ulcers observed by in vivo ESR are associated with protective effects. The enhanced signal decay caused by reactive oxygen species generation in the stomach, contributing to the ulcer formation induced by indomethacin, is additionally instructed to occur at the gastric mucus layer or the interface or the intracellular compartment of epithelial cells. Overall, these results show the potentials of noninvasive assessment of reactive oxygen species production and therefore the sites of damage by in vivo ESR using nitroxyl probes directed to specific subcellular regions [33].

Oxidative stress results in an advanced dysregulation of cell metabolism and cell-cell homeostasis. It plays a very important role in the pathogenesis of insulin resistance

and β-cell dysfunction. Increased oxidative stress in diabetic patients could contribute to the pathogenesis of diabetic angiopathy (common complication of chronic diabetes). These are the two most relevant mechanisms within the pathophysiology of type 2 diabetes and its vascular complications. Then, it would conjointly result in the death in diabetic patients [4]. Sano et al. [34] used a method to work out ESR spectroscopy of reactive oxygen species and free radicals in vivo, by the usage of the nitroxide derivative, carbamoyl-PROXYL, as a probe. Diabetes was induced in rats through streptozotocin injection, and a number of other weeks later, the animals received carbamoyl-PROXYL. ESR was measured at the upper abdominal level at a frequency of 300 MHz. Consequently, the spin clearance rate was drastically greater within the diabetic rats than in control rats. Moreover, the spin clearance rate in the diabetic rats was once appreciably related with urinary malondialdehyde levels, which serve as a marker for lipid peroxidation. It absolutely was verified that noninvasive in vivo ESR measurement could in addition be helpful for evaluating oxidative stress in diabetes.

In vivo detection of a bioradical, generated from the metabolism of nitrosobenzene in live mice, was completed via using L-band ESR spectroscopy with a loop-gap resonator. An extensive three-line ESR spectrum was detected in the buttocks or stomach vicinity of a mouse after intramuscular or intraperitoneal injection of nitrosobenzene. It was suggested that one in all the primary doable targets of nitroso compounds in vivo could in addition be regions of polyunsaturated fatty acid clusters in fats or membranes [35].

4.3 ESR Spectroscopy and Antioxidant Properties of Drugs or Food Factors

Reactive oxygen species scavengers could in addition reduce edema and tissue harm in stroke. Therefore, the neuroprotective properties of anti-stroke agents should be related with their antioxidant properties, indicating reactive oxygen species scavenging endeavor [36, 37]. However, there is very little direct proof of their antioxidant properties, particularly, thanks to an absence of methods for identifying reactive oxygen species and for the evaluation of oxidative stress levels, in vivo (e.g., in stroke animal model). Consequently, extra professional efforts are wanted which used ESR techniques (both in vitro and in vivo) so as to represent antioxidant properties of neuroprotective agents. Miyazaki et al. [12] recommended that in vivo ESR strategy ought to be used clinically for the assessment and evaluation of antioxidant results of novel medicine on oxidative stress-induced illnesses in animal fashions such as stroke-prone spontaneously hypertensive rat.

4.4 Propofol

Antioxidant anesthetics like propofol (2,6-diisopropylphenol) has been related to decrease intracranial pressure and cerebral swelling than volatile anesthesia in brain tumor patients undergoing craniotomy. It directly inhibits lipid peroxidation by

using the formation of reactive oxygen species. The getable neuroprotective impact of propofol may additionally be mediated by its antioxidant properties, which are established to play a role in apoptosis, ischemia-reperfusion injury, and inflammatory-induced neuronal injury owing to the discount of lipid peroxidation via the formation of reactive oxygen species [38, 39]. Antioxidant properties of propofol and a vehicle such as medium-chain triglyceride/long-chain triglyceride using in vitro ESR spin tapping approach have been reported. Propofol medium-chain triglyceride/long-chain triglyceride reduced stroke-prone spontaneously hypertensive rat-induced oxidative stress in the brain [40]. As a result, propofol mixed with medical reagents may well be specifically helpful in adjusting levels of anesthesia in cases of reactive oxygen species-induced brain disease. It can result in the down-regulation of excessive oxidative stress, thanks to scavenging hydroxyl radical, as tested via in vitro or in vivo ESR analysis.

4.5 Crocetin

Crocetin is an herbal apocarotenoid dicarboxylic acid (yellow compound used as spice and natural food colorant) found within the stigmas of saffron (*Crocus sativus* L.) and also the fruits of *Gardenia jasminoides Ellis*. The ESR spectroscopy method was applied in order to analyze the reactive oxygen species scavenging effect of food factors like crocetin and also the decay rate constant of MC-PROXYL within the isolated brain of the stroke-prone spontaneously hypertensive rats [41]. As a result, it absolutely was incontestable that crocetin to stroke-prone spontaneously hypertensive rats was able to decrease reactive oxygen species-mediated oxidative stress in the brain because of the influence of direct antioxidant [41].

4.6 *β*-Carotene

ESR spectroscopy coupled to the spin trapping technique was applied to analysis of the effect of *β*-carotene (a chain-breaking antioxidant) and lutein on the radical adducts of the spin-trap PBN (*N*-*t*-butyl-α-phenylnitrone) generated with the help of the metal-ion breakdown of various tert-butyl hydroperoxide (t-BOOH) concentrations in methylene chloride. Moreover, the antioxidant activity of vitamin E was tested, for comparison with the carotenoids. Within the presence of α-tocopherol, peroxyl and alkoxyl radicals had been quenched, and also the tocopheroxyl radical was once detected [42].

4.7 ESR Spectroscopy and Reactive Oxygen Species Induced via Nanomaterials

One of the vital troubles related to the manufacturing of reactive oxygen species precipitated through nanomaterials is feasible health and environmental dangers related to them. Nanomaterials will have an effect on cell function through the manufacturing of

reactive oxygen species. Therefore, identification of reactive oxygen species for developing nanomaterials and grasp risks related to their use are very important. In other words, qualitative and quantitative evaluations of reactive oxygen species produced on the surfaces of nanomaterials are vital for assessment of their toxicity and toxic mechanisms. In this regard, ESR techniques for the study of reactive oxygen species generation mediated through nanomaterials have quite a few benefits in contrast to different ones [1]. However, it should be noted that the usage of ESR without first considering the physicochemical properties of nanomaterials and proper conditions of the spin trapping agent (e.g., incubation time) could in addition cause misinterpretation of the ensuing data [43]. In one interesting study, ESR approach was developed to learn about the potential of carbon nanostructures (such as carbon nanotubes and graphene oxide) to generate hydroxyl radicals. Using 5,5,-dimethylpyrroline N-oxide as a spin trap, hydroxyl radicals have been made by the usage of carbon nanotubes by using interaction with hydrogen peroxide. This formation of hydroxyl radicals can also be brought on by approach of the existence of carbonaceous and transition metallic impurities. In the study of graphene oxide, functionalized graphene oxide modified with PEGylated poly-L-lysine was found to catalyze the decomposition of hydrogen peroxide to shape hydroxyl radicals. The hydroxyl radicals were captured through 5,5,-dimethylpyrroline N-oxide and detected by using ESR [44, 45]. Furthermore, singlet oxygen can be produced with the aid of photoexcitation of metallic nanoparticles, thanks to their surface plasmon resonance (SPR) properties. TEMP and 4-oxo-TEMP are two standard and usual spin traps used for the detection of singlet oxygen in ESR [46, 47]. For example, Yin et al. [48] investigated the formation of singlet oxygen from irradiated titanium dioxide with the aid of the ESR trapping method using TEMP. They described that ultraviolet A (UVA) irradiation of nano-sized titanium dioxides (TiO_2) can set off considerable cell damage, mediated by using lipid and protein peroxidation. Leonard et al. [49] used ESR and spin trapping to identify short-lived free radical intermediates. As a result, no significant differences in generation of ·OH radical were reported. It was demonstrated that silicon nanowires did not appear to be considerable generators of free radicals. In another research, hydroxyl radical (the most important reactive oxygen species generated by copper(II) oxide nanoparticles) was determined by EPR measurements. As a result, copper(II) oxide nanoparticles generated considerably reactive oxygen species and DNA damage in the presence of ascorbate [50]. Moreover, titanium dioxide nanoparticles promote the formation of reactive oxygen species. ESR spectroscopy has been used to evaluate titanium dioxide nanoparticle safety (e.g., ESR spin-label oximetry and immune-spin trapping techniques). It is suggested that the combination of spin trapping/labeling techniques offers a hopeful method for investigating the oxidative damage caused by these nanoparticles [51]. These techniques are reviewed comprehensively by Li et al. [51].

4.8 Conclusion

In conclusion, ESR-based technique is appropriate and reliable for the recognition of reactive oxygen species within the sort of free radicals in bio-organic tissues and cells, and further, it can be used for willpower of the consequences of reactive

oxygen species-mediated reactions in bio-organic investigations in vitro and in vivo. Indeed, ESR approaches by the usage of spin trap or spin probe are going to be effective and beneficial for assessment of redox status under conditions of oxidative stress in the brain. In other words, in vitro or in vivo ESR methods and strategies may function as a helpful basis for assessing oxidative stress prompted by reactive oxygen species within the brain, and they might also provide beneficial data on pathological traits in the development from hypertension to stroke. Moreover, ESR can be used to check antioxidant consequences on oxidative stress within the brain. It should be mentioned that more advances in the instrumentation used for ESR imaging and the development of optimized nontoxic spin probes will make this technology even further hopeful and favorable for unique clinical evaluation or non-invasive identification of human stroke. Furthermore, in vitro or in vivo ESR assessment may additionally be suitable for the measurement of antioxidant properties of medications or food factors used for clinical therapy of human reactive oxygen species-induced conditions. It seems that in the near future, by using ESR, it will be feasible to find and enhance novel drugs or food elements with such antioxidant properties for the prevention of stroke. In addition, ESR spectroscopy can be used for qualitative and quantitative assessments of reactive oxygen species prompted by nanomaterials, and it is important for consideration of toxicity and toxic mechanisms regarding nanomaterials.

References

1. He W, Liu Y, Wamer WG, Yin JJ. Electron spin resonance spectroscopy for the study of nanomaterial-mediated generation of reactive oxygen species. J Food Drug Anal. 2014;22:49–63.
2. Lee M-C. Assessment of oxidative stress and antioxidant property using electron spin resonance (ESR) spectroscopy. J Clin Biochem Nutr. 2013;52:1–8.
3. Palmieri B, Sblendorio V. Oxidative stress tests: overview on reliability and use. Eur Rev Med Pharmacol Sci. 2007;11:309–42.
4. Pitocco D, Tesauro M, Alessandro R, Ghirlanda G, Cardillo C. Oxidative stress in diabetes: implications for vascular and other complications. Int J Mol Sci. 2013;14:21525–50.
5. Halliwell B. The wanderings of a free radical. Free Radic Biol Med. 2009;46:531–42.
6. Sies H. Oxidative stress: oxidants and antioxidants. Exp Physiol. 1997;82:291–5.
7. Paravicini TM, Drummond GR, Sobey C. Reactive oxygen species in the cerebral circulation: physiological roles and therapeutic implications for hypertension and stroke. Drugs. 2004;64:2143–57.
8. Ignarro LJ, Cirino G, Casini A, Napoli C. Nitric oxide as a signaling molecule in the vascular system: an overview. J Cardiovasc Pharmacol. 1999;34:879–86.
9. Suematsu M, Suzuki H, Delano FA, Schmid-Schönbein G-W. The inflammatory aspect of the microcirculation in hypertension: oxidative stress, leukocytes/endothelial interaction, apoptosis. Microcirculation. 2002;9:259–76.
10. Cuzzocrea S, Mazzon E, Dugo L, Di Paola R, Caputi AP, Salvemini D. Superoxide: a key player in hypertension. FASEB J. 2004;18:94–101.
11. Cooper D, Stokes KY, Tailor A, Granger D-N. Oxidative stress promotes blood cell-endothelial cell interactions in the microcirculation. Cardiovasc Toxicol. 2002;2:165–80.
12. Miyazaki H, Shoji H, Lee M. Measurement of oxidative stress in stroke prone spontaneously hypertensive rat brain using in vivo electron spin resonance spectroscopy. Redox Rep. 2002;7:260–5.

13. Lee MC, Shoji H, Miyazaki H, et al. Measurement of oxidative stress in the rodent brain using computerized electron spin resonance tomography. Magn Reson Med Sci. 2003;2:79–84.
14. Lee MC, Shoji H, Miyazaki H, et al. Assessment of oxidative stress in the spontaneously hypertensive rat brain using electron spin resonance (ESR) imaging and in vivo L-Band ESR. Hypertens Res. 2004;27:485–92.
15. Lee C, Okabe E. Hydroxyl radical-mediated reduction of Ca^{2+}-ATPase activity of masseter muscle sarcoplasmic reticulum. Jpn J Pharmacol. 1995;67:21–8.
16. Ishibashi T, Lee CI, Okabe E. Skeletal sarcoplasmic reticulum dysfunction induced by reactive oxygen intermediates derived from photoactivated rose bengal. J Pharmacol Exp Ther. 1996;277:350–8.
17. Lee C, Miura K, Liu X, Zweier J-L. Biphasic regulation of leukocyte superoxide generation by nitric oxide and peroxynitrite. J Biol Chem. 2000;275:38965–72.
18. Hagiwara T, Lee CI, Okabe E. Differential sensitivity to hydroxyl radicals of pre- and postjunctional neurovascular transmission in the isolated canine mesenteric vein. Neuropharmacology. 2000;39:1662–72.
19. Miura Y, Anzai K, Takahashi S, Ozawa T. A novel lipophilic spin probe for the measurement of radiation damage in mouse brain using in vivo electron spin resonance (ESR). FEBS Lett. 1997;419:99–102.
20. Sano H, Naruse M, Matsumoto K, Oi T, Utsumi H. A new nitroxyl-probe with high retention in the brain and its application for brain imaging. Free Radic Biol Med. 2000;28:959–69.
21. Anzai K, Saito K, Takeshita K, et al. Assessment of ESR-CT imaging by comparison with autoradiography for the distribution of a blood-brain-barrier permeable spin probe, MC-PROXYL, to rodent brain. Magn Reson Imaging. 2003;21:765–72.
22. Halliwell B, Whiteman M. Measuring reactive species and oxidative damage in vivo and in cell culture: how should you do it and what do the results mean? Br J Pharmacol. 2004;142:231–55.
23. Berliner JL, Fujii H. Magnetic resonance imaging of biological specimens by electron paramagnetic resonance of nitroxide spin labels. Science. 1985;227:517–9.
24. Ishida S, Kumashiro H, Tsuchihashi N, et al. In vivo analysis of nitroxide radicals injected into small animals by L-band ESR technique. Phys Med Biol. 1989;34:1317–23.
25. Utsumi H, Muto E, Masuda S, Hamada A. In vivo ESR measurement of free radicals in whole mice. Biochem Biophys Res Commun. 1990;172:1342–8.
26. Takeshita K, Utsumi H, Hamada A. ESR measurement of radical clearance in lung of whole mouse. Biochem Biophys Res Commun. 1991;177:874–80.
27. Kuppusamy P, Chzhan M, Vij K, et al. Three-dimensional spectral-spatial EPR imaging of free radicals in the heart: a technique for imaging tissue metabolism and oxygenation. Proc Natl Acad Sci U S A. 1994;91:3388–92.
28. Kuppusamy P, Afeworki M, Shankar RA, et al. In vivo electron paramagnetic resonance imaging of tumor heterogeneity and oxygenation in a murine model. Cancer Res. 1998;58:1562–8.
29. He G, Shankar RA, Chzhan M, Samouilov A, Kuppusamy P, Zweier J. Noninvasive measurement of anatomic structure and intraluminal oxygenation in the gastrointestinal tract of living mice with spatial and spectral EPR imaging. Proc Natl Acad Sci U S A. 1999;96:4586–91.
30. Ashton T, Rowlands CC, Jones E, Young IS, Jackson SK, Davies B, et al. Electron spin resonance spectroscopic detection of oxygen-centred radicals in human serum following exhaustive exercise. Eur J Appl Physiol. 1998;77:498–502.
31. Grech ED, Dodd NJF, Jackson MJ, Morrison WL, Faragher EB, Ramsdale D-R. Evidence for free radical generation after primary percutaneous transluminal coronary angioplasty recanalization in acute myocardial infarction. Am J Cardiol. 1996;77:122–7.
32. Tortolani AJ, Powell SR, Misik V, Weglicki WG, Pogo GJ, Kramer J-H. Detection of alkoxyl and carbon centred free radicals in coronary sinus blood from patients undergoing elective cardioplegia. Free Radic Biol Med. 1993;14:421–6.
33. Utsumi H, Yasukawa K, Soeda T, Yamada K, Ra S, Yao T, Tsuneyoshi M. Noninvasive mapping of reactive oxygen species by in vivo electron spin resonance spectroscopy in indomethacin-induced gastric ulcers in rats. J Pharmacol Exp Ther. 2006;317:228–35.

34. Sano T, Umeda F, Hashimoto T, Nawata H, Utsumi H. Oxidative stress measurement by in vivo electron spin resonance spectroscopy in rats with streptozotocin-induced diabetes. Diabetologia. 1998;41:1355–60.
35. Fujii H, Koscielniak J, Berliner LJ. In vivo ESR observation of bioradical metabolites in living animals. In: Ohya-Nishiguchi H, Packer L, editors. Bioradicals detected by ESR spectroscopy. Basel: Birkhäuser; 1995. p. 155–62.
36. Hickenbottom SL, Grotta J. Neuroprotective therapy. Semin Neurol. 1998;18:485–92.
37. Tan DX, Reiter RJ, Manchester LC, et al. Chemical and physical properties and potential mechanisms: melatonin as a broad spectrum antioxidant and free radical scavenger. Curr Top Med Chem. 2002;2:181–97.
38. Kevin LG, Novalija E, Stowe D-F. Reactive oxygen species as mediators of cardiac injury and protection: the relevance to anesthesia practice. Anesth Analg. 2005;101:1275–87.
39. Hans P, Bonhomme V. Why we still use intravenous drugs as the basic regimen for neurosurgical anaesthesia. Curr Opin Anaesthesiol. 2006;19:498–503.
40. Kobayashi K, Yoshino F, Takahashi SS, et al. Direct assessments of the antioxidant effects of propofol medium chain triglyceride/long chain triglyceride on the brain of stroke-prone spontaneously hypertensive rats using electron spin resonance spectroscopy. Anesthesiology. 2008;109:426–35.
41. Yoshino F, Yoshida A, Umigai N, Kubo K, Lee M-C. Crocetin reduces the oxidative stress induced reactive oxygen species in the stroke-prone spontaneously hypertensive rats (SHRSPs) brain. J Clin Biochem Nutr. 2011;49:182–7.
42. Iannone A, Rota C, Bergamini S, Tomasi A, Canfield L-M. Antioxidant activity of carotenoids: An electron-spin resonance study on β-carotene and lutein interaction with free radicals generated in a chemical system. J Biochem Mol Toxicol. 1998;12:299–304.
43. Jeong MS, Yu K-N, Chung HH, Park SJ, Lee AY, Song MR, et al. Methodological considerations of electron spin resonance spin trapping techniques for measuring reactive oxygen species generated from metal oxide nanomaterials. Sci Rep. 2016;6:26347.
44. Ge CC, Li Y, Yin JJ, et al. The contributions of metal impurities and tube structure to the toxicity of carbon nanotube materials. NPG Asia Mater. 2012;4:e32.
45. Zhang WD, Wang C, Li ZJ, et al. Unraveling stress-induced toxicity properties of graphene oxide and the underlying mechanism. Adv Mater. 2012;24:5391–7.
46. Pan Y, Leifert A, Ruau D, et al. Gold nanoparticles of diameter 1.4 nm trigger necrosis by oxidative stress and mitochondrial damage. Small. 2009;5:2067–76.
47. Zhao B, Yin JJ, Bilski PJ, et al. Enhanced photodynamic efficacy towards melanoma cells by encapsulation of Pc4 in silica nanoparticles. Toxicol Appl Pharmacol. 2009;241:163–72.
48. Yin JJ, Liu J, Ehrenshaft M, et al. Phototoxicity of nano titanium dioxides in HaCaT keratinocytes-Generation of reactive oxygen species and cell damage. Toxicol Appl Pharmacol. 2012;263:81–8.
49. Leonard SS, Cohen GM, Kenyon AJ, Schwegler-Berry D, Fix NR, Bangsaruntip S, Roberts JR. Generation of reactive oxygen species from silicon nanowires. Environ Health Insights. 2014;8:21–9.
50. Angelé-Martínez C, Nguyen KVT, Ameer FS, Anker JN, Brumaghim JL. Reactive Oxygen Species Generation by Copper(II) Oxide Nanoparticles Determined by DNA Damage Assays and EPR Spectroscopy. Nanotoxicology. 2017;11:278–88.
51. Li M, Yin J-J, Wamer WG, Lo YM. Mechanistic characterization of titanium dioxide nanoparticle-induced toxicity using electron spin resonance. J Food Drug Anal. 2014;22:76–85.

5 Electron Spin Resonance Spectroscopy Investigations on Radiosterilization Feasibilities of Sulfadiazine, Sulfamethoxydiazine and Sulfaquinoxaline

Şeyda Çolak

5.1 Introduction

As a very sensitive method, **Electron Spin Resonance (ESR) spectroscopy** is preferred to be used for qualitative and quantitative detection of the investigated samples that contain free radicals or for the samples which have magnetic property. ESR technique can also be used in the determination of the radiolytical intermediates that can be produced in the gamma irradiated pharmaceuticals. Thus by ESR spectroscopy, radiation sterilization feasibility of the drug/drug raw materials can be determined. Besides, ESR spectroscopy has high sensitivity and high precision, and the sample investigated will not be damaged during the experiments [1–8].

For the sterilization process of pharmaceuticals, ionized radiation, such as gamma rays, is preferred to be used especially for the heat-sensitive drug/drug raw materials [9–14]. EN 552 and ISO 11137 publications recognize standard for radiation sterilization [15, 16]. Radiation sterilization procedure has advantages such as terminal sterilization because of its high penetration property and low cost, and it is also accepted to be a relatively cold technique. But ionized radiation that is used in sterilization process will not only sterilize the pharmaceuticals but also can create different radical species in the irradiated drug/drug raw materials. Detail identification of the radiolytic intermediates that can be produced during the irradiation process of the samples should be done so that the radiosterilized drug and/or drug raw materials can be used safely. ESR spectroscopy is a suitable technique to characterize these radical species induced in the drugs/drug raw materials upon irradiation.

Sulfa group antibacterial agents can treat urinary system infections, meningococcal meningitis prophylaxis, ulcerative colitis, urinary tract infections and dysentery agents and they are widely used both in pharmacy and veterinary medicine [17–19].

Ş. Çolak
Physics Engineering Department, Hacettepe University, Ankara, Turkey
e-mail: seyda@hacettepe.edu.tr

A. K. Shukla (ed.), *Electron Spin Resonance Spectroscopy in Medicine*,
https://doi.org/10.1007/978-981-13-2230-3_5

In literature, radiation sterilization feasibility of "**sulfanilamide**", "**sulfafurazole**", "**sulfathiazole**", "**sulfacetamide sodium**", "**sulfamethazine**" and "**sulfamethoxazole**" by ESR spectroscopy has already been recorded [1, 17, 20–25]. In the present study, detailed ESR experimental data and characterization of gamma irradiated (5–50 kGy) "**sulfadiazine**", "**sulfamethoxydiazine**" and "**sulfaquinoxaline**" will be presented.

5.2 Materials and Methods

The sulfa group drug raw materials named sulfadiazine (hereafter SDZ), sulfamethoxydiazine (hereafter SMDZ) and sulfaquinoxaline (hereafter SQX) were provided from local drug providers, and the samples were stored at room temperature, protected from light. No further purification procedure was performed. ^{60}Co gamma cell with dose rate ~2.5 kGy/h was used for irradiations which was performed at room temperature, at the Sarayköy Establishment of Turkish Atomic Energy Agency in Ankara, Turkey. ESR investigations were performed on gamma irradiated SDZ, SMDZ and SQX drug raw materials at 5 kGy, 10 kGy, 25 kGy and 50 kGy radiation dose values. Sterilization radiation dose value is accepted to be 25 kGy, and the other dose values were also studied so as to determine the dosimetric properties of these investigated samples.

Varian 9″-EL X-band ESR spectrometer operating at about 9.5 GHz were used for ESR measurements. The spectrometer was equipped with a TE_{104} rectangular double cavity containing DPPH standard sample (g = 2.0036) in the rear resonator which remained untouched throughout the experiments. A digital temperature control system (Bruker ER 4111-VT) was used in monitoring the sample temperature inside the microwave cavity. Signal intensities were calculated from first derivative spectra and compared with the signal of standard DPPH under the same spectrometer operating conditions. The results were the average of five replicates for each radiation dose.

ESR experimental conditions held were as follows: central field, 330 mT; sweep width, 10 mT; microwave frequency, about 9.27 GHz; microwave power, 1 mW; modulation frequency, 100 kHz; modulation amplitude, 0.1 mT; receiver gain, 1.25×10^3 to 8×10^3; sweep time, 240 s; time constant, 1 s; and temperature, 110–400 K.

5.3 Experimental Results and Discussion

5.3.1 General Features of SDZ, SMDZ and SQX

Sulfadiazine (SDZ) is an oral sulfonamide antibacterial agent. The chemical formula of SDZ is $C_{10}H_{10}N_4O_2S$; its molecular weight is 250.3 g/mol and has a melting point of 528 K. **Sulfamethoxydiazine (SMDZ)** sulfa group drug has a chemical formula of $C_{11}H_{12}N_4O_3S$ with a molecular mass of 280.3 g/mol. The melting point of SQX is 488 K, and it is not soluble in water but can be soluble slightly in ethanol. The

Table 5.1 Molecular structures of (a) sulfonamides, (b) SDZ, (c) SMDZ and (d) SQX

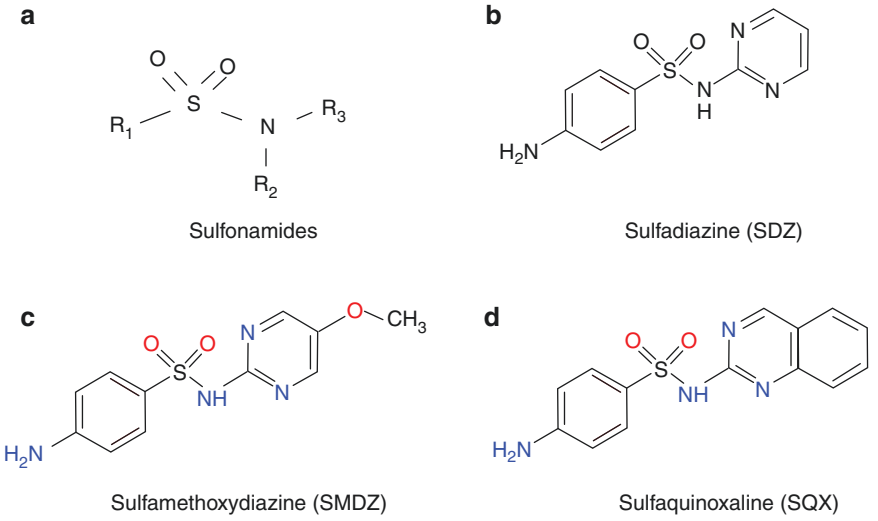

molecular formula of **sulfaquinoxaline (SQX)** is $C_{14}H_{12}N_4O_2S$ with a molecular mass and melting point of 322.3 g/mol and 520 K, respectively. The molecular structures of SDZ, SMDZ and SQX are presented in Table 5.1. They are synthetic bacteriostatic antibiotics with a wide spectrum against most Gram-positive and many Gram-negative organisms. The sulfonamides are widely distributed throughout all tissues [26].

5.3.2 General Features of the ESR Spectra of SDZ, SMDZ and SQX

Unirradiated SDZ, SMDZ and SQX drug raw materials exhibited no ESR signal where gamma irradiated SDZ, SMDZ and SQX drug raw materials showed simple and unresolved ESR spectra with relatively low intensities (Fig. 5.1) which were nearly hardly distinguishable from noise. This relatively low intensity of the resonance lines recorded for the investigated sulfonamides, even for the samples irradiated at high dose levels (50 kGy), indicated that SDZ, SMDZ and SQX drug raw materials have probably radioresistive character. Radioresistive materials are accepted to be good candidates for radiosterilization process. Low amount of radical species are created in radioresistive materials during their irradiation process. The effect of radiation on radiosterilized drug/drug raw materials which are not radiosensitive will be less, thus their active ingredient content will not be much effected by radiation. But still toxicology tests should be held on the radiosterilized drug/drug raw materials.

In the present study, it is observed from experimental data that increase in absorbed dose at room temperature had only increased the ESR resonance line intensities of the irradiated SDZ, SMDZ and SQX but did not create any pattern change in their spectra. Irradiated SDZ represented three characteristic resonance

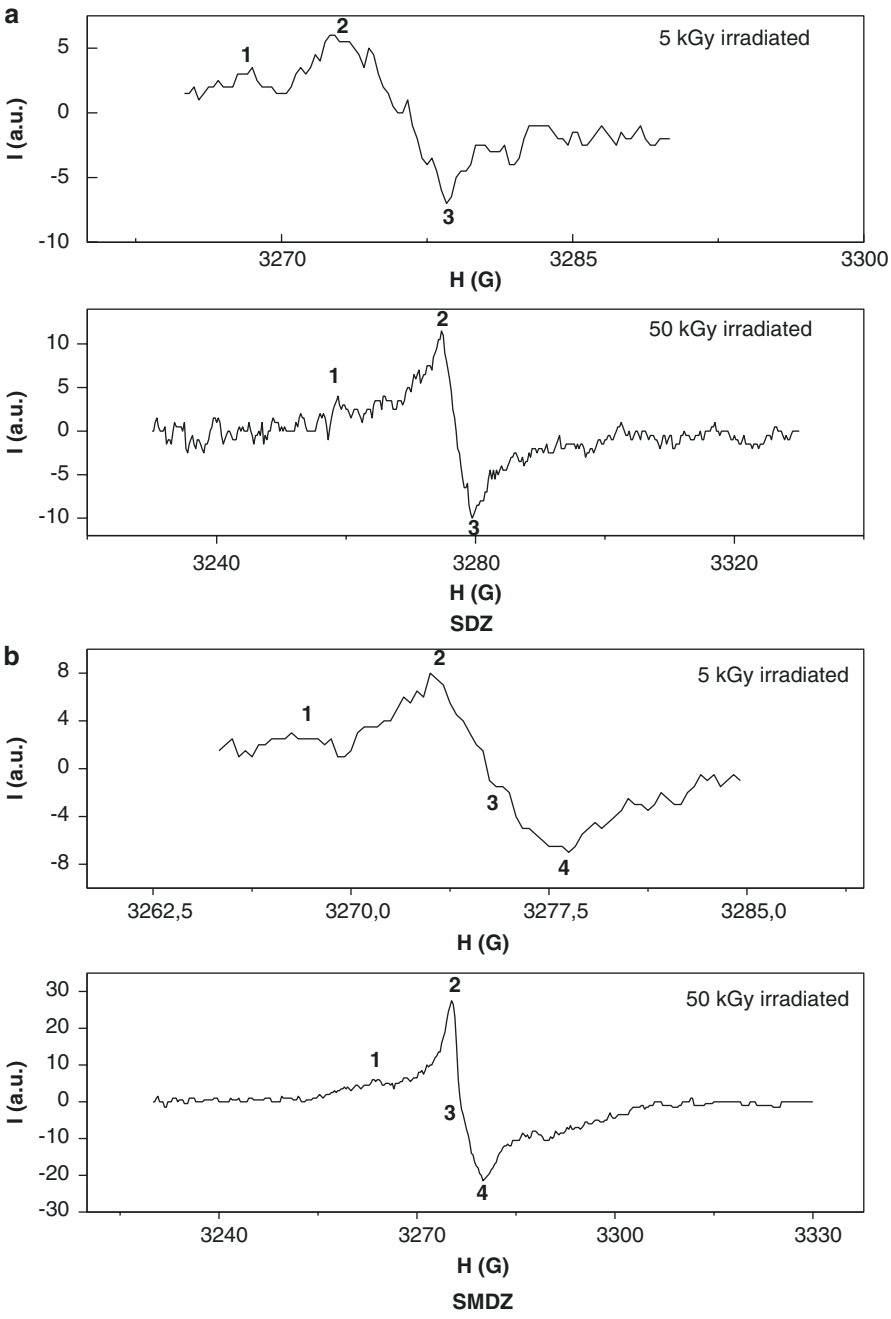

Fig. 5.1 Room temperature ESR spectra of gamma irradiated samples. (**a**) SDZ, (**b**) SMDZ, (**c**) SQX

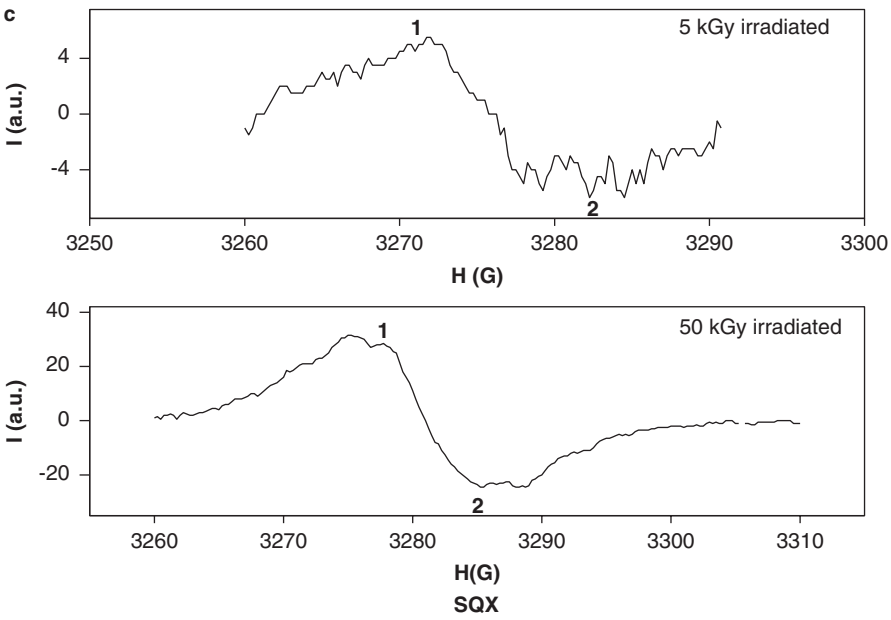

Fig. 5.1 (continued)

lines, and the spectral parameters associated with its central peak are found to be $g = 2.0069$ and $\Delta H_{pp} = 4.7$ G, respectively. Irradiated SMDZ represented an ESR spectrum with four characteristic resonance lines, and the spectral parameters for its central resonance line are found to be $g = 2.0057$ and $\Delta H_{pp} = 4.8$ G. Irradiated SQX has complex and unresolved two resonance lines where its spectral parameters for its central peak are found to be $g = 2.0052$ and $\Delta H_{pp} = 11.5$ G. ESR spectra of SDZ, SMDZ and SQX sulfa drug raw materials irradiated at 5 kGy and 50 kGy are presented in Fig. 5.1.

5.3.3 Microwave Power Saturation Studies of SDZ, SMDZ and SQX

Variations of the resonance peak heights of SDZ, SMDZ and SQX, measured with respect to their base line, with applied microwave power were studied. One of the aims of microwave saturation studies was to determine the optimum microwave power value for the rest of the experiments where no saturation was observed in the resonance lines of the samples. By this study, one can also identify qualitatively the number of radical species that can be induced upon irradiation since the microwave power saturation behaviours of different resonance lines related with different radical species are not expected to be same. By the microwave power saturation studies of SDZ, SMDZ and SQX (Fig. 5.2), it was concluded that at least two radical

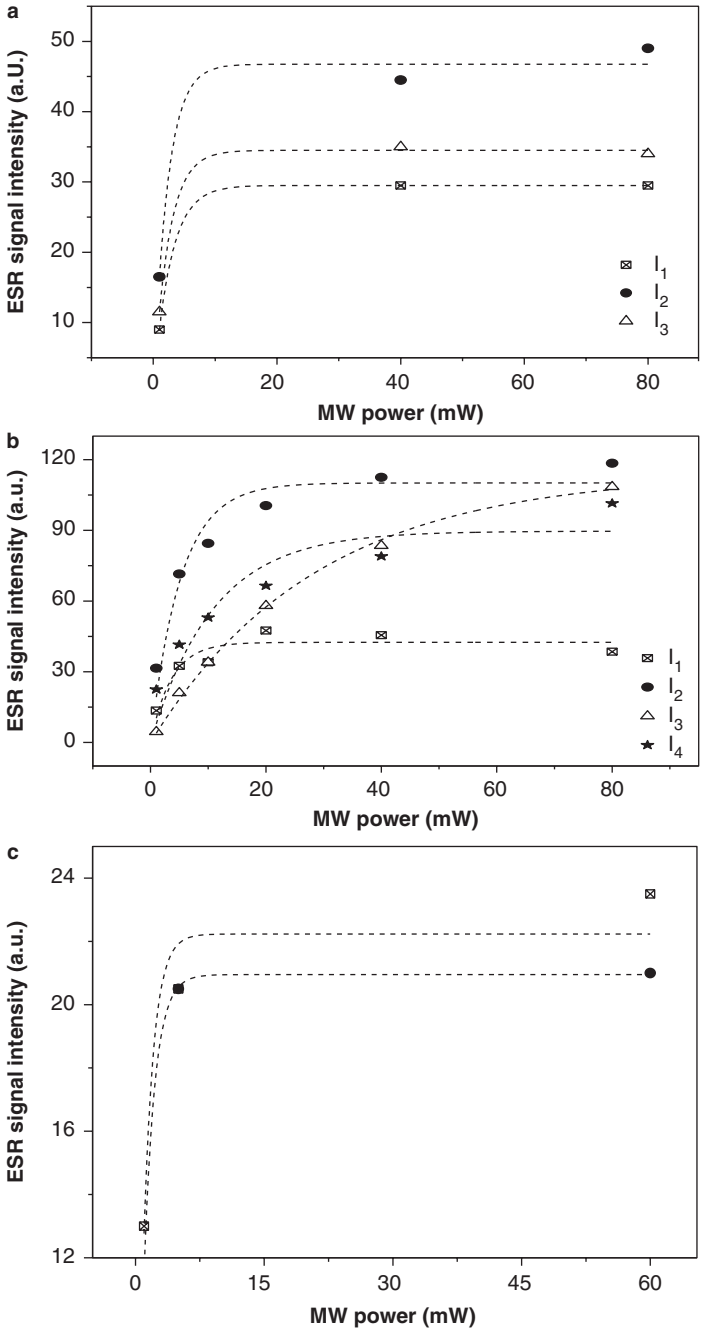

Fig. 5.2 Microwave power studies of 50 kGy gamma irradiated samples at room temperature. (**a**) SDZ, (**b**) SMDZ, (**c**) SQX

species with different saturation characteristics were involved in the irradiated drug raw materials. Theoretical growing function (Eq. 5.1) best fitting to experimental microwave power saturation curves is presented in Fig. 5.2. ESR resonance lines of the investigated 50 kGy gamma irradiated SDZ, SMDZ and SQX were observed to be saturated at relatively high microwave power levels.

$$I = I_0\left(1 - e^{-d\times P}\right) \tag{5.1}$$

5.3.4 Dose-Response Curves of SDZ, SMDZ and SQX

ESR spectroscopy can also give quantitative results about the amount of free radicals induced upon irradiation so that a good dose estimation for the irradiated samples can be obtained. In ESR spectroscopy, radical concentration is proportional with the area of the recorded ESR signal of the investigated samples, or if the linewidths of the signals are not changing with applied dose, radical concentration will also be proportional with the resonance line intensities of the recorded spectrum. Theoretical mathematical function(s) best describing the experimental dose-response curve of the irradiated samples should be determined for the good dose estimation. Dosimetric potentials of SDZ, SMDZ and SQX sulfa group drug raw materials are presented in Fig. 5.3.

The experimental dose-response data recorded for gamma irradiated SDZ, SMDZ and SQX in the dose range of 5–50 kGy are fitted with using different mathematical functions. The mathematical functions and the obtained parameters by fitting process are presented in Table 5.2. It concluded from the findings given in Table 5.2 that *linear fitting* best describes the experimental dose-response data of irradiated SDZ and SMDZ, while *exponential growth* fitting best describes experimental data of irradiated SQX, respectively. Although SDZ, SMDZ and SQX did not indicate good dosimetric behaviours (Fig. 5.3), I_3 resonance line for SDZ ($R^2 = 0.96$), I_1 resonance line for SMDZ ($R^2 = 0.99$) and I_1 resonance line for SQX ($R^2 = 0.56$) can be used in dosimetric studies of these related samples. It was concluded that the discrimination of unirradiated and 5 kGy gamma irradiated SDZ, SMDZ and SQX was possible even after a long storage time interval which was at room conditions (room temperature and atmospheric pressure) and in dark. This result can indicate that SDZ, SMDZ and SQX were relatively stable sulfa drug raw materials.

G value is defined as the number of free radicals induced upon 100 eV of absorbed energy, and this value gives important information about the dosimetric feature of the investigated samples [27]. *G* value of 50 kGy gamma irradiated SDZ, SMDZ and SQX drug raw materials is found to be ~0.1 which confirms that SDZ, SMDZ and SQX are radioresistive materials when compared with *G* value of solid alanine sample ($G = 1$). This result shows that only a small amount

of radical species were trapped in the irradiated SDZ, SMDZ and SQX drug raw materials during the irradiation process, and it is in agreement with the relatively low ESR resonance line intensities recorded for the irradiated samples. Thus radiosterilization method can be feasible in sterilization process of SDZ, SMDZ and SQX.

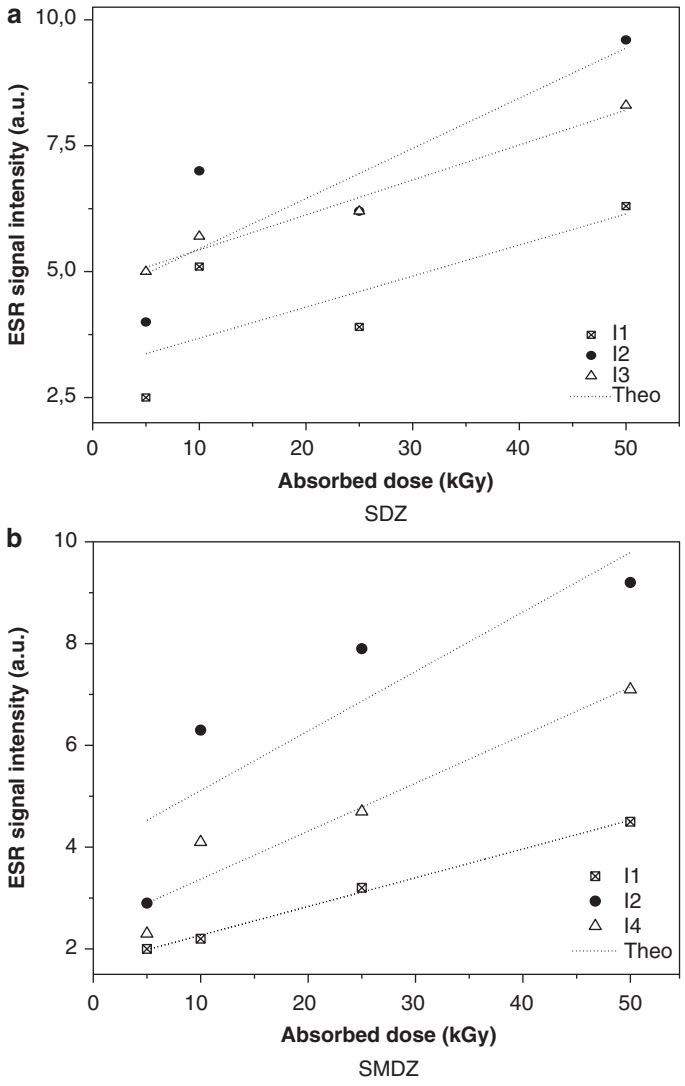

Fig. 5.3 Variations of peak heights with absorbed radiation dose. Dashed lines represent theoretical curves best fitting to experimental data

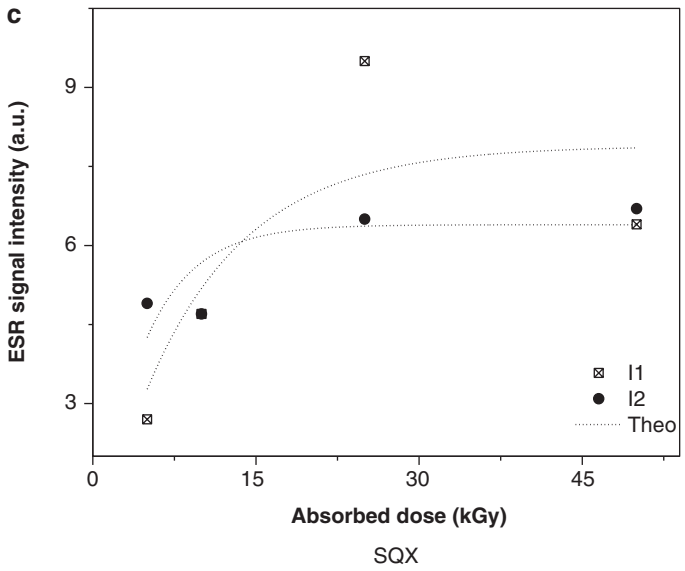

Fig. 5.3 (continued)

Table 5.2 Theoretical functions and derived parameters best fitting to experimental dose-response data of sulfa group drug raw materials. (**a**) SDZ, (**b**) SMDZ, (**c**) SQX

Resonance Line	I_0	a
(a) SDZ: Lineer Fit [$I = I_0 + a \times D$]		
1	3.06 ± 1.05	0.06 ± 0.04
2	4.46 ± 1.14	0.09 ± 0.04
3	4.74 ± 0.23	0.07 ± 0.01
(b) SMDZ: Lineer Fit [$I = I_0 + a \times D$]		
1	1.70 ± 0.07	0.06 ± 0.01
2	3.94 ± 0.35	0.12 ± 0.05
4	2.43 ± 0.55	0.009 ± 0.02
(c) SQX: Exponential Growth Fit [$I = I_o(1 - e^{-dP})$]		
Resonance Line	$\boldsymbol{I_o}$	$\boldsymbol{d}$
1	7.89 ± 1.70	0.11 ± 0.07
2	6.39 ± 0.61	0.22 ± 0.08

5.3.5 Variations of Peak Heights of SDZ, SMDZ and SQX with Temperature

The variation of the 50 kGy gamma irradiated SDZ, SMDZ and SQX samples with varying cavity temperature in the range of 290–400 K was studied, and the results are presented in Fig. 5.4. As seen from the figures for a particular sample, the responses of resonance line intensities of irradiated samples to temperature

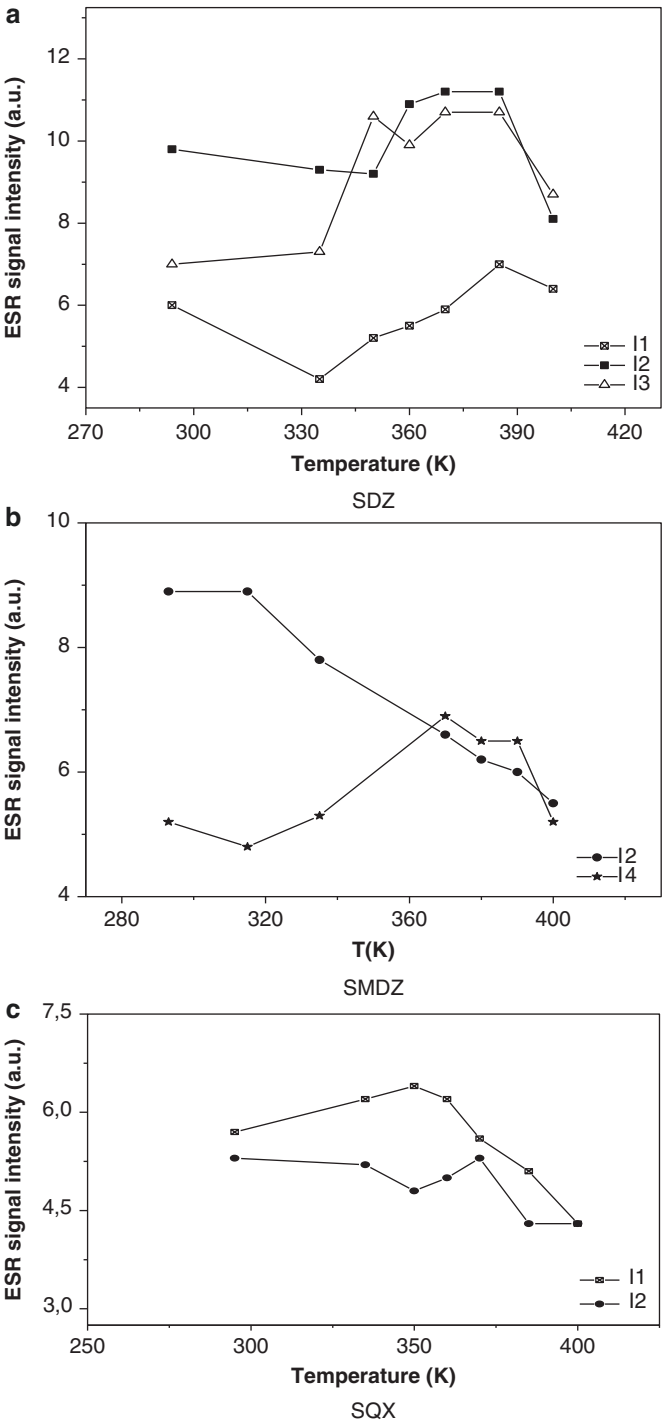

Fig. 5.4 Variation of peak resonance lines of 50 kGy gamma irradiated samples with temperature. (**a**) SDZ, (**b**) SMDZ, (**c**) SQX

variations were not the same. As the temperature dependencies of the resonance lines recorded for the irradiated samples are different from each other, this can be thought also to be a confirmation that at least two radical species have been created during irradiation process of the samples. From the recorded ESR studies held on sulfonamides in literature [1, 17, 20–25], these fundamental radical species were recorded to be **molecular ionic fragment** 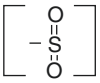 and **SO_2^- ionic radical,** by simulation calculation studies. In the present study, the same radical types are also believed to be responsible from the ESR spectra of irradiated SDZ, SMDZ and SQX.

It was observed that by warming SDZ up to 335 K, resonance line I_1, which was believed to be related with SO_2^- ionic radical, decayed faster than the resonance lines of I_2 and I_3. Thus, SO_2^- ionic radical can be accepted to be dominantly responsible from the existence of resonance line I_1 for SDZ. For the temperature range of 335–385 K, all three resonance lines increased approximately with the same ratio, indicating that some radicals have been also created in SDZ by heat treatment. Above 385 K, continuous decreases in the resonance line intensities of SDZ were observed, and above 390 K, relatively sharp decreases have occurred.

For temperature variation studies of SMDZ, only the resonance peak variations of I_2 and I_4, which are strongly related with SO_2^- ionic radical and molecular ionic fragment 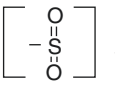 , respectively, are presented in the Fig. 5.4. As seen from the figure, above 370 K, the dominant radical species for SMDZ was SO_2^- ionic radical, and the other resonance line has already been decayed at this related temperature. This result also indicated that SO_2^- ionic radical was relatively stable at high temperatures.

From the experimental data of SQX, up to 290–335 K temperature range, the height of the resonance lines has increased smoothly. This variation can be an indication of the production of similar radical species in SQX by heat treatment, and/or it can be related to the water loss of the irradiated samples. After 335 K, the decay rate of the resonance lines had increased, probably because of the increased recombination rate of the radical species at high temperatures. The observed changes in the intensities of all resonance lines were found to be irreversible at high temperatures (290–400 K).

ESR studies at low temperature ($T = 110$ K) were also studied for 50 kGy gamma irradiated SDZ, SMZ and SQX drug raw materials. As expected, the ESR spectral patterns of the samples were unchanged at low-temperature studies, but the intensities of the resonance lines recorded increased obeying Curie's law.

5.3.6 Annealing Studies of SDZ, SMDZ and SQX

Decay mechanisms of the radical species depend strongly on the sample temperatures (cavity temperature), and the decreases (decays) recorded of the resonance

line intensities of the samples are expected to be irreversible. Besides, the decay rates of the radicals become higher at high temperatures, probably because of the high recombination chance of the induced free radicals. To get detail information about decay mechanisms of SDZ, SMDZ and SQX and to obtain the decay activation energy of these samples, annealing studies were held for 50 kGy gamma irradiated sulfa group drug raw materials at different annealing temperatures such as 323, 333, 348, 365, 378, 393 and 413 K and for predetermined times up to 2 h. Resonance line intensities recorded were normalized to the masses of the samples and to the operating conditions used. Each spectrum of the annealed samples was recorded 5 min after the positioning sample in the microwave cavity after reaching their thermal equilibrium.

At different annealing temperatures, variations of intensities related to central resonance lines of 50 kGy gamma irradiated SDZ [$I_{pp} = I_2 + I_3$], SMDZ [$I_{pp} = I_2 + I_4$] and SQX [$I_{pp} = I_1 + I_2$] are presented in Fig. 5.5. Theoretical parameters calculated by fitting the experimental data of annealed SDZ, SMDZ and SQX to first-order exponential decay (Eq. 5.2) are presented in Table 5.3. Theoretical findings are represented as dotted lines in the figure with their experimental counterparts which correlate well in the studied annealing temperature range of 323–413 K.

$$I_0 e^{-k \times t} \tag{5.2}$$

The decay activation energies of the induced radical species can be calculated from the slopes of $\ln(k)^{-1}/T$ graphs, by using **Arrhenius equation** (Eq. 5.3). In this equation, k is decay constant of the contributing radicals, E_a is activation energy, R is universal gas constant and T is temperature. Decay activation energies of the induced radical species that were responsible from the existence of their central resonance line were calculated to be 13.5 kcal/mol, 18.6 kcal/mol and 9.5 kcal/mol, respectively, by using the results of annealing studies. From these findings, SMDZ can be considered to be more stable when compared with SDZ and SQX.

$$k = A \exp\left(-\frac{E_a}{RT}\right) \tag{5.3}$$

5.3.7 Stability Studies of SDZ, SMDZ and SQX at Normal Conditions

Room temperature stability of the radical species induced in the irradiated drug/drug raw material is also one of the important features to be determined. This type of a study can give an idea about the shelf life of the drug/drug raw materials. Therefore long-term stability studies for SDZ, SMDZ and SQX were held for the samples stored at room conditions (room temperature and atmospheric pressure), for 3 months. Stability features of the samples were found to be independent from the irradiation dose; thus only the resonance line intensity decay data obtained for the 50 kGy gamma irradiated samples were used to get these results. The results are

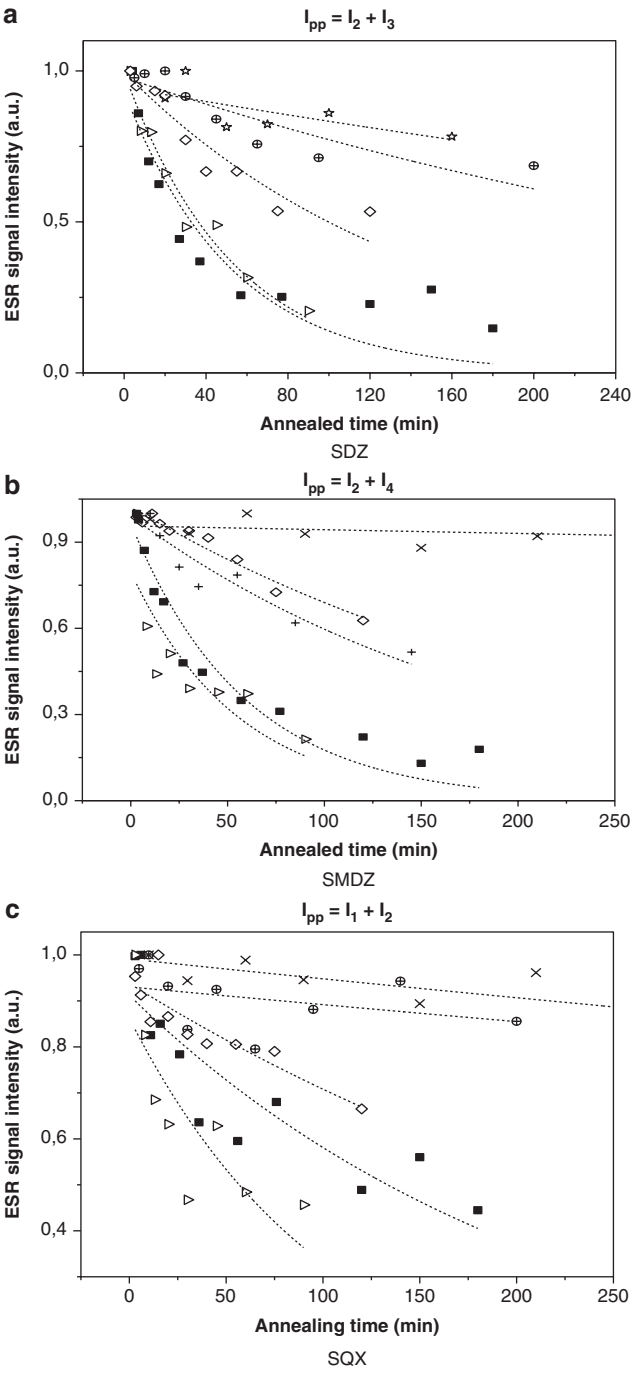

Fig. 5.5 Annealing study results for central resonance line of 50 kGy gamma irradiated SDZ, SMDZ and SQX at different temperatures for different times [× (323 K), ☆ (333 K), ⊕ (348 K), ◇ (365 K), + (378 K), ▷ (393 K), ■ (413 K)]

Table 5.3 Decay constants obtained at different annealing temperature studies of the samples. (**a**) SDZ, (**b**) SMDZ, (**c**) SQX

Annealing temperature (K)	**Resonance line $I_{pp} = [I_2 + I_3]$**
(a) SDZ	
333	$I_0 = 0.95 \pm 0.05$ $k = 0.0013 \pm 0.0007$
348	$I_0 = 0.98 \pm 0.03$ $k = 0.0024 \pm 0.0005$
365	$I_0 = 0.99 \pm 0.04$ $k = 0.0069 \pm 0.0009$
393	$I_0 = 0.99 \pm 0.04$ $k = 0.0189 \pm 0.0019$
413	$I_0 = 0.93 \pm 0.09$ $k = 0.0191 \pm 0.0042$
(b) SMDZ	
Annealing temperature (K)	**Resonance line $I_{pp} = [I_2 + I_4]$**
323	$I_0 = 0.96 \pm 0.02$ $k = 0.0001 \pm 0.0001$
365	$I_0 = 1.02 \pm 0.01$ $k = 0.0039 \pm 0.0004$
378	$I_0 = 0.99 \pm 0.03$ $k = 0.0051 \pm 0.0007$
393	$I_0 = 0.79 \pm 0.11$ $k = 0.0181 \pm 0.0060$
413	$I_0 = 0.97 \pm 0.05$ $k = 0.0170 \pm 0.0020$
(c) SQX	
Annealing temperature (K)	**Resonance line $I_{pp} = [I_1 + I_2]$**
323	$I_0 = 0.99 \pm 0.02$ $k = 0.0004 \pm 0.0001$
348	$I_0 = 0.93 \pm 0.03$ $k = 0.0004 \pm 0.0003$
365	$I_0 = 0.94 \pm 0.02$ $k = 0.0028 \pm 0.0005$
393	$I_0 = 0.86 \pm 0.08$ $k = 0.0096 \pm 0.0030$
413	$I_0 = 0.91 \pm 0.04$ $k = 0.0045 \pm 0.0008$

presented in Fig. 5.6. A slight increase in the height of the resonance lines at the beginning period of storage time was the common behaviour of the samples irradiated at different doses and stored at room temperature. This likely originates from the transformation of the radical species to each other. However, as it is seen from Fig. 5.6, the extent of this transformation is relatively small.

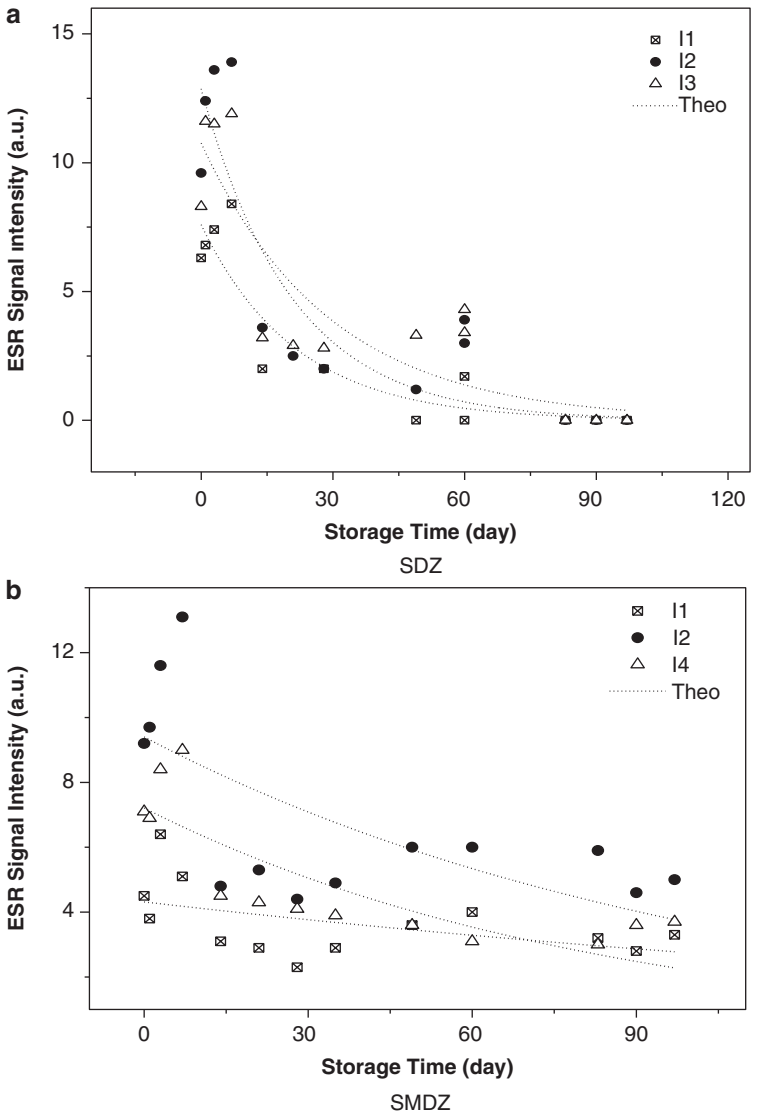

Fig. 5.6 Decays of resonance line intensities of 50 kGy gamma irradiated samples which were stored in normal conditions over a period of 90 days. (**a**) SDZ, (**b**) SMDZ, (**c**) SQX

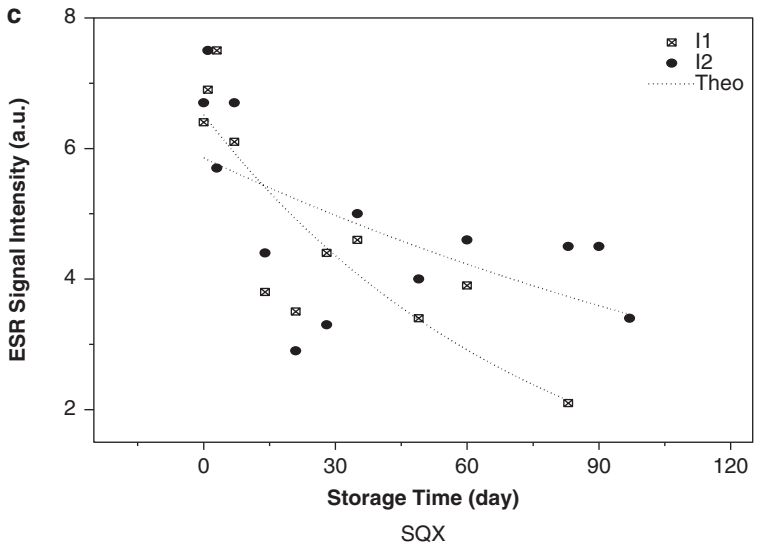

Fig. 5.6 (continued)

Table 5.4 Theoretical parameters of long-term decay data of 50 kGy gamma irradiated samples. (**a**) SDZ, (**b**) SMDZ, (**c**) SQX

Resonance line	
(a) SDZ	
1	$I_0 = 7.59 \pm 0.81$ $k = 0.0465 \pm 0.0141$
2	$I_0 = 12.87 \pm 1.56$ $k = 0.0481 \pm 0.0148$
3	$I_0 = 10.77 \pm 1.31$ $k = 0.0343 \pm 0.0103$
(b) SMDZ	
1	$I_0 = 4.31 \pm 0.45$ $k = 0.0045 \pm 0.0025$
2	$I_0 = 9.39 \pm 1.08$ $k = 0.0094 \pm 0.0035$
4	$I_0 = 7.21 \pm 0.61$ $k = 0.0119 \pm 0.0029$
(c) SQX	
1	$I_0 = 6.51 \pm 0.47$ $k = 0.0134 \pm 0.0031$
2	$I_0 = 5.86 \pm 0.54$ $k = 0.0054 \pm 0.0023$

Decay data recorded for SDZ, SMDZ and SQX stored at normal conditions for 3 months were found best fitting to first-order exponential decay function (Eq. 5.2), and the theoretical parameters calculated by fitting procedure are summarized in Table 5.4.

5.3.8 Proposed Radical Species and Spectral Simulations

SO_2 is the most sensitive group to radiation in sulfa group drugs because of their high electrophilic properties. So, radical species with unpaired electrons that are localized on mostly S atoms are expected to be created during the gamma irradiation of sulfa group antibacterial agents, as in the case of sulphur-containing compounds [28–34]. These radical species do not exhibit hyperfine structure; instead they have g tensor of orthorhombic symmetry with G value range of 2.0037–2.0059. In the present study, *G* values determined for gamma irradiated SDZ, SMDZ and SQX stay also in this range. The molecular ionic fragment 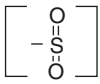 and SO_2^- ionic radical are believed to be the responsible magnetic units from the ESR spectra of irradiated SDZ, SMDZ and SQX drug raw materials. The unpaired electron in SO_2^- ionic radical occupies the antibonding 2b* orbital formed from p orbitals of the S atom. These two radical species produced in irradiated powder samples are randomly oriented, and the motion of molecular ionic fragment 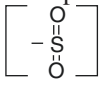 is restricted in large extent because of the big group attached to it. That is why it gives rise to powder ESR spectra with principal *G* values varying between g_{xx} = 2.0022–2.0031, g_{yy} = 2.0015–2.0098 and g_{zz} = 2.0058–2.0066. But SO_2^- ionic radical has a higher motional freedom, it gives rise to a single resonance line with average spectroscopic *G* value in the region of 2.0037–2.0059 [30, 33].

G value of 0.1 was obtained for 50 kGy gamma irradiated solid SDZ, SMDZ and SQX in this present study. This value is quite small when it is compared with the results obtained for sulfonamide aqueous solutions (3.5–5.1) in literature, but it stays in the range of the *G* values that were reported for solid sulfonamides (0.15–0.6) [18, 19].This difference in *G* values is believed to originate from hydrated electrons (e_{aq}^-) and hydroxyl radicals ($^{\cdot}OH$) produced in large amount as radiolytical intermediates in irradiated aqueous solutions of sulfonamides.

Conclusion

Experimental results derived for sulfa group antibacterial agents such as **sulfadiazine (SDZ), sulfamethoxydiazine (SMDZ)** and **sulfaquinoxaline (SQX)** indicated that these samples can be considered to be radioresistive to gamma radiation depending on their recorded low-intensity ESR spectra even for very high absorbed irradiation dose (50 kGy—two times bigger than the accepted sterilization dose) and the low *G* value (0.1) calculated. Therefore, SDZ, SMDZ and SQX could be sterilized by gamma radiation up to a radiation dose of 50 kGy without causing large extent of molecular damages creation during the irradiation process. Although SDZ, SMDZ and SQX do not present good dosimetric features, the detection and discrimination of unirradiated samples from irradiated ones were possible even for 5 kGy gamma irradiated samples. Radical species induced upon irradiation were found to decay faster at higher temperatures.

This point could be a good possibility of decreasing the amount of induced radiolytical intermediates in radiosterilized samples. It was concluded that gamma radiation produced relatively low amount of radiolytic intermediates in the SDZ, SMDZ and SQX sulfa group drug raw materials and ESR spectroscopy could be used as an appropriate technique in monitoring their radiosterilization properties.

Acknowledgement I would like to express my great appreciations to Prof. Dr. Mustafa Korkmaz for his very valuable help and suggestions.

References

1. Çolak Ş, Korkmaz M. Kinetics of the radicals induced in gamma irradiated sulfafurazole: an EPR study. Z Naturforsch A. 2004;59a:481–7.
2. Çolak, Ş. Feasibility of radiation sterilization and dosimetric features of ampicillin: an electron spin resonance study. Radiation Effects & Defects in Solids, Taylor & Francis, Milton Park, Didcot. 2016; 171, 11–12, 904–915.
3. Çolak Ş. Investigation of radiosterilization of benzydamine hydrochloride by electron spin resonance spectroscopy. Radiat Phys Chem. 2016;127:204–9.
4. Çolak Ş, Aktürk C. Synthesis and characterization of undoped and doped (Mn, Cu, Co) Zno nanoparticles: an EPR study. Chapter 7. In: Shukla K, editor. Volume 62 of the series advanced structured materials. India: Springer; 2017. p. 151. https://doi.org/10.1007/978-81-322-3655-9_7. ISBN: 978-81-322-3653-5, Series ISSN: 1869-8433.
5. Korpayev S, Kavaklı C, Çolak Ş, Akkaş Kavaklı P. Preparation and characterization of ethylenediamine modified glycidyl methacrylate-grafted nonwoven cotton fabric adsorbent. Cellulose. 2017;25:813–28.
6. Polat M, Korkmaz M. Effect of radiation on solid paracetamol: ESR identification and dosimetric features of γ-irradiated paracetamol. Radiat Eff Defects Solids. 2006;161(1):51–62.
7. Polat M, Korkmaz M. Detection of irradiated black tea (*Camellia sinensis*) and rooibos tea (*Aspalathus linearis*) by ESR spectroscopy. Food Chem. 2008;107(2):956–61.
8. Tuner H, Bal MO, Polat M. Radiation sensitivity and EPR dosimetric potential of gallic acid and its esters. Radiat Phys Chem. 2015;107:115–20.
9. Abuhanoğlu G, Özer AY. Radiation effects on pharmaceuticals. FABAD. J Pharm Sci. 2010;35:203–17.
10. Erdoğan S, Özer AY, Ekizoğlu M, Özalp M, Çolak Ş, Korkmaz M. Gamma irradiation of liposomal phospholipids. FABAD J Pharm Sci. 2006;31:182–90.
11. Jacobs GP. A review of the effects of gamma radiation on pharmaceutical materials. J Biomater Appl. 1995;10:59–96.
12. Özer AY, Turker S, Çolak Ş, Korkmaz M, Kılıç E, Özalp M. The effects of gamma ırradiation on diclofenac sodium, liposome and niosome ıngredients for rheumatoid arthritis. Interv Med Appl Sci. 2013;5(3):122–30.
13. Turker S, Özer AY, Kılıç E, Özalp M, Çolak Ş, Korkmaz M. Gamma irradiated liposome/niosome and lipogelosome/niogelosome formulations for the treatment of rheumatoid arthritis. Interv Med Appl Sci. 2013;5(2):60–9.
14. Türker NS, Özer AY, Çolak Ş, Kutlu B, Nohutçu R. ESR investigations of gamma irradiated medical devices. Appl Radiat Isot. 2017;130:121–30.
15. EN 552. Sterilization of medical devices: validation and routine control of sterilization irradiation. Brussels, Belgium: CEN, European Committee for Standardization; 1994.
16. ISO 11137. Sterilization of health care products: requirements for validation and routine control. Geneva, Switzerland: Radiation sterilization; International Organization for Standardisation; 1995.

17. Olguner Mercanoğlu G, Özer AY, Çolak Ş, Korkmaz M, Özalp M, Ekizoğlu M, Barbarin N, Tilquin B. Radiosterilization of sulfonamides I: determination of the effects of gamma irradiation on solide sulfonamides. Radiat Phys Chem. 2004;69:511–20.
18. Philips GO, Power DM, Sewart MCG. Effect of gamma irradiation on sodium sulphacetamide. Radiat Res. 1971;46:236–50.
19. Philips GO, Power DM, Sewart MCG. Effect of γ-irradiation on sulphonamides. Radiat Res. 1973;53:204–15.
20. Çolak Ş, Korkmaz M. Investigation of structural and dynamic features of the radicals produced in gamma irradiated sulfanilamide: An ESR study. Int J Pharm. 2003;267(1–2):49–58.
21. Çolak Ş, Korkmaz M. Spectroscopic features of radiolytical intermediates induced in gamma irradiated sulfatiazole: an ESR study. Int J Pharm. 2004;285:1–11.
22. Çolak Ş, Korkmaz M. Investigation of radiosterilization and dosimetric features of sulfacetamide sodium. J Pharm Biomed Anal. 2004;36:791–8.
23. Çolak Ş, Korkmaz M. ESR response of gamma irradiated sulfamethazine. Radiat Eff Defects Solids. 2009;164(12):788–99.
24. Çolak Ş. In: Nenoi M, editor. Ionizing radiation used in drug sterilization, characterization of radical intermediates by electron spin resonance (ESR) analyses (Chapter 12, pp. 281). London: InTech; 2015. https://doi.org/10.5772/61052. ISBN: 978-953-51-2167-1.
25. Çolak Ş. Investigation of radiosterilization feasibility of sulfamethoxazole by ESR spectroscopy. Radiat Eff Defects Solids. 2017;172(11–12):835–50.
26. ChemicalBook, CAS DataBase List., http://www.chemicalbook.com/ChemicalProductProperty_EN_CB4166214.Htm, 2017
27. Ikeya M. New applications of electron spin resonance - dating, dosimetry and microscopy. Singapore: World Scientific Publishing; 1993.
28. Barbas M, Bach A, Mudelsee R, Mangini A. General properties of the paramagnetic center at $g = 2.006$ in carbonates. Quat Sci Rev. 1992;11:165–71.
29. Bershov LV, Martirsyan VO, Marfunin AS, Speranskii AV. EPR and structure models for radical ions in anhydrite crystals. Fortschr Miner. 1975;52:591–604.
30. Huzimura R. ESR studies of radical ion centers in irradiated $CaSO_4$. Jpn J Appl Phys. 1979;18:2031–2.
31. Kai A, Miki T. Electron spin resonance of sulfite radicals in irradiated calcite and aragonite. Radic Phys Chem. 1992;40:469–76.
32. Katzenberger O, Debuyst R, De Canniere P, Dejehet F, Apers D, Barabas M. Temperature experiments on mollusk samples: An approach to ESR signal identification. Appl Radiat Isot. 1989;40:1113–8.
33. Samoilovich MI, Tsinober LI. Characteristics of radiation color centers and microisomorphism in crystals. Sov Phys–Crystallogr. 1970;14:656–66.
34. Walther R, Barbas M, Mangini A. Basic ESR studies on recent corals. Q Sci Rev. 1992;11:191–6.

Free Radicals and Polymerization of Resinous Materials Used in Dentistry

6

Bruno Luiz Santana Vicentin and Eduardo Di Mauro

6.1 Introduction

A composite is generally defined as a material composed of two or more distinct phases. Dental composites consist of a polymerizable resin base containing a ceramic filler that does not interfere on the polymerization reaction. Most dental polymers are based on acrylic resins made up of monomethacrylate, dimethacrylate, or trimethacrylate monomers. The most common restorative materials are based on the bisphenol A-bis(glycidyl methacrylate) (Bis-GMA), which copolymerizes with triethylene glycol dimethacrylate (TEGDMA). Also the dimethacrylate monomers bisphenol A-dimethacrylate (Bis-EMA) and a urethane dimethacrylate (UDMA) are commonly used [1].

Photopolymerizable composite resins are the best substitutes for restoring the lost part of a tooth, both esthetically and practically, because a substitute with similar properties to the human tooth still does not exist. These composite resins polymerize by the absorption of blue visible light which activates the photoinitiator camphorquinone (CQ) from the ground state to an excited state where it reacts with a hydrogen donor and produces an initiating free radical (FR). Thus the excited molecule interacts with other molecules to form FRs capable of starting the radical polymerization by rapid addition of monomers to the chain [1, 2].

B. L. S. Vicentin (✉)
Department of Physics, State University of Londrina, Londrina, Brazil
e-mail: bruno.vicentin@uel.br

E. Di Mauro
Laboratório de Ressonância Paramagnética Eletrônica (LARPE), Departamento de Física – CCE, Universidade Estadual de Londrina, Londrina, Paraná, Brazil
e-mail: dimauro@uel.br

A. K. Shukla (ed.), *Electron Spin Resonance Spectroscopy in Medicine*,
https://doi.org/10.1007/978-981-13-2230-3_6

Besides composite resins used to restore the lost part of the tooth, acrylic resin cements are used to retain intraradicular post for the purpose of assisting the retention of the restoration material. In general, dental resin cements are dual cured to ensure polymerization at deepest points of the restoration where radiation cannot excite CQ, such that photo-cure and self-cure happen simultaneously and independently [1, 3]. Self-curing cements are two-component filled systems based on dimethacrylate monomers with an organic peroxide, usually benzoyl peroxide (BPO). To promote the decomposition of BPO at oral temperature, cold-cure acrylic resins need another chemical, usually an aromatic tertiary amine, to carry out the redox initiation, together with BPO in a short period of time [1, 3].

Intraradicular posts manufactured from a composite of glass fibers and epoxy resin are often used in the treatment of teeth for the purpose of assisting the retention of the restoration material. The fiberglass post became popular in dental practice because of its physical properties, which are very similar to dentin, for its adhesion to root dentin and its esthetic qualities, which differ considerably from the cast metal post. The retention of the fiberglass post with resin material directly depends on the degree of conversion of the cement selected. Thus, translucent fiberglass posts were developed for the purpose of transmitting light and improving cement polymerization throughout the length of the root canal. The efficiency of light transmission by the post, and hence the improvement in the degree of resin cement conversion, is directly proportional to the post diameter [4, 5].

However, these resins do not polymerize completely, and this causes problems that can compromise the restoration. Numerous factors affect polymerization, including chemical composition, polymerization conditions, light intensity, and distance from the device to the resin, which can compromise the restoration and cause problems, such as contraction, poor mechanical strength, color change, and infiltration. In order to avoid these problems and improve the mechanical properties of the restoration, a clearer understanding of the polymerization process is important.

A polymerization reaction encompasses three stages: initiation, propagation, and termination. In the initiation stage, the reaction is started by generating free radicals, and these radicals react with first monomer. In the propagation stage, successive reactions with monomers occur until the reaction is terminated, typically by combination of monomers or disproportionation. Consider R^* being a primary radical (generated by a redox reaction or blue visible light irradiation) and M the monomer molecule.

The general reaction mechanism for the free radical polymerization with termination by combination of monomer is as follows [1]:

Initiation:

$$R^* + M \xrightarrow{k_i} \mathrm{RM}_1^* \tag{6.1}$$

Propagation:

$$\mathrm{RM}_1^* + M \xrightarrow{k_p} \mathrm{RM}_2^* \tag{6.2}$$

$$\mathrm{RM}_2^* + M \xrightarrow{k_p} \mathrm{RM}_3^* \tag{6.3}$$

.
.
.

$$\mathrm{RM}_x^* + M \xrightarrow{k_p} \mathrm{RM}_{x+1}^* \tag{6.4}$$

Termination:

$$\mathrm{RM}_n^* + \mathrm{RM}_m^* \xrightarrow{k_t} \mathrm{RM}_{m+n}R \tag{6.5}$$

In these reactions, k_i, k_p, and k_t denote the reaction rate constants of the initiation, propagation, and termination stages, respectively.

Since these FRs generated are paramagnetic species, electron magnetic resonance (EMR) spectroscopy is a reliable technique for identifying and quantifying the concentration of FRs in the sample without any changes in the material composition. In this way, it is possible to identify the free radicals generated by each initiation mode either to resin composites or to resin cements. In addition, the degree of conversion of monomers into polymer is related to the amount of FRs generated during the initiation step of the polymerization reaction.

This chapter is divided into three parts: (1) multifrequency EMR for identification of radicals, (2) real-time polymerization monitoring by EMR, and (3) influence of the translucent fiberglass post on the depth of polymerization in a root canal.

6.2 Multifrequency EMR for Identification of Free Radicals

6.2.1 Free Radicals in a Photo-Cured Resin Composite

For more than 40 years, EMR spectroscopy has been used to detect, characterize, and monitor the evolution of free radical concentration in dental resins. This spectroscopic technique has been used to study the behavior of the methacrylate radical generated during photopolymerization of dental restoration resins in numerous situations, including irradiation at different wavelengths, required polymerization time as a function of resin composition or sample thickness, resin hardness as a function of the relative number of radicals, conversion degree, analysis of polymerization initiator agents, real-time study of polymerization kinetics, variations in the monomer matrix and influence on the chemical reaction, the effect of the saturation time, evaluation of the behavior of free radicals versus mechanical properties, the relation between the free radicals generated and polymerization depth in resin with different colors, and translucence. Some research has been conducted to elucidate the well-known, though not fully interpreted, nine-line EMR spectrum

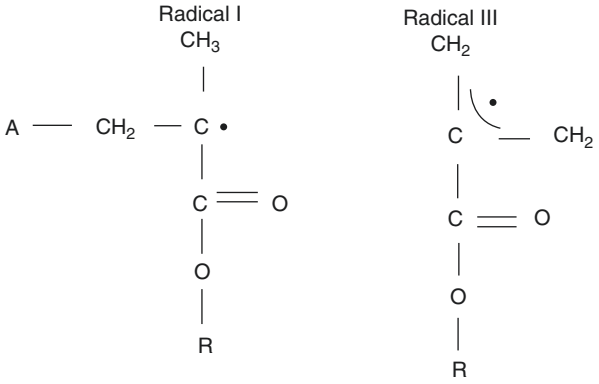

Fig. 6.1 Free radicals generated during the photopolymerization of dental resin Z100 (3 M ESPE) that are responsible for the EMR spectrum formation, where A is the amine monomer and R is dimethacrylate monomer mixture of Bis-GMA and TEGDMA

obtained in X-band for the radicals of methacrylate monomers. Some authors have attributed this spectrum to only one radical specimen. It is currently accepted that this spectrum is due to at least two different free radical types, which are assumed to occur simultaneously in the samples under study. Some authors assumed that the EMR spectrum is formed by the sum "5 + 4" lines; however, the intensities of the lines obtained using this model are different from those in the dental resin spectrum. Truffier-Boutry et al. [6] have assumed that the spectrum is generated from two methacrylate radicals in the solid state (Fig. 6.1), the "propagating" radical (RI) and the allylic radical (RIII). In addition, the methacrylate radical (RII) is probably not observed in the EMR spectrum because it reacts rapidly or the quantity generated is too small to detect, such that the resulting EMR spectrum is formed by the superposition of "9 + 5" lines.

Samples of the commercial resin Z100 (3 M ESPE, Campinas, SP, Brazil), in A2 color indicated for dental enamel, were used in the EMR experiments. It is composed essentially of a dimethacrylate monomer mixture of Bis-GMA and TEGDMA, initiator agents (camphorquinone and amine), and charge particles of zirconium and silica (ZrO_2/SiO_2) (manufacturer's specifications). The light source used for photopolymerization was a LED (Ultra Blue, Dabi Atlante, Ribeirão Preto, SP, Brazil) with an intensity 492 mW/cm^2 for 40 s.

The EMR spectra in X-band (~9 GHz) were obtained in a JEOL (JES-PE-3X) spectrometer at room temperature, and the microwave power (1 mW), modulation amplitude (0.40 mT), and modulation frequency (100 kHz) were set to avoid signal saturation and were maintained constant. A JEOL standard sample MgO:Mn^{2+} was used as intensity standard and g marker. The samples were placed in a 2 × 2 mm silicon mold and 40 s of irradiation [1–6]. The EMR spectra in Q-band were obtained with a VARIAN (E-109) spectrometer, with rectangular cavity, microwave power 0.5 mW, and modulation amplitude 0.40 mT. A MgO:Cr^{3+} was used as intensity standard and g marker, where g = 1.9797. The samples were placed in a 1 × 1 mm silicon mold and irradiated for 40 s. The EMR spectra in W-band were obtained in a Bruker (Elexsys E 680) spectrometer with TerraFlex probe, with sample dimensions of less than 1 mm. The data treatment was

performed with the Origin (OriginLab) software, and simulations were achieved using the WinEPR (Bruker) software.

The free radicals produce an EMR signal with hyperfine splitting, and the resulting spectrum shows an intense signal that remains detectable up to 3 months after the polymerization process began, depending on the storage environment and relative concentration generated.

The EMR spectrum was simulated based on the model proposed by Truffier-Boutry et al. [6]. Radical I is the "propagating" methacrylate radical (CH_2–C*–CH_3) that shows a weak nine-line signal, while the other simulated radical, RIII (CH_2–C*–CH_2), has a strong five-line signal arising from a stable radical, called an allylic radical (Fig. 6.1) [1].

The EMR spectrum of polymethacrylate radicals consists of the superposition of nine-line (RI) and five-line (RIII) sets resulting in a "nine-line spectrum" with peaks of alternating intensities, because the hyperfine interaction of the five-line set is about twofold greater than that of the nine-line set and the first line of both sets are virtually coincident (Fig. 6.2). Thus, the proposed model is a "9+5 line spectrum," and not a "5+4 line spectrum."

Regarding the spectrum simulation, Lorentzian and Gaussian shapes were both considered, with different proportions, because these two line shapes are commonly observed in EMR.

The spin Hamiltonian for radicals I and III can be represented as

$$H_{\mathrm{I}} = \mathrm{g}\beta\mathrm{HS} + \left[\mathrm{AIS} + \mathrm{BIS} + \mathrm{B}'\mathrm{IS}\right], \tag{6.6}$$

for radical I, and

$$H_{\mathrm{III}} = \mathrm{g}\beta\mathrm{HS} + \left[\mathrm{AIS} + \mathrm{BIS}\right], \tag{6.7}$$

for radical III, where gßHS is the Zeeman effect and AIS, BIS, and B′IS are the hyperfine interactions of first and second orders, respectively. The hyperfine structure with nine lines was interpreted and simulated in terms of an unpaired electron interaction, with three equivalent protons of the CH_3 group and two non-equivalent protons of the CH_2 group for radical I, and the interaction of radical III with two CH_2 groups, the radical generated during hydrogen abstraction of the monomer by an amine radical [1–3].

Figure 6.3a shows the EMR simulated spectrum for the radical I with this model, and Fig. 6.3b shows the simulated spectrum for radical III. The sum of these two spectrum gives the nine-line EMR spectrum shown in Fig. 6.3c, which is superimposed with the experiment.

In order to obtain additional information concerning the radicals that participate in the polymerization process, measurements were performed in other EMR bands, aimed at improving the spectrum resolution due to the use of higher frequencies. The same model was tested using the Q- and W-bands, due to their sensitivity, in order to detect other radical species; non-detection can occur when the radical is produced in very small amounts or in the case of species possessing very similar g

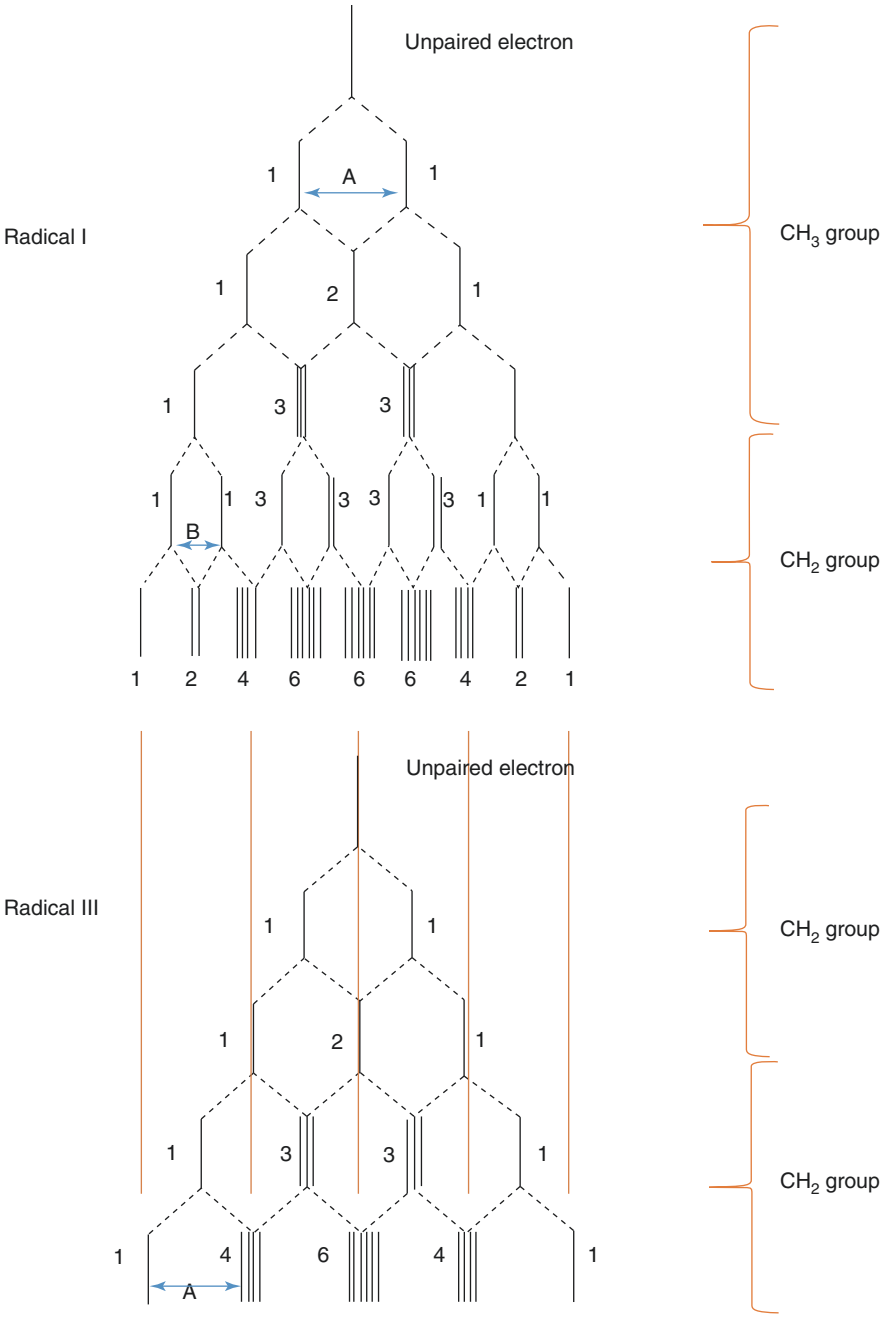

Fig. 6.2 Energy level diagram for the two radicals considered

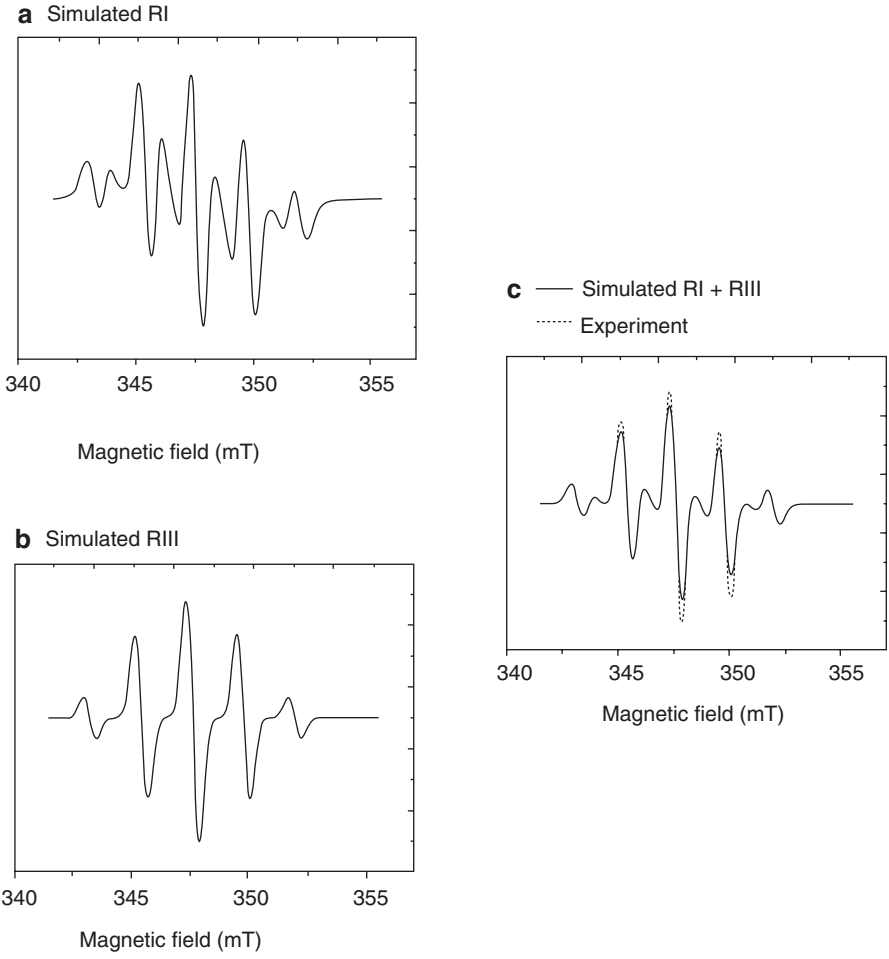

Fig. 6.3 Radical I (**a**) and radical III (**b**) EMR spectra simulations of the composite resin in X-band. (**c**) The superposition of simulated "RI + RIII" and experimental spectra

factors. Figure 6.4a, b shows the simulated spectra for radicals I and III in Q-band and Fig. 6.4c the superposition of simulated RI + RIII with experiment. Again the Hamiltonians and model proposed agree with experiment, as well as in W-band (Fig. 6.5). Since no changes in the spectrum formation were verified, the hypothesis of two radicals was considered valid [2].

The parameters obtained for the simulation in X-band for radical I, with $S = 1/2$ and $I = 1/2$, were $g = 2.0051$ and $A/g\beta = 2.17$ mT for three equivalent 1/2 spin protons belonging to the CH_3 group, $B/g\beta = 1.40$ mT for a non-equivalent proton belonging to the CH_2 group, and $B'/g\beta = 0.85$ mT for a second non-equivalent proton belonging to the CH_2 group. For radical III, the parameters used were $g = 2.0051$ and $A/g\beta = 2.17$ mT for two equivalent 1/2 spin protons belonging to the CH_2 group

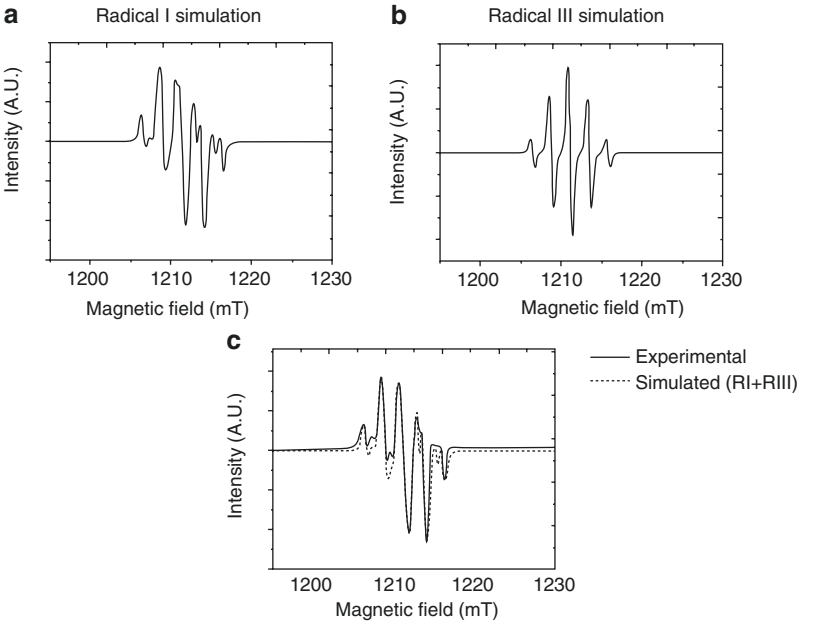

Fig. 6.4 Radical I (**a**) and radical III (**b**) EMR spectra simulations of the composite resin in Q-band. (**c**) Superposition of the simulated "RI + RIII" and experimental spectra

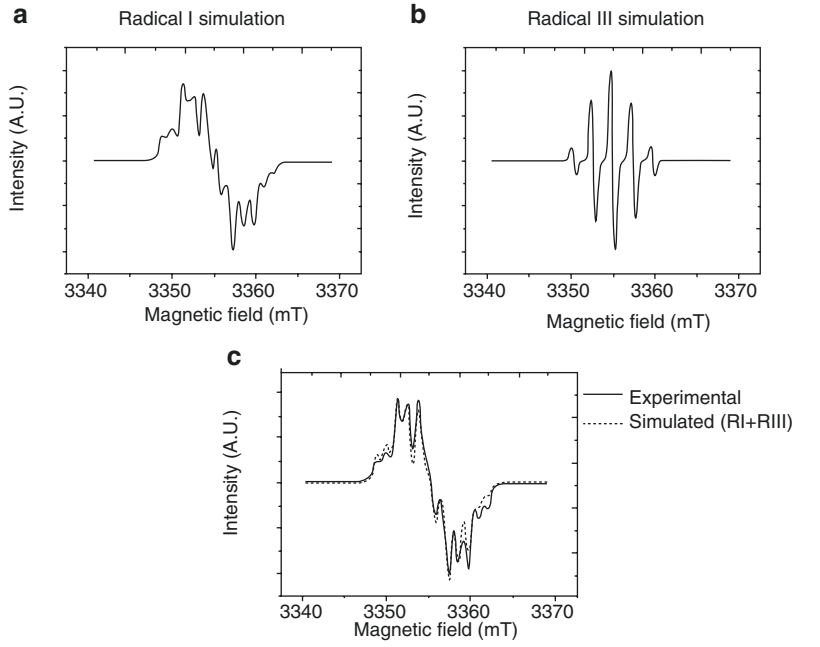

Fig. 6.5 EMR spectrum formation for the dental resin obtained in W-band. Radical I (**a**) and radical III (**b**), and the superposition of the experimental spectrum and the sum of the simulated spectra of radicals I and III (**c**)

and $B/g\beta$ = 2.17 mT for two equivalent 1/2 spin protons belonging to the second CH_2 group [2].

The parameters for the simulation in Q-band with 1/2 spin for radical I were $ACH_3x/g\beta$ = 2.32 mT, $ACH_3y/g\beta$ = 2.32 mT, and $ACH_3z/g\beta$ = 2.33 mT for three protons of the CH_3 group; $BCH_2x/g\beta$ = 1.30 mT, $BCH_2y/g\beta$ = 2.00 mT, and $BCH_2z/g\beta$ = 1.60 mT for one proton of the CH_2 group; $B'1CH_2x/g\beta$ = 0.95 mT, $B'1CH_2y/g\beta$ = 0.75 mT, and $B'1CH_2z/g\beta$ = 0.93 mT for 1 s proton of the CH_2 group; and gx = 2.0015, gy = 2.0023, gz = 2.0023, L/G = 0.5, lx = ly = 0.59 mT, and lz = 0.60 mT. For radical III, $ACH_2xyz/g\beta$ = 2.34 mT and $BCH_2xyz/g\beta$ = 2.34 mT are two CH_2 groups with four equivalent protons, $gxyz$ = 2.0020, lx = ly = 0.55 mT, and lz = 0.61 mT.

The parameters for the simulation in W-band with 1/2 spin for radical I were $ACH_3x/g\beta$ = 2.46 mT, $ACH_3y/g\beta$ = 2.48 mT, and $ACH_3z/g\beta$ = 2.50 mT for three protons of the CH_3 group; $BCH_2x/g\beta$ = 1.30 mT, $BCH_2y/g\beta$ = 1.40 mT, and $BCH_2z/g\beta$ = 1.45 mT for one proton of the CH_2 group; $B'1CH_2x/g\beta$ = 0.95 mT, $B'1CH_2y/g\beta$ = 0.97, and $B'1CH_2z/g\beta$ = 0.90 mT for 1 s proton of the CH_2 group; and gx = 2.00069, gy = 2.0028, gz = 2.0023, L/G = 0.5, lx = ly = 0.59 mT, and lz = 0.65 mT. For radical III, $ACH_2xyz/g\beta$ = 2.34 mT and $BCH_2xyz/g\beta$ = 2.34 mT are two CH_2 groups with four equivalent protons, $gxyz$ = 2.0020, lx = ly = 0.55 mT, and lz = 0.61 mT.

Analysis of the figures revealed that improvement in the EMR spectrum resolution is observed when a higher microwave frequency is used, due to the fact that the free radicals present in the resin are submitted to a more intense magnetic field, which permits the observation of a larger portion of the resonance lines of each radical. The majority the transitions observed in W-band occur in the region of superposed energy levels, hindering clearer identification of the same in X- and Q-bands. The advantage of measuring at higher frequencies is the improved resolution, which should assist in differentiating the paramagnetic species.

In relation to some little differences between experiments and simulations, it is important to remember that we simulate considering the macromolecular system with the unpaired electron interacting only with the closer vicinity, and the Hamiltonian is an approximation for this system in vacuum or water environment. The proper polymerization of the sample can also influence in the result. Considering the number of peaks, line shape, and other parameters, the simulations are in good agreement with experiment [2].

6.2.2 Free Radicals in a Dual-Cured Resin Cement

Samples of resins were dual-cured with cement from AllCem (FGM, Joinville, Brazil) in the color shade A1 were examined by X-, Q-, and W-band EMR. The initial compounds are two pastes separated in a dual-body syringe which are mixed in a self-mixing nozzle that accompanies the kit. The polymerization reaction begins upon mixing the base paste with the catalyst in the nozzle, and it can be accelerated by blue light irradiation. In all experiments, the initial paste and catalyst were mixed

in a 1:1 weight ratio. The particular resin cement was chosen for this study because it has the same composition and showed similar properties and quality compared to others used worldwide for the purpose of translucent fiberglass post cementation. The irradiation of the cement with the blue visible light was produced by a LED (Ultra Blue, Dabi Atlante, Ribeirão Preto, Brazil) with a potency of 492 mW/cm^2. The resin cement samples were separated into two major groups: irradiated for 40 s and not irradiated. Multifrequency EMR spectroscopy aims at improving the spectroscopic information from the use of different field strengths [3].

The X-band (~9 GHz) EMR spectra were obtained with a JEOL JES-PE-3X spectrometer at room temperature using 1 mW microwave power, 0.40 mT modulation amplitude, and 100 kHZ modulation frequency to avoid signal saturation. The samples were placed in a 2 × 2 mm Teflon mold. The Q-band EMR spectra were obtained with a Bruker ER-5106 QT spectrometer at 0.5 mW microwave power and 0.40 mT modulation amplitude. The samples were placed in a 1 × 1 mm Teflon mold. The W-band EMR spectra were obtained with a Bruker Elexsys E 680 spectrometer fitted with a TerraFlex probe, with sample dimensions of less than 1 mm. All experiments were carried out at room temperature. The data treatment was performed with OriginLab software, and simulations were achieved using the WinEPR (Bruker) software [3].

In addition to the self-cure, the dual-cure resin cement has the photo-cure initiators added to its composition. The photoinitiation mechanism by the camphorquinone reaction with a tertiary amine is well described by Truffier-Boutry et al. [6] for the composite resin and was analyzed in previous section. As the EMR spectrum does not depend on the inorganic charges and the self-cure takes place independently of the photo-cure, the model proposed by Truffier-Boutry et al. [6] is applicable to this case, such that the free radicals responsible for the continuity of the polymerization initiated by photo-cure are the propagating (CH_3–C*–CH_2) and the allylic (CH_2–C*–CH_2) radicals.

In the self-cure process, the BPO is degraded releasing two primary radicals and an inert product [3]. Figure 6.6 represents the BPO degradation by interaction with the tertiary amine 4(*N*,*N*-dimethylamino)phenethyl alcohol (DMPOH) [3]. The primary free radicals generated in the self-cure are the N-methylene radical (named PRI) and the benzoyloxy radical (named PRII), while the inert product is benzoic acid [3]. Subsequently PRI and PRII react with monomers leading to the induction step and then to the propagation step, where the active monomer reacts with another monomer molecules. The PRI reacts with monomers by breaking the double bonding or by hydrogen abstraction (Figs. 6.7 and 6.8). The reaction

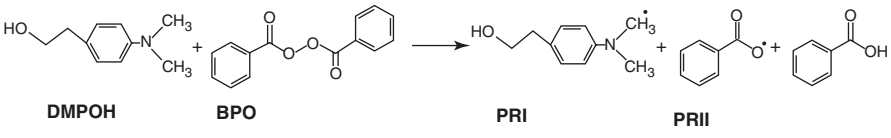

Fig. 6.6 The degradation process of BPO generating two primary radicals, PRI (N-methylene radical) and PRII (benzoyloxy radical), and one inert product

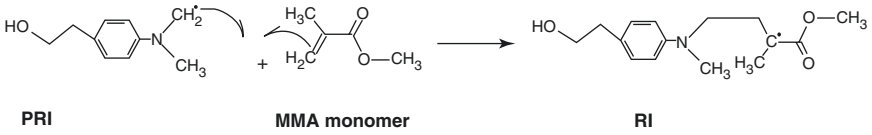

Fig. 6.7 The reaction of PRI with a MMA monomer generating the propagating radical (RI)

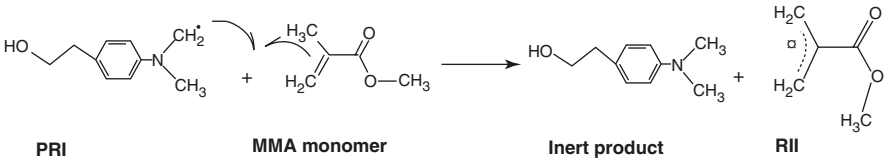

Fig. 6.8 Reaction of PRI with a MMA monomer by hydrogen abstraction generating an inert product and an allylic radical (RII)

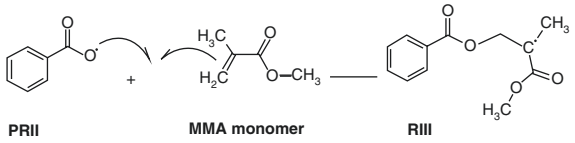

Fig. 6.9 The reaction of PRII with a MMA monomer generating the propagating radical (RIII)

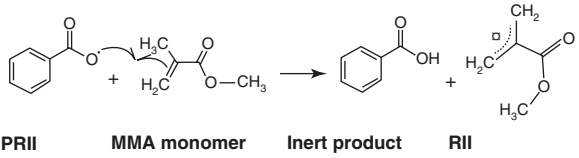

Fig. 6.10 Reaction of PRII with a MMA monomer by hydrogen abstraction generating an inert product and an allylic radical (RII)

generates two different radicals, the propagating radical (RI) and the allylic radical (RII), which can be detected by EMR spectroscopy. Figures 6.9 and 6.10 represent the reaction of the PRII with methacrylate monomer generating two different radicals, RIII and RII.

For mobile radicals, the radical structures RI, RII, and RIII are assumed. It is possible to see that the unpaired electrons in RI and RIII have the same neighborhood (CH_3–C*–CH_2), while RII has the CH_2–C*–CH_2 structure for the closest neighbors. These radicals are the same as the free radicals discussed by Truffier-Boutry et al. [6] to be responsible for the photopolymerization of a composite resin.

6.2.2.1 Multifrequency EMR Experiment

As the polymerization reaction occurs independent of each initiation protocol and the closest neighbors of the unpaired electrons are the same as those found in the composite resin shown by Fontes et al. [2], it is to be expected that the X-band EMR spectrum of the resin cement has nine lines. Figures 6.11 and 6.12a, b show the X-, Q-, and W-band EMR spectra, respectively, of the photo-cured and the self-cured sample.

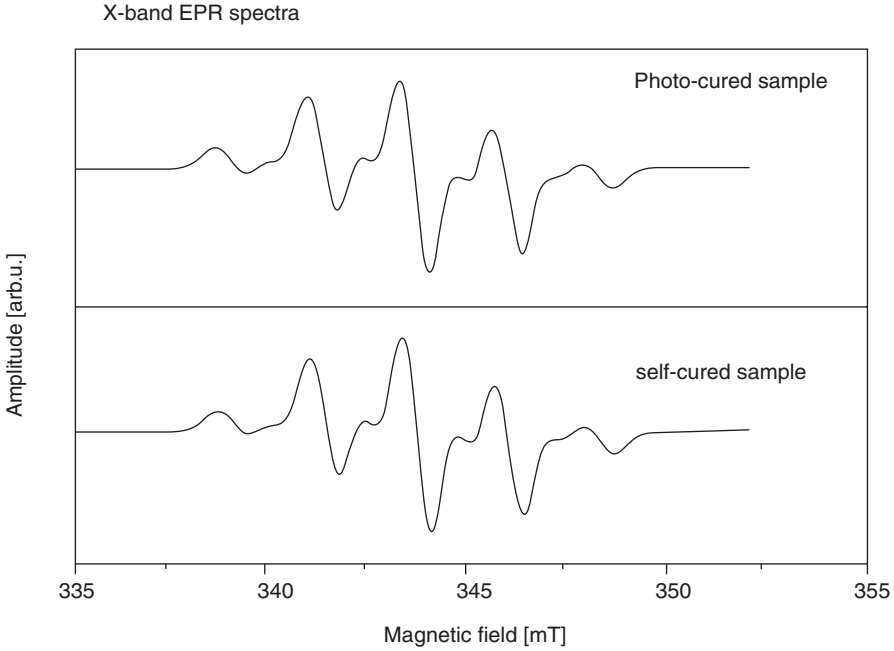

Fig. 6.11 X-band EPR spectra for the photo-cured and the self-cured samples of the dual-cure resin cement AllCem

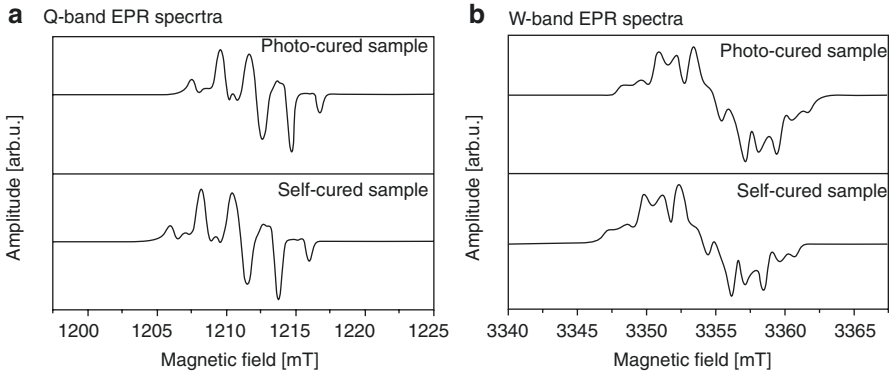

Fig. 6.12 EPR spectra for the photo-cured and the self-cured samples of the dual-cure resin cement AllCem in (**a**) Q-band and (**b**) W-band

No significant differences between photo-cure and self-cure are noticed, and the spectra agrees with the one obtained in previous section for the photopolymerizable dental resin. It is possible to conclude that for the dual-cured resin cement, there are two paramagnetic species forming the EMR spectrum, RI (CH_3–C*–CH_2) and RII (CH_2–C*–CH_2), which are the same radical species formed in the polymerization of the photo-cured composite resin. The radical species are simultaneously present in the sample and occur independently of the polymerization protocol [3].

6.3 Real-Time Polymerization Monitoring in Dental Composite by EMR

In this section, we demonstrate how electron magnetic resonance can be associated with nuclear magnetic resonance (NMR) to study the kinetics of polymerization. Again, the material chosen for the study is the commercial dual-cure resin cement AllCem (FGM).

The NMR-MOUSE (nuclear magnetic resonance mobile universal surface explorer) is a stray-field NMR device suitable to detect the monomer concentration and changes in molecular mobility nondestructively in real time [1]. The NMR-MOUSE can be used to acquire depth profiles locally into the object by varying the distance between the NMR-MOUSE and the object [1].

The concentration of FRs was determined by X-band EMR spectroscopy in real time during the reaction and correlated with the decay curve of mobile monomers obtained by the nuclear magnetic resonance mobile universal surface explorer (NMR-MOUSE). As the EPR signal intensity is proportional to the amount of paramagnetic species in the sample, the second integral of the spectrum gives the number of FRs at the time of measurement. This is a reliable method for determining the amount of radical species in any sample. The EPR experiment does not give information about layers and positions in the sample as does the NMR-MOUSE. The EPR spectrum is always correspondent to the overall mass of the sample inside the resonant cavity [1].

Therefore, while by the time-resolved NMR we can accompany the conversion of monomers into polymers during the reaction, we can probe by EMR the concentration of FRs responsible for the polymerization in the same period [1].

6.3.1 Kinetics of Polymerization of the Self-Cure

Table 6.1 presents the reaction mechanisms for the self-cure.

Table 6.1 Reaction mechanism for the self-polymerization

Initiation:
First step: $A + I \xrightarrow{k_d} A^* + I^* + \text{inert product}$
Second step: $\begin{cases} I^* + M \xrightarrow{k_{i1}} \text{RM}_1^* \\ A^* + M \xrightarrow{k_{i2}} \text{RM}_1^* \end{cases}$
Propagation: $\text{RM}_n^* + M \xrightarrow{k_p} \text{RM}_{n+1}^*$
Termination by combination or disproportionation**: $\text{RM}_n^* + \text{RM}_m^* \xrightarrow{k_t} D_{n+m} \,/\, D_n + D_m$
Radical trapping: $\text{RM}_n^* \xrightarrow{k_b} \text{RM}_{n,b}^*$
Primary radical termination: $\begin{cases} I^* + \text{RM}_n^* \xrightarrow{k_{tp}} D_n \\ A^* + \text{RM}_n^* \xrightarrow{k_{tp}} D_n \end{cases}$
Chain transfer to amine: $\text{RM}_n^* + A \xrightarrow{k_{fA}} D_n + A^*$
Inhibition: $P_n^* + \text{ZA} \xrightarrow{k_Z} D_n$
Benzoyl peroxide side reaction: $I^* + I \xrightarrow{k_I} I^* + \text{inert product}$

**In these equations $n \approx m$

Based on the general kinetics mechanism presented for the self-cure of resin cement, rate equations for all the reacting species can be written as follows [1]:

Initiators:

$$\frac{\mathrm{d}[I]}{\mathrm{d}t} = k_d [I][A] + k_I [I^*][I] \tag{6.8}$$

$$-\frac{\mathrm{d}[A]}{\mathrm{d}t} = k_d [I][A] + k_{fA} [\text{RM}^*][I] \tag{6.9}$$

Primary initiator radicals:

$$-\frac{\mathrm{d}[I^*]}{\mathrm{d}t} = -f_1 k_d [I][A] + k_{i1} [I^*][M] + k_{tp} [I^*][\text{RM}^*] \tag{6.10}$$

$$-\frac{\mathrm{d}[A^*]}{\mathrm{d}t} = -f_2 k_d [I][A] + k_{i2} [A^*][M] + k_{tp} [A^*][\text{RM}^*] + k_{fA} [\text{RM}^*][A] \tag{6.11}$$

Double bonds:

$$-\frac{\mathrm{d}[M]}{\mathrm{d}t} = k_p [\text{RM}^*][M] + k_{i1} [I^*][M] + k_{i2} [A^*][M] \tag{6.12}$$

Active macroradicals:

$$-\frac{\mathrm{d}\left[\mathrm{RM}^{*}\right]}{\mathrm{d}t}=-k_{i1}\left[M\right]\left[I^{*}\right]-k_{i2}\left[M\right]\left[A^{*}\right]+2k_{t}\left[\mathrm{RM}^{*}\right]^{2}+k_{Z}\left[Z\right]\left[\mathrm{RM}^{*}\right]$$
$$+k_{b}\left[\mathrm{RM}^{*}\right]+k_{fA}\left[A\right]\left[\mathrm{RM}^{*}\right]+k_{tp}\left(\left[I^{*}\right]+\left[A^{*}\right]\right)\left[\mathrm{RM}^{*}\right] \tag{6.13}$$

Trapped radicals:

$$\frac{\mathrm{d}\left[\mathrm{RM}^{*}\right]_{b}}{\mathrm{d}t}=k_{b}\left[\mathrm{RM}^{*}\right] \tag{6.14}$$

Inhibitor:

$$\frac{\mathrm{d}\left[Z\right]}{\mathrm{d}t}=-k_{Z}\left[Z\right]\left[\mathrm{RM}^{*}\right] \tag{6.15}$$

In these equations $\left[\mathrm{RM}^{*}\right]=\sum_{n=1}^{\infty}\mathrm{RM}_{n}^{*}$ and k_b is the radical trapping rate constant, which is assumed to be dependent on the fractional free volume of the mixture (V_f) according to $k_\mathrm{b}=k_{\mathrm{b0}}\frac{1}{\mathrm{e}^{-\gamma_\mathrm{b}/V_\mathrm{f}}}$, with k_{b0} the pre-exponential factor, and γ_b is the dimensionless activation volume which governs the rate at which radical trapping increases as a function of fractional free volume. This set of differential ordinary equations can be numerically integrated with the Gear's method to give the time dependence of all reacting species.

During the initial stage of polymerization, where the effect of diffusion-controlled phenomena on the reaction rates is negligible and the steady-state approximation for macroradicals holds, the rate of polymerization (R_p) is given by [1]

$$R_{p}=k_{p}\left(k_{d}\frac{\left(f_{1}+f_{2}\right)}{k_{t}}\right)^{1/2}\left[M\right]\left(\left[I\right]\left[A\right]\right)^{1/2}. \tag{6.16}$$

where k_d is the initiator decomposition rate constant; k_p and k_t represent the propagation and termination rate constant, respectively; and f_1 and f_2 denote the efficiency factors.

6.3.2 Kinetics of Polymerization of the Photo-Cure

The initiator (I) is activated by light irradiation either to a singlet (lifetime in the nanosecond range) or a triplet state (with a lifetime of 50 ms) [1]. Triplet-activated CQ molecules $\left(I_{\mathrm{triplet}}^{*}\right)$ may react with the accelerator molecules (A) and fm two radicals [1], I^* and R^*. I^* shows little reactivity, and the polymerization rate is determined by accelerator radical R^* reacting with the first monomer M. In the propagation stage, the macromolecular chains are formed by successive reaction with monomers. The reaction is terminated typically by combination and/or disproportionation (Table 6.2) [1].

Table 6.2 Reaction mechanisms for the photo-cure

Initiation: $I + h\nu \rightarrow I^*_{\text{triplet}}$
$I^*_{\text{triplet}} + A \rightarrow I^* + R^*$
$R^* + \text{M} \xrightarrow{k_i} \text{RM}^*$
Propagation: $\text{RM}^*_n + \text{M}_1 \xrightarrow{k_p} \text{RM}^*_{n+1}$
Termination by combination or disproportionation**:
$\text{RM}^*_n + \text{RM}^*_m \xrightarrow{k_t} D_{m+n} \,/\, D_n + D_m$

**In these equations $n \approx m$

In these reactions, k_i, k_p, and k_t denote the reaction rate constant of the initiation, propagation, and termination steps, and D_{m+n} stands for the "dead" polymer formed containing $m + n$ monomer units.

The following classical analytical equations are developed for photo-cure kinetics for linear-chain systems [1]. If φ denotes the extinction coefficient assuming an infinite reservoir of accelerator molecules, I_0 the intensity of light absorbed in the surface, α the initiation efficiency, and d the length of the light path in the sample, the rate of production of primary radicals from the photo-sensitizer (R_{PR}) may be expressed by [1]

$$R_{PR} = k_i I_0 t \alpha \mathrm{e}^{-\varphi d}. \tag{6.17}$$

The rate of production of primary radicals can be re-expressed via the following equation:

$$R_{PR} = \beta k_i \left[A\right]\left[I^*_{\text{triplet}}\right], \tag{6.18}$$

where β is the fraction of exciplex "molecules" forming FR. Assuming that the rates of production and consumption of initiator radicals rapidly become equal (steady-state assumption), then R_{PR} is equal to the rate of initiation R_i, meaning $R_{PR} = R_i$ [1]. Approximating the rate of the bimolecular propagation reaction to be independent of the chain length, the propagation rate $R_p$may be expressed by

$$R_p = k_p \left[M\right]\left[\text{RM}^*\right], \tag{6.19}$$

where $[M]$ is the monomer concentration and $[\text{RM}^*]$ the concentration of growing chains. The reaction rate for termination by combination and/or disproportionation is written as

$$R_t = 2k_t \left[\text{RM}^*\right]^2 \tag{6.20}$$

In these reactions, k_i, k_a, k_p, and k_t denote the reaction rate constant of the initiation, rate constant of formation of exciplex from the bimolecular reaction between amine and CQ, and reaction rate of the propagation and termination steps. Assuming a steady state, initiation and termination reaction rates are identical ($R_i = R_t$). Then the steady-state propagation rate of radical polymerization is given by

$$-\frac{\mathrm{d}[M]}{\mathrm{d}t} = k_p \left(\frac{k_i I_0 \alpha e^{-\varphi d}}{2k_t} \right)^{1/2} \sqrt{t}[M]. \tag{6.21}$$

This leads to the time-dependent monomer concentration, $[M](t)$,

$$[M](t) = [M]_0 \, \mathrm{e}^{-\frac{2}{3}\left(\frac{t-t_0}{\tau_P}\right)^{3/2}}, \tag{6.22}$$

with the initial time t_0, $[M]_0$ the initial monomer concentration, and $\tau_P = \left[k_p \left(\frac{k_i I_0 \alpha e^{-\varphi d}}{2k_t} \right)^{1/2} \right]^{-\frac{2}{3}}$ the characteristic time constant for the photo-cure [1].

The self-cure reaction starts as soon as the two components are mixed. The paste-paste self-cure composite has a storage problem, as the BPO mixed with the dimethacrylate monomer is sensitive to heat decomposition. Therefore, inhibitors are added to suppress the polymerization of monomers and prevent premature polymerization. In the case of self-cure composites, inhibitors also provide clinical working time (referred to as the inhibition period, or more commonly, the induction period) to the professional for manipulating materials. When the two pastes of the composite are mixed, the radicals formed by the reaction of the BPO and amine are unable to react with the monomers due to the action of inhibitors and oxygen during the induction period. Thus, inhibitors produce an inert product and completely stop polymerization until the inhibitors are consumed, after which polymerization proceeds at the same rate as if the inhibitor was absent [1]. Meanwhile, the material can be light cured at any time during the chemical (self-)polymerization period. When the resin cement is irradiated, the production rate of primary radical is very high, so that the concentration of inhibitor decreases in a very short time, which explains the rapid decrease in amplitude of the NMR-MOUSE signal in Fig. 6.13a.

It was empirically obtained an expression for the changes in the mobile monomers concentration in the self-cure reaction. During the inhibition time, it is assumed the rate of production of FRs to be identical to the rate of consumption of radicals by the inhibitors, because according to Fig. 6.13, there are no changes in the concentration of mobile monomer during the first minutes. Thereafter, the monomer concentration decays in an exponential way. Considering the rate of self-polymerization in Eq. (6.16), we postulate this rate to be time-dependent [1]:

$$-\frac{\mathrm{d}[M]}{\mathrm{d}t} = \left(K_{\mathrm{SC}}\right) \sqrt[2]{t}[M], \tag{6.23}$$

in which $K_{\mathrm{SC}} = k_p \left(k_d \frac{(f_1 + f_2)}{k_t} \right)^{1/2} \left([I][A]\right)^{1/2}$. This expression can be integrated to give the time-dependent monomer concentration,

$$[M](t) = [M]_0 \, \mathrm{e}^{-\frac{2}{3}\left(\frac{t-t_0}{\tau_{\mathrm{SC}}}\right)^{3/2}}, \tag{6.24}$$

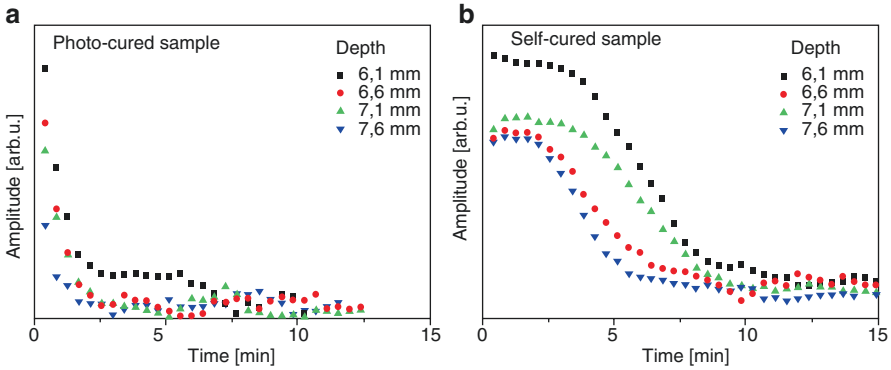

Fig. 6.13 Echo sums as function of time and depth corresponding to the distance to the sensor (**a**) for the photo-cured sample and (**b**) for the self-cured sample

with the initial time t_0 the average time for stopping the inhibition, $[M]_0$ the initial monomer concentration, and $\tau_{SC} = \left(K_{SC}\right)^{-2/3}$ the characteristic time constant of the self-cure reaction [1].

The entire curing process of a dual-cure resin without light irradiation is divided into three stages: the necessary working time for the dentistry professional, the conversion of monomers (curing time), and the cured sample (Fig. 6.14a). The EPR signal intensity for the self-cured sample first increases slowly during the time interval in which the monomers concentration is stable because of the presence of inhibitors to prevent premature reactions. In addition, oxygen trapped in the sample pans can act as an inhibitor [1]. Then the intensity rapidly decays once the concentration of inhibitors is zero. At this point the FRs can react with monomers and start the polymerization reaction. The EPR signal remains zero during the curing time of the resin cement because they are generated in the same rate that are consumed, as assumed in the solution for the rate equations. High initial initiator concentrations are used in commercial polymerizations in order to achieve fully cured products in short reaction times [1]. As the concentration of initiators is too large, FRs continue to be generated even after the monomers are converted into polymers (Fig. 6.14b), so the EPR signal intensity still grows after the curing time.

For the photo-cured sample, the amount of paramagnetic species detected in EPR spectroscopy grows up during the irradiation time and decreases after stopping irradiation (Fig. 6.15). The concentration of FRs rapidly increases up to a maximum value depending on the concentration of initiators, concentration of monomers, and other factors [1]. When irradiation is terminated, the concentration of FRs decreases exponentially due to the consumption of FRs when converting monomers to polymers [1]. The polymerization that occurs after irradiation is slow because the polymeric chain has low mobility in the matrix after irradiation. Figure 6.16 represents the proposed model.

The remaining FRs in a polymerized matrix have been widely studied [1]. During radical polymerization, a gel effect occurs [1], increasing the concentration of FRs which cannot terminate due to their reduced mobility in the matrix. In addition, a

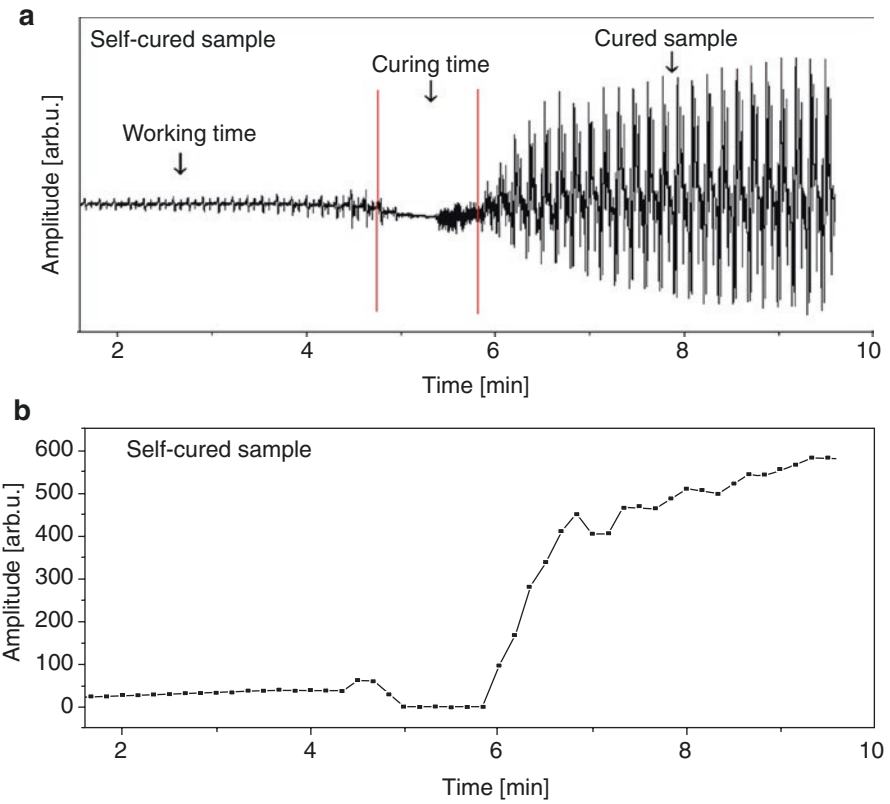

Fig. 6.14 (**a**) EPR spectra of the self-cured sample obtained every 10 s. (**b**) Intensity of the EPR spectra of the self-cured sample obtained every 10 s in a time interval of 10 min

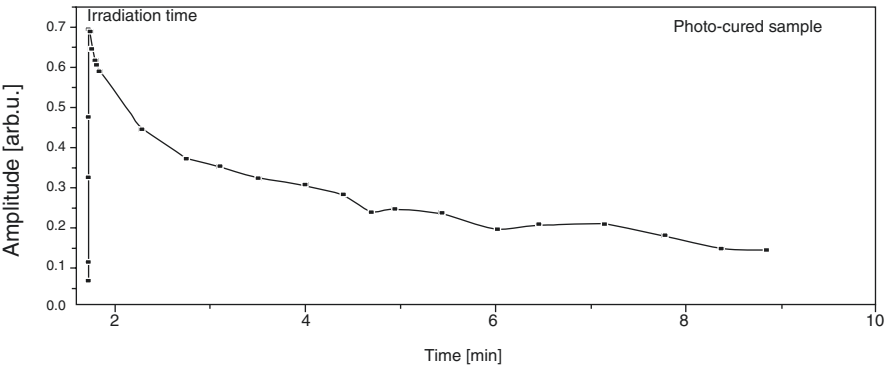

Fig. 6.15 Intensity of the EPR spectra of the photo-cured sample

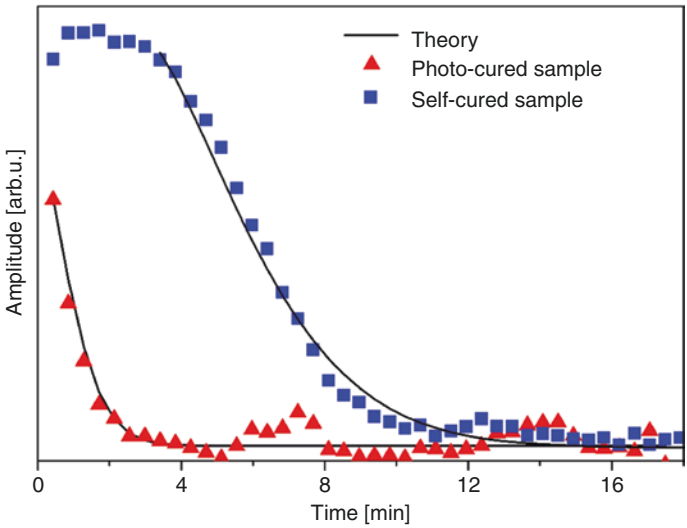

Fig. 6.16 Correlation between theory and experiment for the dual-cured resin cement

vitrification of the matrix occurs, and FRs and remaining double bonds are "quenched" in the organic matrix. Although FRs are present in the sample, the mobility of macromolecules is now in short range.

These results with real-time EPR spectroscopy can be related to the study with the NMR-MOUSE to confirm that the reduction in the concentration of mobile monomers traps FRs in the sample [1], and the model.

6.4 Influence of a Translucent Fiberglass Post on the Depth of Cure in a Root Canal

In this section, we show how EMR spectroscopy is a suitable tool to determine in an indirect way the degree of conversion of monomers into polymers. For this, we use a translucent fiberglass post cemented in a simulated root canal and measure the concentration of FRs in different depths of the post. As the degree of conversion directly depends on the concentration of free radicals generated during the initiation step, this study shows how the translucent fiberglass post effectively transmits the light from the curing device trough the root canal [6].

6.4.1 Influence of the Irradiation Mode and Depth of Cure in Double-Shaped Post

In this present experiment, the relative concentration of free radicals from the dual-cure resin cement, AllCem (FGM, Joinville, SC, Brazil; Table 6.1), of shade A1 was evaluated by electron paramagnetic resonance (EPR) at different restoration points,

after cementation of a prefabricated translucent fiberglass post White Post DC number 1 in a simulated root canal. These materials have properties and qualities that are very similar to others used worldwide. This methodology provides data and basement to understand the influence of a translucent fiberglass post on the degree of conversion of dual-cure resin cement.

The experiment is divided into three major groups: irradiated for 40 s (G1), not irradiated (G2), and irradiated for 40 s with the cementing line sealed (G3). In all groups, the post was cemented and then sectioned in three parts (cervical, middle, and apical thirds). By means of the relative concentration of free radicals, it is possible to study two variables: the influence of sealing the cementing line in the curing of the resin cement and the influence of the fiberglass post in the polymerization of resin cement at different depths (depth of cure of translucent fiberglass post).

After the post cementation for groups 1 and 3, the resin cement was photopolymerized for 40 s using a light-emitting diode (LED) (Radii Plus – SDI®, São Paulo, SP) with 1500 mW/cm^2 potency and in contact with the exposed fiberglass post (2 mm). In G3, the junction between the post and silicone interface was sealed prior to light curing to block light in this region. The resin cement was not photopolymerized after post cementation in G2.

After 10 min from the resin cement mixture, all specimens were removed from the silicone, and the 2 mm section of the fiberglass post that extended from the specimens was sectioned using a double-sided fine-grained diamond disc (Microdont, Socorro, SP, Brasil) at low speed. This sectioning left 18 mm of the post that was cemented, which was divided into three equal parts (6 mm each): the cervical third (closest to the silicon external surface), middle third, and apical third (furthest from the silicon external surface). A 2 mm sample from each third was obtained to study the relative concentration of free radicals: cervical third (CT), middle third (MT), and apical third (AT) (Fig. 6.17).

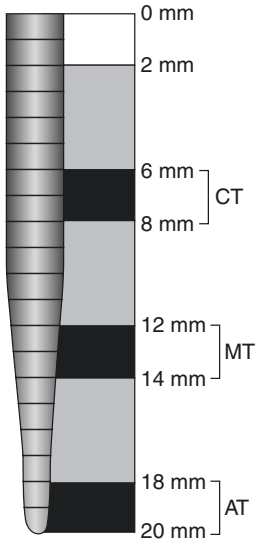

Fig. 6.17 Schematic representation of the double-shaped translucent fiberglass post and the thirds selected for the experiment

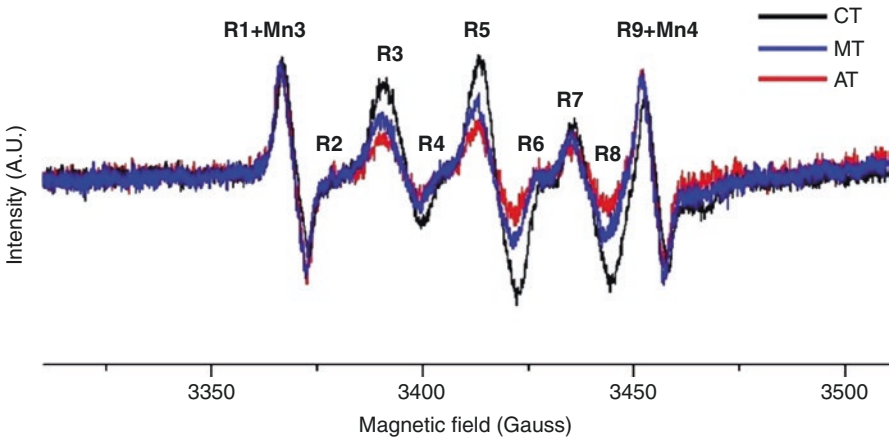

Fig. 6.18 The superposition of X-band EPR spectra for CT, MT, and AT of G1 with the manganese standard

Figure 6.18 shows the superposition of EPR spectra for CT, MT, and AT of G1 and illustrates how the comparison can be done. As CT showed the most intense EPR signal amplitude and thus the greatest concentration of free radicals for all experimental groups, it was taken as the reference point to study the variation on the relative concentration of free radicals between the samples in the group, so that the data presentation is relative to CT (taken as 100%) in each group. The first line in the EPR spectrum (Fig. 6.18) is the superposition of the third line of the MgO:Mn^{2+} standard (called Mn3) with the first line of the free radical (called R1), and the last line in the spectrum is the superposition of the fourth line of the standard (Mn_4) with the ninth line of the free radical (R9). The EPR signal intensity of free radicals for all groups was normalized with the line intensity of the third line of the MgO:Mn^{2+} standard to compare variances in the intensity of the free radical signal (central line) because the superposition is very small and does not change final intensity. As the replicates showed the same results, we used the samples with best signal to noise ratio for data treatment.

EPR spectra in X-band (~9 GHz) were obtained using a JEOL (JES-PE-3X) spectrometer at room temperature, and the microwave power (1 mW), modulation amplitude (20 Gauss), and modulation frequency (100 kHz) were set to avoid signal saturation. A JEOL standard sample MgO:Mn^{2+} was used as an intensity standard and g marker to determine the relative concentration of free radicals. The 2 mm samples from each third of fiberglass posts were inserted into quartz tubes with a 3 mm inner diameter and were analyzed 10 min (T0) and 24 h (T1) after cement mixing. In the time interval from T0 to T1, the samples were stored in aluminum envelopes to remove any influence of external radiation. The data obtained were processed using Origin 8 (OriginLab) and EasySpin (MatLab) software to process the EPR spectra. The estimated error in determining the intensity peak is ±6%.

The EPR spectrum in Fig. 6.18 shows nine-line characteristic of hyperfine interactions. It is concluded that the paramagnetic species in the sample are the "propagating" and "allylic" radicals shown by Fontes et al. [2], which generated during the irradiation of the sample. These radicals are present in the sample even 1 month after the irradiation because of the vitrification phenomenon, although in much less concentration. The reaction kinetics of dental materials is dependent on the initial concentration of monomers and initiators, as well as the light intensity and depth of cure and temperature. This supports the analysis in two different days and light intensity in this study.

6.4.1.1 The Influence of Irradiation Protocol

In relation to the amount of free radicals generated using different initiation methods, the present resin cement displayed a dependence of this quantity with the sample irradiation protocols (Table 6.3).

The chemical cure occurs regardless of the physical cure, a fact verified by the EPR spectrum for the generated free radicals.

In relation to the different irradiation protocols, G1 showed the strongest EPR spectrum signal at T0 and for the CT, with a value of 100%±6%, with all other samples being compared with this result. The concentration of free radicals for G2 at the CT was equivalent to 53%±6% from G1 and 87% ± 6% from G3. Regarding the samples from the middle and apical thirds for all groups, the variation in the intensity of the EPR spectrum was not significant, indicating that the radiation did not influence the free radical formation in the depth correspondent to G1 and G3. Comparatively to G1, the EPR spectrum intensity reduction was 47%±6% for CT in G2 and 13%±6% in G3 (Table 6.4).

Table 6.3 Experimental groups and material evaluated

Group	Sample		Treatment	Factor to be assessed
G1	Three translucent fiberglass posts White Post DC (FGM), number 1	Three sections of the cervical third	Irradiated (40 s)	FR concentration of the cement AllCem (FGM) 10 min (T0) and 24 h (T1) after the cement mixture
		Three sections of the middle third		
		Three sections of the apical third		
G2	Three translucent fiberglass posts White Post DC (FGM), number 1	Three sections of the cervical third	Not irradiated	
		Three sections of the middle third		
		Three sections of the apical third		
G3	Three translucent fiberglass posts White Post DC (FGM), number 1	Three sections of the cervical third	Irradiated (40 s) with the cementing line sealed	
		Three sections of the middle third		
		Three sections of the apical third		

Table 6.4 Relative concentration of free radicals in the samples 10 min after mixing base paste and catalyst

	Sample		
Group	CT	MT	AT
G1	100 ± 6%	No varies	No varies
G2	53 ± 6%	No varies	No varies
G3	87 ± 6%	No varies	No varies

The decrease observed in the relative concentration of free radicals for CT in G2 (Table 6.4) was significant when compared to G1 and G3, because the cement polymerization in G2 was exclusively chemical. When compared to G1, the observed decrease for CT in G3 might have occurred due to the use of a barrier at the post-silicon interface, which limited the passage of the curing light to only through the post.

Comparing G1 and G3 for CT, the light emitted may have been absorbed and transmitted by the cement located at the post-silicon interface, indicating that sealing the cementing line can diminish the initial amount of generated free radicals affecting the conversion degree of monomers to polymer.

It is possible to notice that the translucence and light conduction capability of the post is significant only in the first 8 mm of restoration, once the irradiation protocol did not interfere in the amount of generated free radicals for MT and AT.

6.4.1.2 Depth of Cure of the Translucent Fiberglass Post

The influence that chemical and physical polymerization exerts on the conversion degree of the resin cement can also be observed when evaluating the free radical concentration for samples obtained from the cervical, middle, and apical sections in G1, G2, and G3 and individually at T0 and T1 (Figs. 6.19 and 6.20).

At T0 (Fig. 6.19), the free radical concentration decreased for MT (12–14 mm) and AT (18–20 mm) in relation to CT (6–8 mm) in G1 and G3. In G1, the initial free radical relative concentration is greater than in G3 because the radiation emitted by the curing light is transmitted by the post and the post-silicon interface. This fact contributes to the facilitation of the polymerization of the resin cement; consequently, a faster conversion degree in G1 was observed (Fig. 6.19), considering that the reaction was already started and a portion of the generated free radicals in G1 was already reacted at the time of observation. In turn, G2 did not show decreasing for CT, MT, and AT, because the cement polymerization in all sections was exclusively chemical.

When analyzing points where the light incidence is relevant 10 min after mixing base paste and catalyst (CT, Table 6.4), it is possible to notice that the light can duplicate the concentration of free radicals at these points. Analyzing Fig. 6.19 it is possible to see that the concentration of free radicals decreased about 50% from CT to AT, for G1 and G3, such that it is possible to conclude that the light does not reach the deepest points of the restoration.

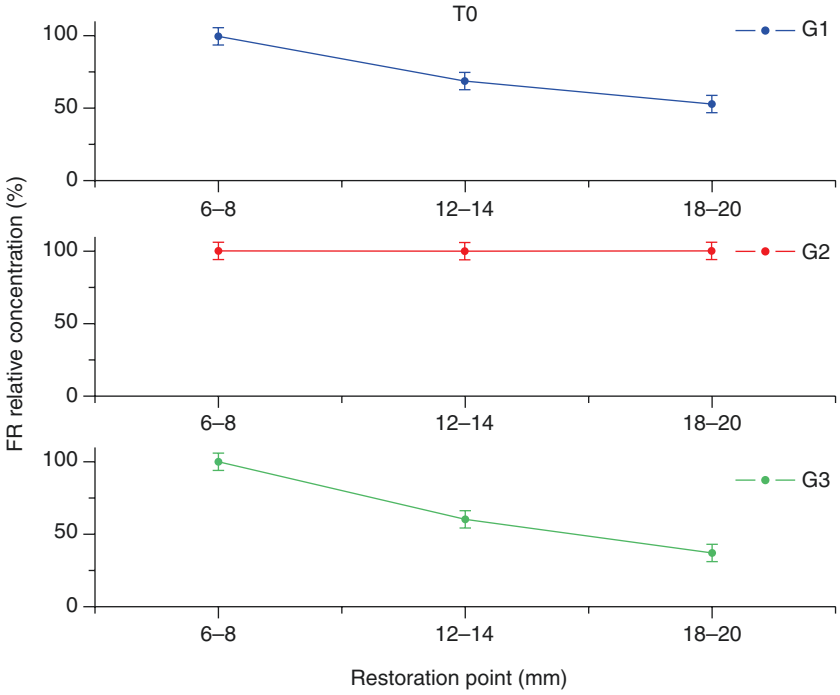

Fig. 6.19 Relative concentration of FR in T0

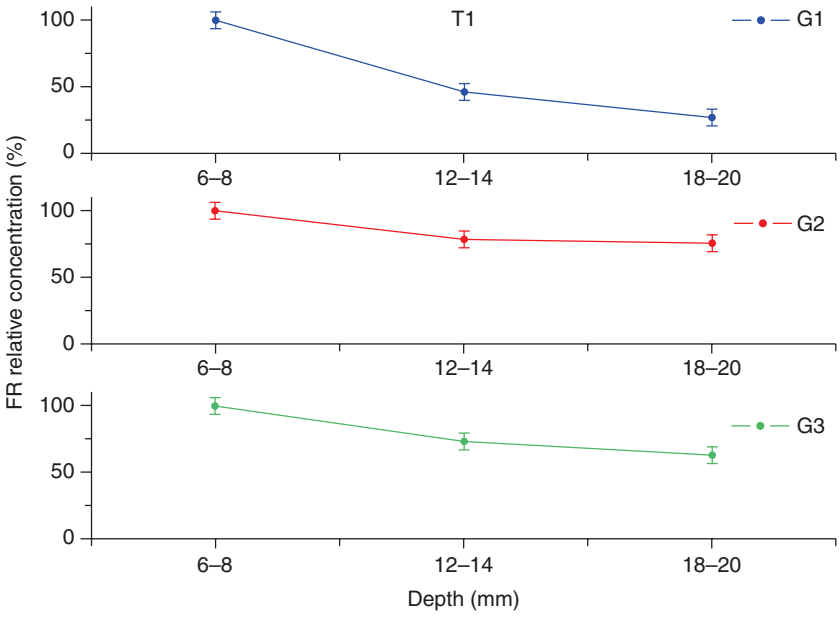

Fig. 6.20 Relative concentration of FR in T1

Twenty four hours after cementation (Fig. 6.20), G1 showed greater decrease in relative concentration of free radicals with depth compared to G3, opposite behavior shown in Fig. 6.19. It occurs because in T0 greater amount of free radicals are generated in G1 than that in G3, which affects the conversion degree. The greater the amount of free radicals generated, the greater is the conversion degree. The decay rate of concentration of initiators depends on the initial concentration of initiators.

The irradiation time, radiation power, and distance from the curing device to the irradiated region directly influence the conversion degree and, consequently, the mechanical properties of a cement and in the bond strength of the fiberglass post to the radicular dentin. Other variables that can influence the amount of generated free radicals and the conversion degree are the post diameter, arrangement of the fibers, composition, translucence degree, and the cementation line thickness. In the present experiment, the power and time were kept constant, 1500 mW/cm^2 and 40 s, respectively, as well as the distance from the curing device to the cemented post. However, based on the present results, a reduction of the luminous intensity with increasing depth of a simulated root canal was observed.

6.4.2 Influence of Geometrical Configuration of the Post on the Depth of Cure

This experiment aimed to evaluate the relative concentration of FRs in samples from the dual-cure resin cement AllCem (FGM, Joinville, SC, Brazil) of shade A1 by electron paramagnetic resonance (EPR) at different restoration points after cementation of a prefabricated translucent fiberglass post White Post DC no. 1 in a simulated root canal (Table 6.5). The post was sectioned to obtain cylindrical and conical samples in order to study the influence of the geometrical configuration of

Table 6.5 Experimental groups and material evaluated

Group		Sample	Curing protocol	Factor assessed
G1	Three cylindrical translucent fiberglass posts, White Post DC (FGM), no. 1 (ClP-1)	Three sections of the cervical quarter	Cement light cured for 40 s	Relative concentration of FR of the cement AllCem (FGM) at two moments in time: T10 min after mixing the cement and T24 h after
		Three sections of the middle quarter		
		Three sections of the deep quarter		
		Three sections of the apical quarter		
G2	Three conical translucent fiberglass posts, White Post DC (FGM), no. 1 (CnP-1)	Three sections of the cervical quarter	Cement light cured for 40 s	
		Three sections of the middle quarter		
		Three sections of the deep quarter		
		Three sections of the apical quarter		

the translucent fiberglass post in the generation of free radicals, which are known to be responsible for the polymerization of the resin cement. Here cervical means the post part closest to the light source and apical the farthest part [5].

After post cementation, the resin cement was photopolymerized for 40 s using a light-emitting diode (LED) (Radii Plus – SDI®, São Paulo, SP) with a potency of 1500 mW/cm^2 and in contact with the exposed ClP-1 and CnP-1. Ten minutes after mixing the resin cement, the set ClP-1/CnP-1 and the AllCem cement was removed from the silicone. With a double-sided fine-grained diamond disc (Microdont, Socorro, SP, Brazil) at low speed, the portion of the posts that remained outside following cementation were sectioned, leaving 8 mm corresponding to the cemented part. This part was sectioned every 2 mm to obtain the samples, cervical quarter (CQ, post portion closest to the polymerization device), middle quarter (MQ), deep quarter (DQ), and apical quarter (AQ), with the samples from ClP-1 allocated to group 1 (G1) and samples from Cn-1 allocated to group 2 (G2) (Fig. 6.20). All samples were obtained in the same conditions of light, temperature, and oxygen.

Figure 6.22a shows EPR spectrum of the dual-cured resin cement due to the superposition of radical I and radical III, and Fig. 6.21b shows the superposition of EPR spectra with MgO:Mn^{2+} standard for cervical, medium, deep, and apical quarters of the conical configuration and illustrates how the comparison can be done. The first line in the EPR spectrum (Fig. 6.22b) is the superposition of the third line of the MgO:Mn^{2+} standard with the first line of the resin cement free radical, and the last line in the spectrum is the superposition of the fourth line of the standard with the last line of the free radical. The EPR signal amplitude of free radicals for all groups was normalized with the line intensity of the third line of the MgO:Mn^{2+} standard to compare variances in the intensity of the free radical signal (central line). As cervical quarter showed the most intense EPR signal amplitude and thus the greatest concentration of free radicals, it was taken as the reference point to study the variation on the relative concentration of free radicals between the samples into the group, so that the data presentation is relative to cervical quarter in each group (taken as 100%).

The EPR spectra in X-band (~9 GHz) were obtained in a JEOL (JES-PE-3X) spectrometer at room temperature, and the microwave power (1 mW), modulation

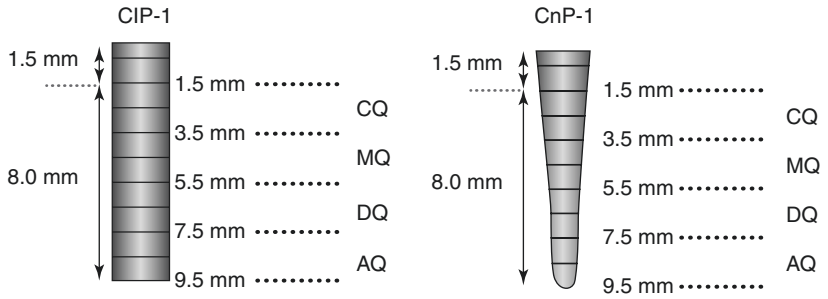

Fig. 6.21 Schematic representation of samples from ClP-1 (G1) and CnP-1 (G2)

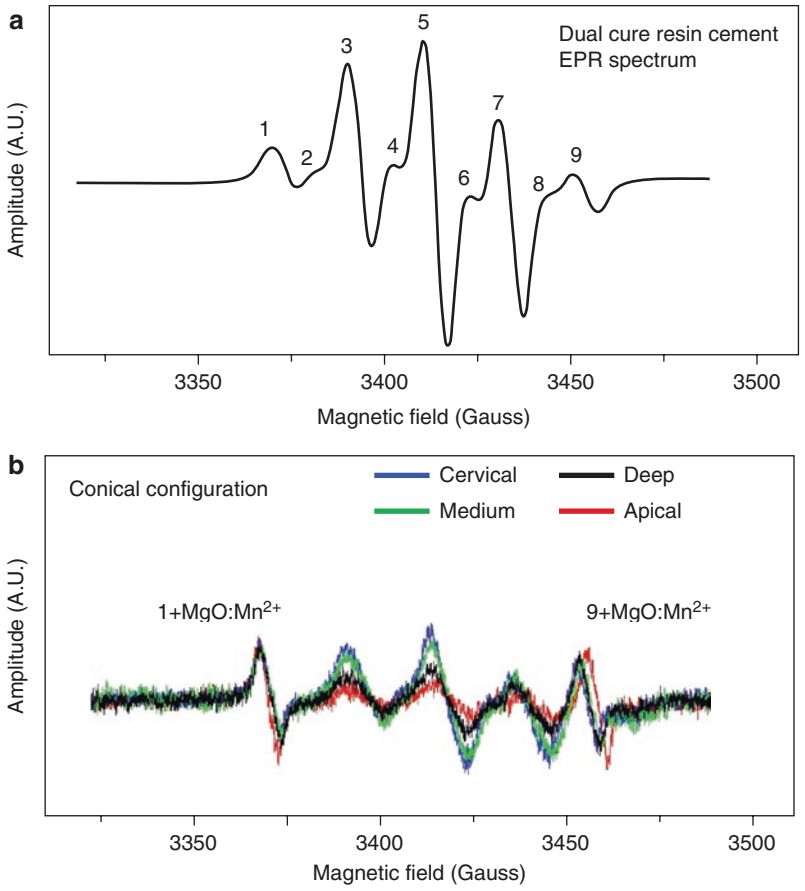

Fig. 6.22 (**a**) Nine-line EPR spectrum of the dual-cured resin cement, characteristic of methacrylate radicals. (**b**) Superposition of EPR spectra obtained from the CQ, MQ, PQ, and AQ of conical configuration at T10 min

amplitude (0.40 mT), and modulation frequency (100 kHz) were set to avoid signal saturation and were maintained constant. A JEOL standard sample MgO:Mn^{2+} was used as an intensity standard and g marker. The 2 mm samples were inserted into the EPR tube (3 mm inner diameter) and investigated immediately after 40 s of irradiation. As the EPR signal intensity is proportional to the amount of paramagnetic species in the sample and this quantity is directly related to the light incidence in the sample, it is possible to use the MgO:Mn2+ as the intensity standard and evaluate differences in the FR concentration for different sections of the post. Each sample was analyzed 10 min (T10 min) and 24 h (T24 h) after mixing the cement. The samples were always carefully handled with tweezers stored in aluminum packets to ensure no influence could be attributed to external light and prevent external contamination.

The best signal to noise ratio among the three replicate EPR spectra obtained for each sample in each experimental group was used for data treatment due to accordance between replicates (Fig. 6.22).

In Fig. 6.22, the first line is the third line of the MgO:Mn^{2+} standard superimposed on the first FR line, and the last line is the fourth resonance line of the standard superimposed on the ninth FR line. The nine lines in the EPR spectrum are typical of methacrylate radicals. The EPR signal intensity for all groups was normalized with the MgO:Mn^{2+} third line intensity. In addition, the EPR signal intensity of the samples in G2 was normalized with respect to the amount of the cement mass, since the resin cement volume is not the same for all samples in this group; because the fiberglass post is conical, a reduction in diameter occurs in the cervical to apical direction. This type of normalization is not required in G1.

For data treatment, it was assumed that the relative FR concentration of the cervical sample (CQ) for G1 and G2 was 100%, because these samples are the first surface and showed the most intense EPR signal and thus the greatest relative FR concentration. The FR concentration for all the other samples in the group was obtained relative to the CQ (Tables 6.6 and 6.7).

Different decay rates were observed in the relative concentrations of FR when comparing the two geometrical configurations (Table 6.6). The G1 MQ showed no variation in the relative concentration of FR with respect to the CQ at T10 min. This indicates that no significant decrease in the light transmission through the cylindrical post occurred that affected the FR concentration at depths up to 5.5 mm. In the DQ, the FR concentration was 84% and in the AQ 70%, clearly indicating that the effectiveness of the light transmission through the post decayed, such that the FR concentration decreased 16% at 6–8 mm in depth and 30% at 8–10 mm. This difference can be explained by the increase in the distance of the DQ and AQ in relation to the radiation source, even when using 1.500 mW/cm^2 of power. In G2, a decrease in the FR concentration was verified for all samples compared with the CQ; the MQ, DQ, and AQ decreased 11, 41, and 72% in relative FR concentration, respectively. The distance between the LED device and the samples analyzed was a significant factor influencing the decay in FR concentration in both G1 and G2. However, for

Table 6.6 Relative FR concentration at T10 min

Group	CQ (1.5–3.5 mm)	MQ (3.5–5.5 mm)	DQ (5.5–7.5 mm)	AQ (7.5–9.5 mm)
G1	100% ± 6%	100% ± 6%	84% ± 6%	70% ± 6%
G2	100% ± 6%	89% ± 6%	59% ± 6%	28% ± 6%

Table 6.7 Relative FR concentration at T24 h

Group	CQ (1.5–3.5 mm)	MQ (3.5–5.5 mm)	DQ (5.5–7.5 mm)	AQ (7.5–9.5 mm)
G1	100% ± 6%	94% ± 6%	98% ± 6%	91% ± 6%
G2	100% ± 6%	83% ± 6%	40% ± 6%	14% ± 6%

This table presents the relative FR concentrations of the samples analyzed 24 h (T24 h) after mixing the base paste and catalyst

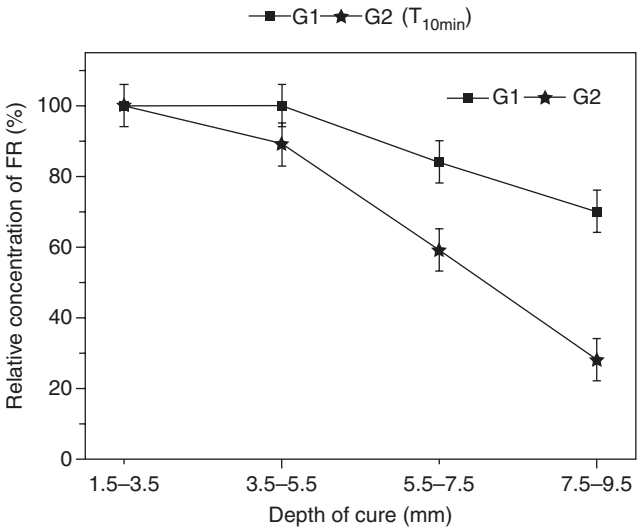

Fig. 6.23 Comparison of the decrease in the relative concentration of free radicals for G1 and G2 in T10 min

G2, the geometrical configuration also influenced light transmission through the post, and thus the relative amount of FR observed in the samples tested was lower (Fig. 6.23).

In our research, it is evident that the shape of the translucent fiberglass post influenced the transmission capacity of the light emitted from the LED device and thus the FR concentration in the dual-cured resin cement, both at T10 min and T24 h.

The diameter of ClP-1 was constant throughout the post length, as well as the amount of epoxy resin and fiberglass. However, in CnP-1, the diameter ranges from 1.6 to 1.25 mm from the cervical to the apical extremities. Considering the variation in FR concentration between G1 and G2 samples, the importance of the diameter of the post in light transmission was confirmed.

In his research, the results showed that the larger the post diameter, the better the results of polymerization of the composite resin at greater canal depth. Regarding the actual effectiveness of transmission of the light emitted by the LED device and its influence on the degree of conversion of FR in resin cement throughout the length of the cemented post, Shadman et al. observed that a translucent quartz fiber post permitted a greater degree of conversion in dual-cured resin cement compared with an opaque post. The authors suggested that this result could be related to the difference in refractive index between glass fiber and epoxy resin in the post. When the light passes through the fiber, it crosses the resin-fiber interface at a higher angle of incidence, which allows reflection to other fibers, resulting in an increase in total light transmittance.

The behavior of light rays emitted by the LED device through interfaces with different refractive indexes could explain the results observed in G1 (Table 6.7), where the DQ showed a higher relative FR concentration compared with the MQ.

A portion of the radiation may have been transmitted through the fiberglass and epoxy resin, while another part may have been absorbed by the mass of the resin cement. The light may also have been directly transmitted by cement located at the post-matrix interface. However, this occurs at low intensity, since the greater part of the light undergoes scattering and absorption when passing from the external environment to the cement mass. Due to changes in the geometrical configuration of CnP-1, the effectiveness of light transmission from the post to the cement is reduced because of the difference in refractive indices.

In relation to the post configuration for ClP-1, at T10 min, no difference was observed between the CQ and MQ. When analyzed at T24 h, the relative FR concentration in the MQ decreased 11% compared with the CQ.

Table 6.7 presents the relative FR concentrations for samples analyzed 24 h (T24 h) after mixing the base paste and catalyst. Compared with the CQ, G1 showed conformity between the relative FR concentrations, such that the MQ, DQ, and AQ showed 94, 98, and 91%, respectively. A larger decrease in the relative FR concentrations was observed for G2 as the depth increased. In this group, the relative FR concentrations were 83, 40, and 14% for the MQ, PQ, and AQ, respectively. During irradiation, the concentration of FR rapidly increases up to a maximum value, depending on the concentration of initiators, depth of cure, and other factors. When irradiation is terminated, the concentration of FR decreases exponentially to zero due to the consumption of FRs when converting monomers to polymers. At depths where the maximum amount of generated FRs is considerably smaller, the EPR spectra obtained 24 h after irradiation shows a relative concentration of FR that is lower than in those samples with a significantly greater concentration of FR.

References

1. Vicentin BLS, Netto AM, Dall'Antonia LH, Di Mauro E, Blümich B. Real-time polymerization monitoring in a dual-cured resin cement by magnetic resonance. Polym Bull. 2017; https://doi.org/10.1007/s00289-017-2007-1.
2. da Silva Fontes A, Vicentin BLS, Valezi DF, da Costa MF, Sano W, Di Mauro E. A Multifrequency (X-, Q-, and W-band) EPR and DFT study of a photopolymerizable dental resin. Appl Magn Reson. 2014;45(7):681–92.
3. Vicentin BLS, Netto AM, Blümich B, Di Mauro E. Identification of free radicals generated by different curing modes in a dental resin cement. Appl Magn Reson. 2016;47(9):1003–14.
4. Vicentin BLS, Salomão FM, Hoeppner MG, Di Mauro E. Influence of geometrical configuration of a translucent fiberglass post on the polymerization of a dual cure resin cement analyzed by epr spectroscopy. Appl Magn Reson. 2016;47(2):211–22.
5. Salomão FM, Vicentin BLS, Contreras EFR, Hoeppner MG, Di Mauro E. The influence of a translucent fiberglass post on the polymerization of dual cure resin cement analyzed by electron paramagnetic resonance. Materi Res. 2015;18(5):1023–8.
6. Truffier-Boutry D, Gallez XA, Demoustier-Champagne S, Devaux J, Mestdagh M, Champagne B, Leloup G. Identification of free radicals trapped in solid methacrylated resins. J Polym Sci A Polym Chem. 2003;41(11):1691–9.

Recent Issues in X-Band ESR Tooth Enamel Dosimetry

7

Shin Toyoda

7.1 Introduction

Tooth enamel, consisting of small crystals of hydroxyapatite, is an excellent material for ESR (electron spin resonance or EPR, electron paramagnetic resonance) dosimetry. It is possible to obtain individual retrospective radiation doses given to humans by ESR tooth enamel dosimetry when extracted teeth are provided by patients. There are many studies investigating retrospective doses received by populations as a result of radiation accidents as recently summarized [1, 2]. Determination of the retrospective doses given by radiation accidents is especially important in epidemiological studies. After many efforts of past researchers, the method of ESR tooth enamel dosimetry is now at a matured stage where its technique has been established for humans. An ISO (International Standard Organization) standard on general aspects was published [3] and one for ex vivo human tooth enamel dosimetry is now in preparation. However, there are still important challenges in technical issues, especially in the low-dose range and for teeth of mammals. The present chapter will summarize such recent issues in X-band ESR tooth enamel dosimetry mainly on technical aspects.

7.2 Principle of ESR Dosimetry

Ionizing radiation creates radicals with unpaired electrons in materials. Many of those radicals are unstable and vanish in a short time; however, in some materials, radicals can be stable enough to survive several days to years. In tooth enamel, radicals created by radiation, the main component of which was identified as CO_2^- [4], are stable enough to be used to date fossils of several hundred thousand years old [5].

S. Toyoda
Department of Applied Physics, Okayama University of Science, Okayama, Japan
e-mail: toyoda@dap.ous.ac.jp

A. K. Shukla (ed.), *Electron Spin Resonance Spectroscopy in Medicine*,
https://doi.org/10.1007/978-981-13-2230-3_7

The intensity of the dosimetric signal is proportional to the given dose in the range of dosimetric applications. The additive dose method was used to determine the given doses at the early stage of the research (e.g., [6]). In this protocol, the sample will be divided into several aliquots and irradiated to different doses with one aliquot left unirradiated. They are then measured by ESR to obtain the intensities of the dosimetric signal which increase linearly with the added dose as shown in Fig. 7.1a. A line is fitted to the points by the least square method, and the line is then extrapolated to the zero ordinate to obtain the retrospective dose as the negative intercept at the dose axis. Alternatively, when the sample amount is not enough to have several aliquots, ESR measurement and gamma ray irradiation can be repeated with the same aliquot, but this is time consuming. Recently, the calibration line method has often been applied to obtain the retrospective radiation doses, the principle of which is shown in Fig. 7.1b. A set of calibration samples are prepared with doses typically up to 1 or 1.5 Gy. Assuming that the dose response of the sample of interest is the same as this set of calibration samples, the dose is obtained as the one corresponding to the signal intensity on the calibration line. As the sensitivity of the signal (the slope of the dose response) is quite uniform in permanent teeth within 10% [7], the calibration method has the advantage that one tooth is enough for determining the dose and that the sample is preserved without any disturbance (without irradiation) if the required precision is about 10%. This precision, however, is usually not attained below 1 Gy.

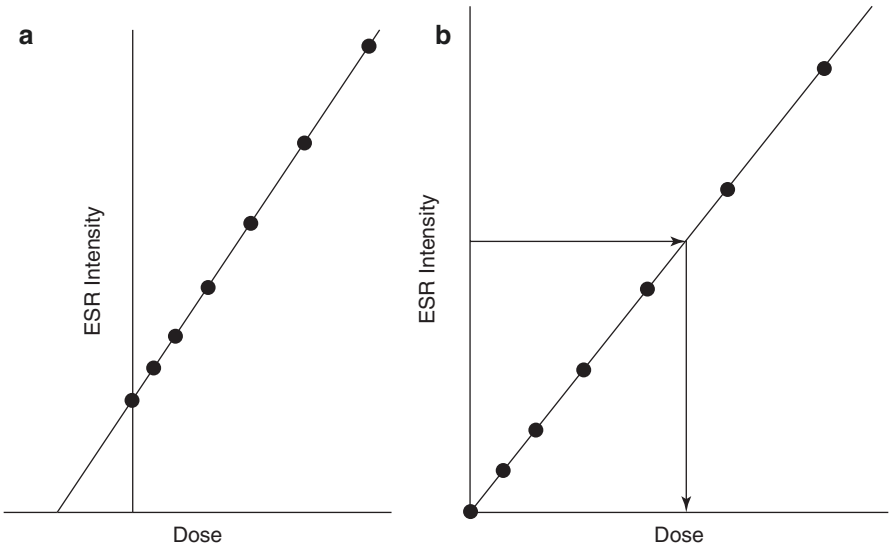

Fig. 7.1 (**a**) The additive dose method. The retrospective dose is the negative value of the intercept at the dose axis which is obtained by extrapolating the regression line to the zero ordinate. (**b**) The calibration method. The dose is obtained as the one corresponding to the ESR intensity on the calibration line

7.3 History of ESR Dosimetry

While the first attempt to use tooth enamel for ESR dosimetry was made nearly 50 years ago [8], the first practical successful application to accidental retrospective radiation dosimetry was to atomic bomb survivors [6]. With improvements to the method, ESR tooth enamel dosimetry has been applied to various cases of radiation accidents such as workers in Mayak (a reprocessing plant of nuclear fuels in former Soviet Union) [9], residents in the reaches of Techa River contaminated by the radioactive wastes of the above plant [10], residents around Chernobyl Nuclear Power Plants [11–14], residents around the Semipalatinsk Nuclear Test Site where the former Soviet Union conducted 467 nuclear explosion tests [15], and victims of JCO accidents in 1999 where nuclear chain reactions occurred in a factory making nuclear fuels [16].

International comparison studies have been conducted already five times in order to test technical improvements and to find the issues and problems with this technique as discussed later in this chapter. The technique has been publicly recognized so that international organizations published technical documents [17] and an ISO standard [3].

7.4 Protocols of ESR Tooth Enamel Dosimetry

7.4.1 Extraction of Tooth Enamel

A human tooth is composed of enamel at its surface and dentin inside. The enamel is made of 96% inorganic material, mostly hydroxyapatite, 3% organic material, and 1% water. Dentin includes only 70% inorganic material, and the rest is organic material and water [17]. As enamel contains a higher concentration of hydroxyapatite crystals, it has a high sensitivity of the dosimetric signal to a given dose. In order to avoid overlaps of interfering organic signal as much as possible, extracting enamel by removing dentin is essentially important in preparing the sample for retrospective dosimetry.

Usually, after cutting out the root, the crown part is cut in half to obtain buccal and lingual halves. This is to check the contribution from dental X-rays which should be effective only in buccal side as the X-rays are not as penetrating as gamma rays. Possible contributions of solar UV would also be checked in the case of front teeth where UV creates a signal identical to dosimetric signal [18]. Nakamura et al. [19] claimed that front teeth show higher doses due to exposure to UV from sunlight.

Chemical and mechanical techniques are used to extract enamel by removing dentin. In the mechanical method, dental drills are used to remove white dentin mechanically leaving gray transparent enamel (e.g., [15]). It is necessary to be careful not to generate much frictional heat with this method. Another chemical method

employs sodium or potassium hydroxide solution. Typically 20% alkaline solution is used at 60 °C with an ultrasonic bath for 24 h [17, 20]. It is possible to combine these two.

After rinsing and drying, the enamel sample is crushed into fragments of about 1 mm [15] or to a powder of about 200 μm [20] to avoid variation of the signal during ESR measurement due to orientation. The c-axis of the hydroxyapatite crystals in enamel is not random but vertical to the tooth surface. When the fragments are too rough, the signal shape varies by changing the orientation of the sample tube in the cavity, which leads to variation in estimating the signal intensity. The mechanically induced signal, however, being similar with the dosimetric signal, is generated when the sample is crushed too much.

7.4.2 ESR Measurements

Currently, most dosimetric work is done with continuous microwave (CW) X-band spectrometers at room temperature. The best measurement conditions are reported, as a microwave power of 2 mW, with modulation amplitude of 0.2 to 0.3 mT [21] for JEOL spectrometers. For Bruker machines, the best microwave power may be different, depending on the cavity type (standard, TMS, spherical, etc.) [22]. It is recommended to set the scan range to 10 mT (±5 mT) to include the third and fourth Mn lines at the left and right ends of the spectrum where available. The author has the time constant of 0.03 s, with the accumulation of scans at least 40 times depending on the signal intensity. The accumulation should be large for small signal intensity where large amplitude has to be chosen. The measurement is repeated at least three times, where the sample tube is removed from the cavity and is shaken before it is returned to the cavity.

7.4.3 Separation of Dosimetric Signal

The dosimetric signal is overlapped by an interfering native signal (sometimes called interfering organic radical signal), as typically shown in Fig. 7.2a. The dosimetric signal due to CO_2^- is most probably generated from carbonate ions included in hydroxyapatite as impurities. As shown in Fig. 7.2b, this dosimetric signal has axial g factors of $g_\perp = 2.0025$ and $g_\parallel = 1.997$ [23], and the symmetric native signal has a g factor of 2.0046 [1]. According to Fattibene and Callens [1], this axial CO_2^- is actually orthorhombic but approximately axial as 2 g factors are very close to each other where Rossi and Poupeau [24] reported g factors of 2.0030, 2.0018, and 1.9977. Ikeya [23] proposed that the signal is axial as the radical is rotating around y-axis.

The dosimetric signal due to CO_2^- has a radiation dose response that can be used for dosimetry, while the native signal also has some dose response, but it is not as

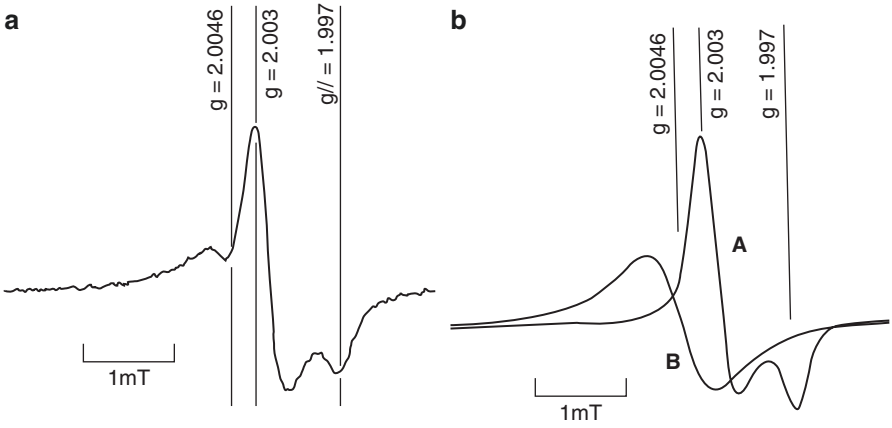

Fig. 7.2 (**a**) A typical ESR spectrum observed in tooth enamel, irradiated to 9 Gy. (**b**) The spectrum is composed of mainly two components: (A) axial CO_2^- (dosimetric) signal and (B) symmetric organic radical. See text for details

such to be used for dose determination. Tooth enamel is known also to be useful to date fossils [23]. For dating, the contribution of the organic signal is negligible as the received dose is high; therefore, usually, the peak to peak signal height in the first derivative spectrum is taken as the signal intensity. Separation of the dosimetic signal from interfering native signal, however, is essentially important for dosimetry below several grays as the peak to peak height has a contribution from the overlapping native signal, resulting in overestimation of the dose. Several methods have been proposed for this separation since the early times of the research. A method was proposed to estimate the contribution of the native signal to the field position to be taken as the peak to peak signal height [25] while utilizing the property that the organic radical signal saturates at lower microwave power, a method to subtract the native signal between the two spectra with different microwave powers [26].

The author proposed a numerical method to find the best contribution parameters by the least square method with two model spectra of dosimetric and the native signals [27]. Recently, there are two main numerical computer programs available for this purpose, which are called Dosimetry [28] and New ER [29]. In these programs, hypothetical Lorentzian functions are used to fit the observed spectra. The main two curves are for the axial dosimetric signal and for isotropic organic signal. An additional unknown broad but small curve is also included to have better fitting of the observed spectra. An example of fitting curves is shown in Fig. 7.3, which are from New ER. The figure shows that the program works well. Toyoda et al. [30] compared the function of the programs and found that New ER is more resistant for unknown disturbances which are sometimes unavoidable in actual samples.

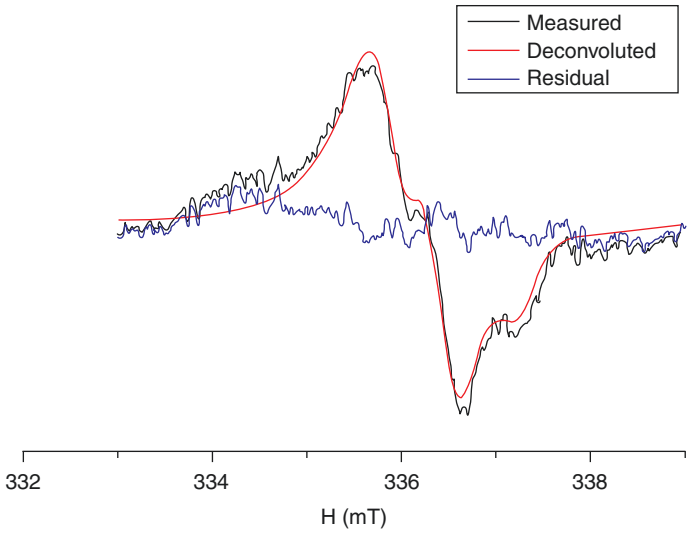

Fig. 7.3 An example of signal separation by New ER for a spectrum observed in tooth enamel with an estimated dose of 252 mGy

7.5 Applications

There have been many application studies to obtain accidental retrospective doses in human teeth by ESR dosimetry as already listed in previous section. The readers interested in such applications should refer to respective papers.

One example is shown here on the Semipalatinsk Nuclear Test Site (SNTS) [31]. Since 1949, the former Soviet Union conducted 467 nuclear tests for 40 years at SNTS, which has an area of about 18,500 km^2 of field in the reaches of the Irtish River. Not only the area of SNTS but also villages near the test site were contaminated by radioactive fallout generated by tests conducted in air.

Tooth samples were collected at Dolon village, one of those villages, from the residents staying the village since the time of the nuclear tests. The retrospective doses were obtained as shown in Fig. 7.4 as a function of enamel formation year where enamel of teeth is formed at certain ages depending on the position as listed in the literature [17]. While the maximum obtained dose was 450 mGy, the doses for the teeth formed after the nuclear tests were less than 100 mGy, indicating that residents were probably exposed to radiation due to contamination at the time of the tests but not much after. The average dose was determined to be 160 mGy, which is consistent with the dose of 300–400 mGy for exposed bricks obtained by the luminescence method after correcting for the duration of the time that people stay outside and inside of houses. The value is also consistent with numerical simulation of contaminated dust fall [31].

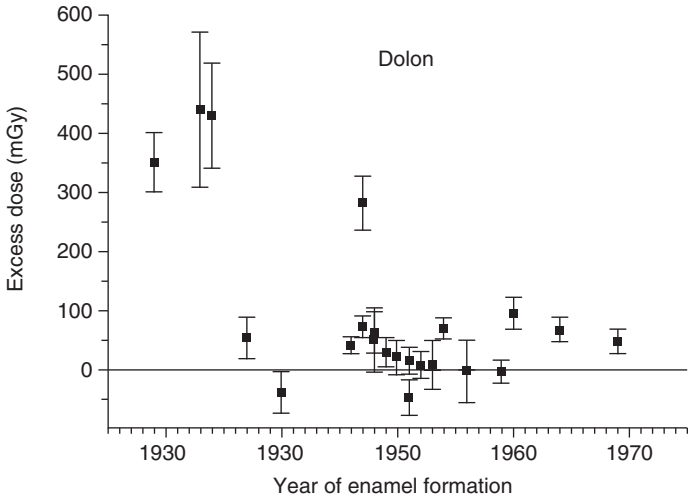

Fig. 7.4 The retrospective radiation doses obtained by ESR tooth enamel dosimetry in teeth provided by residents of Dolon village [31]

7.6 Intercomparisons and ISO Standards

Intercomparisons are important to demonstrate that the technique has been matured so that laboratories in different countries obtain consistent results in estimating the retrospective doses. Five intercomparison projects have been planned and conducted, and the results have already been published [11, 12, 32–37]. Except for the most recent comparison, blind tests were performed, i.e., the doses obtained in participating laboratories were compared. An example of a result obtained in the third intercomparison is shown in Fig. 7.5 for the case of an actual received dose of 176 mGy [36]. The results have improved from the second intercomparison; however, there was still 20% variation among the participating laboratories for the sample irradiated to 704 mGy. While in the first three intercomparisons, the samples were "test" samples; actual samples were used in the fourth intercomparison to check the consistency of the results, instead of correctness. It was shown that it is essentially important to use an appropriate numerical computer program because the results were improved by using the New ER program instead of individual programs [34].

In the most recent intercomparison (the authors claimed that it was the fourth because this was the fourth organized by the same leading group), the participants were asked to measure a series of samples that the organizers had provided. The quality of the measurements was evaluated by the same separation program and the same statistical procedure to obtain the detection limit and the critical doses. The measurement parameters that correlate with the limit and the minimum detection level were investigated but were not clearly found.

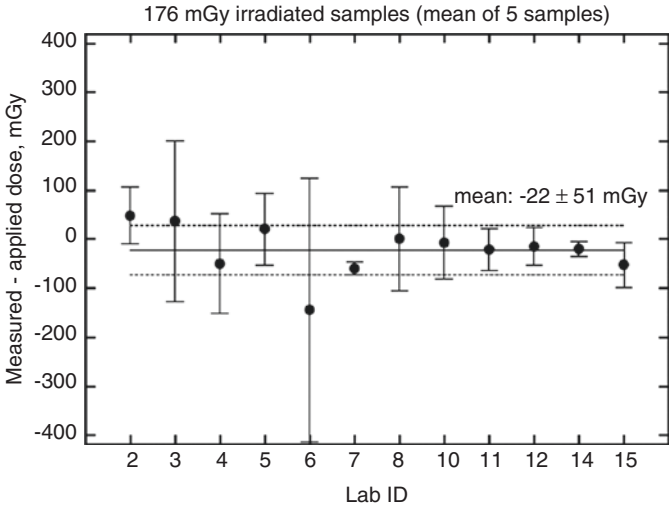

Fig. 7.5 An example of the results obtained in the third intercomparison for a dose of 176 mGy [36]

Based on such developments, an ISO standard was published entitled *Minimum criteria for electron paramagnetic resonance (EPR) spectroscopy for retrospective dosimetry of ionizing radiation – Part 1: General principles* in 2013 on the general aspects of EPR (ESR) biodosimetry [3]. Currently, another standard for ex vivo tooth enamel dosimetry is being prepared. Once it is published, by following the standard, anyone will be able to work on ESR biodosimetry.

7.7 Issues

7.7.1 Detection Limit

The detection limit of the method is one of the most important parameters in order to judge whether the obtained dose values are meaningful or not for the specific applications. There are few papers which discussed the detection limit. The first one was by Romanyukha et al. [38] claiming it to be 29 mGy. Fattibene et al. [32] calculated the doses for the detection limit (DL) defined according to IUPAC [39] for the results of measurements made in the participating laboratories in the most recent intercomparison. As described above, for this intercomparison, the participants were asked to measure the series of samples that the organizers provided and to report the dosimetric signal intensities. The mean of the DL was 205 mGy, where the DL values range from 56 to 649 mGy. The difference should depend on the measurement conditions, the technique of the operator, the ability of the spectrometer, and the numerical procedure that defines the dosimetric signal intensities, but not on the sample. However, at the time of the actual measurements, sample

characteristics are individually different, and the DL depends also on the quality of the set of the standard samples each laboratory has. These factors should be further investigated.

7.7.2 Background Doses

In order to obtain the accidental doses, the background doses have to be subtracted from the value obtained by the measurement. Usually this subtraction is done by estimating the background dose by multiplying the environmental dose rate with the duration of years since the enamel was formed. However, the validity of this way has not yet been experimentally confirmed. There are several papers to investigate the background doses which should vary country to country and region to region (e.g., [40]).

Toyoda et al. [53] examined the doses obtained for 53 extracted teeth and showed the correlation with the ages although quite large variations were observed as shown in Fig. 7.6. Surprisingly, without any accidental dose, a maximum dose of 250 mGy was obtained in Japanese residents in contrast to the results obtained by Rodzi et al. [40] where the maximum obtained dose was below 100 mGy in Malaysia. It is

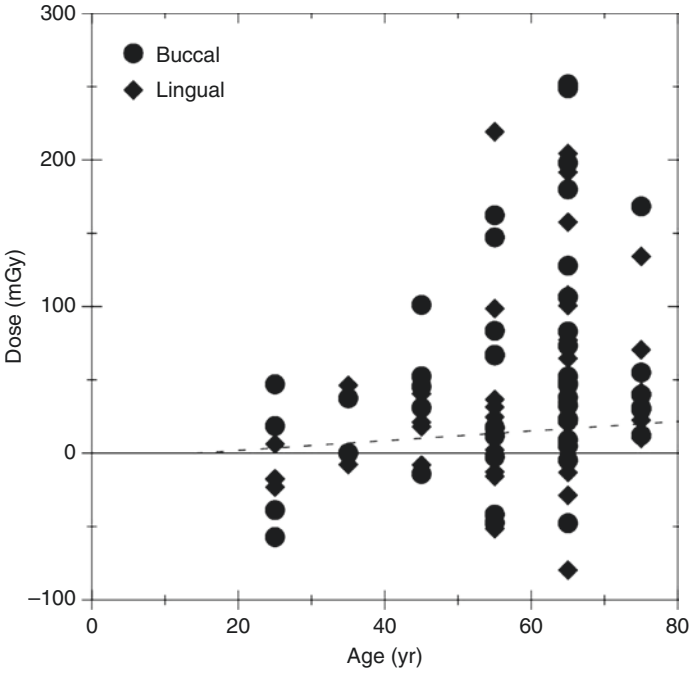

Fig. 7.6 The results of estimated doses of Japanese residents as a function of the age of the donors [53]

possible that it is related to some medical doses, and the work showed that the reality is such without control of record of medical doses. Next, the work should be to investigate background doses with control of medical doses and dental X-ray doses as a function of age, and then natural radiation doses. In the actual retrospective dosimetry in the case of radiation accidents, it is necessary to subtract these background doses. There would be two issues in this aspect. The first would be if the medical doses and X-ray doses in the record are consistent with the measured doses. The second is the variation of the natural doses from country to country and/or from region to region. It is also possible that, in some circumstances, such medical and dental records may not be available, and then typical or averaged such dose estimations would also be necessary.

7.7.3 Standard Samples

It is essential for a laboratory to have a series of standard samples to apply a calibration protocol to obtain a dose. As the dose range of interest is usually up to several hundred mGy, a set of standard samples of 5 to 10 aliquots should be irradiated up to 1 to 1.5 Gy. As one aliquot is about 100 mg, 1 g of tooth enamel is necessary; therefore, usually, enamel powders from several teeth of minimal dosimetric signal intensity are pooled to prepare a set of standard samples. This pooling would also have the effect of averaging the sensitivity variation of the individual samples which is reported to be about 10% for permanent teeth [7].

Although this set of standard samples, which has been prepared in each laboratory, is essentially important, I would like to point out that their quality has never been tested. Our preliminary study (unpublished) indicates there is some variation in dose responses in standard samples which were independently prepared as shown in Fig. 7.7. On the other hand, as the calibration is just a matter of spin numbers in the samples, it might be better just to define a universal standard other than tooth enamel which has some stable ESR signal of known spin numbers.

7.7.4 X-Rays and Low Energy Gamma

It is well known that X-rays produce up to nine times as much dosimetric signal intensity as gamma rays (e.g., [41]) as shown in Fig. 7.8. It is due to the absorption edges of the photoelectric interaction for hydroxyapatite with elements of atomic number higher than water. The absorbed dose we are interested in is that to humans, therefore, which are almost equivalent to water. The absorbed dose is higher for X-rays of photons whose energy is lower than gamma rays, i.e., the absorbed dose to hydroxyapatite is higher than that to water for a similar radiation exposure denoted in C/kg. When the absorbed dose from X-rays is determined with tooth enamel, the obtained dose is to teeth but not the absorbed dose to humans. The correct value to humans by the same X-rays should be much lower. When dental X-ray doses are subtracted, this X-ray efficiency has to be considered.

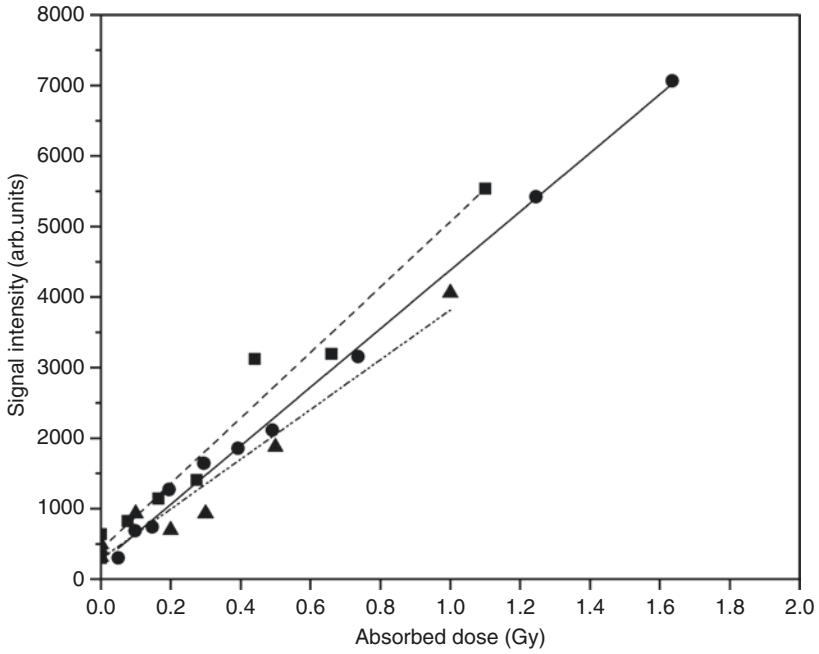

Fig. 7.7 The variation of the dose responses of three "standard" samples of independently prepared

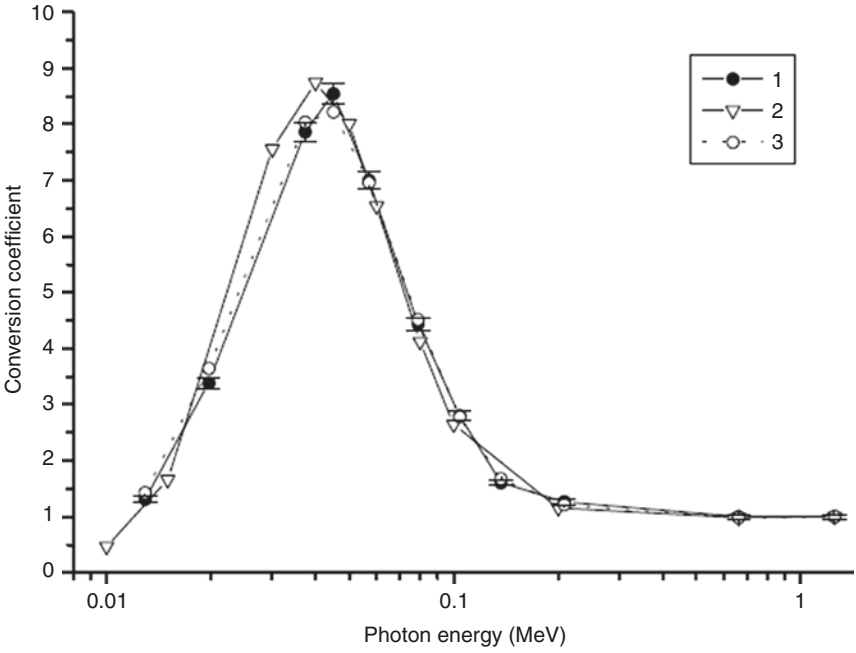

Fig. 7.8 The energy dependence of the dosimetric signals in tooth enamel per unit air dose normalized at 1.25 MeV. (1) Experimental values (2) calculated for monoenergetic X-ray and (3) calculated for actual X-ray spectrum [41]

In most cases of accidental exposure, the photons are usually gamma rays but not X-rays; therefore, this is not the case. However, in an actual situation, gamma rays can be scattered, and due to Compton scattering, the energies of some of the photons can be as low as X-rays. In such cases, this efficiency difference may need to be considered as preliminary done by Hoshi et al. [42].

7.7.5 Neutron Dose

Hydroxyapatite is insensitive to neutron exposure, while it was found that dentin is sensitive to neutrons due to the n–p reactions occurring in organic substances in dentin [43]. As dentin contains hydroxyapatite, it is also sensitive to radiation and can be used for dosimetry where the sensitivity is much lower than enamel and therefore detection limit is much higher. Trompier et al. [43] pointed out that it is possible to obtain both gamma and neutron doses when the doses obtained for enamel and dentin are combined in a radiation field including both neutron and gamma rays (mixed field). However, in an actual case of an accident, the obtained doses were not inconsistent with the previously estimated doses but not determined as expected according to our preliminary study on the JCO accident (unpublished).

7.7.6 ESR Dosimetry with Deciduous and Animal Teeth

While ESR tooth enamel dosimetry has an advantage that individual accumulated radiation doses are obtained, it is a disadvantage that one has to extract a tooth for analysis. Deciduous teeth should be an alternative to such a disadvantage as they naturally fall at certain ages between 5 and 7 years old. The characteristics of the signals in deciduous teeth were investigated [44, 45] and it was found that the sensitivity is about the same as the permanent teeth, while the individual variation is larger, as shown in Fig. 7.9. Also the same numerical computer program for separation of the signals can be used as for permanent teeth, although the organic signal has a wider and more varied signal width.

Animal teeth are also alternatives although the obtained dose are not directly equal to those of humans but an indication of the environmental doses. Teeth of mice, cows, deer, and so on have been investigated so far [46–48]. They can be used for high doses greater than several Gy but were found not to be as sensitive as human teeth.

7.7.7 In Vivo Tooth Enamel Dosimetry

Measurement of teeth without extraction should also be an alternative to the above disadvantage. The idea was already proposed, and preliminary design for an instrument was made quite a long time ago with detection of ESR using microwave

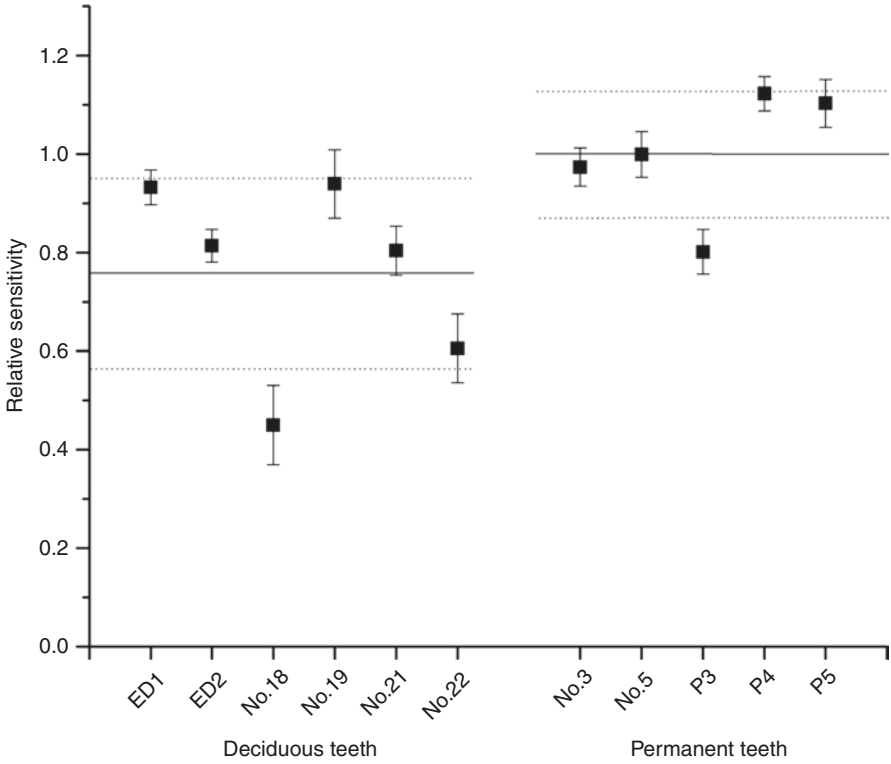

Fig. 7.9 Individual sensitivity to dose of the dosimetric signal in deciduous teeth and permanent teeth [45]

leaking from a slit on an X-band microwave cavity [49]. The instrument system for actual practical measurements was recently developed [50, 51]. As X-band microwaves are absorbed by water, L-band ESR was adopted for this instrument which was designed for screening of exposed people. The authors claimed that currently the instrument is able to distinguish whether the person received a dose more than 2 Gy or less than the value. For screening purposes, this would be practical as a potential patient needs to go to the hospital for some treatment when he/she has received more than 2 Gy, while with a dose below 2 Gy, no serious symptoms will be tentatively observed.

7.7.8 Q-Band

Measuring ESR at higher microwave frequencies (K- and Q-band, etc.) has advantages in having higher sensitivity and higher resolution of the spectra. It is a drawback that the cavity (resonator) volume is smaller; hence, the sample mass to be measured is smaller than that for X-band. If the sample mass for the measurement

is around 100 mg as used in the usual dosimetry studies with X-band, a higher frequency would not have much advantage in sensitivity where typical sample mass for Q-band is about 10 mg. However, higher resolution may possibly contribute in separating dosimetric signal from interfering organic signal, as such a trial has been done with Q-band [52]. Samples with smaller mass will have advantages for measuring smaller doses because the sensitivity is higher in higher frequencies.

7.8 Summary

ESR (EPR) tooth enamel dosimetry is now recognized as a reliable tool for individual retrospective radiation dosimetry. It is based on the principle that a dosimetric signal due to CO_2^- in hydroxyapatite is created by ionizing radiation where the intensity is proportional to the retrospective dose. Separation of enamel from dentin is essentially important in preparation of the samples for measurement. Using a computer program to separate dosimetric signal from interfering native signal is important as well. The calibration method has been recently used in the practical dosimetry studies; therefore, having a series of good standard samples is important. To find the detection limit is one of the important current issues where the statistical standard definition of "detection limit" should be followed. Accumulation of data on background doses, which are to be subtracted in order to obtain accidental doses, should also be an issue which would vary from country to country and/or region to region. As for a new direction of research, dosimetry with deciduous teeth has an advantage in that collection may be easier as they naturally fall out. The doses given to the teeth of other mammals would give information on the environmental doses although they are not direct indications of the doses to humans. L-band in vivo and Q-band measurements are also future important studies.

References

1. Fattibene P, Callens F. EPR dosimetry with tooth enamel: a review. Appl Radiat Isot. 2010;68:2033–116.
2. Wieser A. Review of reconstruction of radiation incident air kerma by measurement of absorbed dose in tooth enamel with EPR. Radiat Prot Dosim. 2012;149:71–8.
3. ISO (2013) Radiological protection – Minimum criteria for electron paramagnetic resonance (EPR) spectroscopy for retrospective dosimetry of ionizing radiation – Part 1: General principles, International Standard, ISO 13304-1.
4. Callens FJ, Verbeeck RMH, Matthys PFA, Martens LC, Boesman ER. The contribution of CO_3^{3-} and CO_2^- to the ESR spectrum near g=2 of powdered human tooth enamel. Calcif Tissue Int. 1987;41:124–9.
5. Schwarcz HP. ESR study of tooth enamel. Nucl Tracks Radiat Meas. 1985;10:865–7.
6. Ikeya M, Miyajima J, Okajima S. ESR dosimetry for atomic bomb survivorsusing shell buttons and tooth enamel. Jpn J Appl Phys. 1984;23:697–9.
7. Wieser A, El-Faramawy N, Meckbach R. Dependencies of the radiation sensitivity of human tooth enamel in EPR dosimetry. Appl Radiat Isot. 2001;54:793–9.

8. Brady JM, Aarestad NO, Swartz HM. In vivo dosimetry by electron spin resonance spectroscopy. Health Phys. 1968;15:43–7.
9. Romanyukha AA, Ignatiev EA, Vasilenko EK, Drozhko EG, Wieser A, Jacob P, Keriim-Markus IB, Kleschenko ED, Nakamura N, Miyazawa C. EPR dose reconstruction for Russian nuclearworkers. Health Phys. 2000;78:15–20.
10. Wieser A, Romayukha AA, Degteva M, Kozheurov V, Petzoldt G. Tooth enamel as a natural beta dosimeter for bone seeking radionuclides. Radiat Prot Dosim. 1996;65:413–6.
11. Chumak V, Bailiff I, Baran N, Bugai A, Bubovsky S, Fedoswov I, Finin V, Haskell E, Hayes R, Ivannikov A, Kenner G, Kirillov V, Khamidova L, Kolesnik S, Liidja G, Likhtarev I, Lippmaa E, Maksimenko V, Meijer A, Minenko V, Pasalskaya L, Past J, Puskar J, Radchuk V, Wieser A. The first international intercomparison of EPR-dosimetry with teeth: first results. Appl Radiat Isot. 1996;47:1281–6.
12. Chumak V, Sholom S, Likhtarev IA. Some results of retrospective dose reconstruction for selected groups of exposed population in Ukraine. In: The radiological consequences of the Chernobyl accident. Report EUR 16544 EN, vol. 1996. Brussels: European Commission; 1996. p. 1059–62.
13. Chumak V, Sholom S, Pasalkaya L. Application of high precision EPR dosimetry with teeth for reconstruction of doses to Chernobyl populations. Radiat Prot Dosim. 1999;84:515–20.
14. Ishii H, Ikeya M, Okano M. ESR dosimetry of teeth of residents close to Chernobyl reactor accident. J Nucl Sci Technol. 1990;27:1153–5.
15. Zhumadilov K, Ivannikov A, Apsalikov KN, Zhumadilov Z, Toyoda S, Zharlyganova D, Tieliewuhan E, Endo S, Tanaka K, Miyazawa C, Okamoto T, Hoshi M. Radiation dose estimation by tooth enamel EPR dosimetry for residents of Dolon and Bodene. J Radiat Res. 2006;47:A47–53.
16. Shiraishi K, Iwasaki M, Miyazawa C, Yonehara H, Matsumoto M. Dose estimation by ESR on tooth enamel from two workers exposed to radiation due to the JCO accident. J Radiat Res. 2002;43:331–5.
17. IAEA (2002) Use of electron paramagnetic resonance dosimetry with tooth enamel for retrospective dose assessment, IAEA-TECDOC-1331, IAEA.
18. Jiao L, Takada J, Endo S, Tanaka K, Zhang W, Ivannikov A, Hoshi M. Effects of sunlight exposure on the human tooth enamel ESR spectra used for dose reconstruction. J Radiat Res. 2007;48:21–9.
19. Nakamura N, Cullings HM, Kodama Y, Watda T, Miyazawa C, Lee K, Awa AA. A method to differentiate between the levels of ESR signals induced by sunlight by ionizing radiation in teeth from atomic bomb survivors. Radiat Res. 2006;165:359–64.
20. Romanyukha AA, Regulla D, Vasilenko E, Wieser A. South Ural nuclear workers: comparison of individual doses from retrospective EPR dosimetry and operational personal monitoring. Appl Radiat Isot. 1994;45:1195–9.
21. Zhumadilov K, Ivannikov A, Skvortsov V, Stepanenko V, Zhumadilov Z, Endo S, Tanaka K, Hoshi M. Tooth enamel EPR dosimetry: optimization of EPR spectra recording parameters and effect of sample mass on spectral sensitivity. J Radiat Res. 2005;46:435–42.
22. Ivannikov AI, Trompier F, Gaillard-Lecanu E, Skvortsov VG, Stepanenko VF. Optimization of recording conditions for the electron paramagnetic resonance signal used in dental enamel dosimetry. Radiat Prot Dosim. 2002;101:531–8.
23. Ikeya M. New applications of electron spin resonance, dating, dosimetry and microscopy. Singapore: World Scientific; 1993. p. 500.
24. Rossi AM, Poupeau G. Radiation damage in bioapatites: the ESR spectrum of irradiated ental enamel revisited. Nuclear Tracks and Radiation Measurements. 1990;17:537–45.
25. Shimano T, Iwasaki M, Miyazawa C, Miki T, Kai A, Ikeya M. Human tooth dosimetry for gamma-rays and dental X-rays using ESR. Appl Radiat Isot. 1989;40:1035–8.
26. Ignatiev EA, Romanyukha AA, Koshta AA, Wieser A. Selective saturation method for EPR dosimetry with tooth enamel. Appl Radiat Isot. 1996;47:333–7.

27. Toyoda S, Sumitomo H, Ikeya M, Ishii H. Separation of CO_2-signal from a spectrum of irradiated tooth enamel in ESR dosimetry. In: Assessment of the health and environmental impact from radiation doses due to released radionuclides, NIRS-M-102. Chiba, Japan: National Institute of Radiological Sciences; 1994. p. 187–205.
28. Koshta AA, Wieser A, Ignatiev EA, Bayankin S, Romanyukha AA, Degteva MO. New computer procedure for routine EPR-dosimetry on tooth enamel. Description and verification. Appl Radiat Isot. 2000;52:1287–90.
29. Ivannikov AI, Skvortsov VG, Stepanenko VF, Tikunov DD, Takada J, Hoshi M. EPR tooth enamel dosimetry: optimization of the automated spectra deconvolution routine. Health Phys. 2001;81:124–37.
30. Toyoda S, Tielewuhan E, Romanyukha A, Ivannikov A, Miyazawa C, Hoshi M, Imata H. Comparison of three methods of numerical procedures for ESR dosimetry of human tooth enamel. Appl Radiat Isot. 2005;62:181–5.
31. Ivannikov A, Zhumadilov K, Tieliewuhan E, Jiao L, Zharlyganova D, Apsalikov KN, Berekenova G, Zhumadilov Z, Toyoda S, Miyazawa C, Skvortsov V, Stepanenko V, Endo S, Tanaka K, Hoshi M. Results of EPR dosimetry for population in the vicinity of the most contaminating radioactive fallout trace after the first nuclear test in the Semipalatinsk Test Site. J Radiat Res. 2006;47:A39–46.
32. Fattibene P, Wieser A, Adolfsson E, Benevides LA, Brai M, Callens F, Chumak V, Ciesielski B, Della Monaca S, Emerich K, Gustafsson H, Hirai Y, Hoshi M, Israelsson A, Ivannikov A, Ivanov D, Kaminska J, Ke W, Lund E, Marrale M, Martens L, Miyazawa C, Nakamura N, Panzer W, Pivovarov S, Reyes RA, Rodzi M, Romanyukha AA, Rukhin A, Sholom S, Skvortsov V, Stepanenko V, Tarpan MA, Thierens H, Toyoda S, Trompier F, Verdi E, Zhumadilov K. The 4th international comparison on EPR dosimetry with tooth enamel part 1: report on the results. Radiat Meas. 2011;46:765–71.
33. Hoshi M, Toyoda S, Ivannikov A, Zhumadilov K, Fukumura A, Apsalikov K, Zhumadilov ZS, Bayankin S, Chumak V, Ciesielski B, De Coste V, Endo S, Fattibene P, Ivanov D, Mitchell CA, Onori S, Penkowski M, Pivovarov SP, Romanyukha A, Rukhin AB, Schultka K, Seredavina TA, Sholom S, Skvortsov V, Stepanenko V, Tanaka K, Trompier F, Wieser A, Wolakiewicz G. Interlaboratory comparison of tooth enamel dosimetry on Semipalatinsk region: part 1, general view. Radiat Meas. 2007;42(6–7):1005–14.
34. Ivannikov A, Toyoda S, Hoshi M, Zhumadilov K, Fukumura A, Apsalikov K, Zhumadilov Z, Bayankin S, Chumak V, Ciesielski B, De Coste V, Endo S, Fattibene P, Ivanov D, Mitchell CA, Nalapko M, Onori S, Penkowski M, Pivovarov S, Romanyukha A, Rukhin AB, Sanin D, Schultka K, Seredavina T, Sholom S, Skvortsov V, Stepanenko V, Tanaka K, Trompier F, Wieser A, Wolakiewicz G. Interlaboratory comparison of tooth enamel dosimetry on Semipalatinsk region: part 2, effects of spectrum processing. Radiat Meas. 2007;42(6–7):1015–20.
35. Wieser A, Mehta K, Amira S, Ararno D, Bercea S, Brik A, Bugai A, Callens F, Chumak V, Ciesielski B, Debuyst R, Dubovsky S, Duliu OG, Fattibene P, Haskell EH, Hayes RB, Ignatiev EA, Ivannikov A, Kirillov V, Kleschenko E, Nakamura N, Nather M, Nowak J, Onori S, Pass B, Pivovarov S, Romanyukha A, Scherbina O, Shames AI, Sholom S, Skvortsov V, Stepanenko V, Tikounov DD, Toyoda S. The 2nd international intercomparison on EPR tooth dosimetry. Radiat Meas. 2000;32(5–6):549–57.
36. Wieser A, Debuyst R, Fattibene P, Meghzifene A, Onori S, Bayankin SN, Blackwell B, Brik A, Bugay A, Chumak V, Ciesielski B, Hoshi M, Imata H, Ivannikov A, Ivanov D, Junczewska M, Miyazawa C, Pass B, Penkowski M, Pivovarov S, Romanyukha A, Romanyukha L, Schauer D, Scherbina O, Schultka K, Shames A, Sholom S, Skinner A, Skvortsov V, Stepanenko V, Tielewuhan E, Toyoda S, Trompier F. The 3rd international intercomparison on EPR tooth dosimetry: part 1, general analysis. Appl Radiat Isot. 2005;62(2):163–71.
37. Wieser A, Debuyst R, Fattibene P, Meghzifene A, Onori S, Bayankin SN, Brik A, Bugay A, Chumak V, Ciesielski B, Hoshi M, Imata H, Ivannikov A, Ivanov D, Junczewska M, Miyazawa C, Penkowski M, Pivovarov S, Romanyukha A, Romanyukha L, Schauer D, Scherbina O, Schultka K, Sholom S, Skvortsov V, Stepanenko V, Thomas JA, Tielewuhan E, Toyoda S, Trompier F. The third international intercomparison on EPR tooth dosimetry: part 2, final analysis. Radiat Protect Dosim. 2006;120(1–4):176–83.

38. Romanyukha AA, Nagy V, Sleptchonok O, Desrosiers MF, Jiang J, Heis A. Individual biodosimetry at the natural radiation background level. Health Phys. 2001;80:71–3.
39. IUPAC. International union of pure and applied chemistry recommendations. Nomenclature in evaluation of analytical methods, including detection and quantification capabilities. Pure Appl Chem. 1995;67:1699–723.
40. Rodzi M, Zhumadilov K, Ohtaki M, Bhattacharjee D, Hoshi M. Estimation of background radiation doses for the peninsular Malaysia population by ESR dosimetry of tooth enamel. Radiat Environ Biophys. 2011;50:451–8.
41. Ivannikov A, Tikunov DD, Borysheva NB, Trompier F, Skvortsov VG, Stepanenko VF, Hoshi M. Calibration of EPR signal dose response of tooth enamel to photons: experiment and Monte Carlo simulation. Radiat Prot Dosim. 2004;108:303–15.
42. Hoshi M, Sawada S, Ikeya M, Miki T. ESR dosimetry for Hiroshima A-bomb survivors, in ESR dating and Dosimetry. Tokyo: IONICS; 1985.
43. Trompier F, Tikunov DD, Ivannikov A, Clairand I. ESR investigation of joint use of dentin and tooth enamel to estimate photon and neutron dose components of a mixed filed. Radiat Prot Dosim. 2006;120:191–6.
44. El-Faramawy N, Wieser A. The use of deciduous molars in EPR dose reconstruction. Radiat Environ Biophys. 2006;44:273–7.
45. Murahashi M, Toyoda S, Hoshi M, Ohtaki M, Endo S, Tanaka K, Yamada Y. The sensitivity vatiation of the radiation induced signal in deciduous teeth to be used in ESR tooth enamel dosimetry. Radiat Meas. 2017;106:450–4.
46. Klevezal GA, Serezhenkov VA, Bakhur AE. Relationships between ESR-evaluated doses estimated from enamel and activity of radionuclides in bone and teeth of reindeer. Appl Radiat lsot. 1999;50:567–72.
47. Serezhenkov VA, Moroz IA, Klevezal GA, Vanin AF. Estimation of accumulated dose of radiation by the method of ESR-spectrometry of dental enamel of mammals. Appl Radiat Isot. 1996;47:1321–8.
48. Toyoda S, Tanizawa H, Romanyukha AA, Miyazawa C, Hoshi M, Ueda Y, Nitta Y. Gamma ray dose response of ESR signals in tooth enamel of cows and mice. Radiat Meas. 2003;37:341–6.
49. Ishii H, Ikeya M. An electron spin resonance system for in-vivo human tooth dosimetry. Jpn J Appl Phys. 1990;29:871–5.
50. Swartz HM, Iwasaki A, Walczak T, Demidenko E, Salikov I, Lesniewski P, Starewicz P, Schauer D, Romanyukha A. Measurements of clinically significant doses of ionizing radiation using non-invasive in vivo EPR spectroscopy of teeth in situ. Appl Radiat Isot. 2005;62:293–9.
51. Williams BB, Dong R, Kmiec M, Burke G, Demidenko E, Gladstone D, Nicolalde RJ, Sucheta A, Lesniewski P, Swartz HM. Development of in vivo tooth tooth EPR for indivisual radiation dose estimation and screening. Health Phys. 2010;98:327–38.
52. Romanyukha A, Trompier F, Reyes RA. Q-band electron paramagnetic resonance dosimetry in tooth enamel: biopsy prodedure and determination of dose detection limit. Radiat Environ Biophys. 2014;53:305–10.
53. Toyoda S, Kondo A, Zhumadilov K, Hoshi M, Miyazawa C, Ivannikov A. ESR measurements of background doses in teeth of Japanese residents. Radiation Measurements. 2011;46(9):797–800.

Dermatological Applications of EPR: Skin-Deep or In-Depth?

8

Martyna Krzykawska-Serda, Dominika Michalczyk-Wetula, and Przemysław M. Płonka

8.1 Introduction: Specificity of Skin and Its Appendages as Materials for EPR Measurements

Electron paramagnetic resonance (EPR; called also electron spin resonance—ESR) is a physical phenomenon and a base for sophisticated techniques of EPR spectroscopy and imaging. In this chapter we focus on the specificity of this technique when applied to dermatology. As its main potential target reader is probably familiar with the physical phenomenon, we would like to pay most of the attention to the biological and medical specificity of the problem. The detailed or simplified description of the physical phenomenon can be found in the wide spectrum of handbooks and reviews, including [1–3] along with the present book. EPR enjoys recently a growing popularity among physicians-scientists, more and more journals publish reviews, and experimental papers concerning applications of EPR to their specific fields [4–9]. Consequently, we would concentrate on the most recent achievements, inventions, and discoveries devoted to the specific field of dermatology and skin as a specific organ for EPR measurements. A wide collection of respective problems enjoying a slightly longer period of "seasoning" will be found in the available reviews.

As an object of EPR measurement, skin is a special organ. It is almost impossible to put the whole organism to the resonant cavity, so as to carry out the *in vivo* EPR investigations of skin *in toto*. Being the most outer layer of the body, skin will also be difficult to access with an endoscope or endoscope-associated research equipment (e.g., an endoscope-coupled surface coil [10]), not to mention the putative problems in executing an EPR imaging (EPRI) experiment [11]. Nevertheless, the

M. Krzykawska-Serda · D. Michalczyk-Wetula · P. M. Płonka (✉)
Department of Biophysics, Faculty of Biochemistry, Biophysics and Biotechnology, Jagiellonian University, Kraków, Poland
e-mail: martyna.krzykawska@uj.edu.pl; dominika.michalczyk@uj.edu.pl; przemyslaw.plonka@uj.edu.pl

A. K. Shukla (ed.), *Electron Spin Resonance Spectroscopy in Medicine*,
https://doi.org/10.1007/978-981-13-2230-3_8

branch of "dermatologic EPR" does develop. This is due both to the possibilities to overcome the difficulties brought about by the organ and (and in the first place) because of the importance and preciousness of the information obtained by EPR. Moreover, a number of papers using EPR to solve dermatologic problems using *ex vivo* or *in vitro* experimental systems prove that the important data can also be gathered indirectly [4].

EPR is a unique research technique (one may say directly—a biological research technique) which delivers qualitative *and* quantitative information on particular paramagnetic centers (free radicals, metal ions, molecular oxygen, nitric oxide, etc.) on different levels of organization of the system, starting from submolecular, ending up on the level of the whole organ. This feature is underlined by many researchers [4, 12–14]. On all the available levels of observation, the main information delivered by EPR concerns unpaired electrons (i.e., of uncompensated spin), and the flow of unpaired electrons via the living system is one of the most important phenomena which make the system actually "alive." This flow may be modified by various factors of their local environment and concern the ongoing metabolic processes (irradiation, hydration, oxygenation, temperature, mechanical stress, etc.) determining the *functions* of the skin, the set of which is substantial. The information concerns also the surrounding tissues (actually—the subcutaneous tissue) and skin appendages. Moreover, it concerns normal, physiological, and pathological conditions, including development of skin tumors. Actually, as the barrier between the inner of the organism and the external world on the one hand, and the junction of the inner of the organism with the external environment on the other hand, the skin (including their EPR-measureable features) conveys information about the condition of the whole organism and on the reaction of the organism as a whole [15, 16]. Sometimes the reaction is not proper, what used to be called "a disease." All these observations strongly justify and explain the interest of dermatologists in EPR and make the skin a special challenge for EPR measurements.

8.2 Skin as the Largest Organ of the Organism

A detailed characterization of skin as the object for EPR measurement is indispensable to gain the view of problems and possibilities of dermatologically oriented EPR spectroscopy. Skin is the largest organ in human body; without subcutaneous tissue its weight reaches 7% of the total body weight of adult humans, almost three times as much as the weight of the liver [17, 18]. It is a layered organ, which determines the primary technique of EPR measurements applicable for skin—application of surface coils. The penetrability of microwaves, besides the wavelength, will strongly depend on the thickness and hydratation of particular layers, and this will create the main axis of further description of the organ. The penetration depth strongly depends on microwave frequency (the higher frequency of microwaves, the worst the penetration), e.g., from 1.05 mm at 20 GHz to 0.78 mm at 38 GHz for human skin *in vivo* [19, 20]. *See* also Fig. 8.1.

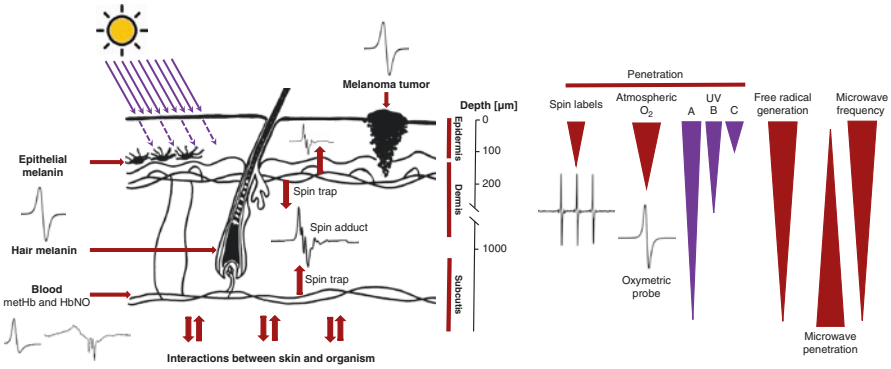

Fig. 8.1 Simplified scheme of human skin showing its structure and experimental EPR accessibility of various types of paramagnetic centers: metHb, HbNO, methemoglobin, and nitrosyl hemoglobin. Phenomena and parameters important for EPR measurements are also displayed [19–25]

It is worth noticing that the total thickness of skin varies according to function and region of the body. On the eyelids, the skin is only 0.5 mm thick, whereas it can be 3–4 mm thick on the soles of the feet [26]. The trunk skin is on average 1–2 mm thick [27].

Its structure includes tissues of epithelial, connective, vascular, muscular, and nervous origin in three main layers: the epidermis of ectodermal origin, the basement membrane which is a form of extracellular matrix composed of proteins created by cooperation of epithelial and mesenchymal skin cells [28–32], and the (primarily) mesodermal dermis. The neural crest also makes an important contribution to the skin, namely, in the form of the pigment cells—melanocytes [17, 33].

Epidermis is the outer part of skin renewing itself continuously and quite fast, namely, within a month. The structure of epidermis is formed by several layers, i.e., from bottom to top: *stratum germinativum* or *basale, stratum spinosum, stratum granulosum, stratum lucidum*, and *stratum corneum* (SC) [34]. The skin is the only organ besides the lungs that is directly exposed to atmospheric oxygen. This automatically determines one of the main topics of EPR application in skin research—oxygen penetration, oxygenation, and oxygen consumption [21, 35, 36]. The epidermis has no vasculature, but oxygen is consumed in all layers of epidermis apart from SC [37]. Cells in the deepest layers of epidermis are oxygenated almost exclusively by the atmospheric oxygen and only to a far lesser degree by blood capillaries extending to the outer layers of the dermis [21, 38]. The atmospheric oxygen can penetrate the upper skin layers down to the depth of 0.25–0.40 mm so that the whole epidermis and the upper corium can be supplied with the atmospheric oxygen [21] (Fig. 8.1). Additionally, the tissue permeability for oxygen is strongly dependent upon the water content (influencing also the EPR signal of, e.g., spin labels [39]) and significantly changes during drying, humidification, or sweating of the skin, but the changes resulting from skin aging do not affect transepidermal oxygen uptake [21].

There are three main pools of cells in the epidermis, namely, keratinocytes, melanocytes, and the Langerhans cells [17]. Epithelial keratinocytes originate from the stem cells residing in the basal layer [40–42]. The differentiating progenitors undergo finally the so-called cornification, which may be qualified as a type of terminal differentiation and of a programmed cellular death at the same time [43]. They undergo deep morphological and biochemical differentiation, i.e., massive production and deposition of keratin, diminution of other organelles, dehydration, and shape remodeling, which inevitably results in cell death. All these changes take place while moving up the strata to SC where they undergo exfoliation [17, 34, 42].

The melanocytes specifically interact with keratinocytes creating the so-called epidermal melanin unit [44] responsible for constitutive color of skin and the reactions to the exposition on the sunlight. The melanin transfer is most probably executed by keratinocyte phagocytosis of tips of melanocytic dendrites. It has been demonstrated that similar transfer takes place between "secondary" keratinocytes [45, 46].

Epidermis and dermis are separated by a thin sheet of proteins, e.g., collagen III, IV, and VII, fibrillin, or laminin, called the basement membrane [28–31, 47]. The main function of the basement membrane is to connect the epithelium to the dermis. It plays the crucial role in remodeling and repairing processes [48]. The layer is also important from the dermatological point of view as crossed by pre-melanocytes and is also necessary to penetrate backward in the process of melanoma metastasizing [49]. This junction is undulated in section: the ridges of the epidermis, known as the so-called *rete ridges*, project into the dermis [33, 47, 48].

The dermis is a supportive, compressible, and elastic tissue structurally divided into two layers: the *papillary region*—the superficial area adjacent to the epidermis—and a deep, thicker area known as the *reticular region*. The dermis is mainly constituted of a matrix of loose connective tissue composed of fibrous proteins (collagen, elastin, reticulin) embedded in an amorphous ground substance making an environment for a few types of cells: fibroblasts supplemented with dermal dendrocytes and mast cells [17, 34].

The dermal layer of skin contains nerve endings which are responsible for the sense of touch and heat and blood vessels that provide nourishment and waste removal from the dermal cells as well as from the *stratum basale* of the epidermis. The dermal vasculature is arranged in two tiers that are parallel to the skin surface: the *superficial plexus* between the papillary and the upper reticular dermis and the *deep plexus* in the lower reticular dermis (Fig. 8.1). Both are connected by perpendicularly orientated communicating vessels. Arcades of capillaries loop upward into the papillae from the subpapillary plexus [37]. The dermis undergoes a continuous turnover, regulated by mechanisms controlling the synthesis and degradation of its protein components [17].

The hypodermis lies below the dermis and is not any part of the skin, but it attaches the skin to the underlying tissue and supplies it with blood vessels and nerves. It also supports skin functions [17].

The integral constituents of the skin are the skin adnexa, i.e., skin-associated and skin-derived structures: hair follicles, *arrector pili* (Latin *musculi arrectores pilorum)*, sebaceous glands, sweat glands, and nails. They are located in dermis and hypodermis [50]. The skin, hair, nails, and the associated glands form the *integumentary system* which enwraps the body [51].

The vital functions of skin as an integumentary system (many of them being potentially accessible with EPR spectroscopy and imaging techniques) are primarily related to isolate the inner of the organism and to protect it against environment factor but also to provide a contact with the environment [15, 52]. The skin protects the underlying tissues from bacteria, viruses, and fungi invasion and provides a barrier against most chemicals and from a mechanical injury. Skin is also involved in thermoregulation through convection, conduction, radiation, and evaporation. It functions as a sophisticated organ of sense (pressure, pain, temperature, touch) and of endocrine action: the skin synthesizes vitamin D and produces POMC and other hormones [17, 50–56].

Special roles in these functions are played by the skin appendages. They are important in such functions as sensation, contractility, lubrication, thermoregulation, and removal of water. Hairs are important in sensation, heat loss, filtering air for breathing, and protection; "arrector pili" (smooth muscles) pulls hairs straight; sebaceous glands secrete sebum onto hair shafts, which oils the hair; sweat glands secrete sweat; and nails have a protective function [50].

The hair (the hair shaft) is a dead product of keratinocytes and melanocytes present in the hair follicle—a sophisticated ecto-mesodermal mini-organ containing various types of cells and histologically differentiated layers. The presence of the hair follicle in the skin must be multiplied by the number of hairs, including also hair follicles which for various reasons do not contain hair shafts [57].

In mice and rats, the whole skin except naked parts is devoid of epidermal melanocytes, and only the hair follicles contain functional melanocytes producing melanin and responding for pigmentation of the hair shaft [58]. Moreover, this process takes place only in anagen III–VI [58, 59]. Anagen is a stage of the hair cycle, i.e., the continuous turnover and remodeling of hair follicles, which may either produce hair shafts (anagen [60]) or remain in an apparently resting phase (telogen [61]). The short period of transformation from anagen to telogen is called catagen (involution of the hair follicle [62]), and recently a separate phase of hair shaft shedding (exogen [63]) and not an obligatory phase of kenogen—"empty" hair follicle [64] (devoid of any hair shafts)—has been described [65].

As a part of skin surface is visible for other people, intact, healthy skin is essential for patient well-being, and every abnormality is a source of malaise, psychical complexes, and problems in social contacts. The same concerns scalp hair [66]. Understanding the normal structure and function of the skin is therefore a prerequisite to understand and manage skin disorders such as psoriasis and decubitus ulcers, alopecia areata, and side effects of cancer chemotherapy [67–69]. Because of skin

size, importance, and tight interconnection with functioning of the inner organs of the body, the knowledge concerning its structure and function is essential to clinicians and researchers. It also provides a large field of research and diagnostics with EPR spectroscopy.

8.3 Paramagnetic Species for EPR Measurements in the Skin

The skin, a normal, living organ, will contain in general the same types of paramagnetic centers as other organs of the body. However, the skin is histologically diversified, so various layers and appendages differ in details and in the type of information conveyed by EPR spectroscopy. In Table 8.1 we have shortly characterized the skin by its "paramagnetomic profile" (*see* also Fig. 8.1 and "Paramagnetomics"—a Chap. 9 in this book). From the medical point of view, the most important are free radicals produced due to oxidative stress, which occurs as an effect of skin irradiation or inflammation. The paramagnetic metal ions are usually blood-borne and may create complexes or react with skin-free radicals.

8.4 Specific Processes for EPR Measurements in the Skin

Paramagnetic centers are mainly short-living, transient species, usually intermediates of important processes of life (primarily—oxidative respiration and photosynthesis) or products of irradiation and participants of any other processes leading to oxidative stress. EPR spectroscopy is a unique technique which is able to identify these species, to follow the processes, and to register their dynamics. As for exogenous paramagnetic probes (spin probes and spin labels), they are often introduced to the organ to follow other processes which may affect the EPR spectra. Some short-living species may prolong their lifetime by making a stable product (spin adduct) with exo- or endogenous spin traps present in the organ (Fig. 8.1). Table 8.2 gathers the most important, recent applications of these EPR techniques (spin labeling and spin-trapping) to follow skin-related biochemical and biophysical processes.

8.4.1 Free Radicals and Redox Processes

It is good to highlight that aging, effects of action of some cosmetic products (e.g., sunscreens), and toxicity of drugs in the skin can be are directly related to skin oxidative stress. The oxidative stress and the related population of free radicals can be successfully investigated by EPR. It is worth mentioning that in biological samples, free radicals are usually not present in concentrations sufficient to give a strong EPR signal. Moreover, the free radical's lifetime is very short, and the reactivity is very fast, which makes a direct measurement challenging. Consequently, the spin probes of a big range of selectivity and sensitivity must be applied in the skin EPR spectroscopy for measurements of oxidative stress (Table 8.2). Generally,

Table 8.1 Selected types of native paramagnetic centers generated in the skin in a natural way or due to irradiation

Endogenous paramagnetic centers	Related biological phenomenon/ material	Character and value of information obtained with EPR, caveats	EPR instrumentation, experimental approach	References
Melanin	Skin pigmentation	Melanization and type of melanin (eumelanin/ pheomelanin ratio) in normal murine melanocytes Production of pheomelanin in amphibian skin	Varian E3 CW X-band, room temperature, and 77 K, *in vitro* cell cultures, skin *ex vivo*	[70, 71]
	Hair pigmentation	Proportion of eumelanin/pheomelanin and total melanization of hair	EPR X-band CW spectroscopy and power saturation, Varian E 3 and ESR-V (Special Constructor Office, Russian Academy of Sciences) Proportion of hyperfine features and apparent *g*-value	[72, 73]
	Melanoma	Assessment of growth stage of pigmented tumors Establishing a link between clear EPR images and tumor invasion state—a correlation between the tumor growth stage and the signal-to-noise ratio (SNR) of the EPR spectrum Limitations: amelanotic melanomas not detectable	X-band EPRI and CW spectroscopy (Bruker E540) *ex vivo* at room temperature	[74–76]
ROS such as $OH^{\cdot}$, $O_2^{-\cdot}$	Oxidative stress Dermal antioxidant activity	Antioxidant-induced radical scavenging activity in the skin	L-band EPR spectrometer LBM MT 03 (Magnettech GmbH, Berlin, Germany) *in vivo* Irradiation with infrared and visible light, oral and topical antioxidants Spin label: TEMPO	[77]
NO	Nitrosative stress Human skin	Determination of NO nonenzymatic photoproduction (blue light) in various layers of skin and of the role of NO in psoriasis	X-band (ESP300 Bruker, BioSpin, Rheinstetten, Germany), 77 K, $Fe^{2+}[DETC]_2$ (diethyldithiocarbamate) spin trapping *ex vivo*, human skin and blood	[78, 79]
	Nitrosative stress Murine melanoma	Detection of nitric oxide generation in melanoma tumors *in situ*	S-band, room temperature, homemade spectrometer, *in vivo* spin trapping with $Fe^{2+}[DTCS]_2$ (diethyl dithiocarboxysarcosine)	[80]

(continued)

Table 8.1 (continued)

Endogenous paramagnetic centers	Related biological phenomenon/ material	Character and value of information obtained with EPR, caveats	EPR instrumentation, experimental approach	References
Methemoglobin Fe^{3+}-transferrin Ceruloplasmin Free radicals	Radiation injuries	Rapid diagnosis of radiation injuries 24 h after exposure in animals, potentially applicable in human, by EPR analysis of blood samples	Blood obtained from irradiated animals, Varian E-12 CW X-band, *ex vivo*, 77 K	[81]
Oxygen tissue pO_2 (partial pressure)	Tissue pO_2 Peripheral vascular Disease (PVD) and radiotherapy Possible extension to other diseases directly or indirectly Linked with tissue pO_2	Sensitive measurement of tissue oxygen up to the depth of 8–10 mm from the surface Skin pO_2 manifestation of status of disease and effects of treatment	Clinical L-band (1.2 GHz) EPR spectrometry *in vivo* in human subjects Surface or implantable resonator Oximetry probes: India ink, polydimethylsiloxane (PDMS) Oxygen-dependent changes in the EPR linewidth	[3] [82] [83] [84] [85] [86]
	Wound healing	Local oxygenation determining process of wound healing to monitor the effectiveness of therapeutic interventions, e.g., in diabetes		[87] [83] [85] [86] [88]
	Intratumor pO_2	Changing of pO_2 in skin tumors over time, optimization of radio- or chemotherapy Noninvasive, fast, and long-term measurement at depths of ≤1 cm (surface resonator) or slightly deeper (implantable resonator)		[82] [83] [85] [88] [89] [90]

Stable free radicals after UV, X, and gamma-irradiation	Keratin of human hair	Absorbed dose of radiation	Varian 900—E line CW X-band spectrometer	[91, 92]
Unstable free radicals after UV Ascorbyl radical ($Asc^{\cdot -}$)	Skin oxidative stress	Radiation-generated $Asc^{\cdot -}$ EPR dosimetry	Bruker ESP-300 (Karlsruhe, Germany) CW, X-band Intact sections of human epidermis (*ex vivo*)	[93]
EPR radiation-induced signal (RIS) of stable free radicals	Keratin of fingernails	Absorbed dose of X-rays EPR dosimetry	Stationary spectrometer: X-band transportable EPR spectrometer, e-scan Bruker BioSpin Portable spectrometer: Q-band spectrometer EMXplus	[94–96]

Melanin can be considered as the exception (i.e., produced only, or mainly in skin), though there are some other organs containing melanin [97]. As examples, besides the eye [98], one should mention the spleen, lymph nodes, and visceral organs [99], *substantia nigra* [100] and *locus coeruleus* [101] in the brain, the leptomeninges [102], and the inner ear [103].

Table 8.2 Variety of spin labels and spin traps with possible application into EPR skin measurement

Spin probes, labels, and traps	What is measured	How/what applied	What EPR technology can be used	References
2,2,6,6-Tetramethyl-1-piperidinyloxyl (TEMPO)	• Intracellular free radicals *in vitro* • Skin antioxidative power *in* and *ex vivo* • Reversible reduction to hydroxylamine depending on oxygen concentration and availability of intracellular glutathione and ascorbate	*In vitro* in solution, (amphiphilic), skin treatment *in vivo*	MiniScope MS 200, X-band L-band EPR (LBM MT 03) ER 200 D-SCR or ERS 221 at 9.5 GHz	[104, 105] [106–109], [110] [111] Limitations: [112]
3-Carboxy-2,2,5,5-tetramethyl-1-pyrrolidinyloxy-3-carboxylic acid (PCA)	• Highly sensitive probes for surrounding microenvironment—free radicals • Probe reacts with $O_2^{-\cdot}$, $OH^{\cdot}$, $LO^{\cdot}$, and $LOO^{\cdot}$ radicals	Topically, observed with a 20–40 min delay (for penetration) (treatment of skin samples/biopsies)	L-band EPR spectrometer, type LBM MT03 X-band EPR system "ELEXSYS E500" X-band EPR (Miniscope 300) W-band EPR	[113–115] [116] [110] [117]
5,5-Dimethyl-1-pyrroline N-oxide (DMPO)	• Free radicals population (hydroxyl spin adduct DMPO-OH)	Treated skin samples	EMXplus 10/12 Bruker BioSpin, X-band	[118–120]
3-Maleimido-proxyl (5-MSL)	• Protein dynamics	Incubation with *stratum corneum*	X-band (9.4 GHz)	[121]
5-Doxylstearic acid (5-DSA)	• Spin label to detect free radicals	Tissue/nail incubated in ~50 μM aqueous solutions (60 min, 37 °C)	JEOL RE-3X 9 GHz EPR 9 GHz Bruker ELEXSYS E500	[122] [123]
N-Tert-butyl-a-phenylnitrone (PBN)	• Free radicals detection • Trapping hydroxyl and carbon-centered free radicals	Skin samples (~1 h incubation), soluble in water/ethanol	X-band EPR system "ELEXSYS E500" ERS 300, 9.52 GHz	[116] [124]
Alpha-(4-pyridyl-1-oxide)-*N*-tert-butylnitrone (POBN)	• Free radicals detection	On epidermis (e.g., for 9 min)	ESP-300 EPR	[119]

Di-tertiary-butyl-nitroxide (DTBN)	• Free radicals imaging	With DMSO as penetration enhancer	X-band, 2D L-band	[11]
Iron-diethyldithiocarbamate $Fe^{2+}(DETC)_2$	• NO is trapped	Blood usage		[79]
1-Hydroxy-3-methoxycarbonyl-2,2,5,5-tetramethylpyrrolidine (CMH)	• Spin trap for reactive oxygen species (ROS)	Skin incubation (200 μM, for 30 min)	Bench-top EPR spectrometer (E-SCAN)	[125]
C-PROXYL 3-Carbamoyl-2,2,5,5-tetramethylpyrrolidine-N-oxyl	• Reactive oxygen species	*i.v.* (e.g., 280 mM; 3 ml/kg body weight)	L-band ESR, Surface coil	[126]
LiPc Lithium phthalocyanine	• Oximetry *in vivo*	Implemented into the tissue, site-specific measurement	EPR S, L-bands, EMX EPR X-band	[87]
OX063 Trityl OX063 radical methyl-tris[8-carboxy-2,2,6,6-tetrakis[2-hydroxyethyl] benzo[1,2-d:4,5-d′] bis[1,3]dithiol-4-yl]-triso-dium salt	• Oximetry	Vein infusion	Pulse EPR, L-band	[127, 128]

three different approaches can be used to detect free radicals in the skin: (a) detection of unstable radicals in a sample at low temperature; (b) spin trapping, e.g., by DMPO; and (c) spin labeling, e.g., with perdeuterated tert-dibutyl nitroxide (DTBN).

An alternative to EPR is application of fluorescent dye, e.g., dichlorofluorescin diacetate (DCFDA, DCFH-DA) which allows one to use flow cytometry or confocal microscopy for time- and spatially resolved detection of reactive oxygen species [116, 129, 130]. Unfortunately, this method has a very low specificity and cannot provide any detailed information about the character of oxidative stress, except of its estimated intensity.

EPR is a useful approach to provide information about UV protection abilities of some drugs. For example, Kawai et al. [131] studied if an antioxidant administered orally or intravenously can penetrate down to epidermis and suppress the anthralin-derived radical generation in the skin epidermis, measured by EPR at X-band [131]. Application of EPR provides the evidence that UVA is responsible for the occurrence of ca. 90% of free radicals in the illuminated skin [124]. Additionally, EPR spectroscopy is a convenient technique to measure nanoparticle-induced intracellular free radicals [104, 105]. Very valuable results were provided by Meinke et al. [113], who showed that the antioxidant status differs between *in vivo* and *ex vivo* skin samples probably due to oxygen effect [113]. Skin samples were also studied for free radical formation under *ex vivo* conditions due to infrared irradiation (e.g., to determine free radical formation and protective β-carotene effect) and solar illumination [114, 116, 118]. Some researchers also compare the human and mouse skin samples after UV irradiation [119].

Skin beautification effect can also be related to free radicals formed and affected by drugs. This effect was successfully studied with an E-109 spectrometer (Varian) [132]. EPR investigation of the skin revealed that different antioxidants protect each other and build an antioxidative network [106].

Nitric oxide spin-trapping technique was successfully used to study nonenzymatic nitric oxide generation in human skin *in vitro* and *in vivo* and proved that blue light irradiation significantly increases the intradermal level of free NO [78].

Free radicals can also be measured as a quantifiable index of a radiobiological effect (e.g., after X-ray irradiation), for example, melanin-derived radicals in the tail skin of a living intact mouse were directly detected in a noninvasive way (TE-mode EPR cavity, 9.45 GHz) [133].

To measure skin ascorbate- and thiol-dependent antioxidant activity *in vitro* and *in vivo*, the quantitative TEMPO radical scavenging can be studied by EPR technique. As described by Fuchs and co-workers [111], cell exposure to the glutathione synthetase inhibitor buthionine-sulfoximine depleted intracellular glutathione and inhibited nitroxide reduction, while exposure to dehydroascorbate or glutathione monoethylester increased intracellular ascorbate or glutathione concentration and stimulated nitroxide reduction [111].

EPR spectroscopy allows for a noninvasive *in vivo* measurement of the radical scavenging capacity in human skin [106]. The application of TEMPO on the human skin allows to perform a noninvasive EPR measurement of the effect of vitamin C intake (100 and 180 mg daily, 4 weeks) by patients to confirm significant increase in the radical scavenging capacity (a significant increase by 22% the capacity of radical scavenging) [107].

The influence of green tea beverages on radical scavenging capacity in skin was also investigated by EPR and TEMPO as a spin probe, and it was confirmed that three cups of freshly prepared green tea can enhance the radical scavenging capacity of human skin [108]. A similar *in vivo* L-band (ca. 1 GHz) EPR methodology was applied in double-blind placebo-controlled human study which revealed the effect of an orally administered natural supplement, which had shown a slow but significant and effective uptake of carotenoids in the skin [109].

8.4.2 Transport and Diffusion

The skin itself is an important target for drug delivery; additionally skin can be a very promising "gate" to systemic delivery of pharmaceuticals, with reduced toxicity. As EPR makes it able to determine some properties of the local environment of paramagnetic centers, such as hydration and polarity, transport and diffusion of cosmeceutics through and in the skin barrier improving the general condition of skin become an important field for skin-related EPR applications [134–136]. To study skin penetration enhancement of some new drug carriers, the spin probe (e.g., PCA) can be used as a cargo, whereupon the probe localization will be investigated by EPR [117]. The penetration of nanoparticles into the skin has also been investigated with EPR with the results remaining in agreement with tests using lipophilic fluorescent dyes [115, 137].

The *stratum corneum* isolated, for example, from pig ear skin has been used to mimic the surface interaction of drugs. Application of several fatty acid spin labels (e.g., 5- and 16-DS spin labels) to monitor the membrane fluidity changes at different depths of the membranes, according to the lipid component of SC, helped at developing of a topical treatment [138, 139].

8.4.3 Oxygen Consumption and Respiration

Oxygen plays a crucial role in majority of biological processes. In the context of skin study, the most interesting seems the engagement of oxygen in wound healing. This multistep process is related to hypoxia episodes and requires new vessels formation (angiogenesis). The different kinetics of wound healing in a diabetic mice model can be studied noninvasively with EPR spectrometers (the implantation of solid spin probe is not affecting the tissue in the long run) [87].

The India ink application as an oxygen-sensitive spin probe turns out a promising technique to monitor skin tissue oxygenation during diabetes in patients. As described by Williams et al. [82], a long-time series of oximetry measurements of the subcutaneous tissue on dorsal and planar foot surfaces have been made in nine volunteers, the longest set of measurements being carried out successfully for as long as over 5 years [82]. This methodology can be used to investigate other skin diseases like psoriasis, vitiligo, etc.

Additionally, more work should be done to elaborate the most useful probes and carriers to measure skin oxygen supply. Some researchers have recently suggested the char of the Bubinga tree (Bubinga, Kevazingo, etc., a group of closely related African trees *Guibourtia* spp.) as the most sensitive EPR oximetry probe in the group of carbon-based markers [36].

Another promising and relatively new access to skin oximetry is pulse EPR imaging with OX063, which has been executed *in vivo*. Triarylmethyl radical (OX063d24, also known as OX071) is extracellular in its distribution and is rapidly cleared from the body through renal excretion with a half-life of ca. 5 min. By using pulse sequences that image the longitudinal relaxation rate, R_1 ($R_1 = 1/T_1$, where T_1 is the longitudinal relaxation time), self-relaxation of the trityl spin probe is reduced to well within the 1 Torr uncertainties of our image voxel pO_2 values [140]. This method has absolute accuracy in oxygen measurement and supremacy over other methods because of a small confounding effect of environmental parameters other than O_2 [127]. During the described above R_{1e} pulse EPR experiment, the highly heterogeneous skin oxygenation is well detectable and sometimes can be even misinterpreted as a noise [128].

8.4.4 Melanization

The main place for melanin synthesis in human and laboratory animals is skin (Fig. 8.1) [141, 142], while its most intriguing physical feature is stable and extremely strong paramagnetism [143] resulting from the presence of semiquinones (eumelanins) and semiquinonimines (pheomelanins) in its amorphous structure [144]. Melanins reveal also other interesting properties like absorbance of light, metals chelation, redox potential, and free radical scavenging [145]. No wonder that EPR spectroscopy and more recently imaging have become the primary method in melanin research [146]. The pigment may be produced in the epithelial melanocytes where it is responsible for skin color [141] and phototype, in hair follicles where it responds for coloration of hair coat [147], and in melanoma tumors or pigmented nevi, where it affects the neoplastic transformation, progression, and metastasizing, as well as resistance to therapies [148]. As the dry, keratinized hair shafts are a perfect material for EPR measurement, the papers concerning EPR-based hair research creates a distinct group of dermatological studies [4]. Moreover, because of different structure of paramagnetic centers detectable in eumelanin and pheomelanin, and different parameters of EPR spectra, there is a possibility to carry out parallel quantitative and qualitative measurements [147, 149], which constitutes a separate group of the EPR papers.

8.5 Specific Biological Phenomena and Pathologies to Follow in the Skin with EPR

The most important practical aspects of medically oriented EPR spectroscopy and imaging concern identification and monitoring of some skin diseases, and the process of treatment, which primarily concerns local delivery and release of drugs. Here we shortly characterize the recent important and interesting applications of EPR in this field, in the context of a general skin physiology.

One of the most "traditional" applications of EPR to medicine is ionizing radiation dosimetry [91]. Hair, finger, and toe nails are convenient natural "dosimeters" because of the simplicity of handling (although, perhaps, not of interpreting radiation-induced EPR signals) and because of keratin—a good trap for radiation-induced radicals [150]. Moreover, information on partial doses of radiation are this way obtainable from various parts of the organism, depending on the place of collection of hair or nails. This field is still developing and improving the methodology [151, 152].

The skin is not only the biggest organ, but also it possesses a substantial surface which gives the opportunity to topically administer drugs. SC effectively prevents the ingress of xenobiotics into the body due to epidermal cell cohesion, keratinization, dehydration, lipid composition, and general organization [53, 153, 154]. The topical administration of drugs is possible but differs in effectiveness, depending on their molecular size and chemical and physical properties [155–157]. It is, however, a tempting opportunity to treat inflammatory skin diseases, and it provides many advantages over the oral or intravenous applications, e.g., preventing the initial pass effect with reduced systemic side effects [158], pain minimization, and a more local targeting of the affected skin with a possible controlled release of the drug [159, 160]. In recent years, the dermatological focus has shifted more and more toward nano-sized carrier systems, as they are able to permeate the SC barrier in an "intelligent" way (i.e., selectively and properly targeting the place of action accordingly to the variable microenvironment) [161–163].

In the broad spectrum of skin pathologies, one can distinguish a few types of skin tumors. The most common types are actinic keratosis, basal cell carcinoma (most common), squamous cell carcinoma, and melanoma. The last one is very interesting from the EPR perspective because it originates from melanocytes and very often is loaded with melanin (amelanotic melanomas are also known in clinic). Melanoma is known for thousands of years and intensively investigated for more than half of the century [164], but still a lot is unknown about the relation of melanin concentration and tumor progression and metastasis [165, 166]. Besides the *in vivo* and *in situ* attempts to image melanin distribution, there are still qualitative and quantitative EPR studies executed *in vitro* and in model systems [167, 168].

The UV exposition is one of the most important risk factors for melanoma; this is why the oxidative stress investigation after skin illumination is a relevant and hot EPR application. The special place in this field belongs to newly tested ointments scavenging free radicals and screening the skin from UV [169]. Additionally,

melanin quality, concentration, and distribution can be studied. The EPR signal from melanin appears to be a good indicator for melanoma development [170, 171]. It was demonstrated that EPR imaging can provide accurate information about the melanotic melanoma dimension (including tumor border, shape, fragmentation, fractal dimension) and the presence of metal ions inside the tumor [74, 172, 173]. Furthermore, Cesareo et al. [174] postulate that EPR signal may represent a reliable marker for melanoma diagnosis in human histological sections (based on the comparison between human melanomas and nevi) [174]. For a long time, melanin has been attempted to be used as an endogenous paramagnetic contrast agent for melanoma EPR imaging [175], and this has finally been achieved recently [176–178]. A progress in melanization or de-melanization in parallel to the development of the tumor may be this way followed *in situ*. Moreover, changes in the spectrum may deliver information not only on the amount and distribution of melanin due to a potential drug (e.g., curcumin or ligands for peroxisome-proliferator-activated receptors—PPARs [168, 179]) but also on other parameters affecting the EPR signal (e.g., oxygen content [180]). This may be of help when designing radiation dose and geometry of application in melanoma radiotherapy [181]. Finally, the ratio between eumelanin and pheomelanin can be studied [174]. This parameter may affect prognosis, but more importantly, it may be correlated with other parameters of tumor growth. One should recall here attempts to correlate melanization with biomechanical properties of tumor cells (plasticity) and with biological properties (metastasizing), which opens up a new field in melanoma research [165]. But EPR may deliver a possibility to monitor the progress of release of even other paramagnetic molecules important for tumor development, like nitric oxide (NO) [80].

A separate group of papers concerns hair as easy to measure indicators of melanogenesis. In this context, a new EPR-based technique of determination of eumelanin/pheomelanin content in regard to the g-factor must be mentioned [72]. The EPR hair studies show the importance of hair melanization as a parameter related to the condition of skin and the whole organism. It turns out that in some murine models, melanin is collected in visceral organs, in particular in the spleen [182–184]. It concerns not only the black C57BL/6 mice where this phenomenon has been described [185] but also wild (agouti) phenotypes [183]. The extradermal transfer of melanin from skin and hair follicles to the visceral organs including humans is an intriguing and still not fully understood phenomenon, studied now for half a century [99]. It concerns even such an important and notorious impairment of pigmentation [186] as chemotherapy-induced alopecia [62, 184]. Another intriguing study has been carried out using transgenic mice revealing knockout of gene encoding the melanocortin MC1 receptor and overexpression of a HGF/SF transcription factor, which performed a sophisticated analysis of the intensity of the melanin EPR signals of hair and skin samples, and their evolution parallel to the postnatal development of skin [73]. This paper concerned an important animal model for melanoma research, resembling in some aspects human melanoma. One must also mention an EPR study on amphibian skin, in which for the first time pheomelanogenesis was

demonstrated in this group of lower tetrapod vertebrates [70]. This study supports the view of a more primitive and evolutionary primordial character of pheomelanin and pheomelanogenesis over eumelanogenesis, a long-disputed controversion. Finally, a study determining the severity of human hair photodamage due to sun exposition [187] and EPR studies on telgen should be noted [65]. An exhaustive table review of older EPR hair studies is published in [4].

Psoriasis is an autoimmune disease the etiology of which has genetic basis and can be triggered by environmental factors. It is estimated that psoriasis affects 2–4% of the Western world population. Nails, skin appendages, are affected by the disease, too, which may be followed with EPR [122] and which is important also from the therapeutic point of view in the context of drug delivery across the nail plate barrier [188]. The role of nitric oxide was also investigated in psoriatic conditions with EPR, and conclusion was made that NO-containing creams would contribute to a partial recovery of disturbed functions and remission of the disease [79]. Nakagawa et al., during his study of skin surface of psoriasis by EPR imaging, concluded in 2016 that this technique can be used to detect and identify the location of abnormality of the SC states [123]. In general, this field will be important for medical EPR development in the future, determining other important functions of skin, affected by the disease, as water penetration and hydration of SC, presently reserved for NMR investigations [189]. While it is commonly considered as a dermatologic pathology, psoriasis affects the organism in-depth [190, 191]. EPR can be here helpful for evaluating conditions of not only skin, but also other parts of the organism, e.g., fluidity of erythrocyte membranes [192–194].

Another important disease affecting the whole organism including skin is diabetes. Diabetic conditions are the primary reason for many pathologies including a typically dermatologic complication—problems with wound healing. It was found that EPR can help at monitoring oxygenation in a noninvasive way in the skin of diabetic mouse models [87]. Interestingly, the effectiveness of treatment of burnt skin can be also investigated with EPR (X-band, Radiopan, Poland), as shown by Olczyk et al. [195].

There are many other "exotic" applications of EPR to study skin diseases or to study rare skin pathologies and diseases. An interesting medical application of EPR spectroscopy is usage of hair to determine iron deficiency and anemia. Petukhov and co-workers proposed in 2013 usage of a Radiopan EPR spectrometer and diethyldithiocarbamate (DETC) as an *in vitro* trap to measure NO activity in such a biological substrate as hair. It was found that the intensity of NO-radical complex signal in the spectrogram depends on the Fe level (again, not only in the analyzed substrate but also in the whole organism) [196]. EPR evaluation of ROS in skin samples from patients with diffuse cutaneous systemic sclerosis suggests that ROS may play an important role in the pathogenesis of fibrosis in scleroderma [125]. Finally, it is worth reminding that EPR was used to monitor the progress of reduction of carcinogenic chromium (VI) on the skin surface [197].

8.6 Specific Newest Experimental Approaches in Dermatologically Oriented EPR

Development of new concepts and techniques is a *conditio sine qua non* for medically oriented EPR to maintain its position as a research and diagnostic method in clinics and laboratories. The present subchapter is focused mainly on summarizing the recent achievements, so as not to recapitulate the contents of the already-existing reviews but to make a prognosis about the directions of the future of dermatological EPR.

Recently we may observe a particular acceleration of several aspects of EPR spectroscopy and imaging, as applied to dermatology. We may notice in particular development of nanocarriers delivering both spin labels and the investigated substances (drugs and cosmeceutics [105, 115, 132, 198–202]), including new-type lipid vesicular carriers—niosomes (nonionic surfactant vesicles [203]). One can observe a wide application of multifrequency EPR spectroscopy [204] and a support of EPR with other refined research and numeric methods [205], such as artificial neural networks [206], confocal microscopies [207], NMR [173, 208, 209], mass spectrometry [210], differential scanning calorimetry [211], atomic force microscopy [165], and others. To overcome the problems with EPR measurement of big, flat surfaces, new types of resonators have been constructed especially for skin research [212–215]. The field of building new resonators and equipment includes also new-type double surface coils for parallel, two-channel acquisition for 3D EPRI [216].

When writing on nanocarriers, it is obligatory to note a new concept of nano- and micro-bubbles as carriers for gases [217, 218]. This approach enables for usage of various gases and for modulation of both pro- and antioxidative activity of the local tissue environment. The redox state of the tissue [218] and its oxygenation [219] may be monitored with EPR [220].

One of the possible applications of EPR is investigation of pharmacokinetic properties of spin-labeled compounds in the skin. It can be a noninvasive technique to study not only skin penetration and stability of compounds but also to study the mechanism of, e.g., free radical generation. The main disadvantage is related to the possibility that nitroxides change the physicochemical properties of the labeled compounds [6]. Another important caveat was introduced by Meinke et al. [113] who compared *in vivo* and *ex vivo* detection of free radicals in skin with EPR and PCA as a spin probe. The results revealed distinct differences in the ROS formation and the antioxidant potential (the experiments *ex vivo* revealed a smaller ROS concentration in the tissue due to oxygen effect) which must be considered during experiments and data interpretation [113].

Another interesting application of EPR is radiation dose reconstruction based on teeth as presented by Demidenko [221]. This illustrates ongoing development of EPR-based dosimetry of ionizing and UV radiation [91].

Skin imaging with EPR is not the newest experimental approach but a very promising direction for the future (especially under *in vivo* conditions) [222]. The surface coil turns out a perfect tool to image skin, for instance, to compare the effectiveness of sunscreens in the same biological conditions *in vivo*. Additionally, imaging of pathologies like human melanoma or psoriasis can

shed new light on the illness classification and therapy optimization [74, 123]. Finally, as it was already mentioned earlier, the application of EPRI for skin research can be related to pharmacokinetics, penetration, and biodistribution study on some paramagnetic or paramagnetic-labeled drugs and beauty products.

Recent years have brought some entirely new concepts in medically oriented EPR. One of them concerns quantitative determination of various kinds of melanins in a pigment [72]. There are two complementary and independent methods of estimation of eumelanin/pheomelanin ratio, which may be important, for example, in determination of prognosis in melanoma treatment [223, 224] or just in estimation of probability of melanoma development [225]. One of them is based on the ratio of specific products of pigment degradation, followed by their quantitative HPLC separation (the "PTCA/AHP" method, colloquially the "Ito" method [175, 226]), and the other one—on the proportion of constituents of hyperfine splitting features of the pigment EPR spectrum [227, 228]—as pheomelanin revealing the splitting, while eumelanin giving a pure singlet line. As the pheomelanin-like paramagnetic centers are of semiquinonimine character, their unpaired electron is localized partially on the sulfur atom of the benzotiazin subunit [144, 229]. The presence of a relatively heavy nucleus (i.e., of a considerable positive charge) in the neighborhood of the unpaired electron causes a low-magnetic-field shift of the EPR signal, resulting from an increase in the g-value [72, 230], which is a phenomenon independent on the mechanism of hyperfine splitting (resulting from the magnetic interactions of the unpaired electron with the nucleus). As a consequence, the researchers have been presented with a new, independent method of estimation of eumelanin/pheomelanin ratio based on the measurement of the g-value, more precisely: a g_{exp} (a resultant of a population of eumelanotic and pheomelanotic paramagnetic centers of various g values and various proportions) or g_{app} value (obtained from a CW X-band measurements) [72, 227].

An important methodological achievement and a good conclusion for this chapter is establishing the RSF—Radical Status Factor [231]—which is defined as a ratio of the number of free radicals in untreated skin to the number of the same area of irradiated skin. It was obtained for pig skin and the UV-IR spectrum of radiation. The RSF makes it able to characterize both a given form of radiation and a given photoprotector (or photosensibilizator)—an ointment, sunscreen, UV filter, etc. This characteristic is a product of the generated oxidative stress, and with some modification it might be calculated directly from parameters of EPR spectra or upon use of spin-trapping techniques, and applied to consider additional sources of free radicals, like melanin. This shows the potential of EPR as applied to prevention and treatment of skin pathologies.

8.7 Conclusions: Skin-Deep or In-Depth?

The main object of interest in dermatologically oriented EPR spectroscopy and imaging is oxidative stress induced by irradiation, intoxication, or inflammation; drug, cosmeceutics, and toxin penetration and delivery, including nanocarrier

delivery systems; and melanin, including melanoma. There are obviously more applications, but in general, the field seems quite narrow and niche. But in the common society, especially in the world of culture and art, the adjective "niche" is often associated with the notion of the so-called high culture. Translating this association to the language of science, it means that a niche application not only is not marginal, and not only may be "mainstream" (because a stream can certainly be narrow), but it may concern the most essential aspects of a discipline, of the biggest impact on its development and cognitive capacities. The processes investigated by EPR seem, indeed, to reveal this kind of importance (see "Paramagnetomics"—Chap. 9 in this book). Regarding the most important functions of skin and its cells [4, 15], one must conclude that they are important not only for the skin itself, and not only for the beauty itself, looking from the cosmeceutical point of view, but also—indirectly or directly—for the organism as a whole [52]. And on the other hand, many processes taking place in the organism as a whole, and some of them being of a pathological character, may manifest themselves in the skin or on the skin. From the content (including the paramagnetic content) of skin melanin, hair, and nails, some aspects of the past of the organism may be read. The oxidative stress and products of inflammation and photoreactivity, including hormones (vitamin D), interleukins, etc., may spread over the whole organisms. Melanoma [148, 224, 232], suspected of being induced by UV, is a deadly threat for the organism. There are numerous other examples of such systemic effects or reasons of what happens in the skin and which may be followed by EPR. The summary chapter is a good opportunity to recapitulate examples of such "in-depth" looks: the most spectacular hair, nail, and skin EPR dosimetry of body irradiation [91, 133], splenic melanosis as a manifestation of normal [182] or chemotherapy-impaired skin/hair pigmentation [184], systemic manifestation of psoriasis [79, 122, 123, 194], skin manifestation of diabetes [132], iron content in hair as a reflex of Fe level in the body [196], or a very interesting hypothesis of the development of the Vogt-Koyanagi-Harada syndrome-related aseptic meningitis in vitiligo patients due to the impairment of leptomeningeal melanocytes [102]. The conclusions drawn from such studies must be of a general character. The amount, quality, and importance of information conveyed by EPR are invaluable and concern the organism as a whole, besides the processes taking place in the skin *in situ*. They all happen literally within the depth of the skin, but many of them are of the systemic, in-depth character. A continual development of the EPR techniques serves for their better understanding and for the better understanding of the connection between what is skin-deep and in-depth in dermatologically oriented EPR.

Acknowledgments The Faculty of Biochemistry, Biophysics, and Biotechnology of the Jagiellonian University in Kraków is a partner of the Leading National Research Center (KNOW) supported by the Polish Ministry of Science and Higher Education. The paper was partially supported from this fund (PMP, grant KNOW 35p/10/2015). The support to MKS from grant PRELUDIUMII NSC, 2011/03/N/NZ4/02019 is also acknowledged.

Conflicts of Interest The authors declare no conflict of interest.

References

1. Łukiewicz SJ, Zweier JL, editors. Nitric oxide in allograft rejection and anti-tumor response. Boston-Dordrecht London: Kluwer Academic Publisher; 1998.
2. Eaton SS, Eaton GR, Berliner JL. Biomedical ESR. Vol 23 of the biological magnetic resonance series. New York-Boston: Kluwer Academic Publishers; 2005.
3. Berliner LJ. The evolution of biomedical EPR (ESR). Biomed Spectrosc Imaging. 2017;5(1):5–26. Available from: http://www.medra.org/servlet/aliasResolver?alias=iospress&doi=10.3233/BSI-150128
4. Plonka PM. Electron paramagnetic resonance as a unique tool for skin and hair research. Exp Dermatol. 2009;18(5):472–84. Available from: https://www.ncbi.nlm.nih.gov/pubmed/19368555
5. Fuchs J, Packer L. Electron paramagnetic resonance in dermatologic research with particular reference to photodermatology. Photodermatol Photoimmunol Photomed. 1990;7(6):229–32. Available from: http://www.ncbi.nlm.nih.gov/pubmed/1966464
6. Cal K, Zakowiecki D, Stefanowska J. Advanced tools for in vivo skin analysis. Int J Dermatol. 2010;49(5):492–9. Available from: http://doi.wiley.com/10.1111/j.1365-4632.2010.04355.x
7. Butt OI, Carruth R, Kutala VK, Kuppusamy P, Moldovan NI. Stimulation of Peri-implant vascularization with bone marrow-derived progenitor cells: monitoring by in vivo EPR Oximetry. Tissue Eng. 2007;13(8):2053–61. Available from: http://www.liebertonline.com/doi/abs/10.1089/ten.2006.0225
8. Kadirov RK, Arkhipova SS, Shahmardanova SA, Rizvanov AA. Structural changes in the pancreas and its blood vessels at the early stages of ischemia. Bionanoscience. 2016;6(4):293–6. Available from: http://link.springer.com/10.1007/s12668-016-0265-2
9. Ziaja M, Pyka J, Machowska A, Maslanka A, Plonka PM. Nitric oxide spin-trapping and NADPH-Diaphorase activity in mature rat brain after injury. J Neurotrauma. 2007;24(12):1845–54. Available from: http://www.liebertonline.com/doi/abs/10.1089/neu.2007.0303
10. Lin Y, Yokoyama H, Ishida S, Tsuchihashi N, Ogata T. In vivo electron spin resonance analysis of nitroxide radicals injected into a rat by a flexible surface-coil-type resonator as an endoscope- or a stethoscope-like device. Magma Magn Reson Mater Physics Biol Med. 1997;5(2):99–103. Available from: http://link.springer.com/10.1007/BF02592239
11. Epel B, Redler G, Tormyshev V, Halpern HJ. Towards human oxygen images with Electron paramagnetic resonance imaging. Adv Exp Med Biol. 2016;876(5):363–9. Available from: http://informahealthcare.com/doi/abs/10.3109/10715769109105220
12. Płonka PM, Elas M. Application of the electron paramagnetic resonance spectroscopy to modern biotechnology. Curr Top Biophys. 2002;26(1):176–89. Available from: http://ctbo.home.amu.edu.pl/
13. Eaton SS, Eaton GR. The world as viewed by and with unpaired electrons. J Magn Reson. 2012;223:151–63. Available from: http://linkinghub.elsevier.com/retrieve/pii/S1090780712002674
14. Hagen WR. Metallomic EPR spectroscopy. Metallomics. 2009;1(5):384. Available from: http://xlink.rsc.org/?DOI=b907919j
15. Chuong CM, Nickoloff BJ, Elias PM, Goldsmith LA, Macher E, Maderson PA, et al. What is the "true" function of skin? Exp Dermatol. 2002;11(2):159–87. Available from: http://www.ncbi.nlm.nih.gov/pubmed/11994143
16. Tobin DJ. Biochemistry of human skin—our brain on the outside. Chem Soc Rev. 2006;35(1):52–67. Available from: http://xlink.rsc.org/?DOI=B505793K
17. Kanitakis J. Anatomy, histology and immunohistochemistry of normal human skin. Eur J Dermatol. 2002;12(4):390–401. Available from: http://www.ncbi.nlm.nih.gov/pubmed/12095893
18. Goldsmith LA. My organ is bigger than your organ. Arch Dermatol. 1990;126(3):301–2. Available from: http://archderm.jamanetwork.com/article.aspx?doi=10.1001/archderm.1990.01670270033005

19. Tamyis NM, Ghodgaonkar DK, Taib MN, Wui WT, Mara UT. Dielectric properties of human skin in vivo in the frequency range 20–38 GHz for 42 healthy volunteers. Proc. of the 28th URSI General Assembly, New Delhi, India, May 23–29, 2005. KP.45(0850), Available from: http://www.ursi.org/Proceedings/ProcGA05/pdf/KP.45(0850).pdf
20. Grant JP, Clarke RN, Symm GT, Spyrou NM. In vivo dielectric properties of human skin from 50 MHz to 2.0 GHz. Phys Med Biol. 1988;33(5):607–12. Available from: http://iopscience.iop.org/article/10.1088/0031-9155/33/5/008/pdf
21. Stücker M, Struk A, Altmeyer P, Herde M, Baumgärtl H, Lübbers DW. The cutaneous uptake of atmospheric oxygen contributes significantly to the oxygen supply of human dermis and epidermis. J Physiol. 2002;538(Pt 3):985–94. Available from: https://www.ncbi.nlm.nih.gov/pubmed/11826181
22. Thiele J, Elsner P. Oxidants and antioxidants in cutaneous biology. In: Thiele J, Elsner P, Burg G, editors. Current problems in dermatology, vol. 29. Zurich: KARGER; 2001. p. 1–203. Available from: https://www.karger.com/Book/Home/224318.
23. Battie C, Verschoore M. Cutaneous solar ultraviolet exposure and clinical aspects of photodamage. Indian J Dermatology, Venereol Leprol. 2012;78(7):9. Available from: http://www.ijdvl.com/text.asp?2012/78/7/9/97350
24. Timares L, Katiyar SK, Elmets CA. DNA damage, apoptosis and langerhans cells–activators of UV-induced immune tolerance. Photochem Photobiol. 2008;84(2):422–36. Available from: http://www.pubmedcentral.nih.gov/articlerender.fcgi?artid=2718731&tool=pmcentrez&rendertype=abstract
25. Zastrow L, Groth N, Klein F, Kockott D, Lademann J, Renneberg R, et al. The missing link—light-induced (280–1600 nm) free radical formation in human skin. Skin Pharmacol Physiol. 2009;22(1):31–44. Available from: https://www.ncbi.nlm.nih.gov/pubmed/19122479
26. Brooker C. Human structure and function: nursing applications in clinical practice. St Louis: Mosby; 1998. p. 1–568.
27. Gerard TJ, Bryan D. Principles of anatomy & physiology. New York: John Wiley & Sons, Inc.; 2012. p. 1–1280.
28. Marionnet C, Pierrard C, Vioux-Chagnoleau C, Sok J, Asselineau D, Bernerd F. Interactions between fibroblasts and keratinocytes in morphogenesis of dermal epidermal junction in a model of reconstructed skin. J Invest Dermatol. 2006;126(5):971–9. Available from: http://linkinghub.elsevier.com/retrieve/pii/S0022202X15328931
29. Smola H, Stark HJ, Thiekötter G, Mirancea N, Krieg T, Fusenig NE. Dynamics of basement membrane formation by keratinocyte-fibroblast interactions in organotypic skin culture. Exp Cell Res. 1998;239(2):399–410. Available from: http://www.ncbi.nlm.nih.gov/pubmed/9521858
30. Marinkovich MP, Keene DR, Rimberg CS, Burgeson RE. Cellular origin of the dermal-epidermal basement membrane. Dev Dyn. 1993;197(4):255–67. Available from: http://www.ncbi.nlm.nih.gov/pubmed/8292823
31. Briggaman RA, Dalldorf FG, Wheeler CE. Formation and origin of basal lamina and anchoring fibrils in adult human skin. J Cell Biol. 1971;51(21):384–95. Available from: http://www.ncbi.nlm.nih.gov/pubmed/4939526
32. Regauer S, Seiler GR, Barrandon Y, Easley KW, Compton CC. Epithelial origin of cutaneous anchoring fibrils. J Cell Biol. 1990;111(5 Pt 1):2109–15. Available from: http://www.ncbi.nlm.nih.gov/pubmed/2229187
33. McGrath JA, Eady RAJ, Pope FM. Anatomy and Organization of Human Skin. In: Burns T, Breathnach S, Neil C, Griffiths C, editors. Rook's textbook of dermatology. 7th ed. Malden, MA: Blackwell Publishing, Inc; 2004. p. 3.1–3.84. Available from. https://doi.org/10.1002/9780470750520.ch3.
34. Montagna W, Parakkal PF. The structure and function of skin. 3rd ed. New York: Academic Press; 1974. p. 433. Available from: http://www.sciencedirect.com/science/book/9780125052634
35. Kristl J, Abramović Z, Sentjurc M. Skin oxygenation after topical application of liposome-entrapped benzyl nicotinate as measured by EPR oximetry in vivo: influence of composition

and size. AAPS PharmSci. 2003;5(1):E2. (1–9). Available from: https://www.ncbi.nlm.nih.gov/pubmed/12713274
36. Krzic M, Sentjurc M, Kristl J. Improved skin oxygenation after benzyl nicotinate application in different carriers as measured by EPR oximetry in vivo. J Control Release. 2001;70(1–2):203–11. Available from:. https://doi.org/10.1016/S0168-3659(00)00351-5.
37. Braverman IM. Ultrastructure and organization of the cutaneous microvasculature in normal and pathologic states. J Invest Dermatol. 1989;93(s2):2S–9S. Available from: https://www.ncbi.nlm.nih.gov/pubmed/2666519
38. Gerlach A. Über das Hautathmen. Arch Anat Physiol. 1851;1:431–79.
39. Raguz M, Mainali L, Widomska J, Subczynski WK. Using spin-label electron paramagnetic resonance (EPR) to discriminate and characterize the cholesterol bilayer domain. Chem Phys Lipids. 2011;164(8):819–29. Available from: http://linkinghub.elsevier.com/retrieve/pii/S0009308411003070
40. Alonso L, Fuchs E. Stem cells of the skin epithelium. Proc Natl Acad Sci U S A. 2003;100(Suppl):11830–5. Available from: http://www.ncbi.nlm.nih.gov/pubmed/12913119
41. Hall PA, Watt FM. Stem cells: the generation and maintenance of cellular diversity. Development. 1989;106(4):619–33. Available from: http://www.ncbi.nlm.nih.gov/pubmed/2562658
42. Watt FM. Terminal differentiation of epidermal keratinocytes. Curr Opin Cell Biol. 1989;1(6):1107–15. Available from: http://www.ncbi.nlm.nih.gov/pubmed/2699799
43. Kroemer G, Galluzzi L, Vandenabeele P, Abrams J, Alnemri ES, Baehrecke EH, Blagosklonny MV, El-Deiry WS, Golstein P, Green DR, Hengartner M, Knight RA, Kumar S, Lipton SA, Malorni W, Nuñez G, Peter ME, Tschopp J, Yuan J, Piacentini M, Zhivotovsky B, Melino G. Nomenclature Committee on Cell Death 2009. Classification of cell death: recommendations of the Nomenclature Committee on Cell Death 2009. Cell Death Differ. 2009;16(1):3–11. Available from: http://www.ncbi.nlm.nih.gov/pmc/articles/PMC2744427/
44. Fitzpatrick TB, Breathnach AS. The epidermal melanin unit system. Dermatol Wochenschr. 1963;147:481–9. Available from: http://www.ncbi.nlm.nih.gov/pubmed/14172128
45. Singh SK, Kurfurst R, Nizard C, Schnebert S, Perrier E, Tobin DJ. Melanin transfer in human skin cells is mediated by filopodia–a model for homotypic and heterotypic lysosome-related organelle transfer. FASEB J. 2010;24(10):3756–69. Available from: http://www.fasebj.org/cgi/doi/10.1096/fj.10-159046
46. Singh SK, Baker R, Sikkink SK, Nizard C, Schnebert S, Kurfurst R, Tobin DJ. E-cadherin mediates ultraviolet radiation- and calcium-induced melanin transfer in human skin cells. Exp Dermatol. 2017;26(11):1125–33. Available from: http://doi.wiley.com/10.1111/exd.13395
47. Stanley JR, Woodley DT, Katz SI, Martin GR. Structure and function of basement membrane. J Invest Dermatol. 1982;79(1):69s–72s. Available from:. https://doi.org/10.1038/jid.1982.13.
48. Breitkreutz D, Mirancea N, Nischt R. Basement membranes in skin: unique matrix structures with diverse functions? Histochem Cell Biol. 2009;132(1):1–10. Available from: http://www.ncbi.nlm.nih.gov/pubmed/19333614
49. Breslow A. Prognosis in cutaneous melanoma: tumor thickness as a guide to treatment. Pathol Annu. 1980;15(Pt 1):1–22. Available from: http://www.ncbi.nlm.nih.gov/pubmed/7443304
50. Walters KAK. Dermatological and transdermal formulations. In: Walters K, editor. Drugs and the pharmaceutical sciences. New York, London: Informa Healthcare; 2002. p. 567. Available from: https://www.google.com/books?hl=pl&lr=&id=4pycGojmdaoC&oi=fnd&pg=PP1&dq=Dermatological+and+transdermal+formulations&ots=lJO8aJVwGB&sig=kHA0nFeCxf3UEX2ceEpBartU6Zc.
51. McLafferty E, Hendry C, Farley A. The integumentary system: anatomy, physiology and function of skin. Nurs Stand. 2012;27(3):35–42. Available from: https://www.ncbi.nlm.nih.gov/pubmed/23248884
52. Slominski AT, Zmijewski MA, Plonka PM, Szaflarski JP, Paus R. How UV Light Touches the Brain and Endocrine System Through Skin, and Why. Endocrinology. 2018;159(5):1992–2007. Available from: https://www.ncbi.nlm.nih.gov/pubmed/29546369

53. Madison KC. Barrier function of the skin:"la raison d'etre" of the epidermis. J Invest Dermatol. 2003;121(2):231–41. Available from: http://www.sciencedirect.com/science/article/pii/S0022202X15303560
54. Slominski A, Zbytek B, Nikolakis G, Manna PR, Skobowiat C, Zmijewski M, Li W, Janjetovic Z, Postlethwaite A, Zouboulis CC, Tuckey RC. Steroidogenesis in the skin: implications for local immune functions. J Steroid Biochem Mol Biol. 2013;137:107–23. Available from: http://linkinghub.elsevier.com/retrieve/pii/S0960076013000277
55. Slominski A, Wortsman J. Neuroendocrinology of the skin. Endocr Rev. 2000;21(5):457–87. Available from: http://www.ncbi.nlm.nih.gov/pubmed/11041445
56. Slominski A, Wortsman J, Pisarchik A, Zbytek B, Linton EA, Mazurkiewicz JE, Wei ET. Cutaneous expression of corticotropin-releasing hormone (CRH), urocortin, and CRH receptors. FASEB J. 2001;15(10):1678–93. Available from: http://www.ncbi.nlm.nih.gov/pubmed/11481215
57. Chao-Chun Yang AT, Chen WC. Handbook of hair in health and disease. In: Preedy VR, editor. Handbook of hair in health and disease. Wageningen: Wageningen Academic Publishers; 2012. p. 51–71. Available from: http://www.wageningenacademic.com/doi/book/10.3920/978-90-8686-728-8.
58. Plonka P, Plonka B, Paus R. Biophysical monitoring of melanogenesis as a tool for pigment and hair research. Arch Dermatol Res. 1995;287(7):687–90. Available from: http://www.ncbi.nlm.nih.gov/pubmed/8534135
59. Slominski A, Paus R, Plonka P, Chakraborty A, Maurer M, Pruski D, Lukiewicz S. Melanogenesis during the anagen-catagen-telogen transformation of the murine hair cycle. J Invest Dermatol. 1994;102(6):862–9. Available from: http://www.ncbi.nlm.nih.gov/pubmed/8006449
60. Müller-Röver S, Handjiski B, van der Veen C, Eichmüller S, Foitzik K, McKay IA, Stenn KS, Paus R. A comprehensive guide for the accurate classification of murine hair follicles in distinct hair cycle stages. J Invest Dermatol. 2001;117(1):3–15. Available from: http://www.ncbi.nlm.nih.gov/pubmed/11442744
61. Geyfman M, Plikus MV, Treffeisen E, Andersen B, Paus R. Resting no more: re-defining telogen, the maintenance stage of the hair growth cycle. Biol Rev. 2015;90(4):1179–96. Available from: http://doi.wiley.com/10.1111/brv.12151
62. Slominski A, Paus R, Plonka P, Handjiski B, Maurer M, Chakraborty A, Mihm MC Jr. Pharmacological disruption of hair follicle pigmentation by cyclophosphamide as a model for studying the melanocyte response to and recovery from cytotoxic drug damage in situ. J Invest Dermatol. 1996;106(6):1203–11. Available from: http://www.ncbi.nlm.nih.gov/pubmed/8752658
63. Milner Y, Sudnik J, Filippi M, Kizoulis M, Kashgarian M, Stenn K. Exogen, shedding phase of the hair growth cycle: characterization of a mouse model. J Invest Dermatol. 2002;119(3):639–44. Available from: http://www.ncbi.nlm.nih.gov/pubmed/12230507
64. Rebora A, Kenogen GM. A new phase of the hair cycle? Dermatology. 2002;205(2):108–10. Available from: http://www.ncbi.nlm.nih.gov/pubmed/12218222
65. Plonka PM, Michalczyk D, Popik M, Handjiski B, Paus R. Electron paramagnetic resonance (EPR) spectroscopy for investigating murine telogen skin after spontaneous or depilation-induced hair growth. J Dermatol Sci. 2008;49(3):227–40. Available from: http://www.ncbi.nlm.nih.gov/pubmed/18061408
66. Cash TF. The psychology of hair loss and its implications for patient care. Clin Dermatol. 2001;19:161–6. Available from: https://www.ncbi.nlm.nih.gov/pubmed/11397595
67. McGarvey E, Baum LD, Pinkerton RC, Rogers LM. Psychological sequelae and alopecia among women with cancer. Cancer Pract. 2001;9:283–9. Available from: https://www.ncbi.nlm.nih.gov/pubmed/11879330
68. Can G, Demir M, Erol O, Aydiner A. A comparison of men and women's experiences of chemotherapy-induced alopecia. Eur J Oncol Nurs. 2013;17:255–60. Available from: https://www.ncbi.nlm.nih.gov/pubmed/22901547

69. Choi M, Kim M, Park S, Park G, Jo S, Cho K, et al. Clinical characteristics of chemotherapy-induced alopecia in childhood. J Am Acad Dermatol. 2014;70:499–505. Available from: https://www.ncbi.nlm.nih.gov/pubmed/24355411
70. Wolnicka-Glubisz A, Pecio A, Podkowa D, Kolodziejczyk LM, Plonka PM. Pheomelanin in the skin of *Hymenochirus boettgeri* (Amphibia: Anura: Pipidae). Exp Dermatol. 2012;21(7):537–40. Available from: https://www.ncbi.nlm.nih.gov/pubmed/22716250
71. Hill HZ, Hill GJ, Cieszka K, Plonka PM, Mitchell DL, Meyenhofer MF, Meyenhofer MF, Xin P, Boissy RE. Comparative action spectrum for ultraviolet light killing of mouse melanocytes from different genetic coat color backgrounds. Photochem Photobiol. 1997;65(6):983–9. Available from: http://www.ncbi.nlm.nih.gov/pubmed/9188277
72. Chikvaidze EN, Partskhaladze TM, Gogoladze TV. Electron spin resonance (ESR/EPR) of free radicals observed in human red hair: a new, simple empirical method of determination of pheomelanin/eumelanin ratio in hair. Magn Reson Chem. 2014;52(7):377–82. Available from: http://www.ncbi.nlm.nih.gov/pubmed/24757073
73. Wolnicka-Glubisz A, Pecio A, Podkowa D, Plonka PM, Grabacka M. HGF/SF increases number of skin melanocytes but does not alter quality or quantity of follicular melanogenesis. PLoS One. 2013;8(11):e74883. Available from: http://www.ncbi.nlm.nih.gov/pubmed/24223113
74. Godechal Q, Leveque P, Marot L, Baurain JF, Gallez B. Optimization of electron paramagnetic resonance imaging for visualization of human skin melanoma in various stages of invasion. Exp Dermatol. 2012;21(5):341–6. Available from: https://www.ncbi.nlm.nih.gov/pubmed/22509830
75. Godechal Q, Defresne F, Danhier P, Leveque P, Porporato PE, Sonveaux P, Baurain JF, Feron O, Gallez B. Assessment of melanoma extent and melanoma metastases invasion using electron paramagnetic resonance and bioluminescence imaging. Contrast Media Mol Imaging. 2011;6(4):282–8. Available from: https://www.ncbi.nlm.nih.gov/pubmed/21861288
76. Katsuda H, Kobayashi T, Saito H, Matsunaga T, Ikeya M. Electron spin resonance imaging of mouse B16 melanoma. Chem Pharm Bull (Tokyo). 1990;38(10):2838–40. Available from: https://www.ncbi.nlm.nih.gov/pubmed/1963815
77. Lohan SB, Lauer A-C, Arndt S, Friedrich A, Tscherch K, Haag SF, Darvin ME, Vollert H, Kleemann A, Gersonde I, Groth N, Lademann J, Rohn S, Meinke MC. Determination of the antioxidant status of the skin by in vivo-electron paramagnetic resonance (EPR) spectroscopy. Cosmetics. 2015;2:286–301. Available from: http://www.mdpi.com/2079-9284/2/3/286
78. Opländer C, Deck A, Volkmar CM, Kirsch M, Liebmann J, Born M, van Abeelen F, van Faassen EE, Kröncke KD, Windolf J, Suschek CV. Mechanism and biological relevance of blue-light (420-453 nm)- induced nonenzymatic nitric oxide generation from photolabile nitric oxide derivates in human skin in vitro and in vivo. Free Radic Biol Med. 2013;65:1363–77. Available from. https://doi.org/10.1016/j.freeradbiomed.2013.09.022.
79. Matoshvili M, Katsitadze A, Sanikidze T, Tophuria D, Richetta A, D'Epiro S. The role of nitric oxide in the pathogenesis and severity of psoriasis. Georgian Med News. 2014;234:61–4. Available from: http://www.ncbi.nlm.nih.gov/pubmed/25341240
80. Pustelny K, Bielanska J, Plonka PM, Rosen GM, Elas M. In vivo spin trapping of nitric oxide from animal tumors. Nitric Oxide. 2007;16(2):202–8. Available from: http://www.sciencedirect.com/science/article/pii/S1089860306004125
81. Konyukhov GV, Nizamov RN, Tarasova NB, Nefedova RV, Petukhov VY, Ibragimova MI, Yusupova GR. Early diagnosis of radiation injuries by methods of immunochemical and EPR analyses. Bali Med J. 2017;6(2):368–70. Available from: http://balimedicaljournal.org/index.php/bmj/article/view/521
82. Williams BB, Khan N, Zaki B, Hartford A, Ernstoff MS, Swartz HM. Clinical Electron paramagnetic resonance (EPR) Oximetry using India ink. Boston, MA: Springer; 2010. p. 149–56. Available from: http://link.springer.com/10.1007/978-1-4419-1241-1_21
83. Khan N, Williams BB, Hou H, Li H, Swartz HM. Repetitive tissue pO measurements by electron paramagnetic resonance oximetry: current status and future potential for experimental

and clinical studies. Antioxid Redox Signal. 2007;9(8):1169–82. Available from: http://www.liebertonline.com/doi/abs/10.1089/ars.2007.1635
84. Abramovic Z, Sentjurc M, Kristl J, Khan N, Hou H, Swartz HM. Influence of different anesthetics on skin oxygenation studied by electron paramagnetic resonance in vivo. Skin Pharmacol Physiol. 2007;20(2):77–84. Available from: https://www.ncbi.nlm.nih.gov/pubmed/17143012
85. Swartz HM, Hou H, Khan N, Jarvis LA, Chen EY, Williams BB, Kuppusamy P. Advances in probes and methods for clinical EPR oximetry. Adv Exp Med Biol. 2014;812:73–9. Available from:. https://doi.org/10.1007/978-1-4939-0620-8.
86. Ahmad R, Kuppusamy P. Theory, instrumentation, and applications of EPR oximetry. Chem Rev. 2011;110(5):3212–36. Available from: https://www.ncbi.nlm.nih.gov/pmc/articles/PMC2868962/
87. Desmet CM, Lafosse A, Vériter S, Porporato PE, Sonveaux P, Dufrane D, Levêque P, Gallez B. Application of electron paramagnetic resonance (EPR) oximetry to monitor oxygen in wounds in diabetic models. PLoS One. 2015;10(12):e0144914. Available from: http://www.ncbi.nlm.nih.gov/pubmed/26659378
88. Swartz HM, Williams BB, Zaki BI, Hartford AC, Jarvis LA, Chen EY, Comi RJ, Ernstoff MS, Hou H, Khan N, Swarts SG, Flood AB, Kuppusamy P. Clinical EPR: unique opportunities and some challenges. Acad Radiol. 2014;21(2):197–206. Available from: https://www.ncbi.nlm.nih.gov/pubmed/24439333
89. Khan N, Hou H, Hein P, Comi RJ, Buckey JC, Grinberg O, Salikhov I, Lu SY, Wallach H, Swartz HM. Black magic and EPR oximetry: from lab to initial clinical trials. Adv Exp Med Biol. 2005;566:119–25. Available from: http://www.ncbi.nlm.nih.gov/pubmed/16594143
90. Khan N, Williams BB, Swartz HM. Clinical applications of in vivo EPR: rationale and initial results. Appl Magn Reson. 2006;30(2):185–99. Available from: http://link.springer.com/10.1007/BF03166718
91. Kubiak T. Advances in EPR dosimetry in terms of retrospective determination of absorbed dose in radiation accidents. Curr Topic Biophys. 2018;41:11–21. Available from: http://ctbo.home.amu.edu.pl/
92. Çolak Ş, Özbey T. An ESR study on biological dosimeters: human hair. Radiat Meas. 2011;46(5):465–72. Available from: https://www.sciencedirect.com/science/article/abs/pii/S1350448710004014
93. Lange BAJ, Buettner GR. Electron paramagnetic resonance detection of free radicals in UV-irradiated human and mouse skin. In: Thiele J, Elsner P, editors. Oxidants and antioxidants in cutaneous biology. Basel: KARGER; 2000. p. 18–25. Available from: https://www.karger.com/Article/FullText/60658.
94. Romanyukha A, Trompier F, Reyes RA, Christensen DM, Iddins CJ, Sugarman SL. Electron paramagnetic resonance radiation dose assessment in fingernails of the victim exposed to high dose as result of an accident. Radiat Environ Biophys. 2014;53(4):755–62. Available from: http://www.ncbi.nlm.nih.gov/pubmed/24957016
95. Marciniak A, Ciesielski B. EPR dosimetry in nails—a review. Appl Spectrosc Rev. 2016;51(1):73–92. Available from: http://www.tandfonline.com/action/journalInformation?journalCode=laps20
96. Trompier F, Queinnec F, Bey E, De Revel T, Lataillade JJ, Clairand I, Benderitter M, Bottollier-Depois JF. EPR retrospective dosimetry with fingernails: report on first application cases. Health Phys. 2014;106(6):798–805. Available from: http://content.wkhealth.com/linkback/openurl?sid=WKPTLP:landingpage&an=00004032-201406000-00023
97. Breathnach AS. Extra-cutaneous melanin. Pigment Cell Res. 1988;1(4):234–7. Available from: http://www.ncbi.nlm.nih.gov/pubmed/3070524
98. Hu D-N, Simon JD, Sarna T. Role of ocular melanin in ophthalmic physiology and pathology. Photochem Photobiol. 2008;84(3):639–44. Available from: http://doi.wiley.com/10.1111/j.1751-1097.2008.00316.x

99. Wassermann HP. Extension of the concept "vertebrate epidermal melanin unit" to embrace visceral pigmentation and leucocytic melanin transport. Nature. 1967;213(5073):282–3. Available from: http://www.ncbi.nlm.nih.gov/pubmed/6030608
100. Zucca FA, Segura-Aguilar J, Ferrari E, Muñoz P, Paris I, Sulzer D, Sarna T, Casella L, Zecca L. Interactions of iron, dopamine and neuromelanin pathways in brain aging and Parkinson's disease. Prog Neurobiol. 2017;155:96–119. Available from: http://www.ncbi.nlm.nih.gov/pubmed/26455458
101. Clewett DV, Lee T-H, Greening S, Ponzio A, Margalit E, Mather M. Neuromelanin marks the spot: identifying a locus coeruleus biomarker of cognitive reserve in healthy aging. Neurobiol Aging. 2016;37:117–26. Available from. https://doi.org/10.1016/j.neurobiolaging.2015.09.019.
102. Goldgeier MH, Klein LE, Klein-Angerer S, Moellmann G, Nordlund JJ. The distribution of melanocytes in the leptomeninges of the human brain. J Invest Dermatol. 1984;82(3):235–8. Available from: http://www.ncbi.nlm.nih.gov/pubmed/6699426
103. Meyer zum Gottesberge AM. Physiology and pathophysiology of inner ear melanin. Pigment Cell Res. 1988;1(4):238–49. Available from: http://www.ncbi.nlm.nih.gov/pubmed/3070525
104. Rancan F, Nazemi B, Rautenberg S, Ryll M, Hadam S, Gao Q, Hackbarth S, Haag SF, Graf C, Rühl E, Blume-Peytavi U, Lademann J, Vogt A, Meinke MC. Ultraviolet radiation and nanoparticle induced intracellular free radicals generation measured in human keratinocytes by electron paramagnetic resonance spectroscopy. Skin Res Technol. 2014;20(2):182–93. Available from: http://www.ncbi.nlm.nih.gov/pubmed/24033792
105. Ahlberg S, Meinke MC, Werner L, Epple M, Diendorf J, Blume-Peytavi U, Lademann J, Vogt A, Rancan F. Comparison of silver nanoparticles stored under air or argon with respect to the induction of intracellular free radicals and toxic effects toward keratinocytes. Eur J Pharm Biopharm. 2014;88(3):651–7. Available from:. https://doi.org/10.1016/j.ejpb.2014.07.012.
106. Haag SF, Taskoparan B, Darvin ME, Groth N, Lademann J, Sterry W, Meinke MC. Determination of the antioxidative capacity of the skin in vivo using resonance Raman and electron paramagnetic resonance spectroscopy. Exp Dermatol. 2011;20(6):483–7. Available from: https://www.ncbi.nlm.nih.gov/pubmed/21366704
107. Lauer A-C, Groth N, Haag SF, Darvin ME, Lademann J, Meinke MC. Radical scavenging capacity in human skin before and after vitamin C uptake: an in vivo feasibility study using electron paramagnetic resonance spectroscopy. J Invest Dermatol. 2013;133(4):1102–4. Available from: http://www.ncbi.nlm.nih.gov/pubmed/23190876
108. Megow I, Darvin ME, Meinke MC, Lademann J. A randomized controlled trial of green tea beverages on the in vivo radical scavenging activity in human skin. Skin Pharmacol Physiol. 2017;30:225–33. Available from: https://www.karger.com/?doi=10.1159/000477355
109. Meinke MC, Friedrich A, Tscherch K, Haag SF, Darvin ME, Vollert H, Groth N, Lademann J, Rohn S. Influence of dietary carotenoids on radical scavenging capacity of the skin and skin lipids. Eur J Pharm Biopharm. 2013;84(2):365–73. Available from:. https://doi.org/10.1016/j.ejpb.2012.11.012.
110. Piazena H, Pittermann W, Müller W, Jung K, Kelleher DK, Herrling T, Meffert P, Uebelhack R, Kietzmann M. Effects of water-filtered infrared-a and of heat on cell death, inflammation, antioxidative potential and of free radical formation in viable skin—first results. J Photochem Photobiol B Biol. 2014;138:347–54. Available from:. https://doi.org/10.1016/j.jphotobiol.2014.06.007.
111. Fuchs J, Groth N, Herrling T, Zimmer G. Electron paramagnetic resonance studies on nitroxide radical 2,2,5,5-tetramethyl-4-piperidin-1-oxyl (TEMPO) redox reactions in human skin. Free Radic Biol Med. 1997;22(6):967–76. Available from: http://www.ncbi.nlm.nih.gov/pubmed/9034235
112. Nardi G, Manet I, Monti S, Miranda MA, Lhiaubet-Vallet V. Scope and limitations of the TEMPO/EPR method for singlet oxygen detection: the misleading role of electron transfer. Free Radic Biol Med. 2014;77:64–70. Available from: https://www.ncbi.nlm.nih.gov/pubmed/25236741

113. Meinke MC, Müller R, Bechtel A, Haag SF, Darvin ME, Lohan SB, Ismaeel F, Lademann J. Evaluation of carotenoids and reactive oxygen species in human skin after UV irradiation: a critical comparison between in vivo and ex vivo investigations. Exp Dermatol. 2015;24(3):194–7. Available from: https://www.ncbi.nlm.nih.gov/pubmed/25431109
114. Darvin ME, Haag SF, Meinke MC, Sterry W, Lademann J. Determination of the influence of IR radiation on the antioxidative network of the human skin. J Biophotonics. 2011;4(1–2):21–9. Available from: https://www.ncbi.nlm.nih.gov/pubmed/24639418
115. Saeidpour S, Lohan SB, Anske M, Unbehauen M, Fleige E, Haag R, Meinke MC, Bittl R, Teutloff C. Localization of dexamethasone within dendritic core-multishell (CMS) nanoparticles and skin penetration properties studied by multi- frequency electron paramagnetic resonance (EPR) spectroscopy. Eur J Pharm Biopharm. 2017;116:94–101. Available from:. https://doi.org/10.1016/j.ejpb.2016.10.001.
116. Albrecht S, Ahlberg S, Beckers I, Kockott D, Lademann J, Paul V, Zastrow L, Meinke MC. Effects on detection of radical formation in skin due to solar irradiation measured by EPR spectroscopy. Methods. 2016;109:44–54. Available from:. https://doi.org/10.1016/j.ymeth.2016.06.005.
117. Haag SF, Fleige E, Chen M, Fahr A, Teutloff C, Bittl R, Lademann J, Schäfer-Korting M, Haag R, Meinke MC. Skin penetration enhancement of core-multishell nanotransporters and invasomes measured by electron paramagnetic resonance spectroscopy. Int J Pharm. 2011;416(1):223–8. Available from:. https://doi.org/10.1016/j.ijpharm.2011.06.044.
118. Fernández E, Fajarí L, Rodríguez G, Cócera M, Moner V, Barbosa-Barros L, Kamma-Lorger CS, de la Maza A, López O. Reducing the harmful effects of infrared radiation on the skin using Bicosomes incorporating β -carotene. Skin Pharmacol Physiol. 2016;29(4):169–77. Available from: https://www.ncbi.nlm.nih.gov/pubmed/27379378
119. Lange BA, Buettner GR. Electron paramagnetic resonance detection of free radicals in UV-irradiated human and mouse skin. Curr Probl Dermatol. 2001;29:18–25. Available from: https://www.ncbi.nlm.nih.gov/pubmed/11225198
120. Clément J-L, Ferré N, Siri D, Karoui H, Rockenbauer A, Tordo P. Assignment of the EPR Spectrum of 5,5-Dimethyl-1-pyrroline N-oxide (DMPO) superoxide spin adduct. J Org Chem. 2005;70(4):1198–203. Available from: http://pubs.acs.org/doi/abs/10.1021/jo048518z?journalCode=joceah
121. Mukherjee S, Yang L, Vincent C, Lei X, Ottaviani MF, Ananthapadmanabhan KP. A comparison between interactions of triglyceride oil and mineral oil with proteins and their ability to reduce cleanser surfactant-induced irritation. Int J Cosmet Sci. 2015;37(4):371–8. Available from: https://www.ncbi.nlm.nih.gov/pubmed/25656133
122. Nakagawa K, Minakawa S, Sawamura D. EPR spectroscopic investigation of psoriatic finger nails. Skin Res Technol. 2013;19(4):450–3. Available from: http://doi.wiley.com/10.1111/srt.12068
123. Nakagawa K, Minakawa S, Sawamura D, Hara H. Skin surface imaging of psoriasis vulgaris by using an electron paramagnetic resonance spin probe. J Dermatol Sci. 2016;81(1):71–3. Available from: https://www.ncbi.nlm.nih.gov/pubmed/26493103
124. Herrling T, Zastrow L, Fuchs J, Groth N. Electron spin resonance detection of UVA-induced free radicals. Skin Pharmacol Appl Ski Physiol. 2002;15(5):381–3. Available from: http://www.ncbi.nlm.nih.gov/pubmed/12239435
125. Bourji K, Meyer A, Chatelus E, Pincemail J, Pigatto E, Defraigne JO, Singh F, Charlier C, Geny B, Gottenberg JE, Punzi L, Cozzi F, Sibilia J. High reactive oxygen species in fibrotic and nonfibrotic skin of patients with diffuse cutaneous systemic sclerosis. Free Radic Biol Med. 2015;87:282–9. Available from: https://www.ncbi.nlm.nih.gov/pubmed/26143738
126. Takeshita K, Chi C, Hirata H, Ono M, Ozawa T. In vivo generation of free radicals in the skin of live mice under ultraviolet light, measured by L-band EPR spectroscopy. Free Radic Biol Med. 2006;40(5):876–85. Available from: https://www.ncbi.nlm.nih.gov/pubmed/16520239
127. Epel B, Sundramoorthy SV, Barth ED, Mailer C, Halpern HJ. Comparison of 250 MHz electron spin echo and continuous wave oxygen EPR imaging methods for *in vivo* applications. Med Phys. 2011;38(4):2045–52. Available from: http://doi.wiley.com/10.1118/1.3555297

128. Epel B, Bowman MK, Mailer C, Halpern HJ. Absolute oxygen R1e imaging in vivo with pulse electron paramagnetic resonance. Magn Reson Med. 2014;72(2):362–8. Available from: http://www.ncbi.nlm.nih.gov/pubmed/24006331
129. Li J, Wei K, Zuo S, Xu Y, Zha Z, Ke W, Chen K, Ge Z. Light-triggered clustered vesicles with self-supplied oxygen and tissue penetrability for photodynamic therapy against hypoxic tumor. Adv Funct Mater. 2017;27(33):E1702108. (1–13). Available from:. https://doi.org/10.1002/adfm.201702108.
130. Pavelescu LA. On reactive oxygen species measurement in living systems. J Med Life. 2015;8(Spec Issue):38–42. Available from: http://www.ncbi.nlm.nih.gov/pubmed/26361509
131. Kawai S, Matsumoto K-I, Utsumi H. An EPR method for estimating activity of antioxidants in mouse skin using an anthralin-derived radical model. Free Radic Res. 2010;44(3):267–74. Available from: https://www.ncbi.nlm.nih.gov/pubmed/20001648
132. Babizhayev MA, Deyev AI, Savel'yeva EL, Lankin VZ, Yegorov YE. Skin beautification with oral non-hydrolized versions of carnosine and carcinine: effective therapeutic management and cosmetic skincare solutions against oxidative glycation and free-radical production as a causal mechanism of diabetic complications and skin aging. J Dermatol Treat. 2012;23(5):345–84. Available from: http://www.ncbi.nlm.nih.gov/pubmed/21756141
133. Ogawa Y, Ueno M, Sekine-Suzuki E, Nakanishi I, Matsumoto K, Fujisaki S. Non-invasive measurement of melanin-derived radicals in living mouse tail using X-band EPR. J Clin Biochem Nutr. 2016;59(3):160–4. Available from: http://www.ncbi.nlm.nih.gov/pubmed/26060345
134. Sahle FF, Metz H, Wohlrab J, Neubert RHH. Lecithin-based microemulsions for targeted delivery of Ceramide AP into the stratum corneum: formulation, characterizations, and in vitro release and penetration studies. Pharm Res. 2013;30(2):538–51. Available from: https://www.ncbi.nlm.nih.gov/pubmed/23135817
135. Sahle FF, Metz H, Wohlrab J, RHH N. Polyglycerol fatty acid ester surfactant-based microemulsions for targeted delivery of ceramide AP into the stratum corneum: formulation, characterisation, in vitro release and penetration investigation. Eur J Pharm Biopharm. 2012;82(1):139–50. Available from: http://www.ncbi.nlm.nih.gov/pubmed/22691416
136. Dos Anjos JLV, de S Neto D, Alonso A. Effects of 1,8-cineole on the dynamics of lipids and proteins of stratum corneum. Int J Pharm. 2007;345(1–2):81–7. Available from: http://www.ncbi.nlm.nih.gov/pubmed/17600646
137. Lohan SB, Icken N, Teutloff C, Saeidpour S, Bittl R, Lademann J, Fleige E, Haag R, Haag SF, Meinke MC. Investigation of cutaneous penetration properties of stearic acid loaded to dendritic core-multishell (CMS) nanocarriers. Int J Pharm. 2016;501(1–2):271–7. Available from:. https://doi.org/10.1016/j.ijpharm.2016.02.004.
138. Alonso L, Mendanha SA, Marquezin CA, Berardi M, Ito AS, Acuña AU, Alonso A. Interaction of miltefosine with intercellular membranes of stratum corneum and biomimetic lipid vesicles. Int J Pharm. 2012;434(1–2):391–8. Available from: https://www.ncbi.nlm.nih.gov/pubmed/22692081
139. Yonar D, Horasan N, Paktaş DD, Abramović Z, Štrancar J, Sünnetçioğlu MM, Sentjurc M. Interaction of antidepressant drug, clomipramine, with model and biological stratum corneum membrane as studied by electron paramagnetic resonance. J Pharm Sci. 2013;102(10):3762–72. Available from: https://www.ncbi.nlm.nih.gov/pubmed/23925997
140. Krzykawska-Serda M, Miller RC, Elas M, Epel B, Barth ED, Maggio M, Halpern HJ. Correlation between hypoxia proteins and EPR-detected hypoxia in tumors. In: Halpern H, La Manna J, Harrison D, Epel B, editors. Oxygen transport to tissue XXXIX Adv Exp Med Biol, vol. 977; 2017. p. 319–25. Available from: http://link.springer.com/10.1007/978-3-319-55231-6_42.
141. Slominski A, Tobin DJ, Shibahara S, Wortsman J. Melanin pigmentation in mammalian skin and its hormonal regulation. Physiol Rev. 2004;84(4):1155–228. Available from: http://www.ncbi.nlm.nih.gov/pubmed/15383650
142. Billingham RE, Silvers WK. The melanocytes of mammals. Q Rev Biol. 1960;35(1):1–40. Available from: http://www.ncbi.nlm.nih.gov/pubmed/13800713

143. Commoner B, Townsend J, Pake GE. Free radicals in biological materials. Nature. 1954;174(4432):689. Available from: http://www.ncbi.nlm.nih.gov/pubmed/13213980
144. Sealy RC, Hyde JS, Felix CC, Menon IA, Prota G, Swartz HM, Persad S, Haberman HF. Novel free radicals in synthetic and natural pheomelanins: distinction between dopa melanins and cysteinyldopa melanins by ESR spectroscopy. Proc Natl Acad Sci U S A. 1982;79(9):2885–9. Available from: http://www.ncbi.nlm.nih.gov/pubmed/6283550
145. Meredith P, Sarna T. The physical and chemical properties of eumelanin. Pigment Cell Res. 2006;19(6):572–94. Available from: http://doi.wiley.com/10.1111/j.1600-0749.2006.00345.x
146. Sarna T, Plonka PM. Biophysical studies of melanin: paramagnetic, ion-exchange and redox properties of melanin pigments and their Photoreactivity. In: Eaton SR, Eaton GR, Berliner LJ, editors. Biomedical EPR, part A: free radicals, metals, medicine, and physiology. New York, Boston: Kluwer Academic Publishers; 2005. p. 125–46. Available from: http://link.springer.com/10.1007/0-387-26741-7_7.
147. Slominski A, Wortsman J, Plonka PM, Schallreuter KU, Paus R, Tobin DJ. Hair follicle pigmentation. J Invest Dermatol. 2005;124(1):13–21. Available from: http://www.ncbi.nlm.nih.gov/pubmed/15654948
148. Brożyna AA, Jóźwicki W, Carlson JA, Slominski AT. Melanogenesis affects overall and disease-free survival in patients with stage III and IV melanoma. Hum Pathol. 2013;44(10):2071–4. Available from: http://www.ncbi.nlm.nih.gov/pubmed/23791398
149. Slominski A, Plonka PM, Pisarchik A, Smart JL, Tolle V, Wortsman J, Low MJ. Preservation of eumelanin hair pigmentation in proopiomelanocortin-deficient mice on a nonagouti (a/a) genetic background. Endocrinology. 2005;146(3):1245–53. Available from: http://www.ncbi.nlm.nih.gov/pubmed/15564334
150. Mishra DR, Soni A, Rawat NS, Bokam G. Study of thermoluminescence (TL) and optically stimulated luminescence (OSL) from α-keratin protein found in human hairs and nails: potential use in radiation dosimetry. Radiat Environ Biophys. 2016;55(2):255–64. Available from: http://link.springer.com/10.1007/s00411-016-0634-9
151. Trompier F, Bassinet C, Wieser A, de Cinzia A, Viscomi D, Fattibene P. Radiation-induced signals analysed by EPR spectrometry applied to fortuitous dosimetry. Ann Ist Super Sanita. 2009;45(3):287–96. Available from: https://www.ncbi.nlm.nih.gov/pubmed/19861734
152. Tepe Çam S, Polat M, Seyhan N. The use of human hair as biodosimeter. Appl Radiat Isot. 2014;94:272–81. Available from: http://www.ncbi.nlm.nih.gov/pubmed/25255305
153. Feingold KR. The importance of lipids in cutaneous function. J Lipid Res. 2007;48(12):2529–30. Available from: http://www.jlr.org/content/48/12/2529.short
154. Hadgraft J. Skin, the final frontier. Int J Pharm. 2001;224(1–2):1–18. Available from: http://linkinghub.elsevier.com/retrieve/pii/S0378517301007311
155. Barry BW. Novel mechanisms and devices to enable successful transdermal drug delivery. Eur J Pharm Sci. 2001;14(2):101–14. Available from: http://www.ncbi.nlm.nih.gov/pubmed/11500256
156. Gill HS, Prausnitz MR. Coated microneedles for transdermal delivery. J Control Release. 2007;117(2):227–37. Available from: http://www.ncbi.nlm.nih.gov/pubmed/17169459
157. Mitragotri S. Modeling skin permeability to hydrophilic and hydrophobic solutes based on four permeation pathways. J Control Release. 2003;86(1):69–92. Available from: http://www.ncbi.nlm.nih.gov/pubmed/12490374
158. Gibaldi M, Feldman S. Pharmacokinetic basis for the influence of route of administration on the area under the plasma concentration-time curve. J Pharm Sci. 1969;58(12):1477–80. Available from: http://www.ncbi.nlm.nih.gov/pubmed/5353263
159. Xie Y, Xu B, Gao Y. Controlled transdermal delivery of model drug compounds by MEMS microneedle array. Nanomedicine. 2005;1(2):184–90. Available from: http://linkinghub.elsevier.com/retrieve/pii/S1549963405000547
160. Singh P, Roberts MS. Skin permeability and local tissue concentrations of nonsteroidal anti-inflammatory drugs after topical application. J Pharmacol Exp Ther. 1994;268(1):144–51. Available from: http://www.ncbi.nlm.nih.gov/pubmed/8301551

161. Venugopal J, Prabhakaran MP, Low S, Choon AT, Zhang YZ, Deepika G, Ramakrishna S. Nanotechnology for nanomedicine and delivery of drugs. Curr Pharm Des. 2008;14(22):2184–200. Available from: http://www.ncbi.nlm.nih.gov/pubmed/18781971
162. Nasir A. Nanotechnology and dermatology: part II–risks of nanotechnology. Clin Dermatol. 2010;28(5):581–8. Available from: http://linkinghub.elsevier.com/retrieve/pii/S0738081X09001394
163. Butoescu N, Jordan O, Burdet P, Stadelmann P, Petri-Fink A, Hofmann H, Doelker E. Dexamethasone-containing biodegradable superparamagnetic microparticles for intra-articular administration: physicochemical and magnetic properties, in vitro and in vivo drug release. Eur J Pharm Biopharm. 2009;72(3):529–38. Available from: http://linkinghub.elsevier.com/retrieve/pii/S0939641109001003
164. Rebecca VW, Sondak VK, Smalley KS. A brief history of melanoma: from mummies to mutations. Melanoma Res. 2012;22(2):114–22. Available from: https://www.ncbi.nlm.nih.gov/pubmed/22395415
165. Sarna M, Zadlo A, Hermanowicz P, Madeja Z, Burda K, Sarna T. Cell elasticity is an important indicator of the metastatic phenotype of melanoma cells. Exp Dermatol. 2014;23(11):813–8. Available from: http://www.ncbi.nlm.nih.gov/pubmed/25180917
166. Slominski RM, Zmijewski MA, Slominski AT. The role of melanin pigment in melanoma. Exp Dermatol. 2015;24(4):258–9. Available from: http://www.ncbi.nlm.nih.gov/pubmed/25496715
167. Wolnicka-Glubisz A, Strickland FM, Wielgus A, Anver M, Merlino G, De Fabo EC, Noonan FP. A melanin-independent interaction between Mc1r and met signaling pathways is required for HGFdependent melanoma. Int J Cancer. 2015;136(4):752–60. Available from:. https://doi.org/10.1002/ijc.29050.
168. Grabacka M, Wieczorek J, Michalczyk-Wetula D, Malinowski M, Wolan N, Wojcik K, Plonka PM. Peroxisome proliferator-activated receptor α (PPARα) contributes to control of melanogenesis in B16 F10 melanoma cells. Arch Dermatol Res. 2017;309(3):141–57. Available from:. https://doi.org/10.1007/s00403-016-1711-2.
169. Lund LP, Timmins GS. Melanoma, long wavelength ultraviolet and sunscreens: controversies and potential resolutions. Pharmacol Ther. 2007;114(2):198–207. Available from: http://www.ncbi.nlm.nih.gov/pubmed/17376535
170. Godechal Q, Gallez B. The contribution of electron paramagnetic resonance to melanoma research. J Skin Cancer. 2011;2011:E273280. (1-6). Available from: http://www.pubmedcentral.nih.gov/articlerender.fcgi?artid=3176523&tool=pmcentrez&rendertype=abstract
171. Godechal Q, Ghanem GE, Cook MG, Gallez B. Electron paramagnetic resonance spectrometry and imaging in melanomas: comparison between pigmented and nonpigmented human malignant melanomas. Mol Imaging. 2013;12(4):218–23. Available from: http://www.ncbi.nlm.nih.gov/pubmed/23651499
172. Okazaki M, Kuwata K, Miki Y, Shiga S, Shiga T. Electron spin relaxation of synthetic melanin and melanin-containing human tissues as studied by electron spin echo and electron spin resonance. Arch Biochem Biophys. 1985;242(1):197–205. Available from: http://www.ncbi.nlm.nih.gov/pubmed/2996430
173. Godechal Q, Mignion L, Karroum O, Magat J, Danhier P, Morandini R, Ghanem GE, Leveque P, Gallez B. Influence of paramagnetic melanin on the MRI contrast in melanoma: a combined high-field (11.7 T) MRI and EPR study. Contrast Media Mol Imaging. 2014;9(2):154–60. Available from:. https://doi.org/10.1002/cmmi.1554.
174. Cesareo E, Korkina L, D'Errico G, Vitiello G, Aguzzi MS, Passarelli F, Pedersen JZ, Facchiano A. An endogenous electron spin resonance (ESR) signal discriminates nevi from melanomas in human specimens: a step forward in its diagnostic application. PLoS One. 2012;7(11):e48849. Available from: https://www.ncbi.nlm.nih.gov/pubmed/23144997
175. Ito S, Jimbow K. Quantitative Analysis of Eumelanin and Pheomelanin in Hair and Melanomas. J Invest Dermatol. 1983;80(4):268–72. Available from: https://www.ncbi.nlm.nih.gov/pubmed/6833784

176. Łukiewicz SJ, Łukiewicz S. In vivo ESR spectroscopy of pigmented Tumors in mice. In: The XIIth international pigment cell conference. Giessen: University of Giessen Press; 1983. p. 133.
177. Berliner LJ, Fujii H, Wan XM, Łukiewicz SJ. Feasibility study of imaging a living murine tumor by electron paramagnetic resonance. Magn Reson Med. 1987;4(4):380–4. Available from: http://www.ncbi.nlm.nih.gov/pubmed/3035320
178. Vanea E, Charlier N, Dewever J, Dinguizli M, Feron O, Baurain JF, Gallez B. Molecular electron paramagnetic resonance imaging of melanin in melanomas: a proof-of-concept. NMR Biomed. 2008;21(3):296–300. Available from: http://www.ncbi.nlm.nih.gov/pubmed/18246539
179. Wolnicka-Glubisz A, Nogal K, Żądło A, Płonka PM. Curcumin does not switch melanin synthesis towards pheomelanin in B16F10 cells. Arch Dermatol Res. 2015;307(1):89–98. Available from: http://link.springer.com/10.1007/s00403-014-1523-1
180. Łukiewicz SJ, Pilas B. A new method of measuring oxygenation in pigmented Tumors growing in situ. In: III European workshop on melanin pigmentation. Prague, Czechoslovakia. Prague: Charles University; 1981. p. 65.
181. Romanowska-Dixon B, Elas M, Swakoń J, Sowa U, Ptaszkiewicz M, Szczygieł M, Krzykawska M, Olko P, Urbańska K. Metastasis inhibition after proton beam, β - and γ-irradiation of melanoma growing in the hamster eye. Acta Biochim Pol. 2013;60(3):307–11. Available from: http://www.ncbi.nlm.nih.gov/pubmed/23819130
182. Plonka PM, Michalczyk D, Popik M, Handjiski B, Slominski A, Paus R. Splenic eumelanin differs from hair eumelanin in C57BL/6 mice. Acta Biochim Pol. 2005;52(2):433–41. Available from: http://www.ncbi.nlm.nih.gov/pubmed/15990923
183. Michalczyk-Wetula D, Wieczorek J, Płonka PM. Splenic melanosis in agouti and black mice. Acta Biochim Pol. 2015;62(3):457–63. Available from: http://www.actabp.pl/#File?./html/3_2015/2015_1053.html
184. Michalczyk-Wetula D, Salwiński A, Popik MM, Jakubowska M, Płonka PM. Splenic melanosis during normal murine C57BL/6 hair cycle and after chemotherapy. Acta Biochim Pol. 2013;60(3):313–21. Available from: http://www.ncbi.nlm.nih.gov/pubmed/23828776
185. Weissman I. Genetic and histochemical studies on mouse spleen black spots. Nature. 1967;215(5098):315. Available from: http://www.ncbi.nlm.nih.gov/pubmed/6059528
186. Płonka PM. Hair pigmentation disorders or 50 years of German-polish alliance for study on a severe side effect of chemotherapy: Kostanecki's legacy. Exp Dermatol. 2015;24(1):10–1. Available from: http://www.ncbi.nlm.nih.gov/pubmed/25279945
187. Fernández E, Barba C, Alonso C, Martí M, Parra JL, Coderch L. Photodamage determination of human hair. J Photochem Photobiol B Biol. 2012;106(1):101–6. Available from: https://www.ncbi.nlm.nih.gov/pubmed/22119660
188. Saner MV, Kulkarni AD, Pardeshi CV. Insights into drug delivery across the nail plate barrier. J Drug Target. 2014;22(9):769–89. Available from: http://www.ncbi.nlm.nih.gov/pubmed/24964054
189. Laule C, Tahir S, Chia CLL, Vavasour IM, Kitson N, MacKay AL. A proton NMR study on the hydration of normal versus psoriatic stratum corneum: linking distinguishable reservoirs to anatomical structures. NMR Biomed. 2010;23(10):1181–90. Available from: http://www.ncbi.nlm.nih.gov/pubmed/20665901
190. Sobchak C, Eder L. Cardiometabolic disorders in psoriatic disease. Curr Rheumatol Rep. 2017;19(10):63. Available from: http://www.ncbi.nlm.nih.gov/pubmed/28844116
191. Pietrzak A, Bartosińska J, Chodorowska G, Szepietowski JC, Paluszkiewicz P, Schwartz RA. Cardiovascular aspects of psoriasis: an updated review. Int J Dermatol. 2013;52(2):153–62. Available from: http://www.ncbi.nlm.nih.gov/pubmed/23347301
192. Górnicki A, Gutsze A. Erythrocyte membrane fluidity changes in psoriasis: an EPR study. J Dermatol Sci. 2001;27(1):27–30. Available from: http://www.ncbi.nlm.nih.gov/pubmed/11457641
193. Górnicki A, Gutsze A. In vivo and in vitro influence of etretinate on erythrocyte membrane fluidity. Eur J Pharmacol. 2001;423(2–3):127–34. Available from: http://www.ncbi.nlm.nih.gov/pubmed/11448476

194. Górnicki A. Domain structure of erythrocyte membranes in psoriasis: an EPR study. J Dermatol Sci. 2002;29(3):214–21. Available from: http://www.ncbi.nlm.nih.gov/pubmed/12234712
195. Olczyk P, Ramos P, Bernas M, Komosinska-Vassev K, Stojko J, Pilawa B. Microwave saturation of complex EPR spectra and free radicals of burnt skin treated with Apitherapeutic agent. Evid Based Complement Alternat Med. 2013;2013:E545201. (1-9). Available from: http://www.ncbi.nlm.nih.gov/pubmed/23781263
196. Petukhov VI, Baumane LK, Reste ED, Zvagule TY, Romanova MA, Shushkevich NI, Sushkova LT, Skavronsky SV, Shchukov AN. Diagnosis of nitrosative stress by quantitative EPR-spectroscopy of epidermal cells. Bull Exp Biol Med. 2013;154(6):734–6. Available from: http://www.ncbi.nlm.nih.gov/pubmed/23658910
197. Liu KJ, Mäder K, Shi X, Swartz HM. Reduction of carcinogenic chromium(VI) on the skin of living rats. Magn Reson Med. 1997;38(4):524–6. Available from: http://doi.wiley.com/10.1002/mrm.1910380403
198. Tosta FV, Andrade LM, Mendes LP, Anjos JLV, Alonso A, Marreto RN, Lima EM, Taveira SF. Paclitaxel-loaded lipid nanoparticles for topical application: the influence of oil content on lipid dynamic behavior, stability, and drug skin penetration. J Nanopart Res. 2014;16(12):2782. Available from:. https://doi.org/10.1007/s11051-014-2782-7.
199. Barua S, Mitragotri S. Challenges associated with penetration of nanoparticles across cell and tissue barriers: a review of current status and future prospects. Nano Today. 2014;9(2):223–43. Available from: http://linkinghub.elsevier.com/retrieve/pii/S174801321400053X
200. Fujimoto T, Ito S, Ito M, Kanazawa H, Yamaguchi S. Induction of different reactive oxygen species in the skin during various laser therapies and their inhibition by fullerene. Lasers Surg Med. 2012;44(8):685–94. Available from: http://doi.wiley.com/10.1002/lsm.22065
201. Haag SF, Chen M, Peters D, Keck CM, Taskoparan B, Fahr A, Teutloff C, Bittl R, Lademann J, Schäfer-Korting M, Meinke MC. Nanostructured lipid carriers as nitroxide depot system measured by electron paramagnetic resonance spectroscopy. Int J Pharm. 2011;421(2):364–9. Available from:. https://doi.org/10.1016/j.ijpharm.2011.10.009.
202. Carlotti ME, Ugazio E, Sapino S, Fenoglio I, Greco G, Fubini B. Role of particle coating in controlling skin damage photoinduced by titania nanoparticles. Free Radic Res. 2009;43(3):312–22. Available from: http://www.tandfonline.com/doi/full/10.1080/10715760802716633
203. Yeom S, Shin BS, Han S. An electron spin resonance study of non-ionic surfactant vesicles (niosomes). Chem Phys Lipids. 2014;181:83–9. Available from: http://linkinghub.elsevier.com/retrieve/pii/S0009308414000425
204. Konkin A, Ritter U, Scharff P, Mamin G, Aganov A, Orlinskii S, Krinichnyi V, Egbed DAM, Ecke G, Romanusa H. Multifrequency X,W-band ESR study on photo-induced ion radical formation in solid films of mono- and di-fullerenes embedded in conjugated polymers. Carbon. 2014;77:11–7. Available from: http://linkinghub.elsevier.com/retrieve/pii/S0008622314003947
205. Olczyk P, Komosinska-Vassev K, Ramos P, Mencner Ł, Olczyk K, Pilawa B. Application of numerical analysis of the shape of electron paramagnetic resonance spectra for determination of the number of different groups of radicals in the burn wounds. Oxidative Med Cell Longev. 2017;2017:1–8. Article ID 4683102 Available from: https://www.hindawi.com/journals/omcl/2017/4683102/
206. Makarova K, Zawada K, Wagner D, Skowyra J. Optimization of antioxidant properties of creams with berry extracts by artificial neural networks. Acta Phys Pol A. 2017;132(1):44–51. Available from: http://przyrbwn.icm.edu.pl/APP/PDF/132/app132z1p09.pdf
207. Lohan SB, Saeidpour S, Solik A, Schanzer S, Richter H, Dong P, Darvin ME, Bodmeier R, Patzelt A, Zoubari G, Unbehauen M, Haag R, Lademann J, Teutloff C, Bittl R, Meinke MC. Investigation of the cutaneous penetration behavior of dexamethasone loaded to nanosized lipid particles by EPR spectroscopy, and confocal Raman and laser scanning microscopy. Eur J Pharm Biopharm. 2017;116:102–10. Available from: http://linkinghub.elsevier.com/retrieve/pii/S0939641116310220
208. Pawlikowska-Pawlęga B, Misiak LE, Zarzyka B, Paduch R, Gawron A, Gruszecki WI. FTIR, 1H NMR and EPR spectroscopy studies on the interaction of flavone apigenin with dipalmi-

toylphosphatidylcholine liposomes. Biochim Biophys Acta. 2013;1828(2):518–27. Available from: http://linkinghub.elsevier.com/retrieve/pii/S0005273612003628
209. Danhier P, Gallez B. Electron paramagnetic resonance: a powerful tool to support magnetic resonance imaging research. Contrast Media Mol Imaging. 2015;10(4):266–81. Available from: http://doi.wiley.com/10.1002/cmmi.1630
210. Hochkirch U, Herrmann W, Stößer R, Linscheid M, Borchert H-H. Distribution profiles of nitroxide spin probes in human skin—a combined study using spatially resolved electron spin resonance spectroscopy and mass spectrometry. Anal Bioanal Chem. 2011;401(3):901–7. Available from: http://link.springer.com/10.1007/s00216-011-5150-9
211. Dragicevic-Curic N, Friedrich M, Petersen S, Scheglmann D, Douroumis D, Plass W, Fahr A. Assessment of fluidity of different invasomes by electron spin resonance and differential scanning calorimetry. Int J Pharm. 2011;412(1–2):85–94. Available from: http://www.ncbi.nlm.nih.gov/pubmed/21527323
212. Sidabras JW, Varanasi SK, Mett RR, Swarts SG, Swartz HM, Hyde JS. A microwave resonator for limiting depth sensitivity for electron paramagnetic resonance spectroscopy of surfaces. Rev Sci Instrum. 2014;85(10):104707. Available from: http://aip.scitation.org/doi/10.1063/1.4898179
213. Petryakov S, Samouilov A, Chzhan-Roytenberg M, Kesselring E, Sun Z, Zweier JL. Segmented surface coil resonator for in vivo EPR applications at 1.1 GHz. J Magn Reson. 2009;198(1):8–14. Available from: http://linkinghub.elsevier.com/retrieve/pii/S1090780708004205
214. Wolfson H, Ahmad R, Twig Y, Kuppusamy P, Blank A. A miniature electron spin resonance probehead for transcutaneous oxygen monitoring. Appl Magn Reson. 2014;45(10):955–67. Available from:. https://doi.org/10.1007/s00723-014-0593-8.
215. Nakagawa K, Ohba Y, Epel B, Hirata H. A 9 GHz EPR imager for thin materials: application to surface detection. J Oleo Sci. 2012;61(8):451–6. Available from: http://jlc.jst.go.jp/DN/JST.JSTAGE/jos/61.451?lang=en&from=CrossRef&type=abstract
216. Enomoto A, Hirata H. Parallel image-acquisition in continuous-wave electron paramagnetic resonance imaging with a surface coil array: proof-of-concept experiments. J Magn Reson. 2014;239:29–33. Available from: http://linkinghub.elsevier.com/retrieve/pii/S1090780713003133
217. Asada R, Kageyama K, Tanaka H, Matsui H, Kimura M, Saitoh Y, Miwa N. Antitumor effects of nano-bubble hydrogen-dissolved water are enhanced by coexistent platinum colloid and the combined hyperthermia with apoptosis-like cell death. Oncol Rep. 2010;24(6):1463–70. Available from: http://www.spandidos-publications.com/or/24/6/1463
218. Tada K, Maeda M, Nishiuchi Y, Nagahara J, Hata T, Zhuowei Z, Yoshida Y, Watanabe M, Ohmori M. ESR measurement of hydroxyl radicals in micro-nanobubble water. Chem Lett. 2014;43(12):1907–8. Available from: http://www.journal.csj.jp/doi/10.1246/cl.140691
219. Orel VB, Zabolotny MA, Orel VE. Heterogeneity of hypoxia in solid tumours and mechanochemical reactions with oxygen nanobubbles. Med Hypotheses. 2017;102:82–6. Available from: http://linkinghub.elsevier.com/retrieve/pii/S0306987716305758
220. Drzał A, Delalande A, Pichon C, Elas M. Oxygen release by ultrasound sensitive O_2 microbubbles in solution and in vivo: temporal study. In: International Conference on Electron Paramagnetic Resonance Spectroscopy and Imaging of Biological Systems (EPR-2017), Morgantown, Virginia; July 16–22 2017. p. 56.
221. Demidenko E, Williams BB, Sucheta A, Dong R, Swartz HM. Radiation dose reconstruction from L-band in vivo EPR spectroscopy of intact teeth: comparison of methods. Radiat Meas. 2007;42(6–7):1089–98. Available from: https://www.ncbi.nlm.nih.gov/pubmed/18591987
222. Fuchs J, Groth N, Herrling T, Packer L. In vivo Electron spin resonance imaging of skin. Methods Enzymol. 1994;233:140–9. Available from: https://www.ncbi.nlm.nih.gov/pubmed/8015452
223. Napolitano A, Panzella L, Monfrecola G, D'Ischia M. Pheomelanin-induced oxidative stress: bright and dark chemistry bridging red hair phenotype and melanoma. Pigment

Cell Melanoma Res. 2014;27(5):721–33. Available from: http://doi.wiley.com/10.1111/pcmr.12262
224. Brożyna AA, Van Middlesworth L, Slominski AT. Inhibition of melanogenesis as a radiation sensitizer for melanoma therapy. Int J Cancer. 2008;123(6):1448–56. Available from: http://www.ncbi.nlm.nih.gov/pubmed/18567001
225. Maresca V, Flori E, Picardo M. Skin phototype: a new perspective. Pigment Cell Melanoma Res. 2015;28(4):378–89. Available from: http://www.ncbi.nlm.nih.gov/pubmed/25786343
226. d'Ischia M, Wakamatsu K, Napolitano A, Briganti S, Garcia-Borron JC, Kovacs D, Meredith P, Pezzella A, Picardo M, Sarna T, Simon JD, Ito S. Melanins and melanogenesis: methods, standards, protocols. Pigment Cell Melanoma Res. 2013;26(5):616–33. Available from:. https://doi.org/10.1111/pcmr.12121.
227. Sealy RC, Hyde JS, Felix CC, Menon IA, Prota G. Eumelanins and pheomelanins: characterization by electron spin resonance spectroscopy. Science. 1982;217(4559):545–7. Available from: http://www.ncbi.nlm.nih.gov/pubmed/6283638
228. Vsevolodov EB, Ito S, Wakamatsu K, Kuchina II, Latypov IF. Comparative analysis of hair melanins by chemical and electron spin resonance methods. Pigment Cell Res. 1991;4(1):30–4. Available from: http://www.ncbi.nlm.nih.gov/pubmed/1656423
229. Gordy W, Ard WB, Shields H. Microwave spectroscopy of biological substances. I. Paramagnetic resonance in X-irradiated amino acids and proteins. Proc Natl Acad Sci U S A. 1955;41(11):983–96. Available from: http://www.pnas.org/cgi/doi/10.1073/pnas.41.11.983
230. Harriman JE. Theoretical foundations of electron spin resonance: physical chemistry: a series of monographs. New York-San Francisco-London: Academic Press; 1978. p. 1–399. Available from: https://books.google.pl/books?id=Q7M3BQAAQBAJ&pg=PR3&lpg=PR3&dq=John+E.+Harriman.+Theoretical+Foundations+of+Electron+Spin+Resonance:+Physical+Chemistry:+A+Series+of+Monographs.+Academic+Press,+New+York-San+Francisco-London+1978&source=bl&ots=hc21itaBa7&s
231. Herrling T, Jung K. The radical status factor (RSF): a novel metric to characterize skin products. Int J Cosmet Sci. 2012;34(4):285–90. Available from: https://www.ncbi.nlm.nih.gov/pubmed/22563768
232. Brożyna AA, Jóźwicki W, Roszkowski K, Filipiak J, Slominski AT. Melanin content in melanoma metastases affects the outcome of radiotherapy. Oncotarget. 2016;7(14):17844–53. Available from: http://www.ncbi.nlm.nih.gov/pubmed/26910282

Paramagnetomics

9

Przemysław M. Płonka

9.1 Introduction: The Position of EPR Spectroscopy in Life Sciences

EPR (ESR) spectroscopy is a refined research method deeply rooted in physics, while its field of application in biology and biomedical research is wide. For the purpose of the present chapter, I prefer the name "electron paramagnetic resonance" (EPR) [1], although presently both are equivalently recommended by the International EPR (ESR) Society. So far, EPR spectroscopy and imaging have been traditionally attributed to physics and physicists. Its theory and practice are traditionally considered as a branch of physics, quantum physics, solid-state physics, etc. The position of an EPR spectroscopist in the so-called "life science domain" is exotic, and the spectroscopist himself/herself is considered by biologists as a stranger or alien. In this chapter, I would like to convince the readers that there is a clearly defined place of the EPR spectroscopy in biology and the subject of its interest is a part of life sciences, which can also find its reflex in medicine. This is because of the particular status of the species containing unpaired electron and the processes which they determine, processes crucial for the phenomenon of life. I postulate, in the age of systems biology, in the age of establishing new branches of biology crosswise the traditional genetics, biochemistry etc., to establish a new "-omics" and to determine its position among other "-omics".

P. M. Płonka
Department of Biophysics, Faculty of Biochemistry, Biophysics and Biotechnology, Jagiellonian University, Kraków, Poland
e-mail: przemyslaw.plonka@uj.edu.pl

A. K. Shukla (ed.), *Electron Spin Resonance Spectroscopy in Medicine*,
https://doi.org/10.1007/978-981-13-2230-3_9

9.2 Definition of Life is Biophysical

The phenomenon of life belongs to the most mysterious in the Universe, and its emergence and maintenance are as extraordinary and unbelievable as the beginning and maintenance of the Universe itself. Biologists are concentrated on analysis and description of life, which in the long run should lead to its better or maybe total understanding. However, paradoxically, to be a good biologist, a good specialist in one's own discipline—biology—one does not need to precisely define the phenomenon of life. Similarly, to be a good physician, one does not need to precisely define the human. Biology deals with sophisticated and enormously developed systems, and a biologist has to devote tens of years to understand its own field, e.g. taxonomy of beetles or regulation of cell division. The life *in toto* should be defined looking from a different level [2].

Consequently, there is no satisfactory definition of life; all the existing definitions are rather descriptions including the main features of life and, even more frequently, living systems [2]. The discipline of biological sciences which is probably closest to defining life is the biophysics. And this is because a biophysicist must possess a tool or a criterion to tell the difference between life and other processes ongoing in the Universe. Therefore, the biophysicist considers the life as one of many other physical processes and phenomena. A living system is similar to other systems in the sense of being built of the same matter and being based of the same physical processes and principles. So, the biophysicist must be able to recognize living systems among other systems of the Universe. As a consequence, the best definitions of life used by many mainstream biologists are the "biophysical" ones, no matter what the original field of their biological interest is, and many of them include the notion of the electron or derivatives (e.g. oxidation or reduction meaning subtraction or addition of the electron, etc.) to their definition of life.

While defining biophysics (or defining life) is not the exact aim of this chapter, one should possess a well-defined starting point, which in this case is a certain definition of life. It is not, however, taken from any handbook on biophysics but on ecology: *"Life and Evolution of Biosphere*" by a Polish ecologist Professor January Weiner from Jagiellonian University in Kraków [3]. He writes that "*Life is an endoenergetic physicochemical process being a cyclic oxidation and reduction of carbon compounds, executed by autocatalytic, self-reproducing macromolecules ("organisms"). The process is continuous, and the biosphere remains in the state far from thermodynamic equilibrium, for the replication of macromolecules progresses with errors, so the composition of macromolecules changes permanently and randomly*" ([3], the citation translated by PMP). The biophysical ("thermodynamic") character of this definition is self-evident, but so as not to be accused of bias, let me support this definition with the definition by John Desmond Bernal: "Life is a partial, continuous, progressive multiform and conditionally interactive self-realization of the potentialities of atomic electron states…" [4]. The relation to electron phenomena seems indispensable in defining or characterizing in general terms the phenomenon of life.

The Weiner's definition [3] reveals a symptomatic dichotomy. It consists of two overlapping parts, as if representing two general aspects of life: thermodynamics and energy flow versus genetic information and information flow. The first part

reads: “Life is an endoenergetic physicochemical process being a cyclic oxidation and reduction of carbon compounds, executed by autocatalytic, self-reproducing macromolecules (“organisms”). “The process is continuous, and the biosphere remains in the state far from thermodynamic equilibrium (…),” and the second part: “(…) The process is continuous, and the biosphere remains in the state far from thermodynamic equilibrium, for the replication of macromolecules progresses with errors, so the composition of macromolecules changes permanently and randomly.”

The common, mainstream biology based its development (in particular in the second half of the twentieth century) on the development of the information-related aspects of the definition, focusing on various modes of encryption, expression and metabolic implementation of genetic information, which I am going to start with, too. The first, bioenergetic part, perhaps neglected a little, underinvested, let us transiently neglect, too. I would analyse it later, considering some conclusions from the first task.

9.3 The Information-Related Part of the Definition of Life: A Modern Approach Originating from Mendel’s Genetics

Gregor Mendel (1822–1884) might be considered as the precursor of not only genetics but also modern biophysics. Following the detailed description of modern biophysics given by a Czech biophysicist, Professor Vaclav Prosser [2], one can find many determinants of common biophysics in the Mendel’s works [5]. Mendel performed one of the first *par excellence* biophysical experiments, in which he used the methodology of physics. Starting from multiannual observations of cultivars (which was the methodology typical of the early nineteenth-century biology), he put a hypothesis which resulted from a causal question—why is there a heredity in the alive world, despite the existence of variability? The hypothesis was that there must exist some material, discrete, elementary, eternal carriers of characters, the recombination of which results in phenotypic polymorphism. Next, Mendel predicted (i.e. calculated mathematically) the ratio of segregation in F1, F2, etc. and then intentionally selected the material for further experiments (his famous peas) in such a way that if the segregation followed the calculations, the alternate hypothesis would prove false, i.e. the only way to accept the actual and factual results would be to accept the above-mentioned hypothesis. His work was appreciated only almost 50 years after its announcement, which was soon followed by discoveries of other genetic phenomena and creation of new notions as the gene, the mutation, the crossing over, etc. Shortly, it had ended up with realizing that what really matters in living systems, what “makes” them alive, was an abstract which possesses a material carrier (form), namely, information encrypted in DNA, called today the genetic information. The essence of life was then believed to be possible to be reduced down to the sequence of nucleotides in DNA, which would be expressed (transformed) into the sequence of amino acids in a polypeptide [6], each of whom representing and performing a strictly determined function in the metabolism (the “one gene-one peptide” or “one gene-one enzyme” hypothesis [6]). A complete analysis

of organisms seemed then to be reduced to the analysis of genetic texts—genomes. Today this analysis serves in some branches of bioinformatics to compare various genetic texts (or rather their representations as streams of characters) and concludes about their relations [7].

Unfortunately, among all the chemical reactions being the base of the mechanisms of the expression and replication of genomes and genetic information, there are no redox reactions but only the reactions of estrification, hydrolysis and condensation, in which ATP is utilized, but no oxidation state changes (i.e. no electron is transferred between a donor and its acceptor).

In 1962 took place an interesting discovery which may be a good example that the phenomenon of life cannot be boiled down to the simple linear sequence of deoxyribonucleotides in DNA. It was the discovery of the "*nude*" mutation in mice [8]. The wild-type *Foxn1* gene encodes the FOXN1 protein which is a transcription factor [9]. Actually, this protein performs many functions in the sense of variable phenotypic manifestations of the mutation [9, 10]. Many genes different than *Foxn1*, e.g. those encoding keratins [9], undergo expression depending on the expression of gene *Foxn1*. If the content of the latter does not undergo proper expression, no keratin can be produced by the cell despite possessing proper genes encoding keratins. Consequently, the portion of genetic information (or better—"meta-information") concerning expression of keratins must be somehow encrypted in *locus nude* as well. The simple view that one gene encrypts one protein, and therefore one phenotypic function, cannot be maintained any more. This conclusion can be further supported by multiple experiments and observations, including the theory of operon [11], etc., which finally lead to the conclusion that the "structure" of genetic information is multidimensional and that there is a "meta-information", "meta-meta-information", etc. Actually it is closely supported by the theory of natural language [12] which presumes that a natural language is its own metalanguage [13]. Anyway, it lets one to conclude that there is something at least as important as genetic information itself, which makes a system alive, and this is the interaction (interactions) between particular parts of genetic information and between particular constituents of genomes. This is the base to treat the living system in general as a dynamic system of various interactions and flows, which is more than a static though very complicated structure [14]. Following the classical and molecular genetics which mainly describe genes localized in *loci*, collected into genomes and transferred between (or among) generations, there occurred genomics or functional genomics focused on the action of genomes—systems of genes or systems of genes and their expression, characteristic for particular cells, organs and organisms or developmental stages of them [7, 15]. In particular, focused on what genes at all are present in the genetic material, what sequences code proteins, which ones are regulatory, and what are other functions? What genes remain under control of other genes? What signal pathways are turned on or off, when and where (in what cells)? The expression of genetic information may be further analysed also on the level of RNA (transcriptomics and transcriptome [16]) and proteins (proteomes and proteomics [17]), which are often considered as integral parts of functional genomics, or its phenotypic implementation (*see* also Table 9.1).

Table 9.1 Definitions of the basic "-omes" and "-omics" studying the phenomenon of life in general

"omics"	"-ome"	Object of investigations	Remarks
Genomics [15]	Genome [18]	Full genetic material. In a narrow sense: "full set of genes[a] of a biological system[b], their interactions and interdependence" (functional genomics [19, 20])	[a]However, a precise definition of gene is necessary [b]Here and below—"biological system" means an organellum, cell, tissue, organ, organism or biome
Transcriptomics [16][a]	Transcriptome [16, 21]	Full set of RNAs being transcribed in a biological system[b]	[a]Understood as extension of genomic methods for mRNA analysis [b]Initially "full set of mRNA particles"
Proteomics [17]	Proteome [22]	The supplementation of the genome and the transcriptome, i.e. the full set of proteins undergoing transcription and translation in a given biological system	
Metagenomics [23][a]	Metagenome [24][b]	A set of genomes characteristic of a given biome or microbiome	[a]Perversely, this study was devoted to rRNA sequences (or their genes. Cited after [25] as the first example of metagenomic approach)—so better "metatranscriptomics" [b]An inconvenient term, as apparently related to genetic "metainformation" which is something different than "information contained in a metagenome". See the text
Lipidomics [26]	[a]Lipidome [26]	Full set of lipids characteristic of a given biological system (usually a cellular lipidome)	[a]A subset of the metabolome
Glycomics [27]	[a]Glycome [28]	Full set of carbohydrates, sugar residues or their modifications (full set of glycans) typical of a given biological system	[a]A subset of the metabolome

(continued)

Table 9.1 (continued)

"omics"	"-ome"	Object of investigations	Remarks
Metallomics [29, 30]	Metallome [29]	Metals and metalloids, their compounds, ions and complexes present in a biological system	
Metabolomics [31]	Metabolome [32]	The full set of metabolites resulting from the expression of a given genome (the "metabolic profile") attributed to a given biological system	
Interactomics [33]	Interactome [34]	The full set of molecular interactions[a] characteristic of a given biological system	[a]Understood as physical interactions—complexing, associations, agglomerations, aggregations, attachments, etc.
Paramagnetomics[a]	Paramagnetome[a]	A full set of permanent or transient, endo- or exogenous paramagnetic centres detectable in (or derived from) a given biological system by EPR spectroscopy	[a]This issue

The fact that the information-related part of the definition of life [3] is not enough to satisfactorily describe the whole phenomenon is a manifestation of two other important facts. The first one is the lack of a satisfactory definition of information [35, 36] and—consequently—of genetic information [36, 37]. For the purpose of this chapter, it can be described as the biologically relevant information encrypted in the form of a nucleotide sequence in a nucleic acid [37]. But the problem persists and may often be observed as, for example, erroneous identification of the information with its encryption and with its material carrier, erroneous identification of genetic information with the sequence of nucleotides and with DNA or erroneously calling mutations "changes in the genetic code". While we are still not able to precisely define information, we can provide some important features of this phenomenon. Information is something dealing with or influencing on the following: (1) dynamic process of exchange (flow) of energy between systems; (2) the resulting change of the (thermodynamic) state of a system; (3) the system itself (e.g. the living system) being non-equilibrial and non-linear; (4) improbability, uncertainty and entropy; (5) something which chooses a particular state from the repertoire of the putative states of the system; and (6) the system's possession of the memory of states [14, 35–40].

The second fact is that despite such an intricacy in defining genetic information, many of the functions or characters of the organisms are *not* encrypted directly in the genetic information [36, 37].

9.4 "Omics"

Bob Kuska described the moment of invention of the word "genomics" as "an activity, a new way of thinking about biology" [15]. And indeed, realizing that there is no satisfactory definition of genetic information and that not everything is encrypted in the genetic information inevitably leads to the necessity to describe biological phenomena not analytically, but synthetically, as numerous phenomena acting in a context and acting on each other in the form of extremely complicated nets. In the names of the systems of such nets, the suffix "-ome" appears, *per analogiam* to "the genome"—the first "-ome" consciously analysed as the system of items. Similarly, the names of new, respective branches of biological sciences end up with the suffix "-omics" (*per analogiam* to "genomics") [41].

The set of selected "-omics" and "-omes" described in the literature is collected in Table 9.1. Establishing them is a result of the necessity of a systemic thinking in biology, which is the final result of the developmental tendency initiated by Gregor Mendel.

The fascination with genetics directed some biologists to the presumption that everything which means "alive" is encrypted in DNA [37], so that deciphering DNA would equal a complete understanding of the phenomenon of life (thus the ultimate possibility of defining it) and reducing it to a purely chemical or physical phenomenon [42, 43]. Meanwhile, based on the purely physical rules and principles, the phenomenon of life *in toto* does not simply result from the sequence of nucleotides, physical or chemical properties of DNA [36]. This conflict was manifested as early as in the 1950s by several famous scientists, including a great American biophysicist and biologist, Barry Commoner, representing the fraction of "systems biologists' (speaking in the nowadays language), and Isaac Asimov representing the "DNA-centric" fraction [42, 43]. This hot discussion is important for the present chapter also because Barry Commoner was the scientist who (in parallel to Lev Alexadrovich Blumenfeld in Europe [44]) actually introduced EPR to the biological and biomedical sciences [45, 46]. And it inevitably leads us to focus on the first "electron" or "thermodynamic" part of the Weiner's definition of life [3].

9.5 "*Materia Electronica*"

The discovery of the electron, the theoretical prediction and further experimental confirmation of the electron spin and the idea of the dual, corpuscular-wave character of the electron not only established chemistry in its present foundations, and changed the way of thinking in physics [47, 48], but also strongly influenced the development of modern biochemistry and bioenergetics. Nowadays we think about the process of life in general, as a series of redox reactions in which the energy is conveyed in a form of the electron (or its lack) [3, 4, 46]. The intermediates which are produced by this way reveal paramagnetic properties, as being free radicals, or transient metal ions [49]. There are also stable paramagnetic products of the metabolism—dioxygen [49], nitric oxide [50] and melanin [45].

The importance of the particles with unpaired electrons for the phenomenon of life was probably appreciated for the first time by Leonor Michaelis who observed that obligatory intermediates in the metabolic pathways related to the transfer of the electron, being therefore mainly the single-electron-transfer reactions, must be of a free radical character [49, 51–53]. This assumption must have prompted Barry Commoner to put biological materials into the EPR resonant cavity and to register first EPR free radical signals of biological samples. He and his co-authors—Jonathan Townsend and George C. Pake—wrote in 1954: "In the light of the suggestion of Michaelis and others that free radicals occur as intermediates in biological electron-transfer processes, it is of considerable interest to investigate the association between free radical content and metabolic activity" ([45], p. 690). When reading this paper nowadays, it appears striking up to date and sharpens the view of the engagement of unpaired electrons in the metabolic processes, in particular in two principle processes of life intensively studied at present with EPR: photosynthesis [54, 55] and oxygen respiration [56–60]. This is exactly what Barry Commoner wrote about when analysing his EPR spectra. Paradoxically, Isaac Asimov preparing his Ph.D. thesis worked on similar processes of catechol oxidation [61]. Biology investigates, therefore, the flow of electrons through the living system and the flow driven by external sources of energy (the Sun), resulting from its strong non-equilibrial (non-linear) character [3]. So, the first part of the definition of life—the thermodynamic one—is boiled down to the functioning of "*materia electronica*" (Fig. 9.1).

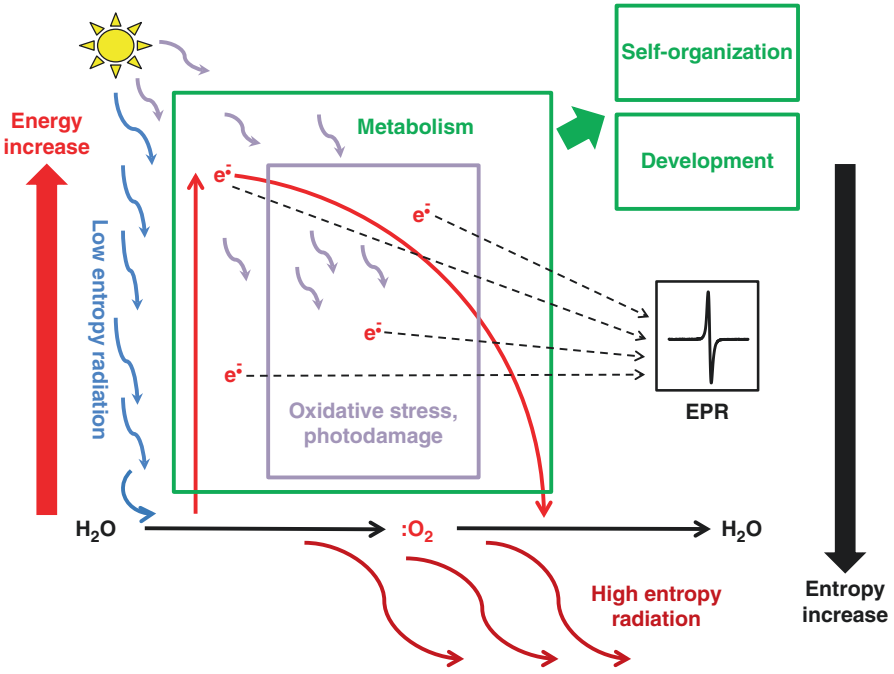

Fig. 9.1 "*Materia electronica*"—a simplified view of the phenomenon of life according to [3] and [62] and on the position and role of EPR and paramagnetomics in investigating the living systems. *See* also [63]

9.6 The Notion of the Paramagnetic Centre

In EPR spectroscopy, instead of using the term "free radical", it is more convenient and instructive to use terms reflecting the macroscopic feature being the essence of this method—the paramagnetism, namely, the paramagnetic centre. The paramagnetic centre may be a part of a bigger molecule or macromolecule, or of a system of small molecules bound by physical interactions, like biological membranes. It can be defined as a particle, atom, ion, molecule or a part of it, which contains in its atomic or molecular orbital an electron with uncompensated (unpaired) spin. This term is widely used in the EPR spectroscopy, and it originates probably from the early 1960s or late 1950s. Commoner did not use it in 1954 [45], but that was probably one of the earliest papers on biologically oriented EPR, when the characteristic nomenclature of biologically oriented EPR had not been established yet. The earliest usage of this term in the title of a paper, according to "Web of Science™", comes from a paper by Professor Machbuba Kayumovna Pulatova published in1963 [64, 65]. It was transferred to biologically oriented EPR from solid-state physics and crystallography, probably from the nomenclature of radiation-induced defects in inorganic crystals. One says, for example, on "the F-centres". The F-type centre is an unpaired electron which replaces the anionic vacancy in a crystal of metallic oxide. Such an electron can absorb electromagnetic radiation from the visible band, which results in colouration of the crystal (F-centre comes from the German "Farbzentrum"—a "colour centre") and at the same time responds for the paramagnetic properties of the crystal [66]. The paramagnetic centre in biological systems must have initially concerned "the part of a protein or nucleic acid molecule which possesses an unpaired electron due to interactions of the system with ionizing radiation" and was used in opposition to "free radicals" being a result of biochemical reactions or radio- or photolysis of water, but gradually it has gained today's meaning.

Such unpaired-electron-containing free radical intermediates cannot be attributed to a single particular cellular compartment out of the various compartments of the cell; however, they can be easily detected by means of EPR and, moreover, detected *in situ*, i.e. with no necessity to be subjected to other biological methods of fractionation or separation followed by any specific or non-specific staining or "blotting" and staining. Instead, the specific "staining" called the spin trapping and the spin labelling can be used. In a similar way, the spatial distribution of paramagnetic centres in a living biological system can be obtained by means of EPR imaging [67, 68]. This creates a specific, unique "picture" of the biological system, in which paramagnetic centres, and only they, can be characterized qualitatively, quantitatively and mapped spatially. The dynamics of changes in this "picture" following transformation (annihilation or creation) of paramagnetic centres can be even registered in a kinetic aspect in serial EPR measurements in various timescales.

9.7 The Notion of the Paramagnetome

Here it is proposed to encompass, by the notion of "the paramagnetome", all the paramagnetic centres which appear in the living cell (however, with the possibility to escape to the environment) and which can be detected directly or indirectly with EPR

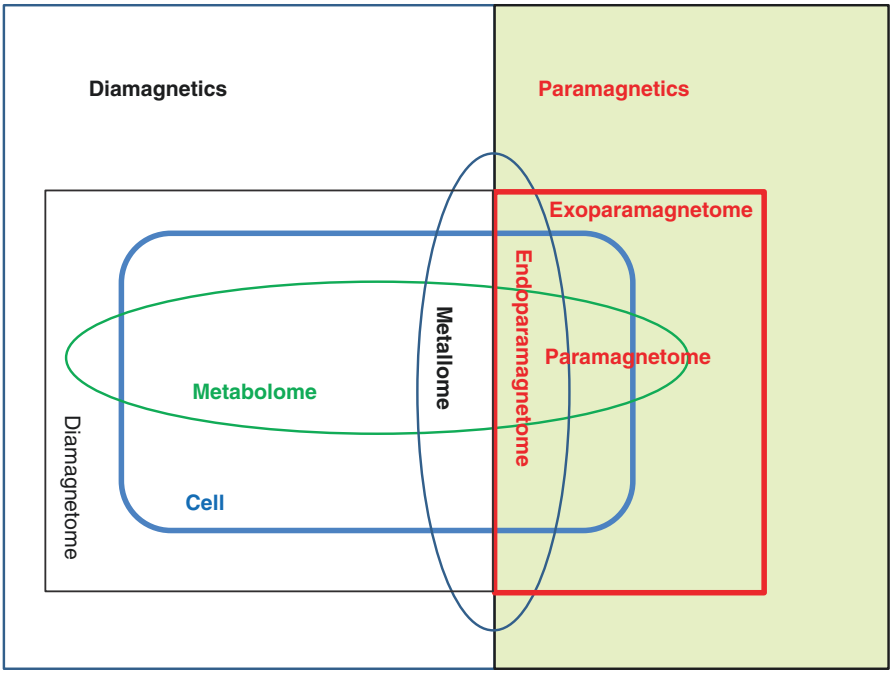

Fig. 9.2 The paramagnetome—its special position in relation to other "-omes". The proportion between particular components of the figure and the number of the included species is not maintained. To express the relation of the metallome to other "-omes", I referred to [69] and in particular to [70]

spectroscopy. It includes both transient and permanent species revealing paramagnetic properties (Fig. 9.2). An important but distinctly separated part is the exogenous paramagnetome ("exoparamagnetome"), which consists of paramagnetic probes and spin labels (or paramagnetic centres in spin-labelled molecules) but also spin adducts created from exogenous spin traps and short-living radicals. In opposition to the "exoparamagnetome" stays the "endoparamagnetome"—the pool of paramagnetic centres generated by the living system itself. It must be observed that some part of the "exoparamagnetome" may be a product of the activity of other cells and organisms and some—the artefacts—intentionally or unintentionally generated by human (who is a living organism him-/herself). The so-defined paramagnetome can also be divided into a dynamic and a stable fraction, the first consisting of short-living reactive species and the other of stable particles in which paramagnetic properties are "trapped" or "hidden". Both can include the exogenous and endogenous paramagnetic centres.

This pool of paramagnetic centres in a living organism creates a specific and dynamic being, which is quickly spoiled (but not necessarily annihilated) once the system dies (Fig. 9.3). It interacts with the rest of the system, and it makes these interactions very symptomatic for some important processes and features of the biological system. The most important processes which form the paramagnetome of a living system are:

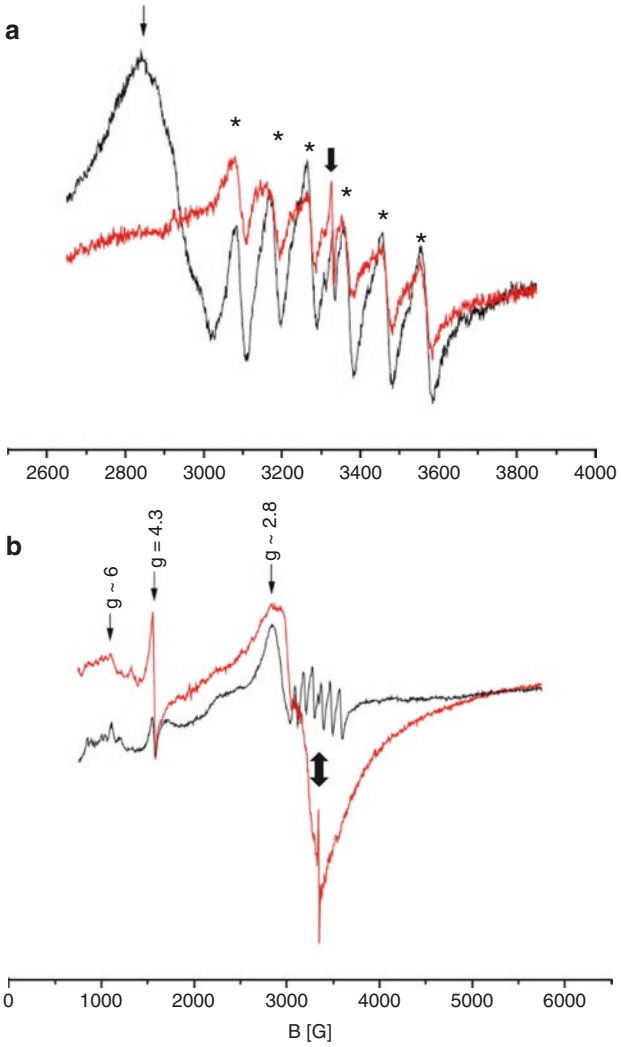

Fig. 9.3 Paramagnetomes of a true slime mould *Fuligo septica* (Wigg F.H.) and their changes due to necrosis. (**a**) The changes observed in the necrotizing plasmodium (red line, the native plasmodium; black line, the necrotic plasmodium). Thin arrow, a wide $g \approx 2.08$ signal of decomposing haem iron (low-spin Fe(III), "hemichrome" [71, 72]); thick arrow, the free radical signal ($g \approx 2.00$); asterisks, hyperfine structure of the EPR signal of Mn(II) complexes. (**b**) The EPR signal of the necrotic plasmodium compared with the spectrum of the author's lyophilized blood (red line). Note a decrease in the free radical signal of metabolic origin [73, 74], a change in the shape of the Mn(II) complex signals towards more regular (better resolution and symmetry of the hyperfine structure characteristic for low-molecular $[Mn(OH_2)_6]^{2+}$ complexes) [75] and the occurrence of the low-spin Fe(III) signals. $g = 6$ and $g = 4.3$—the signals of high-spin haem ($g = 6$) and non-haem Fe(III) ($g = 4.3$) [73, 74]. The strong free radical signal in the dried blood (thick double-headed arrow) is due to paramagnetic products of lipid peroxidation [72]. The plasmodium was collected and measured at ambient temperature in a Pasteur pipette, and left in the same conditions for 5 days, whereupon measured again at X-band using a Bruker EPR spectrometer at modulation amplitude—5 G, microwave power 21 (plasmodia) or 30 mW (blood)

1. Photosynthesis [45, 46, 55]
2. Oxidative respiration ([45, 46, 56–60] and oxygen transport [76, 77])
3. Synthesis of DNA, i.e. reduction of ribonucleotides to deoxyribonucleotides ([78]; see also further in this chapter)
4. Inflammation and related processes of defence [79, 80]
5. Cellular signalling [81, 82]
6. Cellular detoxification and recycling [82–84]
7. Activity of other oxidoreductases and other redox reactions—e.g. melanogenesis [85, 86], synthesis of nitric oxide [50], oxidation and reduction of metal ions [87], Fenton reaction [88], etc.
8. Interactions with ionizing radiation and UV (e.g. [63, 89–93])
9. Inter-radical reactions (e.g. recombination [94–96]), all of which being generalized as the process of life [3].

The possession of unpaired electron results with the non-zero magnetic momentum, responsible for the paramagnetic properties of the whole molecule. Such a magnetic momentum interacts with the external magnetic field in a positive way, i.e. pulling the particle into the magnetic field. This is strongly contrasted with the diamagnetic reaction, which is repulsive, and which results from the Lenz's law and which pushes away the particle out of the magnetic field [97, 98]. But it also entitles us to call the opposite part of the living system metabolome—the "diamagnetome" (Fig. 9.2). This measure may seem much more artificial than establishing the paramagnetome, because the species with unpaired electrons play unique and crucial roles in the phenomenon of life, while the diamagnetome is "all what does not belong to the paramagnetome". This notion, however, may appear useful when analysing the dynamics of interactions between the paramagnetome and the rest of the metabolome.

The notion of the paramagnetome includes:

1. Free radicals and hydrated electrons [89]—products of metabolism [45, 53–60], products of action of radiation (including UV) [63] on other "-omes", and products of secondary reactions of the primary products with other "-omes" [64–66, 79, 90–95, 99–102]
2. Paramagnetic gases: oxygen [97, 103], nitric oxide [50, 81, 104, 105], nitric dioxide [104, 106]
3. Paramagnetic ions of transient metals and metalloids, mainly Fe [56, 59, 73, 74, 105, 107], Cu [107–109], Mn [75, 110, 111], V [112], Cr [113, 114], Mo, Co, Ni [107] and others
4. Melanin [45, 115, 116]
5. Some defects in crystals of biominerals [66, 117]
6. Donor-acceptor complexes with strong charge transfer, e.g. in photosynthetic centres [118, 119].

It is important to note that from the chemical point of view, the difference between these categories is more or less arbitrary, and sometimes even metal ions are colloquially called "free radicals".

9.8 The Special Position of Melanin in the Paramagnetome

Melanin is a paramagnetic biopolymer of unique chemical and physical properties [116]. Its main (but not the only one) function in the organism is pigmentation of the skin, hair and iris [120]. Its paramagnetism is extraordinarily high as compared to other paramagnetic biological substances, unbelievably stable, e.g. preserved over millions of years in fossilized paleontological material [121]. It is an end product of polymerization of aromatic amino acids and their derivatives, and, as opposite to other biopolymers, it is produced by oxidative polymerization [85]. Its paramagnetic properties are of a mixed character, predominantly determined by free radicals, with admixture of paramagnetic metal ions [115, 116]. The free radical paramagnetic centres, mainly of semiquinone or semiquinonimine character, are trapped within the amorphic structure of the polymer, which makes the paramagnetism particularly resistant to almost all methods of degradation, except of oxidative ones [116]. Its position in the paramagnetome of a pigment cell, such as melanocyte or melanoma cell, is very special [120] and responsive for some features of these cells, besides pigmentation, e.g. of the resistance to various methods of therapy, including radiotherapy [122]. It is not clear what the evolutionary origin of melanin is, but there are hypotheses that it was an end product or the butt end of some biochemical reactions which appeared when the atmosphere in the Earth became oxidative [123] and which otherwise might have led to a total destruction of the cells by oxygen. Other authors suppose that it is a by-product of oxidation of quinones which may have been used as a "chemical weapon" due to their high chemical activity [85, 124]. In the pigmented cell, melanin may be just a "cleaner of the diamagnetome" which sweeps of the paramagnetic transient and highly active species or even participates in the metabolism by driving the unpaired electrons through the carriers. Such a role of this substance has been implied since the already cited paper by Commoner et al. [45]. For the present chapter, it is important to note that many cells, e.g. keratinocytes in the skin epidermis or in hair follicles [120, 125, 126], do not produce melanin but obtain it directly from melanocytes, from other keratinocytes [126] or by phagocytosis of ectopic melanin or apoptotic bodies [127]. For phagocytic cells, melanin, a product of endogenous metabolism of other cells, may be, therefore, an important constituent of the "exoparamagnetome". One of its supposed biological functions is the role of a "redox buffer", delivering or accepting electrons in the case of their overproduction or deficiency in the living system [116]. They can interfere with the paramagnetome as "stabilizers" or, perhaps, as destabilizers [128, 129] of the endo- but also of the exoparamagnetome and the general internal or external environment. In some cases it is difficult to an unambiguous determination of their paramagnetomic position, just like in the case of marine or soil bacteria which may use melanin and humic substances as shuttle vectors for electrons in the process of anaerobic respiration, in which the excess of electrons generated by the cells due to oxidation of particular substrates is transiently saved in the form of "reduced melanin" to reduce further an inorganic acceptor (e.g. iron(iii)) [130, 131]. This seems to be a new step in the evolution of melanin but also a new paramagnetomic quality in the biosphere [132, 133].

9.9 Dynamics of Paramagnetomes in Time and Space - Examples

One of the most important features of EPR as a method useful in biology is the possibility to monitor the same paramagnetic species on different levels of the organization of biological systems, from the ecosystem [133], through single organisms (e.g. alive developing embryos [134]), organs [135], tissues [136], cells [50] and pure substances [75, 112], to the level of molecular electron "bus bars" [56, 119]. Important paramagnetomes act in plants, their leaves [54, 55, 109] and germinating seeds [45]. It is also possible to study "paleoparamagnetomes", i.e. paramagnetomes of fossils, because some paramagnetic centres may be trapped in particularly stable and resistant materials. To such materials belong i.a. biominerals (bones, teeth [137]), melanin or its external equivalent contained in humic substances [121] and various forms of fossil carbon, which itself may serve as a paramagnetic probe, e.g. in EPR oxymetry [138, 139]. As on each level, the paramagnetic centres may interact with other constituents of the system and the paramagnetomes with other "-omes"; EPR appears as a really powerful tool, which has been pointed out many times in the past as the unique characteristics of EPR techniques [68, 140–142].

The amino acid free radicals are often products of irradiation and oxidative stress and interact with other macromolecular and usually diamagnetic components of the cell. As belonging to a rich set of xenobiotics, the damaged macromolecules may further induce inflammation-related oxygen burst, generate a secondary pool of free radicals and escalate the oxidative stress responsible, for example, for some autoimmune degenerative disorders [90, 91, 143].

The soluble guanyl (called also guanylate or guanylyl) cyclase belongs to the very small group of the haem-containing enzymes whose haem group is not engaged in the catalytic activity [144, 145]. As a consequence, this enzyme is not an oxidoreductase but a lyase, responding, however, to a paramagnetic, parahormonal ligand—NO [50, 81, 105, 146]—and itself being paramagnetic [147]. But the vast majority of haem-containing enzymes belongs to the first class of enzymes—the oxidoreductases—which change the oxidation state of their substrates. While the full cycle of the enzymatic activity should regenerate the initial redox and spin state of the enzyme [148], the transient reactions may be associated with reduction or oxidation of the metal of its catalytic centre (ferroxidase-ceruloplasmin [86], L-phenylalanine hydroxylase [87], nitric oxide synthases [148], etc.). The enzyme may also change its oxidation state due to activation or inactivation (e.g. tyrosinase [85, 149]). Finally, the main factors determining enzymatic activities of oxidoreductases are often amino acid free radicals [148]. As a consequence, the oxidoreductases stay paramagnetic over the substantial part of their existence in the cell. Therefore, the proteomic paramagnetome plus melanin (in pigment cells) seem to hold the central and the most stable position in the cellular paramagnetome.

In the majority of cases, the EPR signal of free radicals is a result of transient, short-living species (e.g. semiquinones, except of these trapped within the structure of melanin), which when overlapped with the signals of "working" enzymes may be treated as the "signal of life", the manifestation of a given system being alive [45,

73, 74]. But in this point, it must be stressed that not every redox reaction which takes place in the metabolome reveals the engagement of unpaired electrons in the mechanism. For instance, the production of NADH in the process of oxidation of phosphoglycerol aldehyde in glycolysis does not involve free radical intermediates [150]. The primary electron donor for NADP+ is the hydride anion (H^-) [151], whose two electrons reveal by definition compensated spins, so that the activity of the enzyme (GAPDH—glyceraldehyde-3-phosphate dehydrogenase) is based solely on amino acid residues of the apoenzyme and the phosphate group of the substrate [150, 151]. Anyway, in the respiratory chain, the NAD^+ reductase acts as a typical oxidoreductase with the unpaired electron intermediates [152]. A more interesting case is represented by the nitric oxide synthase [148], which produces NO in two independent steps. In the first monooxygenase reaction, the free radical intermediate is centred on an amino acid residue of the apoenzyme, while in the second the free radical appears as an L–Arg–$O^{\cdot}$ radical of the "second" substrate (N–OH–L–Arg). Everything is orchestrated by the iron of the haem prosthetic group upon control of BH_4 (also controlling the spin state of the catalytic iron(III)), FAD and FMN, with NADPH as a co-substrate. The system of the electron carriers is extraordinarily complicated, one of the substrate (O_2) is paramagnetic, and, besides the intermediate free radicals and the permanently changing iron [148, 153], the product itself is a paramagnetic particle: NO. Examples for non-unpaired electron- and unpaired electron-engaged reactions of oxidoreductases can be multiplied.

The endoparamagnetomes may interact with the environment and the exoparamagnetomes. The most important example of this interaction is, again, photosynthesis which has produced over the substantial part of the evolution the whole resource of atmospheric, paramagnetic oxygen [154–156]. This element is also the dominant final acceptor of the electrons in the catabolic processes delivering energy available for living systems, thus creating the continual flow of electrons and energy, facilitating self-organization and setting the machinery of life in motion—in other words, maintaining the biosphere in the state of life [3, 46, 154].

The signal or, better, the EPR signals from the paramagnetome may also deliver important information on the actual quality of the ongoing processes of oxidative damage, e.g. mitochondrial dysfunction due to septic shock [73] or a change of the balance between various pools of iron due to the progress of dilated cardiomyopathy [74]. The signal of paramagnetic centres trapped in calcium carbonate crystals [117] or in keratin of finger- and toenails [157] inform on the doses of radiation absorbed by an organism. From the shape and strength of the EPR signals of spin adducts [158, 159], one can deduce on the proper functioning of other life processes, difficult to a direct monitoring with EPR, like oxygen burst [76, 79, 92, 159], production of nitric oxide due to activation of non-specific immunity [50, 79, 135, 158–161], etc. Similar information can be extracted from the changes in the EPR spectra of EPR probes and spin labels [162]. Finally, the oxygen supply and consumption, as well as vascularisation of an organ (e.g. a tumour), may be observed not only in the dynamic but also the spatial aspect upon use of EPR imaging (EPRI) [163, 164]. The spatial distribution of melanin in a solid tumour of melanoma has

recently been registered using EPRI [165]. Such EPR spectrum-derived (i.e. paramagnetome-derived) information may be applied to monitor some other features of the inner environment of the organism, organ or cells, like fluidity, polarity, pH, etc. [68, 140, 142, 159, 162]. All these data are important to design therapeutic procedures and to define the applicative aspect of the paramagnetome [142, 166].

9.10 The Sense and Usefulness of Paramagnetomic Approach to Biology

So far, some constituents of the paramagnetome have been discussed in a wider context of the metabolome (let's cite as an example the title of a session during the Xth International Workshop on EPR in Biology and Medicine in Kraków; the session, and the workshop as a whole, contained presentations and posters with EPR/ESR data [167]) and/or the metallome [141]. Such approach is to some degree justified, as free radicals are inevitable side products and intermediates of metabolism and the biologically important metal ions are often paramagnetic; moreover, this importance resulted from their being paramagnetic. In both cases, however, the usage of EPR as the main method of investigation of paramagnetic species makes it exotic and unusual, and somehow strange for the metabolomics [32], and even more importantly, almost the entire metabolome is diamagnetic. There are biologically important metals, even such that in general can change their oxidation state (e.g. zinc), which in biological systems are only diamagnetic and do not undergo redox reactions (zinc II, magnesium, calcium) [168], despite belonging to the metallome. Biological EPR is wholly dedicated to the paramagnetome, while to investigate diamagnetic substances, incomparably more methods have been created. The living organisms are almost entirely diamagnetic, but it is the very few paramagnetic constituents that make them unique and living. As a result, distinguishing the paramagnetome from the metabolome and the metallome, followed by creation of the "paramagnetomics", seems specially justified.

Application of EPR and analysis of the EPR spectra are the common denominators for the cross-sectional analysis of paramagnetic centres of the metabolome and the metallome. In other words, EPR techniques, as dedicated to the paramagnetome, and *only* to the paramagnetome, make the paramagnetome exceptional. Moreover, this analysis, no matter if metallomic or metabolomic, concerns processes crucial for living cells.

At this point, there remain, however, still three other reasons justifying the selection of the paramagnetome as a separated, autonomic "-ome" in the biological system:

(a) From the physical and even chemical point of view, the existence of paramagnetic molecules, ions or atoms in a system is important only from the point of view of the direct environment, i.e. the environment directly neighbouring in time and space the present system or the present state of the system. For the alive, biological system, everything, which precedes the current state from the

beginning of the existence, matters, and the present state of the system is given by the integral of the function of response over the whole time of existence, given by all the parameters with their own history and transient states [2]. Only the integral analysis of the transient paramagnetic species over time (and space), given as a system— as an "-ome"—leads to the anticipated goal. In other words, the transient state of a biological system, in which the paramagnetic species play the main role, is the state of the whole paramagnetome and its history. For instance, for a biological system, it *does* matter whether the molecule of superoxide radical was generated as a goal product of NADPH oxidase or a side product of photosynthesis.

(b) As it has already been pointed out, the phenomenon of life possesses its dynamic, ephemeric, transient dimension, as being rather a process of transformation, change or flow, than a structure (while the structure being still important, it still undergoes transformation [14]). The dynamic approach is indispensable to understand, e.g. the function of a macromolecule, a lipid bilayer [169], a biological subsystem or a whole system. The paramagnetic centres are usually transient species, which mark the given pathway of changes and whose fugacity can be overcome by spin-trapping. EPR measurement makes it able to register the kinetics of the process. More metaphorically, electrons still flow through the living system [14, 46, 55, 56, 119, 170], and EPR –makes it able to directly "trace" this flow, thence, the phenomenon of life. It can be executed against the diamagnetic background without the necessity to purify any transient paramagnetic species, which would hardly be possible in the case of "diamagnetomic" constituents.

(c) Constituents of paramagnetomes are often the only remnants of once-alive systems (the so-called EPR fingerprints [133]). The paramagnetic substance is sometimes the only proof that a given environment was, indeed, inhabited by alive organisms [121, 138, 139], so its remnants can be called "life fingerprints".

Finally, there are some paramagnetic species, the position of whom is problematic, e.g. dioxygen, which is a product of enzymatic photosynthesis, and the main final substrate of oxidative respiration, however, being a chemical element of clearly "inorganic" character. A similar problem concerns nitric oxide—one of the simplest heteroatomic molecules in the Universe. The same problem that metal ions are not directly encoded in the genes and are actually of the external origin, as not possible to be generated or created by the living system, leads to the establishment of the metallomics [29, 30].

One can say that EPR itself defines the paramagnetome. The paramagnetome is all this of the substances present in any living system, which can be measured directly by EPR, which can be reflected in an EPR spectrum and, a lot of this, which makes the system alive.

The chemical nature of the paramagnetome makes its constituents actively interact with one another; in other words, the metallomic paramagnetome creates the constituents of metabolomic paramagnetome, which interacts within itself and

which may interact with other "-omes". But here, there is a start of a very long and substantial discussion, to be carried out in another book akin to the present one. However, one should note that some attempts have already been undertaken several times, from the position of metallomics [29, 141] and metabolomics [30, 162, 167], from the position of physics and biophysics [46, 171] and even from the point of view of applicative sciences like biotechnology [140] or dermatology [68] (actually, the whole present book is a proof that the "EPR approach" to biology and medicine, and the paramagnetome, exist). All those attempts limited themselves to pinpoint of advantages and versatility of EPR spectroscopy, without making a step forward—to call this approach by name. So far, the keyword "paramagnetome" or "paramagnetomics" delivers no entry in the available Internet resources, except of my invited lecture which has been given on May 21, 2017, during the VI International Conference of Biophysics Students in Kraków [172].

9.11 The Paramagnetome and Genetic Information

The paramagnetome as a real being in the living system can be in the best way portrayed in relation to other similarly defined systems ("-omes") perhaps better analysed and deeper rooted in the common biology. So far, the talk has concerned some paramagnetomic aspects of proteome, metabolome and metallome. The lipidomic and glycomic aspects of paramagnetomics have also been noted, as the "biologically oriented EPR" has partially developed from the EPR study of biological membranes [162]. But when following the main plot of this chapter (definition of life), the question about the genetic information and its paramagnetomic associations arises in the first place.

Many processes of interactions between the paramagnetome and classical "-omes", in particular the genome, the transcriptome and the proteome, reveal a remarkable stigma of pathology and destruction of living systems, which on the level of genetic information means randomization of the sequence of nucleotides [173]. In this context, the unpaired electrons and paramagnetic centres as the primary or secondary products of ionizing irradiation are the factors of damage to DNA and RNA [140] potentially leading to the destruction of genetic information and the living system [173].

One has, however, to remember that the process of mutagenesis leads to the production of new genetic information and probably new biological functions [175]. Actually, mutations and their further evolutionary verification are the only, primary, natural processes of creation of qualitatively new genetic information encrypted in a qualitatively new variant of a nucleotide sequence [155, 175]. This variant may be further multiplied and rearranged creating yet newer portion of genetic information [37]. There is a hypothesis that the existing genomes may have evolved from a limited number of short oligomeric sequences which generated the present genomes by multiplication and recombination [176], but to achieve the present length and variability of genomic sequences, and the corresponding polypeptides, it must have been supported by point mutations [177, 178].

There is a given error rate, over which the given genome must inevitably undergo such an above-mentioned randomization over the next several generations (the so-called Eigen limit) [175, 179]. As the matter of fact, the entire genetic information is a manifestation of the permanent interaction between the biological systems and the environment which undergoes also permanent changes. The process of environmental changes (except of extreme environments) is, however, much longer and slower than the lifetime of a generation of organisms. Therefore, in the short run, it pays to preserve genetic information rather than to develop it (and this was what Gregor Mendel actually discovered [5]). The adaptative value of the mutations is also permanently verified in new environmental conditions, and a "bad" mutation not necessarily must remain "bad" in the future. As a result, it would also pay if any new genetic information (i.e. the new mutations) were somehow stored in the genetic material. The biological system must possess a genetic memory [154].

Earlier I wrote that in the process of the expression of genetic information, "*unfortunately*", no redox reaction takes place, therefore apparently eliminating the unpaired-electron-involving phenomena from the stream of the expression of genetic information. Mutagenesis does engage the paramagnetome. It can be accelerated by artificial irradiation of generative forms of life, and this is the way to obtain new mutations in classical genetics [180]. UV irradiation may lead to the electron-excited states in DNA of highly reactive though not necessary paramagnetic character; however, it is an important inducer of the oxidative stress and free radicals in a similar way generating mutations [79, 80, 89, 91, 174, 181]. But the development and expansion of genetic information, thanks to mutagenesis, are easily imaginable without recourse to the radiation or UV-induced mutagenesis [182]. The point mutations understood as random, hereditary changes of the number or quality of single nucleotides in the nucleotide sequences may be induced chemically or may just be the effects of erroneous replication [179, 182, 183]. Consequently, the engagement of the paramagnetome as an indispensable factor in the biological evolution might seem exaggerated (hence the above mentioned word "unfortunately"). Perhaps the existence of the paramagnetome is an exotic curiosity which has nothing important to the establishing, maintaining and expression of genetic information, thus the life. Is this the case?

There is one crucial difference between ionizing radiation-induced and UV-induced mutagenesis. In the case of free radical intermediates, the unpaired electrons cannot annihilate nor dissipate but only recombine, i.e. pair with other paramagnetic species [95, 184] or interact with a diamagnetic species leaving another paramagnetic centre [185]. Meanwhile, in the case of the electron-excited states, the active intermediates, besides the possibility of utilizing the excess of energy to break or form a covalent bond, may dissipate the excess of energy in the form of heat (thus increasing the entropy of the surrounding [62]). A particular efficiency of this process can be supplied by hydrogen bonds in the DNA double helix and Watson-Crick base pairing [186]. As a result, almost every excitation of a base in a double helix of DNA by UV can be dissipated. As the most important mutagenic factor on the early Earth was UV, this was probably the most important reason for establishing DNA as the main, most stable and inert carrier of genetic

information [186]. The other reason is the relatively low Eigen limit enabling to maintain only genomes as long as ca. 100 nucleotides if the genetic information were encrypted in RNA [179, 183]. DNA not only turned out relatively inert to UV-induced mutagenesis but also made it able to substantially lengthen the existing genomes [175]. As a result, the present living cell *does* possess a genetic memory [154] and a representation of states to choose from in response to the changes in the environment [40]. But it leads to a paradoxon—the development of DNA as the ultimate carrier of genetic memory would move the evolution of genetic information apparently towards independence on the unpaired electron-containing, mutagenic paramagnetome. Is this, indeed, the case?

The answer to these questions—no, it is not the case!—does not concern the resistance to mutagenicity but the production of DNA, in particular deoxyribonucleotides, which are the reduced forms of ribonucleotides due to the activity of ribonucleotide oxidoreductases (RNR) [78, 187–191]. Let it be illustrated first by a citation from Michelle C. Y. Chang, Cyril S. Yee, JoAnne Stubbe and Daniel G. Nosera who wrote in 2004 ([189], p. 6882): "The central role of RNRs in nucleic acid metabolism, their exquisite control of free radical chemistry, and the proposed part they play in the conversion of an RNA to a DNA world, have fascinated scientists since their discovery". RNRs are oxidoreductases, obviously dealing with free radical species and transient metal ions (and being studied with EPR [78, 191]). The obligatory step in this process is reduction of carbon 2′ of the substrate's ribose in the active centre of the enzyme. One of the peculiarities of these enzymes is a direct replacement of the 2′-OH group with a hydrogen (from the thiol residue of Cys 462 of the apoenzyme [188]). The origin of the unpaired electron, however, is the thiol radical of another cysteinyl residue—Cys 439 situated in the active centre of the enzyme. And interestingly, it is the 3′ carbon of the ribose of the substrate that is initially reduced by the Cys 439 thiol radical, and only then is the unpaired electron transferred on 2′ carbon [188]. The full mechanism of the process is much more sophisticated, in details described in the substantial literature (e.g. [78, 188–190], etc.) not to mention that there are three main classes of RNR [188–190]. The important point here seems a complicated, multistep series of free radical reactions and transient paramagnetic species which take place in the molecule of the substrate during the full process of reduction driven by external paramagnetic centres of the apoenzyme. The actual origin of the unpaired electron (nonhaem iron complex and tyrosyl radical, cobalamin, or glycyl radical generated with another nonhaem iron complex) segregates the enzymes into these three main classes (RNR I, RNR II and RNR III, respectively; e.g. [188–190]). The unpaired electron in RNR I is probably generated by a photochemical reaction [189] and transferred to the reactive centre of the enzyme via a chain of amino-acid radical intermediates situated on the inter-domain surface of the enzyme [189]. So, the "control of free radical chemistry by RNRs" is "exquisite", indeed ([189], p. 6882). Thanks to amino acid, and transient metal paramagnetic centres, not only new genetic information is produced but DNA itself.

Is this process related to oxidative stress? Demand for deoxyribonucleotides is created in the cell by two main factors—DNA replication (which is self-evident) and also

DNA repair, which is a direct result of oxidative damage to DNA [174]. The more recent study of already cited [64, 65] Professor Machbuba K. Pulatova revealed that irradiation itself increases the activity of ribonucleotide reductases [192]. The increased supply of free radicals must result in the increased DNA damage, which increases the demand for deoxyribonucleotides for the repair systems. Another evidence is the dependence of the process of RNR Ib maturation (i.e. generation of the "external electron donor", the tyrosyl radical) on the semiquinone-manganese (II) complex which is created with the engagement of superoxide anion-radical [191], i.e. the main factor of oxidative stress [76, 77, 79, 80, 160]. It must be emphasized that the putative light-primed activation and the engagement of nonhaem iron complexes in the class I RNR denote an ancient origin of this group of enzymes. Unexpectedly, it is the RNR III class that is suggested as the most ancestral representative of RNR [190].

The discovery of RNRs [187] and their mechanism of action strongly reinforced the view that DNA must have evolved in the RNA world with RNA genes encoding proteins and that DNA must be a relatively young evolutionary invention [189, 193, 194]. Another evidence is the fact that it is the ribonucleotide, not the ribose, which is reduced by RNRs [188, 189]. The variability of different nucleotide sequences may have been achieved in the "RNA world" and then transferred and preserved in the much more stable DNA [193, 194]. The paramagnetome must have, consequently, appeared earlier than DNA-based genetic memory which preserves the repertoire of states and makes it possible to control metabolism. The co-localization of the sites of DNA repair and DNA replication [195, 196] suggests that the origin of DNA replication may have something in common with DNA repair. The other important reason for this assumption is that double breaks of DNA are the main type of DNA damage due to irradiation [174], such damage being a substitute of "melting", i.e. dissociating of the nucleic-acid double strand, making a sort of replicatory fork necessary to initiate primordial replication. It is important, as the necessity to dissociate is one of the problems when re-constructing the evolution of replication [197]. Such partial dissociation is necessary to facilitate semi-conservative replication. Templates loosely bound into double strands achieve this easier than the more stable, tightly bound double strands. But loose bound means pairing with the monomers in the process of replication with a lower fidelity. It also increases the probability of hydrolysis into monomers—and randomization [173, 197]. This lowers the Eigen's error threshold and shortens the putative genomes which may be maintained over a big number of generations.

The described phenomena really place the paramagnetome in the centre of the life processes connected with the production and transfer of genetic information. In the context of the work by Berggren [191], Pulatova [192] and colleagues, it directs the topic of the relations between the paramagnetome and the genome towards the hottest stream of discussions on the evolutionary origin of genetic information. One should end up with a provocative statement that the definition of life given by Professor Weiner [3] is as a matter of fact a variant of the definition of the paramagnetome.

Table 9.2 Features of paramagnetomics as a representative of "omics"

"Omics"	Paramagnetomics
Functional	EPR signal—the signal of redox processes (transient species), the record of *par excellence* functions
Interdisciplinary	"Biologically oriented EPR" is by definition and even by name interdisciplinary
Investigating living systems in a "cross-cutting" manner and "in a context"	EPR spectroscopy as the only method to directly investigate paramagnetomes understood as the life *in esse*
Operating (usually)—on *big* sets of data	Whatever big the sets of the EPR data are, they demand special skills to interpret them
Basing on newest analytical methods in particular addressed to big data systems	Specific method: EPR spectroscopy and imaging
Demanding therefore refined IT (information technology)…	Digital acquisition of EPR spectra and their numeric simulations…
…and refined IT specialists	…demand omnipresent IT specialist

9.12 Conclusions: Paramagnetomics—Is There a Necessity to Create Yet Another "-Omics"?

In 2007 Satya Yadav counted 829 entries containing suffix "-omics" [41]. Inventing and establishing this way new branches of biology became a fashion and even a matter of competition among scientists. One of the reasons (or maybe an opportunity) for this is a thorough redesign of life sciences [198]. But, while "to bring something into existence" often means "to name it", is the other way round also true: does "to name something" automatically mean "to bring it into existence"? Whatever the answer is, in my opinion, the paramagnetomics has already been created; the only step to do is to call it by name.

Paramagnetomes may be described as systems of biologically relevant paramagnetic centres interacting with other "-omes", created and annihilated in biologically relevant processes (some key biological processes). This placement of paramagnetomes in a very special position towards other "-omes" makes the EPR spectroscopy a unique and convenient tool for biologically oriented research and entitles one to call the full discipline engaging EPR to biology as "paramagnetomics" rather than "biologically (and medically) oriented EPR/ESR spectroscopy". Table 9.2 compares the features of paramagnetomics with other "-omics". Paramagnetomics possesses a clearly determined object of investigations—biologically relevant paramagnetic centres—and a clearly defined field of research, processes taking place in living systems with the participation of paramagnetic centres, as well as sharply outlined directions of further development. It also possesses the specially dedicated research method—EPR spectroscopy and imaging. Of course there are other research methods serving to investigate paramagnetic centres, including polarimetry [199], fluorimetry [200] and UV/VIS spectroscopy [201], mass spectrometry [202], Mössbauer spectroscopy [203], NMR and NMRI [107, 166, 204] and others [116]. But all of them, except EPR, may also serve to investigate directly diamagnetic molecules and atoms, i.e. the

Table 9.3 Paramagnetomics as a "new science" according to Stafford Beer [205] and updated

The feature	Implementation in paramagnetomics	Remarks
The object of investigations	Living systems or their remains (soil, fossils) and their models	
The topics of research	Paramagnetomes	As defined in this chapter
The scope (field) of research	Paramagnetic centres on various levels of organization of the living system and their interactions	
The primary method of research	EPR spectroscopy and imaging	
The theory	Theory of magnetic resonance In silico simulation of EPR spectra and of pulse EPR data (e.g. [206, 207])	"Pure science"
The resource of predicative sentences	Description of paramagnetomes, their dynamics and interactions including free radicals, paramagnetic transient metals, spin trapping and spin labelling	"Actual knowledge"
The applicative aspect	"Application of EPR in biology and medicine"	"Implementation"
Main directions of the future development	– Deepening the existing knowledge on paramagnetomes – Theoretical studies (modelling and simulations) on sophisticated aspects of EPR and on big systems of paramagnetic centres – Integration with techniques other than EPR – Interactions of paramagnetomes with other "-omes" – Clinical, environmental, evolutionary, astrobiological EPR – Further developing the definition of life	

"diamagnetomic" part of the metabolome. On the other hand, EPR may be used to investigate other "-omes", e.g. transcriptomes [140], which well documents the "inter-omic" interactions and unifies the processes, the understanding of which is possible only using the approach of the systems biology.

The "paramagnetomics" fully deserves the status of a "new science" (in the sense of "a new branch of science") fulfilling the criteria of being a distinct, complete discipline of science, i.e. according to Stafford Beer [205], possessing its theory (the so-called pure science—the principles of concluding and the scaffolding for the assemblage of the knowledge into an organized system), the resource of predicative sentences (i.e. the resource of the actual knowledge) and the applicative aspect of the theory and the actual knowledge. The brief characteristics of "paramagnetomics" are shown in Table 9.3.

Paramagnetomics understood previously as "biologically and biomedically-oriented EPR (ESR) spectroscopy and imaging" is a clearly defined, modern interdisciplinary branch of science. In contrast to the previous determinations, however, it appears as a discipline of biological rather than of physical sciences.

Acknowledgements I would like to recall the memory of two excellent scientists from Kraków, who actually created the topic and the subject of this chapter: Professor Stanisław J. Łukiewicz (1927–2005) and Professor Aleksander Koj (1935–2016). Professor Łukiewicz established "The Kraków School of Biophysics", but I particularly appreciate his monographic course entitled "The electron phenomena in living systems and the ways of their investigations" which I attended in 1985/1986 and which actually in detail outlined and designed paramagnetomics. Professor Koj, a famous Polish biochemist, and a Rector of the Jagiellonian University in Kraków, was a supporter of systemic approach in modern biology, fascinated by functional genomics—with the term itself and the genomic approach to biochemistry. He had always encouraged me to head crosswise the standard pathways of thinking in biology and to look for new qualities in the process of "making the science". I would like to express my particular gratitude to all the students of mine (some of whom being now professors) who have always inspired me to do so and who invited me to their conference in 2017 [172]. In particular, I must acknowledge Dr. Sebastian Pintscher, who in 2010 carried out under my supervision the EPR measurements exhibited in Fig. 9.3 and let me publish the spectra under my name.

The Faculty of Biochemistry, Biophysics and Biotechnology of Jagiellonian University is a partner of the Leading National Research Centre (KNOW) supported by the Polish Ministry of Science and Higher Education. The paper was partially supported from this fund (PMP, grant KNOW 35p/10/2015).

Conflict of Interest I have no conflict of interest to disclose.

References

1. Kon H. Recommendations for EPR/ESR nomenclature and conventions for presenting experimental data in publications. Pure Appl Chem. 1989;61:2195–200.
2. Prosser V. Postavení a úloha biofyziky v ostatních přírodních védách. [The position and role of biophysics in other natural sciences.]. In: Prosser V, collective, editors. Eksperimentální metody biofyziky [Experimental methods of biophysics]. Praha: Academia; 1989. p. 21–31. [In Czech].
3. Weiner J. Życie i ewolucja biosfery. Podręcznik ekologii ogólnej [Life and evolution of biosphere. A handbook on general ecology]. Warszawa: PWN; 1999. p. 53. [in Polish]
4. Bernal JD. The origin of life. Cleveland, Ohio: The World Publishing Company; 1967. Preface, p. xv
5. Mendel J/G, Wilczyński J, Tschermak E. Prace naukowe Jana/Grzegorza Mendla [*The scientific works of John/Gregor Mendel*], Spółdzielnia Wydawnicza Książka, Warszawa 1948. [in Polish, Translation of the 6 Edition and Forward by J. Wilczyński, Commentaries by E. Tschermak].
6. Beadle GW, Tatum EL. Genetic control of biochemical reactions in Neurospora. Proc Natl Acad Sci U S A. 1941;27:499–506.
7. Higgs PG, Attwood TK. Bioinformatyka i ewolucja molekularna [Bioinformatics and molecular evolution], Polish Scientific Editors PWN, Warszawa 2012. [in Polish, transl. by Murzyn K, Liguziński P and Kurdziel M, Murzyn K transl. editor, of 1 ed. Blackwell Sci Ltd, a Blackwell Publishing Company, 2005].
8. Flanagan SP. 'Nude', a new hairless gene with pleiotropic effects in the mouse. Genet Res Camb. 1966;8:295–309.
9. Mecklenburg L, Nakamura M, Sundberg JP, Paus R. The nude mouse skin phenotype: The role of Foxn1 in hair follicle development and cycling. Exp Mol Pathol. 2001;71:171–8.
10. Pantelouris EM. Absence of thymus in a mouse mutant. Nature. 1968;217:370–1.
11. Jacob F, Perrin D, Sánchez C, Monod J. "L'opéron: groupe de gènes à expression coordonnée par un opérateur" [Operon: a group of genes with the expression coordinated by an operator]. C R Hebd Seances Acad Sci. 1960;250:1727–9. [in French]

12. Searls DB. The language of genes. Nature. 2002;420:211–7.
13. Tarski A. Pojęcie prawdy w językach nauk dedukcyjnych [The notion of truth in languages of deductive/formal sciences]. Warszawa: Towarzystwo Naukowe Warszawskie; 1933. [in Polish]
14. Ji S. The Bhopalator–a molecular model of the living cell based on the concepts of conformons and dissipative structures. J Theor Biol. 1985;116:399–426.
15. Kuska B. Beer, Bethesda, and Biology: How "Genomics" Came Into Being. J Natl Cancer Inst. 1998;90:93.
16. Piétu G, Mariage-Samson R, Fayein NA, Matingou C, Eveno E, Houlgatte R, Decraene C, Vandenbrouck Y, Tahi F, Devignes MD, Wirkner U, Ansorge W, Cox D, Nagase T, Nomura N, Auffray C. The Genexpress IMAGE knowledge base of the human brain transcriptome: a prototype integrated resource for functional and computational genomics. Genome Res. 1999;9:195–209.
17. James P. Protein identification in the post-genome era: the rapid rise of proteomics. Q Rev Biophys. 1997;30:279–331.
18. Winkler HL. Verbreitung und Ursache der Parthenogenesis im Pflanzen- und Tierreiche [Occurrence and cause of parthenogenesis in plants and animals]. Jena: Verlag Fischer; 1920. [in German]
19. Olivier SG. From DNA sequence to biological function. Nature. 1998;379:597–600.
20. Hicks GG, Shi EG, Li XM, Li CH, Pawlak M, Ruley HE. Functional genomics in mice by tagged sequence mutagenesis. Nat Genet. 1997;16:338–44.
21. Velculescu VE, Zhang L, Zhou W, Vogelstein J, Basrai MA, Bassett DE Jr, Hieter P, Vogelstein B, Kinzler KW. Characterization of the yeast transcriptome. Cell. 1997;88:243–51.
22. Wasinger VC, Cordwell SJ, Cerpa-Poljak A, Yan JX, Gooley AA, Wilkins MR, Duncan MW, Harris R, Williams KL. Humphery-Smith I. Progress with gene-product mapping of *Mycoplasma genitalium*. Electrophoresis. 1995;16:1090–4.
23. Olsen GJ, Lane DJ, Giovannoni SJ, Pace NR, Stahl DA. Microbial ecology and evolution: A ribosomal RNA approach. Annu Rev Microbiol. 1986;40:337–65.
24. Handelsman J, Rondon MR, Brady SF, Clardy J, Goodman RM. Molecular biological access to the chemistry of unknown soil microbes: a new frontier for natural products. Chem Biol. 1998;5:R245–9.
25. Chen K, Pachter L. Bioinformatics for whole-genome shotgun sequencing of microbial communities. PLoS Comput Biol. 2005;1:106–12.
26. Han X, Gross RW. Global analyses of cellular lipidomes directly from crude extracts of biological samples by ESI mass spectrometry: a bridge to lipidomics. J Lipid Res. 2003;44:1071–9.
27. Hirabayashi J, Kasai K. Glycomics, coming of age! Trends Glycosci Glycotechnol. 2000;12:1–5.
28. Feizi T. Progress in deciphering the information content of the 'glycome'–a crescendo in the closing years of the millennium. Glycoconj J. 2000;17:553–65.
29. Williams RJP. Chemical selection of elements by cells. Coord Chem Rev. 2001;216–217:583–95.
30. Szpunar J. Advances in analytical methodology for bioinorganic speciation analysis: metallomics, metalloproteomics and heteroatom-tagged proteomics and metabolomics. Analyst. 2005;130:442–65.
31. Fiehn O, Kopka J, Dörmann P, Altmann T, Trethewey RN, Willmitzer L. Metabolite profiling for plant functional genomics. Nat Biotechnol. 2000;18:1157–61.
32. Oliver SG, Winson MK, Kell DB, Baganz F. Systematic functional analysis of the yeast genome. Trends Biotechnol. 1998;16:373–8.
33. Cesareni G, Ceol A, Gavrila C, Palazzi LM, Persico M, Schneider MV. Comparative interactomics. FEBS Lett. 2005;579:1828–33.
34. Sanchez C, Lachaize C, Janody F, Bellon B, Röder L, Euzenat J, Rechenmann F, Jacq B. Grasping at molecular interactions and genetic networks in *Drosophila melanogaster* using FlyNets, an Internet database. Nucleic Acids Res. 1999;27:89–94.

35. Devlin DKJ. Goodbye, Descartes: the end of logic and the search for a new cosmology of the mind. Chichester: John Wiley & Sons, Inc; 1997.
36. Williams RJP. Signalling: basics and evolution. Acta Biochim Pol. 2004;51:281–98.
37. Jura J, Węgrzyn P, Jura J, Koj A. Regulatory mechanisms of gene expression: complexity with elements of deterministic chaos. Acta Biochim Pol. 2006;53:1–9.
38. Shannon CE. A mathematical theory of communication. Bell Syst Tech J. 1948;27:379–423.
39. Mazur M. Jakościowa teoria informacji [Qualitative Information Theory]. Warszawa: Wydawnictwa Naukowo Techniczne; 1970. [in Polish]
40. Chmielecki A. Między mózgiem i świadomością: próba rozwiązania problemu psychofizycznego [Between the brain and the consciousness: an attempt to solve the psychophysical problem]. Warszawa: Wydawnictwo Instytutu Filozofii i Socjologii PAN; 2001. [in Polish]
41. Yadav SP. The Wholeness in Suffix -omics, -omes, and the Word Om. J Biomol Tech. 2007;18:277.
42. Commoner B. In defense of biology. The integrity of biology must be maintained if physics and chemistry are to be properly applied to the problems of life. Science. 1961;133:1745–8.
43. Asimov I, Najarian HH, Commoner B. Modern Biology. Science. 1961;134:1020–4.
44. Salikhov KM. Voevodsky Award 2001 to Prof L. A. Blumenfeld. EPR Newsletter. 2001;12(1):3.
45. Commoner B, Townsend J, Pake GW. Free radicals in biological materials. Nature. 1954;174:689–91.
46. Blumenfeld LA. Problemy Fizyki Biologicznej [Problems of biological physics]. Warszawa: PWN;1978. [in Polish, transl. by Berens K and Wartoń A from Russian "Проблемы биологической физики". Издательство "Наука"; Москва 1974. Available also in English: Blumenfeld LA, author, Haken H editor. Problems of biological physics. Springer-Verlag; Berlin-Heidelberg-New York 1981].
47. Pauli W, Über den Zusammenhang d. Abschlusses der Elektronenbahnen im Atom mit der Komplexstruktur der Spektren [On the connection between the completions of the electron orbitals in atoms with complex structure of their spectra]. Z Phys. 1925;31:765–85. [in German]
48. Uhlenbeck GE, Goudsmit S. Spinning electrons and the structure of spectra. Nature. 1926;117:264–5.
49. Michaelis L. Oxidation-reduction systems of biological significance. VI. The mechanism of the catalytic effect of iron on the oxidation of cysteine. J Biol Chem. 1929;84:777–87.
50. Lancaster JR Jr, Hibbs JB Jr. EPR demonstration of iron-nitrosyl complex formation by cytotoxic activated macrophages. Proc Natl Acad Sci U S A. 1990;87:1223–7.
51. Michaelis L. The formation of semiquinones as intermediary reduction products from pyocyanine and some other dyestuffs. J Biol Chem. 1931;92:211–32.
52. Michaelis L. Theory of the reversible two-step oxidation. J Biol Chem. 1932;96:703–15.
53. Michaelis L. Semiquinones, the intermediate steps of reversible organic oxidation-reduction. Chem Rev. 1935;16:243–86.
54. Huber M. Introduction to magnetic resonance methods in photosynthesis. Photosynth Res. 2009;102:305–10.
55. Tikhonov AN. Induction events and short-term regulation of electron transport in chloroplasts: an overview. Photosynth Res. 2015;125:65–94.
56. Świerczek M, Cieluch E, Sarewicz M, Borek A, Moser CC, Dutton PL, Osyczka A. An electronic bus bar lies in the core of cytochrome bc1. Science. 2010;329:451–3.
57. Sarewicz M, Dutka M, Pintscher S, Osyczka A. Triplet state of the semiquinone-rieske cluster as an intermediate of electronic bifurcation catalyzed by cytochrome bc1. Biochemistry. 2013;52:6388–95.
58. Kuleta P, Sarewicz M, Postila P, Róg T, Osyczka A. Identifying involvement of Lys251/Asp252 pair in electron transfer and associated proton transfer at the quinone reduction site of *Rhodobacter capsulatus cytochrome bc1*. Biochim Biophys Acta. 2016;1857:1661–8.

59. Pintscher S, Kuleta P, Cieluch E, Sarewicz M, Osyczka A. Tuning of hemes *b* equilibrium redox potential is not required for cross-membrane electron transfer. J Biol Chem. 2016;291:6872–81.
60. Sarewicz M, Bujnowicz Ł, Bhaduri S, Singh SK, Cramer WA, Osyczka A. Metastable radical state, nonreactive with oxygen, is inherent to catalysis by respiratory and photosynthetic cytochromes bc1/b6f. Proc Natl Acad Sci U S A. 2017;114:1323–8.
61. Asimov I, Dawson CR. On the reaction inactivation of tyrosinase during the aerobic oxidation of catechol. J Am Chem Soc. 1950;72:820–8.
62. Ksenzhek O. Money: virtual energy. Economy through the prism of thermodynamics. Boca Raton, Florida: Universal-Publishers; 2007.
63. Slominski AT, Zmijewski MA, Plonka PM, Szaflarski JP, Paus R. How UV Light Touches the Brain and Endocrine System Through Skin, and Why. Endocrinology. 2018;159:1992–2007.
64. Pulatova MK. Localization of paramagnetic centre in gamma irradiated protein. Biophysics (USSR). 1963;8:700–3.
65. Pulatova MK. On the problem of the localization of the paramagnetic center of proteins irradiated with gamma rays. Biofizika. 1963;8:632–4. [Article in Russian]
66. Atkins PW, Symons MCR. The structure of inorganic radicals. An application of electron spin resonance to the study of molecular structure. Amsterdam-London-New York: Elsevier Publishing Company; 1967. [Russian transl. by Germanv ED, Dyatkina ME editor. "Спектры ЭПР н строение неорганичецких радикалов". Издателство "Мир"; Москва 1970, p. 56–65].
67. Berliner JL, Fujii H. Magnetic resonance imaging of biological specimens by electron paramagnetic resonance of nitroxide spin labels. Science. 1985;227:517–9.
68. Plonka PM. Electron paramagnetic resonance as a unique tool for skin and hair research. Exp Dermatol. 2009;18:472–84.
69. Schaumlöffel D. The position of metallomics within other omics fields. In: Michalke B, editor. Metallomics: analytical techniques and speciation methods. Weinheim: Wiley-VCH Verlag GmbH & Co. KGaA; 2016. p. 3–16.
70. Haraguchi H. Metallomics: the history in the last decade and a future outlook. Metallomics. 2017;9(8):1001–13. https://doi.org/10.1039/C7MT00023E.
71. Rachmilewitz EA, Peisach J, Blumberg WE. Studies on the stability of oxyhemoglobin A and its constituent chains and derivatives. J Biol Chem. 1971;246:3356–66.
72. Miki T, Kai A, Ikeya M. Electron spin resonance of bloodstains and its application to the estimation of time after bleeding. Forensic Sci Int. 1987;35:149–58.
73. Svistunenko DA, Davies N, Brealey D, Singer M, Cooper CE. Mitochondrial dysfunction in patients with severe sepsis: An EPR interrogation of individual respiratory chain components. Biochim Biophys Acta. 2006;1757:262–72.
74. Elas M, Bielanska J, Pustelny K, Plonka PM, Drelicharz L, Skorka T, Tyrankiewicz U, Wozniak M, Heinze-Paluchowska S, Walski M, Wojnar L, Fortin D, Ventura-Clapier R, Chlopicki S. Detection of mitochondrial dysfunction by EPR technique in mouse model of dilated cardiomyopathy. Free Radic Biol Med. 2008;45:321–8.
75. Reed GH. Electron-paramagnetic-resonance studies of Mn(II) complexes with enzymes and substrates. Biochem Soc Trans. 1985;13:567–71.
76. Wever R, Oudega B, Van Gelder BF. Generation of superoxide radicals during the autoxidation of mammalian oxyhemoglobin. Biochim Biophys Acta. 1973;302:475–8.
77. Tsuruga M, Matsuoka A, Hachimori A, Sugawara Y, Shikama K. The molecular mechanism of autoxidation for human oxyhemoglobin. Tilting of the distal histidine causes nonequivalent oxidation in the β chain. J Biol Chem. 1998;273:8607–15.
78. Lendzian F. Structure and interactions of amino acid radicals in class I ribonucleotide reductase studied by ENDOR and high-field EPR spectroscopy. Biochim Biophys Acta. 2005;1707:67–90.
79. Kohno M. Applications of electron spin resonance spectrometry for reactive oxygen species and reactive nitrogen species research. J Clin Biochem Nutr. 2010;47:1–11.

80. Pucciariello C, Pierdomenico P. New insights into reactive oxygen species and nitric oxide signalling under low oxygen in plants. Plant Cell Environ. 2017;40:473–82.
81. Palmer RMJ, Ferrige AG, Moncada S. Nitric oxide release accounts for the biological activity of endothelium-derived relaxing factor. Nature. 1987;327:524–6.
82. Ortiz de Montellano PR, Wilks A. Heme oxygenase structure and mechanism. Adv Inorg Chem. 2001;51:359–407.
83. Hlavica P. N-oxidative transformation of free and N-substituted amine functions by cytochrome P450 as means of bioactivation and detoxication. Drug Metab Rev. 2002;34:451–77.
84. Wilks A, Heinzl G. Heme oxygenation and the widening paradigm of heme degradation. Arch Biochem Biophys. 2014;544:87–95.
85. Land EJ, Ramsden CA, Riley PA. Quinone chemistry and melanogenesis. Methods Enzymol. 2004;378:88–109.
86. Pey AL, Martinez A, Charubala R, Maitland DJ, Teigen K, Calvo A, Pfleiderer W, Wood JM, Schallreuter KU. Specific interaction of the diastereomers 7(R)- and 7(S)-tetrahydrobiopterin with phenylalanine hydroxylase: implications for understanding primapterinuria and vitiligo. FASEB J. 2006;20:E1451–64.
87. Daniel J, Kosman DJ. Multicopper oxidases: a workshop on copper coordination chemistry, electron transfer, and metallophysiology. J Biol Inorg Chem. 2010;15:15–28.
88. Fenton HJH. Oxidation of tartaric acid in presence of iron. J Chem Soc Trans. 1894;65:899–910.
89. Wang W, Zafiriou OC, Chan IY, Zepp RG, Blough NV. Production of hydrated electrons from photoionization of dissolved organic matter in natural waters. Environ Sci Technol. 2007;41:1601–7.
90. Nikitaki Z, Mavragani IV, Laskaratou DA, Gika V, Moskvin VP, Theofilatos K, Vougas K, Stewart RD, Georgakilas AG. Systemic mechanisms and effects of ionizing radiation: A new 'old' paradigm of how the bystanders and distant can become the players. Semin Cancer Biol. 2016;37-38:77–95.
91. Hawkins CL, Davies MJ. Detection and characterisation of radicals in biological materials using EPR methodology. Biochim Biophys Acta. 2014;1840:708–21.
92. Davies MJ, Hawkins CL. EPR spin trapping of protein radicals. Free Radic Biol Med. 2004;36:1072–86.
93. Chikira M, Ng CH, M P. Interaction of DNA with Simple and Mixed Ligand Copper(II) Complexes of 1,10-Phenanthrolines as Studied by DNA-Fiber EPR Spectroscopy. Int J Mol Sci. 2015;16:22754–80.
94. Haber F, Weiss J. Über die Katalyse des Hydroperoxydes. (On the catalyse of hydrogen peroxide). Naturwissenschaften. 1932;20:948–50. [in German].
95. Blough NV, Zafiriou OC. Reaction of superoxide with nitric oxide to form peroxonitrite in alkaline aqueous solution. Inorg Chem. 1985;24:3502–4.
96. Beckman JS, Beckman TW, Chen J, Marshall PA, Freeman BA. Apparent hydroxyl radical production by peroxynitrite: implications for endothelial injury from nitric oxide and superoxide. Proc Natl Acad Sci U S A. 1990;87:1620–4.
97. Curie P. Lippmann M. Propriétés magnétiques des corps à diverses températures (note de P. Curie, prèsentée par M. Lippmann). [Magnetic properties of bodies in various temperatures]. Comptes Rendus Hebdomadaires de Séances de l'Académie des Sciences 116. Paris: Gauthier-Villars et Fils, Imprimeurs-Libraires des C. R., 1893: 136–139. [in French]
98. Langevin M P. La théorie cinétique du magnétisme et les magnétons [The kinetic theory of magnetism and the magnets]. Rapport présenté à la Conférence Solvay, Bruxelles, 30 oct.-3 nov. 1911, In: Langevin P. La physique depuis vingt ans. Paris: Douin, 1923: 171–188. [in French]
99. Gordy W, Ard WB, Shields H. Microwave spectroscopy of biological substances. I. Paramagnetic substances in X-irradiated amino acids and proteins. Proc Natl Acad Sci U S A. 1955;41:983–96.
100. Landar A, Giles N, Zmijewski J, Watanabe N, Oh J-Y, Darley-Usmar V. Modification of lipids by reactive oxygen and nitrogen species: the oxy-nitroxy-lipidome and its role in redox cell signaling. Future Lipidol. 2006;1(2):203–11.

101. Buettner GR, Wagner BA, Rodgers VGJ. Quantitative redox biology: An approach to understand the role of reactive species in defining the cellular redox environment. Cell Biochem Biophys. 2013;67:477–83.
102. Lohan SB, Müller R, Albrecht S, Mink K, Tscherch K, Ismaeel F, Lademann J, Rohn S, Meinke MC. Free radicals induced by sunlight in different spectral regions—in vivo versus ex vivo study. Exp Dermatol. 2016;25:380–5.
103. Lennard-Jones JE. The electronic structure of some diatomic molecules. Trans Faraday Soc. 1929;25:668–86.
104. Uehara H, Arimitsu S. Gas-phase electron paramagnetic resonance detection of nitric oxide and nitrogen dioxide in polluted air. Anal Chem. 1973;45:1897–9.
105. Vanin AF, Mordvintsev PI, Kleshchov AL. Nitrogen oxide appearance in animal tissues in vivo. Studia Biophys. 1984;192:135–43.
106. Castle JG Jr, Beringer R. Microwave magnetic resonance absorption in nitrogen dioxide. Physiol Res. 1950;80:114–5.
107. Lowe DJ. ENDOR and EPR of metalloproteins. Prog Biophys Mol Biol. 1992;5:1–22.
108. Antholine W, Mailer C, Reichlin B, Swartz HM. Experimental considerations in biological ESR studies. 1. Identity and origin of the 'tissue lipid signal': A copper-dithiocarbamate complex. Phys Med Biol. 1976;21:840–6.
109. Kakuda T, Tanaka H, Kimoto E, Morishige F. Electron paramagnetic resonance spectrum of human serum copper. Appl Spectrosc. 1980;34:276–80.
110. Stegmann HB, Schuler P, Ruff H-J. Investigation of damage to forest by EPR spectroscopy *in vivo*. Photochem Photobiol. 1989;50:209–11.
111. Rakoczy L, Płonka PM. Akumulacja manganu w plazmodiach śluzowca (*Myxomycetes*) *Metatrichia vesparum*. [Accumulation of manganese in the plasmodia of a true slime mould (*Myxomycetes*) *Metatrichia vesparium*]. Ochrona Środowiska i Zasobów Naturalnych, Instytut Ochrony Środowiska. Warszawa. 1999;18:299–308. [In Polish]
112. Ramos S, Moura JJG, Aureliano M. Recent advances into vanadyl, vanadate and decavanadate interactions with actins. Metallomics. 2012;4:16–22.
113. Gutierrez P, Sarna T, Swartz HM. Experimental considerations in biological ESR studies. 11. Chromium-tissue complexes detected by electron spin resonance. Phys Med Biol. 1976;21:949–54.
114. Liu KJ, Mader K, Shi X, Swartz HM. Reduction of carcinogenic chromium(VI) on the skin of living rats. Magn Reson Med. 1997;38:524–6.
115. Blois MS, Zahlan AB, Maling JE. Electron spin resonance studies on melanin. Biophys J. 1964;4:471–90.
116. Meredith P, Sarna T. The physical and chemical properties of eumelanin. Pigment Cell Res. 2006;19:572–94.
117. Fattibene P, Callens F. EPR dosimetry with tooth enamel: A review. Appl Radiat Isot. 2010;68:2033–116.
118. Hauska G, Schoedl T, Remigy H, Tsiots G. The reaction center of green sulfur bacteria. Biochim Biophys Acta. 2001;1507:260–77.
119. Barry BA. Reaction dynamics and proton coupled electron transfer: Studies of tyrosine-based charge transfer in natural and biomimetic systems. Biochim Biophys Acta. 2015;1847:46–54.
120. Slominski A, Tobin DJ, Shibahara S, Wortsman J. Melanin pigmentation in mammalian skin and its hormonal regulation. Physiol Rev. 2004;84:1155–228.
121. Glass K, Ito S, Wilby PR, Sota T, Nakamura A, Bowers CR, Vinther J, Dutta S, Summons R, Briggs DEG, Wakamatsu K, Simon JD. Direct chemical evidence for eumelanin pigment from the Jurassic period. Proc Natl Acad Sci U S A. 2012;109:10218–23.
122. Brozyna AA, Jozwicki W, Roszkowski K, Filipiak J, Slominski AT. Melanin content in melanoma metastases affects the outcome of radiotherapy. Oncotarget. 2016;7:17844–53.
123. Wood JM, Jimbow K, Boissy RE, Slominski A, Plonka PM, Slawinski J, Wortsman J, Tosk J. What's the use of generating melanin? Exp Dermatol. 1999;8:153–64.
124. Riley PA. *Materia melanica*: further dark thoughts. Pigment Cell Res. 1992;5:101–6.

125. Slominski A, Wortsman J, Plonka PM, Schallreuter KU, Paus R, Tobin DJ. Hair follicle pigmentation. J Invest Dermatol. 2005;124:13–21.
126. Singh SK, Kurfurst R, Nizard C, Schnebert S, Perrier E, Tobin DJ. Melanin transfer in human skin cells is mediated by filopodia–a model for homotypic and heterotypic lysosome-related organelle transfer. FASEB J. 2010;24:3756–69.
127. Tobin DJ, Slominski A, Botchkarev V, Paus R. The fate of hair follicle melanocytes during the hair growth cycle. J Investig Dermatol Symp Proc. 1999;4:323–32.
128. Lembo S, Di Caprio R, Micillo R, Balato A, Monfrecola G, Panzella L, Napolitano A. Light-independent pro-inflammatory and pro-oxidant effects of purified human hair melanins on keratinocyte cell cultures. Exp Dermatol. 2017;26:592–4.
129. Płonka PM, Picardo M, Slominski AT. Does melanin matter in the dark? Exp Dermatol. 2017;26:595–7.
130. Menter JM, Willis I. Electron transfer and photoprotective properties of melanins in solution. Pigment Cell Res. 1997;10:214–7.
131. Turick CE, Tisa LS, Caccavo F Jr. Melanin production and use as a soluble electron shuttle for Fe(III) oxide reduction and as a terminal electron acceptor by *Shewanella algae* BrY. Appl Environ Microbiol. 2002;68:2436–44.
132. Plonka PM, Grabacka M. Melanin synthesis in microorganisms–biotechnological and medical aspects. Acta Biochim Pol. 2006;53:429–43.
133. Perrette Y, Poulenard J, Protiere M, Fanget B, Lombard C, Miege C, Quiers M, Nafferchoux E, Pepin-Donat B. Determining soil sources by organic matter EPR fingerprints in two modern speleothems. Org Geochem. 2015;88:59–68.
134. Sarna T, Lukiewicz S. Electron spin resonance on living cells. IV. Pathological changes in amphibian eggs and embryos. Folia Histochem Cytochem. 1972;10:265–78.
135. Plonka PM, Wisniewska M, Chlopicki S, Elas M, Rosen GM. X-band and S-band EPR detection of nitric oxide in murine endotoxaemia using spin trapping by ferro-di(N-(dithiocarboxy) sarcosine). Acta Biochim Pol. 2003;50:799–806.
136. Jakubowska M, Sniegocka M, Podgorska E, Michalczyk-Wetula D, Urbanska K, Susz A, Fiedor L, Pyka J, Plonka PM. Pulmonary metastases of the A549-derived lung adenocarcinoma tumors growing in nude mice. A multiple case study. Acta Biochim Pol. 2013;60:323–30.
137. Gruen R, Eggins S, Aubert M, Spooner N, Pike A, Mueller W. ESR and U-series analyses of faunal material from Cuddie Springs, NSW, Australia: implications for the timing of the extinction of the Australian megafauna. Quat Sci Rev. 2010;29:596–610.
138. Vahidi N, Clarkson RB, Liu KJ, Norby SW, Wu M, Swartz HM. In-vivo and in-vitro EPR oximetry with fusinite - a new coal-derived, particulate EPR probe. Magn Reson Med. 1994;31:139–46.
139. Ligeza A, Tikhonov AN, Subczynski WK. In situ measurements of oxygen production and consumption using paramagnetic fusinite particles injected into a bean leaf. Biochim Biophys Acta. 1997;1319:133–7.
140. Płonka PM, Elas M. Application of the electron paramagnetic resonance spectroscopy to modern biotechnology. Curr Top Biophys. 2002;26(1):175–89.
141. Hagen WR. Metallomic EPR spectroscopy. Metallomics. 2009;1:384–91.
142. Eaton SS, Eaton GR. The world as viewed by and with unpaired electrons. J Magn Reson. 2012;223:151–63.
143. Namazi MR. Cytochrome-P450 enzymes and autoimmunity: expansion of the relationship and introduction of free radicals as the link. J Autoimmune Dis. 2009;6:4.
144. Ignarro LJ. Haem-dependent activation of guanylate cyclase and cyclic GMP formation by endogenous nitric oxide: a unique transduction mechanism for transcellular signaling. Pharmacol Toxicol. 1990;67:1–7.
145. Ignarro LJ. Regulation of cytosolic guanylyl cyclase by porphyrins and metalloporphyrins. Adv Pharmacol. 1994;26:35–65.
146. Denninger JW, Marletta MA. Guanylate cyclase and the NO/cGMP signaling pathway. Biochim Biophys Acta. 1999;1411:334–50.

147. Gunn A, Derbyshire ER, Marletta MA, Britt RD. Conformationally distinct five-coordinate heme-NO complexes of soluble guanylate cyclase elucidated by multifrequency electron paramagnetic resonance (EPR). Biochemistry. 2012;51:8384–90.
148. Alderton WK, Cooper CE, Knowles RG. Nitric oxide synthases: structure, function and inhibition. Biochem J. 2001;357:593–615.
149. van Gastel M, Bubacco L, Groenen EJ, Vijgenboom E, Canters GW. EPR study of the dinuclear active copper site of tyrosinase from *Streptomyces antibioticus*. FEBS Lett. 2000;474:228–32.
150. Segal HL, Boyer PD. The role of sulfhydryl groups in the activity of D-glyceraldehyde 3-phosphate dehydrogenase. J Biol Chem. 1953;204:265–81.
151. Dalziel K, McFerran NV, Wonacott AJ. Glyceraldehyde-3-phosphate dehydrogenase. Philos Trans R Soc Lond Ser B Biol Sci. 1981;293:105–18.
152. Wu K, Li W, Yu L, Tong W, Feng Y, Ling S, Zhang L, Zheng X, Yang M, Tian C. Temperature-dependent ESR and computational studies on antiferromagnetic electron transfer in the yeast NADH dehydrogenase Ndi1. Phys Chem Chem Phys. 2017;19:4849–54.
153. Migita CT, Salerno JC, Masters BS, Martasek P, McMillan K, Ikeda-Saito M. Substrate binding-induced changes in the EPR spectra of the ferrous nitric oxide complexes of neuronal nitric oxide synthase. Biochemistry. 1997;36:10987–92.
154. Smith JM. Evolution and information. In: Koj A, Sztompka P, editors. Images of the World: Science, Humanities, Art. Kraków: The Jagiellonian University; 2001. p. 13–7.
155. Muh F, Zouni A. Light-induced water oxidation in photosystem II. Front Biosci (Landmark Ed). 2011;16:3072–132.
156. Müh F, Glöckner C, Hellmich J, Zouni A. Light-induced quinone reduction in photosystem II. Biochim Biophys Acta. 2012;1817:44–65.
157. Marciniak A, Ciesielski B. EPR dosimetry in nails—A review. Appl Spectrosc Rev. 2016;51:73–92.
158. Hong H, Sun J, Cai W. Multimodality imaging of nitric oxide and nitric oxide synthases. Free Radic Biol Med. 2009;47:684–98.
159. Spasojević I. Free radicals and antioxidants at a glance using EPR Spectroscopy. Crit Rev Clin Lab Sci. 2011;48:114–42.
160. Plonka PM, Chlopicki S, Plonka BK, Jawien J, Gryglewski RJ. Endotoxaemia in rats: detection of nitrosyl-haemoglobin in blood and lung by EPR. Curr Top Biophys. 1999;23(1):47–53.
161. Szczygiel D, Pawlus J, Plonka PM, Elas M, Szczygiel M, Plonka BK, Łukiewicz SJ. Nitric oxide in the interaction between primary and secondary tumor of L5178Y lymphoma. Nitric Oxide. 2004;11:279–89.
162. Subczynski WK, Widomska J, Feix JB. Physical properties of lipid bilayers from EPR spin labeling and their influence on chemical reactions in a membrane environment. Free Radic Biol Med. 2009;46:707–18.
163. Elas M, Magwood JM, Butler B, Li C, Wardak R, DeVries R, Barth ED, Epel B, Rubinstein S, Pelizzari CA, Weichselbaum RR, Halpern HJ. EPR oxygen images predict tumor control by a 50% tumor control radiation dose. Cancer Res. 2013;73:5328–35.
164. Krzykawska-Serda M, Miller RC, Elas M, Epel B, Barth ED, Maggio M, Halpern HJ. Correlation between hypoxia proteins and EPR-detected hypoxia in tumors. Adv Exp Med Biol. 2017;977:319–25.
165. Godechal Q, Ghanem GE, Cook MG, Gallez B. Electron paramagnetic resonance spectrometry and imaging in melanomas: comparison between pigmented and nonpigmented human malignant melanomas. Mol Imaging. 2013;12:218–23.
166. Danhier P, Gallez B. Electron paramagnetic resonance: a powerful tool to support magnetic resonance imaging research. Contrast Media Mol Imaging. 2015;10:266–81.
167. Metabolism, Metabolomics, Imaging in Cancer. Cherukuri MK, Kalyanaraman B (Chairs). Session 6th, Wednesday, October 5th, 2016. Xth International Workshop on EPR in Biology and Medicine, Kraków, October 02–06, 2016. www.eprworkshop.info [Access: Aug 29th, 2017].

168. McCall KA, Huang C, Fierke CA. Function and mechanism of zinc metalloenzymes. J Nutr. 2000;130:1437S–46S.
169. Pasenkiewicz-Gierula M, Murzyn K, Róg T, Czaplewski C. Molecular dynamics simulation studies of lipid bilayer systems. Acta Biochim Pol. 2000;47:601–11.
170. Symons MC. Electron movement through proteins and DNA. Free Radic Biol Med. 1997;22:1271–6.
171. Szent-Györgyi A. Wstęp do biologii submolekularnej. Warszawa: PWN; 1961. [Polish, transl. by Stolarek J from English "Introduction to a submolecular biology". New York: Academic Press; 1960].
172. VI International Conference of Biophysics Students. Biophysics Students' Association 'Nobel' and Faculty of Biochemistry, Biophysics and Biotechnology, Jagiellonian University, Cracow, Poland, 19th-21st May 2017. Programme Book. http://www.nobel.wbbib.uj.edu.pl/ [Access: Aug 30th, 2017].
173. Benenson Y, Adar R, Paz-Elizur T, Livneh Z, Shapiro E. DNA molecule provides a computing machine with both data and fuel. Proc Natl Acad Sci U S A. 2003;100:2191–6.
174. Nickoloff JA. Paths from DNA damage and signaling to genome rearrangements via homologous recombination. Mutat Res. 2017;806:64–74. https://doi.org/10.1016/j.mrfmmm.2017.07.008.
175. Küppers B-A. Geneza informacji biologicznej. Filozoficzne problem powstania życia. [The genesis of biological information. On philosophical problems of the origin of life]. Warszawa: PWN; 1991. [in Polish, transl. by Ługowski W from German "Der Ursprung biologischer Information. Zur Naturphilosophie der Lebenentstehung". B. Piper Verlag GmbH & Co. K.G. Munich 1986. Available also in English: Information and the origin of life. The MIT Press, Cambridge/Mass. 1990].
176. Ohno S. Evolution from primordial oligomeric repeats to modern coding sequences. J Mol Evol. 1987;25:325–9.
177. Arodź T, Płonka PM. Effects of point mutations on protein structure are nonexponentially distributed. Proteins. 2012;80:1780–90.
178. Arodź T, Płonka PM. Sequence and structure space model of protein divergence driven by point mutations. J Theor Biol. 2013;330:1–8.
179. Eigen M. Selforganization of matter and the evolution of biological macromolecules. Naturwissenschaften. 1971;58:465–523.
180. Muller HJ. Artificial transmutation of the gene. Science. 1927;66:84–7.
181. Howard BD, Tessman I. Identification of altered bases in mutated single-stranded DNA III. Mutagenesis by ultraviolet light. J Mol Biol. 1964;9:372–5.
182. Tessman I, Poddart RK, Kumar S. Identification of the altered bases in mutated single-stranded DNA I. In vitro mutagenesis by hydroxylamine, ethyl methanesulfonate and nitrous acid. J Mol Biol. 1964;9:352–63.
183. Cech TR. RNA chemistry. Ribozyme self-replication? Nature. 1989;339:507–8.
184. Niziolek M, Korytowski W, Girotti AW. Chain-breaking antioxidant and cytoprotective action of nitric oxide on photodynamically stressed tumor cells. Photochem Photobiol. 2003;78:262–70.
185. El-Agamey A, Lowe GM, McGarvey DJ, Mortensen A, Phillip DM, Truscott TG, Young AJ. Carotenoid radical chemistry and antioxidant/pro-oxidant properties. Arch Biochem Biophys. 2004;430:37–48.
186. Schultz T, Samoylova E, Radloff W, Hertel IV, Sobolewski AL, Domcke W. Efficient deactivation of a model base pair via excited-state hydrogen transfer. Science. 2004;306:1765–8.
187. Reichard P, Baldesten A, Rutberg L. Formation of deoxycytidine phosphates from cytidine phosphates in extracts from *Escherichia coli*. J Biol Chem. 1961;236:1150–7.
188. Jordan A, Reichard P. Ribonucleotide reductases. Annu Rev Biochem. 1998;67:71–98.
189. Chang MC, Yee CS, Stubbe J, Nocera DG. Turning on ribonucleotide reductase by light-initiated amino acid radical generation. Proc Natl Acad Sci U S A. 2004;101:6882–7.
190. Nordlund P, Reichard P. Ribonucleotide reductases. Annu Rev Biochem. 2006;75:681–706.

191. Berggren G, Duraffourg N, Sahlin M, Sjöberg BM. Semiquinone-induced maturation of *Bacillus anthracis* ribonucleotide reductase by a superoxide intermediate. J Biol Chem. 2014;289:31940–9.
192. Pulatova MK, Sharygin VL, Todorov IN. The activation of ribonucleotide reductase in animal organs as the cellular response against the treatment with DNA-damaging factors and the influence of radioprotectors on this effect. Biochim Biophys Acta. 1999;1453:321–9.
193. Poole AM, Jeffares DC, Penny D. The path from the RNA world. J Mol Evol. 1998;46:1–17.
194. Jeffares DC, Poole AM, Penny D. Relics from the RNA world. J Mol Evol. 1998;46:18–36.
195. Zhao H, Dobrucki J, Rybak P, Traganos F, Halicka HD, Darzynkiewicz Z. Induction of DNA damage signaling by oxidative stress in relation to DNA replication as detected using "click chemistry". Cytometry A. 2011;79:897–902.
196. Berniak K, Rybak P, Bernas T, Zarębski M, Biela E, Zhao H, Darzynkiewicz Z, Dobrucki JW. Relationship between DNA damage response, initiated by camptothecin or oxidative stress, and DNA replication, analyzed by quantitative 3D image analysis. Cytometry A. 2013;83:913–24.
197. Joyce GF, Orgel LE. Prospects for understanding the origin of RNA world. In: Gesteland RF, Atkins JF, editors. The RNA world. New York, NJ: Cold Spring Harbour Laboratory Press; 1993. p. 1–25.
198. Plume A. "Omics": 'genomics' offspring shed light on biodiversity. Res Trends. 2010;19:6–7.
199. Malinski T, Taha Z. Nitric oxide release from a single cell measured in situ by a porphyrinic-based microsensor. Nature. 1992;358:676–8.
200. Soh N, Katayama Y, Maeda M. A fluorescent probe for monitoring nitric oxide production using a novel detection concept. Analyst. 2001;126:564–6.
201. Mal A, Chatterjee IB. Mechanism of autoxidation of oxyhaemoglobin. J Biosci. 1991;16:55–70.
202. Batthyány C, Bartesaghi S, Mastrogiovanni M, Lima A, Demicheli V, Radi R. Tyrosine-nitrated proteins: proteomic and bioanalytical aspects. Antioxid Redox Signal. 2017;26:313–28.
203. Mak PJ, Denisov IG. Spectroscopic studies of the cytochrome P450 reaction mechanisms. Biochim Biophys Acta. 2018;1866(1):178–204. https://doi.org/10.1016/j.bbapap.2017.06.021.
204. Di Giuseppe S, Placidi G, Sotgiu A. New experimental apparatus for multimodal resonance imaging: initial EPRI and NMRI experimental results. Phys Med Biol. 2001;46:1003–16.
205. Beer S. Cybernetyka a zarządzanie [Cybernetics and management]. Warszawa: PWN; 1966, pp. 67–74. [in Polish, transl. by Ś. Sorokowski of the 1st Edition, The English London: University Press Ltd; 1959].
206. Pasenkiewicz-Gierula M, Sealy RC. Analysis of the ESR spectrum of synthetic dopa melanin. Biochim Biophys Acta. 1986;884:510–6.
207. Subczynski WK, Kusumi A. Dynamics of raft molecules in the cell and artificial membranes: approaches by pulse EPR spin labeling and single molecule optical microscopy. Biochim Biophys Acta. 2003;1610:231–43.